Lawrence Berkeley National Laboratory
Recent Work

Title
MEASUREMENT AND INTERPRETATION OF LIMITING CURRENTS

Permalink
https://escholarship.org/uc/item/26p2m03j

Author
Seljman, Jan Robert.

Publication Date
1971-06-01

eScholarship.org Powered by the California Digital Library
University of California

Jan Robert Selman

UCRL-20557
c.2

MEASUREMENT AND INTERPRETATION OF LIMITING CURRENTS

Jan Robert Selman

(Ph. D. Thesis)

June 1971

AEC Contract No. W-7405-eng-48

TWO-WEEK LOAN COPY

This is a Library Circulating Copy which may be borrowed for two weeks. For a personal retention copy, call Tech. Info. Division, Ext. 5545

LAWRENCE RADIATION LABORATORY
UNIVERSITY of CALIFORNIA BERKELEY

UCRL-20557
c.2

DISCLAIMER

This document was prepared as an account of work sponsored by the United States Government. While this document is believed to contain correct information, neither the United States Government nor any agency thereof, nor the Regents of the University of California, nor any of their employees, makes any warranty, express or implied, or assumes any legal responsibility for the accuracy, completeness, or usefulness of any information, apparatus, product, or process disclosed, or represents that its use would not infringe privately owned rights. Reference herein to any specific commercial product, process, or service by its trade name, trademark, manufacturer, or otherwise, does not necessarily constitute or imply its endorsement, recommendation, or favoring by the United States Government or any agency thereof, or the Regents of the University of California. The views and opinions of authors expressed herein do not necessarily state or reflect those of the United States Government or any agency thereof or the Regents of the University of California.

Table of Contents

Abstract v

Introduction 1

Chapter 1. Applicability of the limiting current method

Part I. The limiting current method

1.1. The limiting current 3

1.2. Measurement of mass transfer rates 5

1.3. Model reactions 7

1.4. Historical 11

Part II. Review of applications

1.5. Simple laminar flows 14

1.6. Laminar flow with complications 25

1.7. Turbulent flows and mixed convection 40

1.8. Restricted cells with agitation 52

1.9. Cells with gas-evolution 55

1.10. Particulate flow systems 58

1.11. Electrochemiluminescence 61

1.12 Conclusions 61

Chapter 2. Validity of the limiting current method

Part I. Basic concepts of electrochemical mass transfer

2.1. Migration and diffusion 67

2.2. Polarization 77

2.3. Current and potential distribution 91

Part II. Conditions for validity

2.4. Definition of the limiting current plateau 105

2.5. Conditions for valid measurement 105

2.6. Conditions for valid interpretation 106

Chapter 3. Rotating disk integral diffusivities of Cu^{++} ion in $CuSO_4$-H_2SO_4-H_2O

3.1. Introduction 108

3.2. Experimental 110

3.3. Results 118

3.4. Discussion: migration effect 138

3.5. Discussion: deposit roughness 147

3.6. Conclusions 157

Chapter 4. Unsteady state effects in electrochemical flow cells

Part I. Review

4.1. Introduction 161

4.2. Free convection 162

4.3. Forced convection 169

4.4. Interaction with potential distribution at elongated electrodes 172

Part II. Unsteady state at a rotating disk electrode

4.5. Experimental 177

4.6. Results 179

4.7. Discussion 194

4.8. Conclusions 208

Conclusions and Recommendations 210

Acknowledgments 213

Appendices

A. Program for calculation of a theoretical limiting current curve 214

B. Flux at a rotating disk electrode after a concentration step at the surface, in the limit of high Schmidt numbers . . 216

C. Degree of dissociation of HSO_4^- ion in the system $CuSO_4$ $-H_2SO_4-H_2O$ 237

D. Migration at a rotating disk electrode in acidified solutions of $CuSO_4$ characterized by the bisulfate dissociation parameter $I/K_B' = 5$ 250

E. Theoretical solutions for transient convective diffusion . . 256

F. Transient diffusion following linear potential decrease at a redox electrode 261

G. Transient diffusion following linear potential decrease for a deposition reaction, taking electrode kinetics into account 270

Nomenclature 288

References 295

MEASUREMENT AND INTERPRETATION OF LIMITING CURRENTS

Jan Robert Selman

Inorganic Materials Research Division, Lawrence Radiation Laboratory
Department of Chemical Engineering
University of California, Berkeley, California

June 1971

ABSTRACT

Applications of the limiting current method for measuring mass transfer rates are reviewed. To date almost 100 publications using this method have appeared, with recent applications in the area of stirred tanks, particulate systems, mixed convection and turbulence.

The conditions for valid measurement and interpretation of limiting currents are discussed. An ideal limiting current curve is constructed for the copper deposition model reaction. The effect of migration due to the electric field is computed for this reaction, taking into account that the bisulfate ion is not completely dissociated. The use of integral diffusivities, which reflect the effect of migration as well as that of variable physical properties, is required in the correlation of mass transfer coefficients calculated from limiting currents.

Rotating disk integral diffusivities are reported for cupric ion in acidified solutions of cupric sulfate. In solutions containing less than 0.1 molar cupric sulfate the product of viscosity and integral diffusivity is independent of the ionic strength of the solution. In more concentrated solutions the effect of surface roughness developing near the limiting current is discernible in high diffusivity values. Some semi-quantitative considerations on the development and extent of this roughness effect are given.

Unsteady-state effects in limiting current measurements are reviewed from the viewpoint of nonstationary convective diffusion. The complicating effect of the presence of an electric field is discussed, and it is shown that apparent, nonsimultaneous, sectional limiting currents can be expected to occur at elongated electrodes. Unsteady-state limiting currents at a rotating disk electrode are investigated experimentally, using the ferricyanide-ferrocyanide redox system. The minimum time to reach a steady-state limiting current by linear current increase is an order of magnitude larger than that necessary if a linear potential scan is applied. Apparent limiting currents due to fast current increase or potential scan rates can be satisfactorily interpreted in terms of a pure-diffusion model.

This thesis is dedicated to the memory of my father

Jan Selman

a chemist and a teacher, who first taught me the value of understanding.

INTRODUCTION : STRUCTURE OF THE THESIS

Electrochemical measurements of mass transfer rates by the limiting current technique have been employed in recent decades with increasing frequency. The present work aims to contribute to the methodology of limiting current measurements by a unifying review of applications and of conditions for validity, as well as by a detailed study of some critically important aspects.

In the first Chapter the basic features of the method are described, its advantages and limitations. The variety of mass transfer situations towhich it has been applied, is reviewed.

Chapter 2 gives a synopsis of those concepts of electrochemical mass transfer theory which are necessary for an analysis of the limiting current condition. The requirements for an effective measurement and a valid interpretation of the results, are reviewed.

Three practical aspects of the limiting current technique are singled out for a detailed investigation: diffusivity values appropriate to the method; unsteady-state mass transfer during the approach of the limiting current; and the effect of current distribution below and at the limiting current, due to the presence of an electric field.

Chapter 3 treats the problem of appropriate diffusivities to be used in limiting current studies, in particular for the copper deposition reaction frequently used in free-convection studies. It is shown that migration and surface roughness formed near the limiting current both have a considerable effect on the integral diffusivities measured at a rotating disk electrode. The conditions under which the surface roughness

effect is minimal are investigated.

Chapter 4 deals with the unsteady state due to mass transfer. Available information concerning transients in convective diffusion is reviewed. From a comparison with experimental limiting current curves at planar, sectioned electrodes it can be inferred that transient effects are more persistent than expected. This is shown to be related to the current distribution below the limiting current.

The second part of Chapter 4 is devoted to a study of unsteady-state mass transfer at a rotating disk electrode, using a redox reaction where such current distribution effects are not important. The apparent limiting currents observed in fast current ramps or potential scans are explained in terms of a pure-diffusion model.

Chapter 1. APPLICABILITY OF THE LIMITING CURRENT METHOD

Part 1. The limiting current method

1.1. The limiting current.

The term "limiting current density" is used to describe the maximum rate at which a particular electrode reaction can proceed in the steady state, with 100% current efficiency. This rate is determined by the composition and transport properties of the electrolytic solution on the one hand, and on the other by the hydrodynamics of the electrochemical cell. In a given situation the limiting current at an electrode can only be exceeded by increasing the cell potential until another consecutive, electrode reaction starts occurring at finite rate.

The limiting current may be due to a slow, rate-determining step in the electrode reaction (kinetic limiting current). However, in the majority of cases where a limiting current is encountered it is caused by the slowness of transport of ionic or uncharged species through the solution. The ions (or molecules) move toward the electrode where they are consumed in the electrode reaction, or a reaction coupled with it. Electrode reactions, by their nature, are surface reactions and cause local changes in composition. A thin diffusion layer, impoverished in the reacting species, develops at the electrode surfaces. The ions or molecules move across the diffusion layer by diffusion down concentration gradients. Ions move also under the influence of the electric field, i.e., they migrate.

Limiting currents are usually associated with cathodic reactions (e.g., in metal deposition), although anodic reactions are by no means excluded. Whenever the supply of a dissolved species from the solution to the electrode surface becomes a rate limiting factor, limiting current phenomena

may be observed. Agar and Bowden[122] showed that diffusion of H_2O limits O_2 evolution in fused NaOH. Hoar and Rothwell[28] observed anodic limiting currents in electropolishing of copper, due in part to a dissolution diffusion layer, and in part to a solid oxide film.

In most cases the diffusion layer is not a stagnant layer, as presented in the early Nernst-Whitman model. Where no forced convection is maintained free convection usually sets in due to the density gradient developing in the diffusion layer. The convective velocity, although it vanishes at the wall, enhances the diffusion toward the electrode. It steepens the concentration gradient of the reacting species at the electrode and therefore increases the maximum current obtainable.

Equivalently this is often expressed as a decrease of the Nernst layer thickness. In the stagnant layer model referred to above the concentration profile of the reacting ion is linear, with the thickness δ_N chosen so as to give the actual concentration gradient at the electrode. This fictitious δ_N is always smaller than the real diffusion layer thickness, but better defined since the actual concentration profile tapers off very gradually to the bulk value.

Clearly the maximum gradient for a certain rate of stirring, i.e., a given hydrodynamic condition near the electrode, is that gradient whereby the concentration at the electrode is reduced to zero, or virtually zero. This situation corresponds, in an electrochemical cell, to the limiting current condition.

1.2. Measurement of mass transfer rates.

If the rate of the reaction is not restricted by the kinetics of the reaction mechanism, the reaction is called "reversible" and its rate is transport-controlled. The current density, $\underline{i}$, is proportional to the reacting ion (or molecule) flux, $\underline{N}_i$, by Faraday's law:

$$s_i \underline{i} = -nF\underline{N}_i \tag{1.1}$$

Here s_i is the number of molecules of species i participating in the transfer of n electrons to or from the electrode.

Therefore, if the driving force of the mass transfer process can be expressed in a practical form, e.g., as a concentration gradient of the reacting species, or as a concentration difference between electrode and bulk solution, one can relate the mass transfer rate in a general way to the concentration driving force. If the concentration gradient is known, an effective diffusivity can be defined:

$$\underline{N}_i = -D_i^{eff} \nabla c_i \quad . \tag{1.2}$$

More often, only the concentration difference electrode/bulk is known, and in such cases the mass-transfer coefficient can be calculated:

$$\underline{N}_i = k(c_{i,o} - c_{i,b}) . \tag{1.3}$$

In the limiting current method of measuring mass transfer coefficients, the reacting ion concentration at the electrode is made vanishingly small by applying a large potential. In that case only the current density and the bulk concentration need to be known.

If the concentration at the electrode is not zero, it can still be measured by optical techniques, in particular by interferometric methods. Such measurements, however, are relatively simple only in dilute solutions, because refraction occurs in addition to interference.[115] Moreover, they are restricted to solutions where only the reacting species concentration varies, i.e., to solutions of a single salt. If the solution contains two electrolytes with dissimilar concentration profiles in the diffusion layer, a second, independent, measurement is needed to establish the reactant concentration at the electrode.

In practice such multicomponent electrolytic solutions are used much more frequently than those of single salts. In binary solutions the current exceeds the expected current due to convective diffusion by a factor of approximately two. This excess current is due to migration of the reacting ion in the electric field. It can be suppressed by increasing the conductivity of the solution, thereby lowering the electric field strength. Thus, in mass transfer measurements, a large amount of "supporting" or "inert" electrolyte is usually added to the solution. The complications associated with the presence of non-reacting ions in the diffusion layer have been discussed extensively elsewhere.[113,114] They are of special importance in free convection, where the driving force, i.e., a density difference, is affected by the accumulation or deficit of non-reacting ions at the electrode. In both forced and free convection it is important to know the ion flux contributed by migration, which is never completely absent. Chapter 2 deals with this problem in quantitative terms.

Since current measurements can be made very exactly, the limiting current technique is a convenient and precise method of measuring mass transfer rates. The limiting current makes itself known as a plateau or inflection point in the plot of current versus electrode overpotential (Figure 3.6). In principle the accuracy of mass transfer measurements is limited only by the precision with which this limiting current plateau, or point, can be read. Further, the electrode area, current distribution and reactant bulk concentration have to be known accurately.

1.3. Model reactions.

The electrochemical reactions most often used for the study of limiting currents are listed in Table 1.1. Oxygen reduction was used in early experiments with a rotating disk.[87] Later many investigators made use of copper deposition from acidified solution. This reaction has the disadvantage of changing the cathode surface, especially near the limiting current where the deposit becomes rough (see section 3.5).

For forced convection studies copper deposition has been largely supplanted by the reduction of ferricyanide at a nickel or platinum surface. Usually, an equimolar mixture of ferri- and ferrocyanide is used. The oxidation of ferrocyanide at the anode compensates, at least in part, for the cathodic depletion of ferricyanide, if anolyte and catholyte are not separated by a diaphragm. The ferrocyanide oxidation reaction has also been used occasionally as the controlling reaction, but it has the disadvantage of a shorter limiting current plateau. In addition, oxygen evolution passivates a nickel anode. (Both electrodes

Table 1.1. Model reactions in electrochemical mass transfer studies.

		E^o(v)	electrode metal	supporting electrolyte	reference
CATHODIC					
1	$Fe(CN)_6^{3-} + e \rightarrow Fe(CN)_6^{4-}$	+0.360	Ni,Pt	NaOH KOH	many 51
2	$O_2 + 2H_2O + 4e \rightarrow 4OH^-$	+0.401	Pt,Ag	NaOH NaCl	2,87 81
3	$I_3^- + 2e \rightarrow 3I^-$	+0.536	Pt	KI	59,88
4	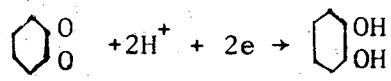	+0.699	Ag	fosfate buffer	2
5	$Zn^{2+} + 2e \rightarrow Zn$	-0.763	Zn(Hg)	KOH	
6	$Cd^{2+} + 2e \rightarrow Cd$	-0.352	Cd(Hg)	none	4
7	$Cu^{2+} + 2e \rightarrow Cu$	+0.337	Cu	H_2SO_4 none	many 7,9,23
8	$Ag^+ + e \rightarrow Ag$	+0.799	Ag	$HClO_4$	5
ANODIC					
9	$CuCl_4^{3-} \rightarrow CuCl_4^{2-} + e$	+0.153	Pt	$CaCl_2$	15
10	$Fe(CN)_6^{4-} \rightarrow Fe(CN)_6^{3-} + e$	+0.360	Ni,Pt	NaOH KOH	many 51

are susceptible to CN^- poisoning. The correct procedure to activate nickel electrodes before use has been described by Eisenberg c.s.[6])

For studies of free convection mass transfer, or combinations of forced and free convection, the copper deposition reaction remains the preferred reaction, in spite of the precautions necessary to prevent excessive surface roughening near the limiting current. The advantage that copper deposition offers in such studies is a considerably larger driving density difference, due to (1) its higher solubility; (2) the larger densification (see Table 1.2).

In the case of the redox reaction the opposite effects of reactant depletion and product accumulation cancel each other to a large extent. The densification due to ferrocyanide is larger than that due to ferricyanide (each larger than that for $CuSO_4$), so that the redox reaction makes the catholyte denser and the anolyte less dense.

The actual densification is also influenced by the effect of migration. As shown in the third line of Table 1.2, the relative densification in acidified cupric sulfate is less than in binary cupric sulfate solution. In the case of the supported redox reaction the migration effect makes the density difference larger than expected from over-all reaction stoichiometry.

None of the other reactions listed in Table 1.1 have attained the popularity of ferricyanide reduction and copper deposition. The oxygen and iodine reduction reactions satisfy the requirements of a reasonably long plateau (> 250 mv, depending on the supporting electrolyte pH) and do not change the surface. They are however restricted to forced convection situations with large flow rates, since the bulk concentrations are

Table 1.2. Maximum densification in cupric sulfate and alkaline equimolar ferri-and ferrocyanide solutions, at 25°C.

	$CuSO_4$	$CuSO_4$ +1.5M H_2SO_4	equimolar ferri/ferrocyanide +2.0M NaOH	
			cathodic	anodic
Δc_R (M)	1.4	0.9	0.2	0.2
α_R (M^{-1})	0.140	0.140	0.167	0.226
$\Delta\rho/\rho$	0.140	0.125	-0.0706	0.0832
ρ(g/ml)	1.214	1.217	1.50	
μ(cp)	1.824	1.914	1.647	
ν(cst)	1.502	1.573	1.432	
$\Delta\rho$(g/ml)	0.170	0.137	-0.0812	+0.0957

Values of α_R and $\Delta\rho/\rho$ taken from Ref. 114.

of the order of 10^{-3}M at most. Reducible impurities and gases (e.g., O_2 if iodine is the reactant) have to be rigorously excluded. In the case of oxygen reduction, maintaining a known oxygen concentration in the bulk is not a trivial problem because of the tendency to super-saturation, and the extreme sensitivity of the solubility to the salt concentration in solution.

The silver and zinc deposition reactions have only occasionally been used. Dendritic deposits form very easily unless organic inhibitants are added, which complicates the electrode kinetics to the point of obscuring the limiting current.

In the present study only ferricyanide reduction and copper deposition were employed.

1.4. Historical.

The dependence of current density on the rate of stirring was first clearly established by Nernst[116] and Brunner[117] (1904). They interpreted this by means of the stagnant layer concept first used by Noyes and Whitney. The thickness of this layer ("Nernst diffusion layer thickness") was correlated simply with the speed of the stirring impeller or rotating electrode tip.

The lack of hydrodynamic definition was recognized by Eucken,[99] who considered convective diffusion transverse to a parallel flow and obtained an expression analogous to the Lévêque equation of heat transfer. Experiments with Couette flow between a rotating cylinder and a stationary outer cylinder did not confirm his predictions. At very low rotation rates, where such a flow is stable, it does not contribute to the diffusion process since there is no velocity component in the radial

direction. At higher rotation rates secondary flow patterns form (Taylor vortices) and finally the flow becomes turbulent. Neither flow regime satisfies the conditions of the Lévêque equation.

However, flow generated by a cylinder rotating at high speed was subsequently used by others, in particular King and co-workers[118,119] to demonstrate that dissolution processes are diffusion limited, and electrochemical corrosion processes as well. The dependence of the mass-transfer coefficient on the 0.7 power of rotation rate and diffusivity of the dissolving species was established (cf. Table 1.3, eq. 31).

Of considerable importance for the conceptual development of limiting current measurement was the work of Agar and Bowden[122] on the current-overpotential relationship at nickel electrodes in fused sodium hydroxyde, where water transport is the limiting step:

$$2OH^- \rightarrow \frac{1}{2}O_2 + H_2O + e$$

A more detailed review of this, and other, early work in ionic mass transfer is given by Tobias, Wilke and Eisenberg.[100]

The full development of electrochemical techniques of mass transfer measurement had to await the formulation of a quantitative insight into the role of convective diffusion in electrode processes. This was first successfully provided by the groundbreaking work of Levich on the rotating disk electrode,[105,106] so that by 1947 the conditions were fulfilled for a matching of theory and practice.[87] Agar[107] pointed out that electrochemical mass transfer correlations should be closely similar to those known for heat transfer. The first test of the theory of convective diffusion in free convection was made by Wagner.[1] From 1951 on limiting

current measurements have been used with increasing frequency and confidence to establish mass transfer rates at reactive surfaces in flow situations where they cannot be predicted on theoretical grounds, or where the theory needs confirmation.

Only a few reviews have appeared in which the application of the method is discussed from a chemical engineering viewpoint. In the review already mentioned Tobias, Wilke and Eisenberg[100] examined the available knowledge about electrochemical mass transport at the beginning of its application (1950). The same authors developed correlations for predicting the limiting current in laminar free convection at vertical electrodes, as well as in turbulent flow between cylindrical electrodes, with the inner cylinder rotating and the outer one stationary.

Ibl[8] reviewed early work on free convection, to which he and his co-workers contributed notably by the development of optical methods for the study of the diffusion layer.[101,7,9] A discussion of their application falls outside the scope of this review and has been given by Muller.[104]

In a survey of 1963, Ibl[102] lists 13 mass transfer correlations established by the limiting current method. Only 4 of these were known from quantitative theoretical predictions. The total number of publications since 1963 has almost quadrupled (references 1-88). The majority of these concern flow situations where theoretical predictions are at most of a qualitative nature. An increasing number of publications deal with model studies of complex situations, e.g., packed and fluidized beds, and with hydrodynamic studies.

Part II. Review of Applications

For the purpose of this review we will distinguish experimental studies of mass-transfer in: (a) simple laminar flow; (b) laminar flow with complications; (c) turbulent flow and mixed convection; (d) stirred vessels; (e) cells with gas-evolution; (f) particulate flow systems.

A related technique of mass transfer measurement will also be discussed briefly.

1.4. Simple laminar flows

For the flow situations listed as number 1 through 5 in Table 1.3 the mass transfer rate can be derived directly from a solution of the equation of convective diffusion. The velocity profile near the electrode is known, and the equation is simplified by appropriate similarity transformations. Newman[103] has reviewed these solutions in detail. Here we only want to comment on the nature of the velocity profile near the electrode, and on the agreement between theory and experiment.

In the case of the rotating disk there is a uniform axial velocity towards the disk, which depends only on the normal distance from the disk, so that the mass transfer rate is also uniform. If the center of the disk is non-reactive, the flux to the active ring is higher than it otherwise would be, and the electrode is no longer uniformly accessible. The maximum rate is found at the inner edge of the ring, where radial convection is no longer uniform. Thus, the maximum is due to the non-coincidence of the uniform hydrodynamic boundary layer and the diffusion layer (relaxation process).

Table 1.3. Mass transfer correlations obtained by limiting current measurements.

	System	Correlation	Range	Parameters	Electrolyte	Authors
1a	Rotating disk	$Nu=0.62Re^{1/2}Sc^{1/3}$ $Re=\omega r^2/\nu$ $Nu=kr/D$	$Re<2.7\times10^5$	r=radius r_i=inner radius r_o=outer radius	O_2 Cu^{++} $Fe(CN)_6^{3-}$ I_3^-	Siver,Kabanov[87] Hsueh,Newman[98] Okada, et al.[10] Newson,Riddiford[88] Daguenet[59]
b	Rotating ring	$Nu=Nu_{disk,r_o}(1-r_i^3/r_o^3)^{2/3}$	$Re<2.7\times10^5$		I_3^-	Daguenet[59]
2	Coaxial flow in annular tube	(a)*$Nu=1.62(ReSc\ d/L)^{1/3}$ $r_i/r_o=0.5$ $Re=\bar{v}d_e/\nu$ $Nu=kd_e/D$	$1.6\times10^4<$ $ReSc\ d/L<1.1\times10^6$ $300<Sc<3000$	$d_e=r_o-r_i$	O_2 $Fe(CN)_6^{3-}$ quinone $Fe(CN)_6^{4-}$	Lin, et al.[2]
		(b)$Nu=1.94(ReSc\ d/L)^{1/3}$ $r_i/r_o=0.5$	$1.7\times10^4<$ $ReSc\ d/L<9\times10^7$		Cu^{2+}	Ross,Wragg[36] Wragg,Ross[63]
3	Parallel flow in rectangular channel	$Nu=1.85(ReSc\ d/L)^{1/3}$ $d/h>1.85$ $Re=\bar{v}d_e/\nu$ $Nu=kd_e/D$	$75<Re<7000$ $600<Sc<12000$ $0.05<d/L<20$	h=height d=eq.diameter	Cu^{2+}	Tobias,Hickman[32]
4	Free convection at a vertical wall (plate,wide cylinders)	(a)$Nu=0.67(GrSc)^{1/4}$ $Gr=g\Delta\rho L^3/\nu^2\rho$	$5\times10^6<GrSc<5\times10^{12}$ $500<Sc<80000$	L=height	Cu^{2+}	Wagner[1] Wilke,et al.[3] Wilke,et al.[5]
		(b)**$Nu=0.45(GrSc)^{1/4}$	$9\times10^9<GrSc<4.6\times10^{11}$ $2350<Sc<3650$	V=electrode velocity L=transfer length	$Fe(CN)_6^{3-}$	Fouad,Gouda[31]
5	Moving continuous cylinder	$Nu=1.13Pe^{1/2}$ $Pe=vL/D$ $Nu=kL/D$	$4000<\sqrt{Pe}<40000$ $Sc>700$		$Fe(CN)_6^{3-}$	Rotte[73] Rotte,Tummers[74]

*See however page 17 of text. Expected constant is 1.939 for $r_i/r_o=0.5$ (cf. eq. 1-6 text)

**See page 23 of text. Expected constant is 0.67.

(continued on p. 26)

A maximum in the mass transfer rate at the entering edge of the electrode occurs in all cases where the main flow is parallel to the electrode. This is the case in flow through pipes and channels, but also, e.g., at a flat plate, where the velocity near the plate has a transverse component. In all such cases the parallel velocity component close to the electrode can be considered linearly dependent on the distance from the electrode. This is justified by the extreme thinness of the diffusion layer compared to the region of velocity variation (large Schmidt number).

Similarity transformations lead then to two types of correlations: the boundary layer type,

$$Nu = C Re^{1/2} Sc^{1/3} \quad , \tag{1.4}$$

valid for boundary layers which have transverse velocity components; and the Lévêque type,

$$Nu = C (ReSc\ d_e/L)^{1/3} \quad , \tag{1.5}$$

valid for parallel flows. The rotating disk correlation 1a in Table 1.3 is an example of the first. Numbers 2 and 3 belong to the Lévêque type. All are characterized by the exponent 1/3 on the Schmidt number, corresponding to a ratio of boundary layer thicknesses (hydrodynamic/mass transfer) of the same order of magnitude:

$$\delta_{m.t.}/\delta_h \sim Sc^{-1/3}$$

The correlation of Table 1.3, for mass-transfer at infinitely extended parallel plates, to which Hickman's[32] experimental channel is

a good approximation (aspect-ratio 10 to 15), is a special case of that in annular channels. The general expression[103] for such channels is:

$$Nu = 1.615(\phi ReSc\ d_e/L)^{1/3} \quad , \qquad (1.6)$$

where ϕ is a function of the geometric parameter κ the ratio between inner and outer radius. Re and Nu are based on the equivalent diameter, i.e., the difference between inner and outer diameter. Figure 1.1 shows $\phi^{1/3}$ as a function of κ.

The limiting case $\kappa \to 1$ ($r_o = r_i$, $d_e = 2h$ where h is the channel height) gives

$$Nu = 1.8488\ (ReSc\ d_e/L)^{1/3} \quad , \qquad (1.7)$$

which is identical with the expression first found empirically by Norris and Streid[32] for heat transfer in flat rectangular channels, and confirmed by Hickman, with a scatter of about 7% around the theoretical values.

The correlation 2 of Table 1.3, established by Lin a.o.[2] for coaxial flow in annuli with $\kappa = 0.5$, was originally compared by them with the other limiting case of (6), $\kappa \to 0$ ($r_i \to 0$), i.e., mass transfer to the wall of a circular tube:

$$Nu = 1.615\ (ReSc\ d_e/L)^{1/3} \quad . \qquad (1.8)$$

This procedure was criticized by Friend and Metzner[128] who calculated that the constant should actually be 1.939 for the radial ratio 0.5. Part of the 19% discrepancy between the experimental results and the theoretical prediction can be ascribed to the use of incorrect diffusivities. For the experiments using the ferri-/ferrocyanide redox reaction an estimate of the

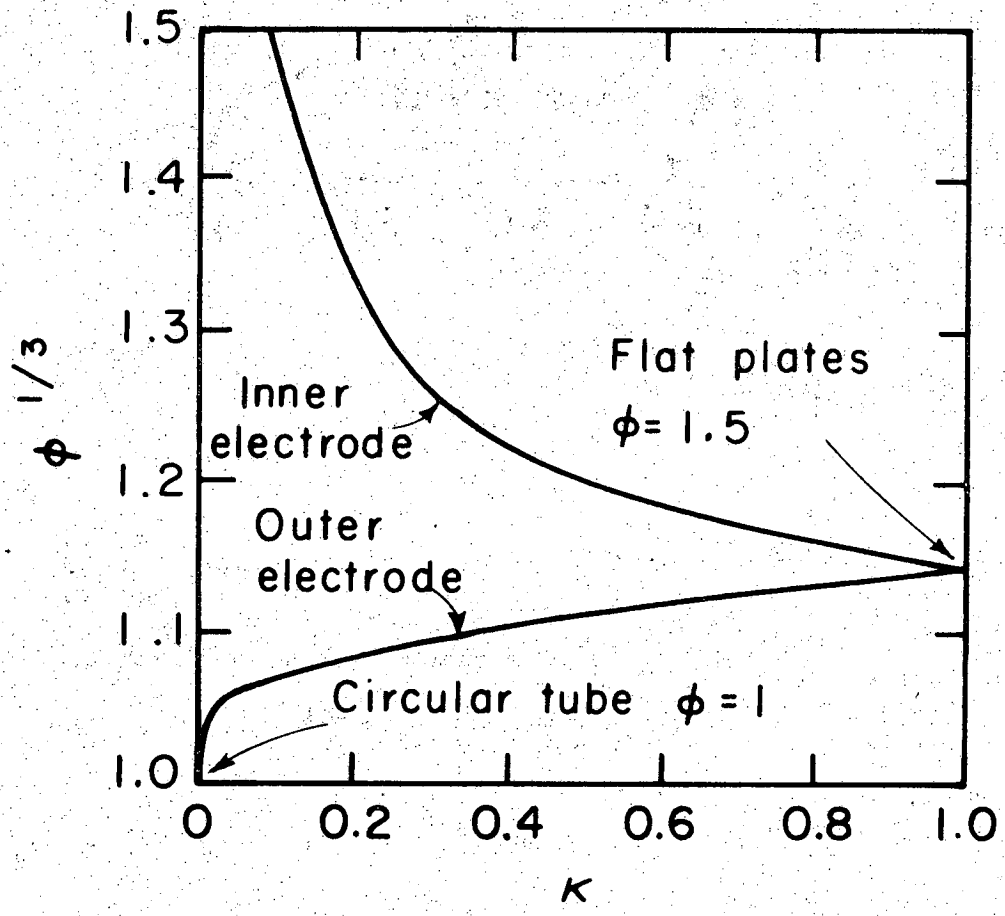

MUB-13771

Figure 1.1. The constant ϕ in the Lévêque correlation (1.7) for an annulus:

$$Nu = 1.615\ (\phi ReSc\ d_e/L)^{1/3} ,$$

as a function of the radial ratio $\kappa = r_i/r_o$.

error is possible. The value of the mobility product $\mu D/T$, based by Lin c.s. on the mobility at infinite dilution, is 6-20% lower according to more recent measurements using the rotating disk (The concept of the rotating disk integral diffusivity will be discussed below). Table 1.4 lists these values. Also given are $\mu D/T$ for oxygen in NaOH as used by Lin c.s., and according to recent measurements by Davis a.o.[52] in KOH. The latter value is no less than 25% lower than that used by Lin c.s. Since, according to (6) the mass transfer coefficient

$$k = \text{constant} \times D^{2/3} \quad ,$$

a discrepancy of approximately 31% in the diffusivities would be necessary to cause a deviation of 19% in the constant, assuming all other properties unchanged. Consequently, the discrepancy between the results of Lin c.s. and equation (3) cannot be attributed entirely to the use of incorrect diffusivities.

The theoretical relation (6) was tested also by Ross and Wragg[36,63] in annuli of the same radial ratio 0.5 as used by Lin c.s., and a few other ratios. They used the copper deposition reaction in acidified solution, the solutions being 0.01 or 0.05 M in $CuSO_4$. The expression originally presented to correlate their data fell 10% below the theoretical one based on (6). In a later review the data were re-correlated using rotating disk integral diffusivities measured by Arvia a.o., instead of the older diffusivity data of Cole and Gordon from diaphragm cell measurements. The latter had been expressed by Fenech in the form of a $\mu D/T$ correlation with weak dependence on $CuSO_4$ and H_2SO_4 concentration. The value of $\mu D/T$ found by Arvia a.o. for solutions dilute in $CuSO_4$ (and not containing glycerol)

Table 1.4. Values of μD/T for three reactant species.

reactant	$K_3Fe(CN)_6$ equimolar				$K_4Fe(CN)_6$ equimolar				method
+ excess	KOH	NaOH	KCl	KNO_3	KOH	NaOH	KCl	KNO_3	
Lin[2]	2.67	2.67	2.67	2.67	2.31	2.31	2.31	2.31	LM
Eisenberg[97]		2.50				2.15			CC
Arvia[51]	2.78	2.52	2.00		2.52	2.09	1.75		RDE
Gordon[47]	2.34 + 0.014I				1.87 + 0.034I				RDE
Van Shaw[22]		2.30*							LFA
Rotte[53]		2.27*							DS
Sih[173]				1.49*					RDE
Smyrl[174]								1.81	RDE

reactant	O_2		
in	0.015 M KOH	2M KOH	
Lin[2]	7.37		ICT
Davis[52]	5.40	4.36	RDE,CC
Gubbins[120]	5.46	5.60	POL

*based on measurements with one composition only

CC capillary cell

DS diffusion to a sphere

ICT International Critical Tables

LFA Laminar flow annular cell (Lévêque relation)

LM Limiting mobility

POL Polarography

RDE Rotating disk electrode

was 20% lower. Re-correlation on this basis yielded results very close to the theoretical expression.[63]

These two tests of mass-transfer theory by means of the limiting current method point to the importance of correct diffusivity data to be used in correlating the results. From an analysis of the mass-transfer process, which will be discussed in Chapter 2, it can be shown that diaphragm cell measurements do not necessarily provide the best effective diffusivity values to be used in limiting current calculations. A theoreticaly correct diffusivity to be used in multicomponent solutions cannot

be defined or constructed from binary diffusivities. The only valid statement that can be made is that, in the limit of infinite dilution, this diffusivity must be identical with the Nernst-Einstein diffusivity calculated from the limiting ionic mobility:

$$D_i = R_o T u_i = \frac{R_o T \lambda_i}{|z| F^2} \qquad (1.9)$$

Early experimenters were therefore forced to use either diaphragm cell data, scarce for multicomponent systems, or limiting diffusivities, which were known to be too high. In the face of this dilemma later investigators increasingly resorted to the use of effective, integral, diffusivities. Capillary cell diffusivities are attractive because of the convenient method of measurement but from a viewpoint of diffusional similarity the rotating disk integral diffusivity is more appropriate for work in convective mass transfer.

The use of rotating disk diffusivities means, in effect, that a mass transfer correlation for a well defined convection profile, once its

validity established by theory or independent experiment,* can be inverted to calculate effective diffusivities from (and for) limiting current measurements in the same regime and the same electrolytic solution. This stratagem could, in principle, be applied quite generally but it has, so far, been restricted to rotating disk mass transfer. In Chapter 2 the concept and applicability of these diffusivities will be discussed, and in Chapter 3 such diffusivities are calculated for the Cu^{2+} ion in acidified cupric sulfate solutions.

Diaphragm cell data have been used all along because they were the only ones available, e.g., the effectiveness of the limiting current method for mass transfer measurement was demonstrated quite early by the results of Tobias and co-workers in free convection at vertical electrodes (number 4 in Table 1.3). Excellent agreement was obtained with the theoretically predicted correlation. These experiments were carried out with the copper deposition reaction, which provides a large density difference at high concentrations. The diffusity data used were diaphragm cell data of Cole and Gordon. These data, correlated by Fenech,[11] were also used in later work on horizontal electrodes. The important question whether the Cole and Gordon data were adequate for the work in question, provided a key motivation for the study of rotating disk integral diffusivities in the $CuSO_4$-H_2SO_4 system, to be reported in chapter 3.

---

*In this connection it should be noted that the most careful studies[88,59] undertaken to confirm the rotating disk correlation (1a and b, Table 1.3), used the iodine reduction reaction with very small reactant concentrations, and employed diaphragm cell diffusivities of KI_3 in KI.

Later measurements by Fouad and Gouda,[31] who used the ferri-/ferrocyanide redox reaction, yielded a much lower coefficient in the free convection correlation 4 of Table 1.3. However, as theoretical calculations of the migration effect in free convection[113] show, the small density difference driving the convection in the case of the redox reaction, in combination with the presence of highly mobile OH^- ions, tends to destabilize the velocity profile. It is not unlikely that this effect, and the uncertainty about the interfacial composition, are responsible for the discrepancy between the result obtained with the copper deposition system and that with the redox system.

The application to free convective mass transfer is a particularly severe test of the limiting current method because the driving density difference, which enters into the correlation:

$$Nu = C(GrSc)^{1/4}$$

by way of the Grashof number:

$$Gr = \Delta\rho g L^3/\nu^2\rho \quad ,$$

is influenced by the accumulation or depletion of supporting electrolyte at the electrode.

Thus there is an interaction not only of diffusion and convection, expressed in the coupling of the equation of motion and the equation of convective diffusion, but also of electromigration and convective diffusion. This is true for well supported electrolytes, and a fortiori for solutions concentrated in $CuSO_4$ as used frequently in free convection studies. The situation has been analyzed in detail elsewhere.[113]

In free convective mass transfer at electrodes, as well as in forced convection, the diffusion layer extends only over a very small part of the hydrodynamic boundary layer. Whereas in laminar forced convection the ratio δ_d/δ_h was on the order of $Sc^{-1/3}$, it is in laminar free convection:

$$\delta_d/\delta_h \sim Sc^{-1/4}$$

There is an important qualitative difference, too, in that there is an inner part of the boundary layer, where the velocity increases to a maximum determined by a balance of viscous and buoyancy forces. The diffusion layer thickness, in fluids of high Sc, is of the same order of magnitude as this inner part of the boundary layer. In the outer part of the boundary layer, where the velocity decays, the buoyancy force is unimportant.

Again different as far as concerns the velocity profile in the region of varying concentration, is mass transfer at a moving continuous electrode, exemplified by correlation 5 of Table 1.3. Next to the uniformly moving continuous flat plate, the flow generated by a moving, continuous (e.g., extruded) cylinder is the simplest of a class of laminar boundary layer flows first investigated by Sakiadis.[129] In high Sc number liquids the diffusion layer is contained in a region near the moving electrode, where the liquid velocity is practically equal to that of the cylinder. The mass transfer rate should follow then a penetration type correlation, involving the Péclet number (vL/D, where v is the electrode velocity; L the transfer length):

$$Nu = (2/\sqrt{\pi})Pe^{1/2} \qquad (1.10)$$

Experiments where the electrode is circulated into and out of the solution are difficult to realize without electrolyte and current leaks. Rotte,[74] using a nickel wire circulated through ferri-/ferrocyanide solution, found only approximate agreement with equation 10; mass transfer rates were mostly too low and showed considerable scatter.

1.6. Laminar flow with complications*

It is remarkable that the well-known boundary layer flow along a flat plate has not been used in electrochemical studies. The expected equation:

$$Nu_L = 0.677\ Re_L^{1/2} Sc^{1/3} \quad (Re_L < 10^5) \qquad (1.11)$$

has been used by Wranglen and Nilsson[16] to correlate their results obtained in a rectangular channel. The hydrodynamic entrance length was not enough to assure a fully developed parallel flow, so that they had recourse to the flat plate correlation extended by a relaxation assumption (as in 1b of Table 1.3):

$$Nu_x = Nu_{x,plate}\left(1 - \frac{x_i^{3/4}}{x_o^{3/4}}\right)^{-1/3} \qquad (1.12)$$

Their results, however, were still 24% too high compared with this correlation. The velocity profile must have been steeper than would correspond to flat plate theory. This was ascribed to the merging of the boundary layers.

---

*Numbers 6 through 20 of Table 1.3

Table 1.3. (continued from p. 15)

	System	Correlation	Range	Parameters	Electrolyte	Authors
6	Rotating and stationary disk in restricted housing	no correlation $i_{stat}<i_{rot}$	$30<\omega<3000$ r_o=6cm h=0.19-2cm	h=distance disks r_o=radius	Cu^{2+}	Okada, et al.[10]
7	Developing flow in rectangular channel ($L_e/d<0.01Re$)	no general correlation $k\sim\nu^{1/2}$	$825<Re<3000$ d/L=0.343 d/h=1.14	L_e=entrance length d=eq.diameter L=transfer length h=height	$Fe(CN)_6^{3-}$	Wranglen,Nilsson[16]
8a	Developing flow in annular channel ($L_e/d<0.01Re$)	*$Nu=3.647Re_L^{1/2}Sc^{1/3}$		L=transfer length	$Fe(CN)_6^{3-}$	Bazan[34]
b		*$Nu=0.525Re_d^{1/2}Sc^{1/3}(L/d)^{3/4}$		d=eq.diameter	Cu^{2+}	Bazan[35]
9	Developed flow over isolated strips	$Nu=1.43(ReSc\ d/L)^{1/3}$ $Re=vd/\nu$	d/L=8.1 or 9.2 L=0.15cm $4x10^5<ReSc\ d/L<1.6x10^7$	d=eq.diameter L=transfer length	Cu^{2+}	Palade de Iribarne, et al.[78]
10	Falling liquid film	$Nu=1.21(ReSc\ d/L)^{1/3}$	$Re=\Gamma/\mu=g\delta^3/3\nu$ $Nu=k\delta/D$ $70<Re<700$ $1400<Sc<18500$	δ=film thickness Γ=mass flow rate	$Fe(CN)_6^{3-}$	Iribarne,Gosman,et al.[56]
11a	Transverse flow around cylinders	**(a)$Nu=1.08Re^{0.44}Sc^{1/3}$ $d/d_{tube}=0.2$ **(b)$Nu=1.20Re^{0.42}Sc^{1/3}$ $d/d_{tube}=0.1$ $Re=vd/\nu$	$160<Re<1000$	d=diameter cylinder	$Fe(CN)_6^{3-}$	Grassman,Ibl,et al.[13]

*See, however, p. 27 of text. Eq. 1-12 text gives the expected correlation.

**Results of 11b appear to be more generally applicable.

(continued on p. 31)

Bazan and Arvia[34,35] also used equation (11) to correlate results obtained in internal flows, this time in annuli with insufficient hydrodynamic entrance provisions. Some of their data fitted the form of (11) with only a slightly smaller coefficient.

There appears to be no reason why equation (11) could not be tested in a flow channel of sufficient height provided with a suitable flow-straightening section. The results should be relevant to many corrosion processes occurring in maritime structures.

The Lévêque mass transfer model has also been tested for flow of a liquid film under gravity (10 in Table 1.3), where it should hold for Reynolds numbers in the laminar range in spite of the presence of surface waves on the film. The latter caused small local oscillations of the mass transfer rates, on the order of 2% in the laminar range but higher in the turbulent range which was also investigated (see below). In these measurements Iribarne c.s.[56] found rates slightly below those predicted by the Lévêque relation, but the difference is not significant.

Of considerable interest is the use of small isolated electrodes, in the form of strips or disks embedded in the wall, to measure <u>local mass transfer rates, or rate fluctuations</u>. In fully developed channel or pipe flow, the mass transfer to such electrodes according to the Lévêque model is given by:

$$k_{avg} \doteq 0.8075(D^2S/L)^{1/3} \quad , \qquad (1.13)$$

where S is the velocity gradient at the electrode and L its length. Equation 6, 7 and 8 are specific forms of this general relation.

Iribarne a.o.[78] measured k at an array of electrodes each 1.5 mm

long in the flow direction and 1 cm wide, spaced 5 mm apart along the wall of a rectangular channel. The actual rates found were considerably below those predicted by equation 7, even if allowance was made for the rectangular shape of the channel cross-section. Considerable scatter characterized the data. Probably the electrode spacing was not large enough to assure decay of the concentration profile in between electrodes.

Interestingly, the use of such extremely short sections may complicate the Lévêque mass transfer model which neglects longitudinal diffusion. At the leading edge of electrodes this assumption is not correct, and the flux is actually increased, over a distance of the order of $d_e/\sqrt{ReSc}$. Newman[130] treated this problem for the case of pipe flow and obtained for the local mass transfer rate, in the limit of very small transfer lengths:

$$Nu/Nu_{Lévêque} = 0.5519\ Pe^{-1/12}\left(\frac{d}{x}\right)^{1/6} \qquad (1.14)$$

For a Pe number of 10^4, a typical lower limit in laminar flows, and a channel diameter of 2 cm, the region of axial diffusion is 0.2 mm and the average rate in this region is roughly 10% larger than according to (13).

The influence of axial diffusion will not normally be felt when larger Pe numbers are involved. The use of strip or spot electrodes has been developed extensively by Hanratty and co-workers, who used these in particular to record mass-transfer fluctuations in turbulent flows. They used disks of diameters 0.38 to 1.63 mm (effectively equivalent to rectangles of L equal 0.82 times the disk diameter) and rectangular shapes 0.51-1.57 mm wide, and 0.076 mm to 0.53 mm long in the flow direction.

Since they were interested principally in the intensity of the mass transfer fluctuations, the coefficient in (6) is of less importance.

From the mass transfer intensity one can obtain information about the turbulent velocity intensity near the wall. In turbulent flow the diffusion layer is an order of magnitude smaller than the viscous sub-layer, at least for electrolytic solutiosn. Therefore, the velocity fluctuations as well as the average velocity transverse to the wall are negligible compared to the longitudinal quantities, and the Lévêque model applies again, but with a time-dependence. For small frequencies, f, Hanratty and Reiss[19,20] deduced a simple relationship between fluctuating mass transfer and velocity gradient, in terms of the dimensionless frequency:

$$\tilde{n} = \frac{2\ fL^{2/3}}{D^{1/3}S^{2/3}} \quad , \tag{1.15}$$

by means of which the velocity intensity can be calculated from the mass transfer intensity and the spectral distribution function of mass transfer fluctuations. By thus measuring and correlating mass transfer fluctuations at strip electrodes in longitudinal and circumferential arrays, Hanratty and co-workers[19,20,22,27,49] obtained information about the structure of turbulent flow very close to the wall, where hot-wire anemometer techniques become unreliable. A concise review of this work has been given by Hanratty.[50]

When electrically insulated strip or spot electrodes are <u>embedded in a larger electrode</u>, and the turbulent flow is fully developed, the steady mass transfer rate gives information about the eddy diffusivity in the viscous sub-layer very close to the electrode (see section 6, below).

The fluctuating rate does not give information about velocity variations and is markedly affected by the size of the electrode. The longitudinal, circumferential and time scale of the mass transfer fluctuations lead Hanratty[50] to postulate a surface renewal model with fixed time intervals based on the median-energy frequency.

The basic Lévêque relation (13) was also used by Hanratty and co-workers[89,67] to study surface velocity gradients in laminar and separated flow around a cylinder, in the ranges $60 < Re < 360$ (where vortex shedding first occurs) and $5000 < Re < 100{,}000$ (region of constant drag). Local velocity gradients were measured by embedding strip electrodes in an inert cylinder surface and measuring the time-averaged current. Local mass-transfer rates were also measured, with the entire cylinder surface as cathode and insulated disks as measuring cathodes. The recorded rate-distribution over the circumference was in good agreement with the shear-stress distribution calculated from the measurements on the inert cylinder. Only at very low Reynolds numbers did free convection interfere with the velocity field, in particular at the forward and rear stagnation points. Also, velocity gradients at the rear and near the separation point are small, so that (11) becomes inaccurate.

The separation point was determined with an accuracy of within 1° by the use of twin strip electrodes of length 125μ, separated by 50-70μ insulation. The electrode giving a diminished signal when the other one is activated, is in the wake of the other. With a proper choice of electrode configuration, this procedure can be employed to measure quantitatively the direction of surface velocity gradients in three-dimensional boundary layers.[64] The extreme care with which embedded electrodes for such

Table 1.3. (continued from p. 26)

	System	Correlation	Range	Parameters	Electrolyte	Authors
11b		$Nu=0.38Sc^{-0.2}$ $(+0.56Re^{0.5}+0.001Re)Sc^{0.33}$ $d/d_{tube}<0.05$ $Re=vd/\nu$	$S<Re<100$ $1300<Sc<2000$	d=diameter cylinder	$Fe(CN)_6^{3-}$	Vogtländer,Bakker[25]
12	Flow through a gauze	(a)$Nu=0.64Sc^{1/5}$ $+0.52Re^{1/2}Sc^{1/3}$ open area 66% (b)$Nu=1.03Sc^{1/5}+0.61Re^{1/2}Sc^{1/3}$ open area 56% $Re=vd/\nu$	$1<Re<50$ $1300<Sc<2000$	d=diameter gauze wire v=free velocity	$Fe(CN)_6^{3-}$	Vogtländer,Bakker[25]
13a	Free convection around a horizontal cylinder	$Nu=0.53(GrSc)^{1/4}$ $Nu=kd/D$ $Gr=g\Delta\rho d^3/\nu^2\rho$	$1.2x10^7<GrSc<10^9$ transition at $GrSc=3x10^8$	d=diameter cylinder	Cu^{2+}	Schütz[24]
13b		$Nu=0.23(GrSc)^{0.3}$	$2.3x10^6<GrSc<10^9$		$Fe(CN)_6^{3-}$	Weder[54]
14	Free convection around a sphere	$Nu=2+0.59(GrSc)^{1/4}$ Nu,Gr see 13	$2.3x10^8<GrSc<1.5x10^{10}$	d=diameter sphere	Cu^{2+}	Schütz[24]
15	Free convection at a vertical gauze	$Nu=0.45(GrSc)^{1/4}$ Nu,Gr see 13	$2x10^5<GrSc<5x10^{10}$	d=diameter gauze wire	$Fe(CN)_6^{3-}$	Wragg[61]
16	Free convection at a vertical wire	$Nu=f(Y_L)$;see Fig.4 $Y_L=L/R(Gr_LSc)^{-1/4}$	$0.11<Y_L<6.8$ $2x10^7<GrSc<6x10^{12}$	L=length(height) R=radius	$Fe(CN)_6^{3-}$	Ravoo, et al.[77]
17	Combined thermal and diffusional free convection at a vertical plate	$Nu=0.636(Gr^*Sc)^{1/4}$ Gr^*see eq.(1.18) text $Nu=kL/D$ for opposing and for cooperating body forces	$4x10^7<Gr^*Sc<2x10^8$ $Gr=g\alpha\Delta CL^3/\nu^2=7000$ $Sc=2000$ $\Delta T=0-13°C$	L=height	Cu^{2+}	Marchiano,Arvia[66]

(continued on p. 38)

hydrodynamic measurements have to be prepared, is demonstrated in a paper by Son and Hanratty.[67]

Altogether, these investigations are a remarkable example of the versatility of the electrochemical mass transfer model. Implicitly the method is considered reliable enough that generalized correlations, e.g., (13), can be used in the reverse manner, to measure convection profiles at a reacting surface.

In their work on cylinders, Hanratty c.s. did not measure over-all mass transfer rates, which are important from a chemical engineering viewpoint. For cylinders in transverse flow this had been done before, by Grassmann, Ibl and Trueb,[13] and by Vogtländer and Bakker.[25] (The former also were the first to report measurements of local rates, by means of a strip of 0.45 mm length embedded in the cylindrical cathode. They reported a minimum at the forward stagnation point, not confirmed by Son and Hanratty measurements and perhaps caused by free convection). The results of Grassmann c.s. are somewhat higher than those of Vogtländer and Bakker, who measured over a lower range of Re numbers and fitted their results to an empirical heat transfer correlation. This apparently accounted well for free convection contributions, by the presence of a term in Sc only. Also, the wires used by Vogtländer and Bakker were very thin compared to the flow tube diameter, while this was not the case in the others' measurements. The expressions 12 (Table 1.3) for gauzes are 10 to 20% higher than those for a single wire, if based on the approach velocity.

Free convection flow around horizontal cylinders is also laminar in nature, for moderate values of GrSc, and follows a relation of the same

type as that for vertical plate electrodes:

$$Nu \sim (GrSc)^{1/4} \tag{1.16}$$

Schütz[24] observed local transition above GrSc = $3x10^8$, by the use of an insulated strip electrode. The correlation obtained by Weder[54] has a somewhat higher exponent, interpreted as an indication of local transition at the highest GrSc numbers dealt with.

Wragg[61] investigated free convection mass transfer to vertical gauzes and found likewise good agreement with an expression similar to (16).

For free convection at a sphere Schütz obtained the correlation:

$$Nu = 2 + 0.59(GrSc)^{1/4} \quad , \tag{1.17}$$

which takes the effect of pure diffusion into account by means of the constant. The flow here is not laminar, according to his measurements with local spot electrodes, but already in transition to turbulence for the GrSc range in question.

Free convection at vertical cylinders differs from that along vertical plates because of the influence of curvature. The effect is important only if the diffusion layer thickness is no longer small compared to the diameter. Since the diffusion layer thickness increases with x, this can be expressed as

$$x/R \sim O(Gr_x Sc)^{1/4}$$

where x is the vertical coordinate and R the cylinder radius. Ravoo a.o.[77]

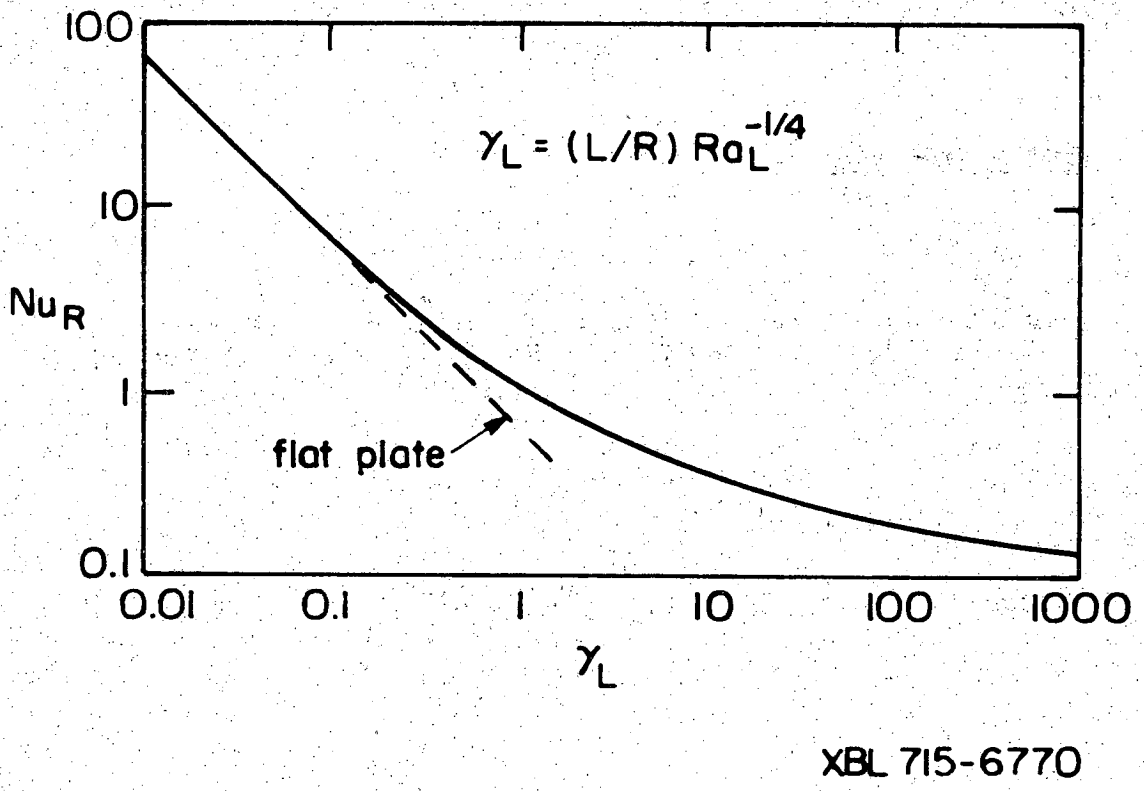

Figure 1.2. Relation between Nusselt number and free convective curvature parameter for a vertical cylinder (after Ravoo a.o.[77]).

developed an approximate solution for this case and, using wires of diameter 0.1 to 2.64 mm, length 1 to 374 cm, found fairly good agreement with the theory. (Fig. 1.2).

Another case of free convection with some complications, but amenable to solution, is that due to combined temperature and concentration differences. Marchiano and Arvía[66] tested a theoretical solution for mass transfer in such a laminar flow along a vertical plate, which employs a combined Grashof number as follows:

$$Gr = \{(\alpha\Delta c)^{3/4} + (\zeta\Delta T)^{3/4}(\frac{Sc}{Pr})^{1/4}\}^{4/3} \frac{gL^3}{\nu^2} \quad , \qquad (1.18)$$

where α is the concentration densification coefficient and ζ that due to temperature. They found fair agreement except for an unstable flow region if the temperature densification was of opposite sign but not large enough to cancel the concentration effect. For stronger cooling of the cathode the flow became stable again and mass transfer rates satisfied the theory.

Earlier, de Leeuw den Bouter a.o.[65] had already experimented with such combined free convective transfer, assuming complete analogy if the Grashof number employed is:

$$Gr = \{\alpha\Delta c + \zeta\Delta T(\frac{Sc}{Pr})^{1/2}\} \frac{gL^3}{\nu^2} \qquad (1.19a)$$

Their results for cooperating body forces come very close to a confirmation of this complete analogy, since the expressions (18) of Table 1.3 are also valid for the heat transfer rate which was measured simultaneously:

$$Nu_h = 0.64\,(Gr_h^* Pr)^{0.252} \tag{1.20}$$

where $$Gr_h^* = \{\zeta\Delta T + \alpha\Delta c\,(\frac{Pr}{Sc})^{1/2}\}\,\frac{gL^3}{\nu^2} \tag{1.19b}$$

The expression (18) appears to have a weaker theoretical basis, too, since it approximates flow profiles by a single quadratic function of the distance.

A more complicated case of combined thermal and diffusional free convection is that around a horizontal cylinder. This has been investigated by Weder,[54] who likewise used a combined Grashof number of type (19) but corrected for the higher exponent found in isothermal mass transfer (13b of Table 1.3). The correlation finally obtained is:

$$Nu = 0.23\,(Ra^*)^{0.28} \tag{1.21}$$

with $$Ra^* = (GrSc)^{1.07} + 1.49\,(Gr_h Sc)\,(\frac{Sc}{Pr})^{1/2} \tag{1.22}$$

Weder's experiments were all carried out with opposing body forces, and large current oscillations were found as long as the (negative) thermal densification was smaller than the diffusional densification. (Note that the Grashof numbers in (22) are based on absolute magnitudes). Local mass transfer rates oscillated by 50%, and total currents by 4%. When the thermal densification dominates, the stagnation point moves to the other side of the cylinder and the boundary layer, which separated in purely diffusional free convection, remains attached.

Free convection in restricted spaces has been investigated by Böhm, Ibl and Frei,[48] and earlier by Schmidt.[90] The latter author restricted the

distance between parallel plate electrodes in halogene redox reactions (without supporting electrolyte) to such small values that convection could hardly develop. Similar experiments, also using closed cells but with larger electrode distance were reported by O'Brien and Mukherjee.[30] Böhm c.s. did restrict the liquid movement by varying the distance between vertical cathode and vertical diaphragm from 6 to 0.15 mm, but did not enclose the electrolyte between these. Various experiments with impeded inflow and outflow were also reported. A critical distance between vertical electrode and diaphragm exists, below which the current is less than for a single vertical plate with distant counter-electrode. This critical distance is given by:

$$a_{cr} = 5.48L(GrSc)^{-0.3} \qquad (1.24)$$

Conspicuous is the high exponent on the GrSc number in the mass transfer correlation (20) of Table 1.3. Since the current is almost independent of D, this must mean that the reacting ion is depleted at the downstream end of the narrow slit between cathode and diaphragm so that the total current is largely determined by the convective transport of reactant into the slit, which depends on the density difference but not on diffusivity.

Investigations like the one just discussed are very important from an engineering point of view. Mass transfer processes rarely take place in the simple configurations leading to the classical correlations for forced and free convection. By examining the influence of flow obstructions and secondary flows, one can gain insight to what extent practical mass transfer situations deviate from the theory. On the other hand, the

Table 1.3. (continued from p. 31)

	System	Correlation	Range	Parameters	Electrolyte	Authors
18		(a)$Nu=0.79(Gr^{*}Sc)^{0.243}$ for opposing and for cooperating forces (b)$Nu=0.64(Gr^{*}Sc)^{0.252}$ for cooperating body forces only Gr^{*} see eq.(1.19) text	$6x10^{9}<Gr^{*}Sc<2\ 10^{11}$ $2x10^{6}<Gr^{*}Pr<5x10^{7}$	L=height	Cu^{2+}	de Leeuw den Bouter, et al.[65]
19	Combined thermal and diffusional free convection at a horizontal cylinder	$Nu=0.23(Ra^{*})^{0.28}$ Ra^{*} see eq(21)text opposing body forces	$2.3x10^{6}<GrSc<1.5x10^{10}$ $5.5x10^{3}<Gr_{h}Pr<8.7x7x10^{6}$ $2x10^{7}<Ra^{*}<4x10^{10}$	d=diameter cylinder	$Fe(CN)_6^{3-}$	Weder[54]
20	Free convection at vertical cathode in a restricted space	$Nu_{L}=0.0225(a/L)^{2}(Gr_{L}Sc)^{0.85}$	$2x10^{6}<GrSc<2x10^{8}$ $0.005<a/L<5.48(GrSc)^{-0.3}$	a=distance electrode-diaphragm L=height electrode	Cu^{2+} $Fe(CN)_6^{3-}$	Böhm, et al.[48]
21	Mass transfer entrance regime in channels with fully turbulent flow	$Nu=0.276Re^{0.58}(Sc\ \frac{L}{d})^{1/3}$ $Nu=kd/D$	$5000<Re<75,000$ $0.018<L/d<4.31$ $Sc=2400$	d=diameter pipe $L/d<5000Re^{-7/8}$	$Fe(CN)_6^{3-}$ Cu^{2+}	Shaw, et al.[22] Schütz[38]
22	Mass transfer entrance regime in turbulent falling film	$Nu=1.080(ReSc\ \delta/L)^{1/3}$ $Re=g\delta^{3}/3\delta$	$Re>10^{3}$ $L/\delta<900\ \nu/g\delta^{3}$	δ=film thickness	$Fe(CN)_6^{3-}$	Iribarne, et al.[56]

(continued on p. 39)

Table 1.3. (continued from p. 38)

	System	Correlation	Range	Parameters	Electrolyte	Authors
23	Mass transfer fully developed in turbulent flow (annulus)	$Nu=0.023Re^{0.8}Sc^{1/3}$	$2100<Re<30,000$ $300<Sc<3000$	$d=2(r_o-r_i)$	O_2 $Fe(CN)_6^{3-}$ quinone $Fe(CN)_6^{4-}$ Cd^{2+}	Lin, et al.[2] Lin, et al.[4]
24a	" (pipe)	$k_{+\infty}=0.115Sc^{-3/4}$ (Deissler)	$5000<Re<50,000$ $Sc=2170$		Cu^{2+}	Schütz[38]
24b	" (channel)	$Nu=(f/2)ReSc^{1/3}$ (Chilton-Colburn)	$7000<Re<60,000$ $1700<Sc<30,000$	d=eq.diameter	$Fe(CN)_6^{3-}$	Hubbard, Lightfoot[42]
25	" (pipe)	$k_{+\infty}=3.52x10^{-4}$ $k_{+\infty}$ see eq.1.25,1.26 text	$8000<Re<50,000$ $Sc=2400$		$Fe(CN)_6^{3-}$	Shaw, Hanratty[27] Son, Hanratty[91]
26	" (falling film)	$k_{+\infty}=0.115Sc^{-3/4}$ (Spalding-Van Driest) $Re=g\delta^3/3\nu$	$Re>1000$ $1000<L/\delta\sqrt{g\delta^3/\nu}<5000$ $1400<Sc<18,500$	δ=film thick thickness	$Fe(CN)_6^{3-}$	Iribarne[S6]
27a	Fully developed turbulent flow at a rotating disk	$Nu=0.00726Re^{0.4}Sc^{1/3}$ $Re=\omega r^2/\nu$	$2.7x10^5<Re<1.5x10^6$ $345<Sc<6450$	ω=rotation rate r=radius disk	I_3^-	Daguenet[59]
b	"	$Nu=0.0117Re^{0.896}Sc^{0.249}$	$8.9x10^5<Re<1.18x10^7$ $34<Sc<1400$		O_2	Ellison, Cornet[81]
28	Fully developed turbulent flow at a rotating ring	$Nu=Nu_{disk,r_o}$ $(1-(r_i/r_o)^{5/2})^{4/5}$	$2.7x10^5<Re<1.5x10^6$ $345<Sc<6450$	r_i=inner radius r_o=outer radius	I_3^-	Daguenet[59]

(continued on p. 46)

blind labor involved in copying and investigating one or another industrial configuration is avoided.

Rather surprisingly, research on forced flow in restricted geometries is also scarce. An example is work by Okada a.o.[10] on a rotating disk flow where the electrolyte is completely enclosed between the rotating disk and the counter-electrode. Mass transfer was measured at the rotating as well as at the stationary disk. The distance between the disks was varied. At low rotation rates the flux at the rotating disk was higher than predicted by the Levich equation (1 of Table 1.3). The flux at the stationary disk followed a relation of the Levich type but with a constant roughly 2/3 that of the rotating disk equation.

Flow patterns in agitated vessels can be profitably studied starting with disks and cylinders rotating freely in restricted cells. Investigations of this kind will be reviewed below, after a survey of the better defined turbulent flows.

1.7. Turbulent flows and mixed convection*

Forced convective turbulent mass transfer relations are of interest for two reasons: their practical importance since turbulence efficiently increases transfer rates; and the insight one can gain from them into the mechanism of turbulence very close to the wall, where the usual hydrodynamic probes (hot wire anemometer) disturb the phenomenon to be measured.

A variety of turbulent mass-transfer relationships are listed in Table 1.3. The most important ones are those for channels and tubes, but several other ones have been investigated for their hydrodynamic interest.

Turbulent flow theory is not able to predict mass transfer rates quantitatively, except in the region of developing mass transfer where a

* Numbers 21 through 37 in Table 1.3

Lévêque type correlation between rate and friction coefficient can be established:

$$\frac{k}{\bar{v}} = 0.8075\left(\frac{D^2\lambda}{2\nu L}\right)^{1/3} \quad , \quad \text{or} \tag{1.25}$$

$$k/v^* = k_+ = 0.8075\ L_+^{-1/3}Sc^{-2/3} \quad , \tag{1.26}$$

where subscript + denotes quantities made nondimensional with respect to the wall shear stress τ_o by the "friction velocity" $v^* = (\tau_o/\rho)^{1/2} = \bar{v}(f/2)^{1/2}$.

By substituting the well-known Blasius relation for the friction factors, equation 21 of Table 1.3 is obtained, which van Shaw, Hanratty and Reiss[22] tested by limiting current measurements on short pipe sections. They found Re and (L/d) dependence according to the theory but rates on the average 7% lower than expected. In a later publication[50] this was traced to incorrect flow rate calibration. Schütz[38] also found good agreement with this mass transfer entrance equation for small values of L/d. The condition for validity can be expressed as $L^+ < 10^3$.

Iribarne, Gosman and Spalding[56] showed that the Lévêque relation is also valid for turbulent flows in films, with the same entrance condition and $Re > 10^3$.

When the concentration profile is fully developed the mass transfer rate becomes independent of the transfer length. Spalding[131] has given a theory of turbulent convective transfer based on the hypothesis that profiles of velocity, total (molecular + eddy) viscosity and total diffusivity possess a universal character. In that case the transfer

rate k_+ (see 26) can be expressed as a single, universal function of the transfer length L_+ and fluid properties, expressed in a molecular and a turbulent Schmidt number:

$$k_+ = k_+(L_+, Sc, Sc_t) \tag{1.27}$$

Equation (26) is the asymptotic form of (27) for small L_+. The specific form of (27) for larger L_+ can only be derived with the help of a particular hypothesis about the distribution of the eddy diffusivity (or viscosity) in the turbulent boundary-layer, in particular near the wall, in the inner part of the viscous sub-layer. Since the mass-transfer rate attains a constant value for very large L_+ ($>10^4$), the dependence of this asymptotic k_+ on the Schmidt number has been the objective of numerous experimental investigations, whereby the limiting current method had decisive advantages over earlier dissolution methods.

An equally important objective of these turbulent mass transfer measurements was the establishment of the exact dependence of k on the Reynolds number. According to the well-known empirical Chilton-Colburn equation for turbulent transfer one should have:

$$Nu = \frac{\lambda}{2} ReSc^{1/3} \tag{1.28}$$

which corresponds to an additional dependence of k_+ on the Reynolds number. Semi-empirical modifications of the Chilton-Colburn equation have been proposed,[132] which also imply this additional dependence. Table 1.5 lists some expressions valid in the limit of large L^+ and high Sc.

Son[90] has reviewed the experimental evidence from electrochemical and other model experiments. He concludes that the eddy diffusivity varies with

Table 1.5. Expressions for fully developed turbulent mass transfer.

Author	Expression	Basis
(1) Chilton-Colburn	$Nu = \lambda/2 ReSc^{1/3}$	empirical
	$k_+ = \sqrt{\lambda}/2\ Sc^{-23}$	
(2) Deissler[133]	$Nu = 0.0789\sqrt{\lambda}\ ReSc^{1/4}$	$D_t \sim y_+^4$
	$k_+ = 0.112\ Sc^{-3/4}$	
(3) Lin, Moulton, and Putnam[4]	$Nu = 0.057\sqrt{\lambda}\ ReSc^{1/3}$	$D_t \sim y_+^3$
	$k_+ = 0.081\ Sc^{-2/3}$	
(4) Vieth, Porter, and Sherwood[132]	$Nu = 4.586(u_{max}/u_{avg})\frac{\lambda}{2} ReSc^{1/3}$	semi-
	$k_+ = 4.586\ u_{max}/u_{avg}\ \frac{\sqrt{\lambda}}{2} Sc^{-2/3}$	empirical
(5) Spalding[131]	$Nu = 0.053\ \lambda\ ReSc^{1/4}$	semi-
	$k_+ = 0.0746\ Sc^{-3/4}$	empirical

the fourth power of the distance from the wall, assuming that the friction factor takes care of the Reynolds number dependence. Hubbard and Lightfoot[42] earlier concluded to a $Sc^{1/3}$ dependence on the basis of measurements in which the Schmidt number was varied over a very large range. These did not exclude a lower Reynolds exponent than 0.88, and re-affirmed the value of the classical Chilton-Colburn equation for practical purposes.

By more refined measurements using strip electrodes at different orientations with respect to the mean flow, Sirkar and Hanratty[69] later showed that the transverse velocity fluctuations play a significant part in the turbulent transport very close to the wall, and that the eddy diffusivity may indeed be dependent on the cube of the distance y_+, leading to a $Sc^{1/3}$ dependence of mass transfer correlations.

The laminar boundary layer on a rotating disk becomes turbulent at Reynolds numbers above 10^5. Mass transfer to disks and rings in turbulent, or almost completely turbulent, flows has been measured by Daguenet[59] and by Ellison and Cornet.[81] The latter found a dependence on $Sc^{1/4}$, in accordance with Deissler's model (Table 1.5) Daguenet,[59] who used a higher Sc range, concluded to agreement with the Lin-Moulton-Putnam model, with a dependence on $Sc^{1/3}$.

Summarizing, it can be said that a conclusive investigation of the turbulent transport process is still extant, and that it will be necessary to synthesize inferences from optical as well as mass transfer measurements. The latter will have to be made at very high Reynolds numbers (>50,000 in channel flow) and at very high Schmidt numbers (>10,000) to yield critical information about the transfer process.

Flow between rotating cylinders has been referred to in the historical introduction (1.3) since it was recognized early that Couette flow can be realized if the inner cylinder rotates more slowly than the outer cylinder, or is stationary. Experimentally this is hard to realize, and so far only work with a rotating inner cylinder has been reported, where Taylor instability occurs at low rotation rates. The other inherent advantage of concentric cylinders is the uniform current distribution, which makes this model extremely attractive for applications.

The over-all results for the turbulent regime are in good agreement with those obtained by dissolving cast metal or salt cylinders.[118,119] Rotating cylinders have also been used to measure the influence of surface roughness on the turbulent mass transfer rate.[121]

Turbulent free convection has early attracted attention in limiting current studies, because the laminar free convection boundary layer becomes turbulent at a certain height, approximately characterized by the Rayleigh number

$$Ra_L = Gr_L Sc \approx 10^{11} \text{ to } 10^{13} \qquad (1.29)$$

Fouad and Ibl[12] have suggested that the transfer rate in free convective turbulent flow is expected to follow a $Ra^{1/3}$ dependence. Fouad and Ibl[12] found a dependence slightly lower, probably due to the partly laminar regime on such plates. Because the exponent is not fixed by theoretical considerations, there is considerable variation in the coefficients of turbulent free convection correlations. (Inaccuracies in the calculation of the density driving force may also be responsible for this, in particular in the ferricyanide reduction reaction).

Table 1.3. (continued from p. 39)

	System	Correlation	Range	Parameters	Electrolyte	Authors
29	Turbulent Couette flow between a rotating and a stationary cylinder	(a)$Nu_{rotor}=0.0791Re^{0.7}Sc^{0.356}$ $Re=\omega d_i^2/\nu$	$10^3<Re<10^5$ $835<Sc<11,490$ $0.093<d_i/d_o<0.83$	d_i=inner diameter (rotor)	$Fe(CN)_6^{3-}$ $Fe(CN)_6^{4-}$	Eisenberg, et al.[6]
		(b)$Nu_{stator}=0.0791Re^{0.7}Sc^{0.356}(d_i/d_o)^{0.7}$ $Re=\omega d_i^2/\nu$	$10^3<Re<5.3x10^4$ $Sc=2450$ $0.22<d_i/d_o<0.68$	d_o=outer diameter (stator)	Cu^{2+}	Arvia,Carrozza[17]
30	Transitional and turbulent Couette flow between rotating cylinders				$Fe(CN)_6^{3-}$	Heitz,Hauptmann[84]
31a	Turbulent free convection at a vertical plate	$Nu=0.31(GrSc)^{0.28}$ $Gr=g\Delta\rho L^3/\nu^2\rho$	$4x10^{13}<GrSc<10^{15}$	L=height plate	Cu^{2+}	Fouad,Ibl[12]
b		$Nu=0.15(GrSc)^{0.29}$	$4.57x10^{11}<GrSc<10^{14}$ $2400<Sc<3700$		$Fe(CN)_6^{3-}$	Fouad,Gouda[31]
32	Transitional and turbulent free convection at a horizontal plate	(a)$Nu=0.64(GrSc)^{1/4}$ (transitional)	$3x10^4<GrSc<2.5x10^7$	L=width plate	Cu^{2+}	Wragg[60]
		(b)$Nu=0.16(GrSc)^{1/3}$ (turbulent) $Nu=kL/D$ $Gr=g\Delta\rho L^3/\nu^2\rho$	$2.5x10^7<GrSc<10^{12}$ $2200<Sc<2300$			

(continued on p. 47)

Table 1.3. (continued from page 46)

	System	Correlation	Range	Parameters	Electrolyte	Authors
32	Turbulent free convection at a horizontal plate	(c) $Nu=0.19(GrSc)^{1/3}$ (d) $Nu=0.122(GrSc^{9/18})^{1/3}d_n$	$10^8<GrSc<1.4\times10^{12}$ $2100<Sc<52,000$ $d_n=1.0$ for plate surrounded by vertical walls; <1.0 for embedded electrodes	L=length plate	Cu^{2+} $Fe(CN)_6^{3-}$	Fenech, Tobias[11] Fenech[11a] Boeffard[46]
		(e) $Nu=0.152(GrSc)^{1/3}$ $Gr=a\Delta\rho L^3/\nu^2\rho$	$6\times10^6<GrSc<5\times10^{12}$ $2000<Sc<40,000$ $1<a/g<420$	a=centrifugal acceleration	Cu^{2+} $Fe(CN)_6^{3-}$ $Fe(CN)_6^{4-}$	Ravoo[79] Ravoo[80]
33	Turbulent free convection at a vertical cylinder with strong curvature	$Nu=0.57(Gr_RSc)^{0.11}$	$2.9<Gr_RSc<400$ $2500<Sc<3800$ $3700<L/R<78,000$	R=radius cylinder	$Fe(CN)_6^{3-}$	Ravoo[77]
34	Free convection at an inclined plate	$Nu=0.3(C\ GrSc)0.28$ C=f(angle of inclination)	$6\times10^{10}<GrSc<7\times10^{13}$ $1750<Sc<3000$	L=height plate	Cu^{2+}	Fouad, Ahmed[75]
35	Free convection at a roughened plate	$Nu=A(GrSc)^{0.32}$ A=f(h/δ)	$2.2\times10^{10}<GrSc<2.5\times10^{13}$ $2400<Sc<3400$	h=height roughness δ=diff. layer thickness	$Fe(CN)_6^{3-}$	Fouad, Zatout[76]
36a	Combined free and forced convection at vertical surface in coaxial annular flow; aiding flow	$Nu=1.96(ReSc\ d_e/L + 0.04(GrSc\ d_e/L)^{0.75})^{1/3}$	$1.3\times10^7<GrSc<d_e/L<1.1\times10^9$ $7\times10^3<ReSc<d_e/L<2.5\times10^5$	L=length r_i=inner radius r_o=outer radius $d_e=2(r_o-r_i)$	Cu^{2+}	Wragg, Ross[93]
b	same; opposing flow	no correlation			Cu^{2+}	Wragg[83]

(continued on page 50)

It is interesting to notice that free convection on a rough surface (number 35 of Table 1.3) follows a higher GrSc dependence than for the same Ra range on a smooth plate. The roughness definitely appears to ease the transition to turbulence.

Fouad and Ahmed[75] investigated free convection at inclined plates, expressing the results in the form of a dependence on $(CGrSc)^{0.28}$ where C = 1 for a vertical plate and equation (34) of Table 1.3 is obtained. The constant C corresponds roughly to cos θ, θ being the angle of inclination from the vertical, as long as the densification is stable, i.e., in the direction of gravity. For unstable densification C increases sharply with θ, and least squares analysis gives a GrSc dependence which appears to approach the exponent 1/3 as the plate becomes horizontal.

Free convection on a horizontal plate has been studied extensively. Fenech and Tobias first established the $(GrSc)^{1/3}$ dependence of this kind of turbulent transport. The rate per unit area is independent of plate dimension, provided edge effects are unimportant. Another condition investigated was the presence of an opposite parallel surface (a diaphragm) which did not influence the mass transfer unless closer than approximately 0.5 cm. An alternative equation for plates embedded in an inert surface was also given, which takes advection into account (eq. 35b of Table 1.3).

At low Rayleigh numbers Wragg[60] found a lesser Ra dependence, more resembling that for laminar free convection. In this range a cellular flow pattern is believed to exist in analogy to thermal and surface-tension driven cellular convection (Bénard cells). In the region where the convection is turbulent the $Ra^{1/3}$ dependence has been confirmed over 7 decades of Ra by Ravoo,[79] who used a centrifuge to vary the body force

at constant composition.

As a general comment on free convection limiting currents it should be remarked that several experimenters[11,48] report difficulties in trying to obtain steady limiting current plateaus of good readability in those solutions where the driving force is small. In extreme cases curves with maxima and minima were obtained, and a limiting current could not be assigned. This aspect of free-convection mass transfer will lead us to investigate mass transfer transients more closely in a later chapter.

Combinations of forced and free convective mass transfer (mixed convection) are amenable to theoretical analysis so long as the free convective flow is in the same direction as the forced flow (aiding flows). This is e.g., the case in free convection with forced flow in vertical channels. Ross and Wragg[93] have experimentally investigated such a situation and found a smooth transition from the forced convective Lévêque correlation to the $(GrSc)^{1/4}$ dependence typical for laminar free convection. In opposing flows of this type a more complex behavior was found,[83] where the mass transfer rate is minimal at a certain critical combination of length, Reynolds number and Grashof number. Very likely at this point the leading edge of the diffusion layer moves from one end of the transfer section to the other. The flow instability becomes apparent in marked current oscillation and poor reproducibility.

Hickman and Tobias[32] have been the only investigators to study combined free and forced convection in horizontal channel flow. They found a remarkably sharp separation of forced-convection dominated, as opposed to free-convection dominated, mass transfer. The critical Grashof number based on the diffusion layer thickness in forced convection, is:

Table 1.3. (continued from p. 47)

	System	Correlation	Range	Parameters	Electrolyte	Author
37	Combined free and forced convection at horizontal plate in channel flow	(a)$Nu=0.85(ReSc\ d/L)^{1/3}$ $Gr_\delta<920$ (b)$Nu=0.19(GrSc)^{1/3}$ $Gr_\delta>920$ Gr_δ see eq.(1.30) text.	75<Re<3000 600<Sc<12,000 0.05<d/L<20	d=eq. diameter L=transfer length	Cu^{2+}	Tobias,Hickman[32]
38a	Flow at a freely rotating cylinder in a baffled cylindrical cell	$Nu_d=1.83Re^{0.58}Sc^{1/3}$ $Re=\omega dh/\nu$		d=diameter cylinder h=distance	Cu^{2+} $Fe(CN)_6^{4-}$	Krishna, Jagannadharaju[40]
b	Flow at ring electrodes in the bottom of same cell	$Nu_d=2.41Re^{0.62}Sc^{1/3}$ $C^{-0.32}$ $Re=\omega dh/\nu$		C=distance rotor-bottom of cell		
39	Flow at a rotating sphere	$Nu=10+0.43Re^{1/2}Sc^{1/3}$ $Re=\omega d^2/\nu$	800<Re<27000 500<Sc<2000 $1.2sec^{-1}<\omega<31sec^{-1}$ d=2.53 cm	ω=rotation rate d=diameter	Cu^{2+} $Fe(CN)_6^{3-}$	Noordsij, Rotte[53]
40	Flow at a sphere in oscillating motion	$Nu=2+0.42(ReSc)^{1/2}$ $Pe=fad/\nu$ $Nu=kd/D$	100<Re<1600 d=2.53cm 500<Sc<2000 $3sec^{-1}<f<35sec^{-1}$ 0.075cm<a<0.157cm	a=amplitude d=diameter f=frequency	Cu^{2+} $Fe(CN)_6^{3-}$	Noordsij,Rotte[53]
41	Flow at a vertical cylinder in horizontal transverse vibration	$Nu_d=0.41Re^{0.62}Sc^{1/3}$ $Nu=kd/D$ $Re=fad/\nu$	$60<Re<10^4$ $1.6sec^{-1}$ f<25sec^{-1} 0.24cm<a<3.7cm 0.177cm<d<1.02cm 800<Sc<2240	a=amplitude d=diameter f=frequency	$Fe(CN)_6^{4-}$	Somasundara, et al.[33]

(continued on p. 51)

Table 1.3. (continued from p. 50)

	System	Correlation	Range	Parameters	Electrolyte	Authors
42a	Flow at a vertical plate in vibration perpendicular to the width	$Nu_W=0.476Re_1^{0.56}Sc^{1/3}(1+W/L)^{0.7}$ $Re_1=faW/\nu$	$165<Re_1<8850$ $145<Re_2<4160$ $1.6sec^{-1}<f<23.3\ sec^{-1}$ $0.13cm<a<2.0cm$ $1cm<W,L<4cm$	W=width L=height T=thickness d=L+WT/(W+T) a=amplitude f=frequency	$Fe(CN)_6^{3-}$	Raju, et al.[71]
42b	Flow at a vertical plate in vibration perpendicular to the thickness	$Nu_d=0.437Re_2^{0.74}Sc^{1/3}(W/T)^{0.5}$ $Re_2=fad/\nu$				
43a	Flow at one wall of a diaphragm cell stirred by magnetic stirrer	$Nu_d=0.050Re_d^{0.79}Sc^{0.38}$ $Re=\omega d^2/\nu$	$200<Re<4000$ $2500<Sc<62,000$ $5.4x10^9<GrSc<1x10^{10}$ $d=2.5cm$ cell volume $125cm^3$	d=length stirrer bar ω=rotation rate	Cu^{2+}	Holmes, et al.[21]
b	Same in free convection	$Nu_r=0.57(Gr_rSc)^{1/4}$	$5.4x10^9<GrSc<1x10^{10}$	r=radius diaphragm (side wall)		
44	Oscillating flow transverse to a horizontal plate	(a)$Nu_d=0.24Re^{0.62}Sc^{1/3}$ $Re=fad/\nu<150$ (b)$Nu_d=0.066Re^{0.87}Sc^{1/3}$ $150<Re<960$	$18<Re<960$ $850<Sc<1100$ $3.3sec^{-1}<f<42sec^{-1}$ $0.05cm<a<0.77cm$	d=diameter f=frequency a=amplitude	$Fe(CN)_6^{3-}$	Raju, et al.[57]
45	Annular cell with tangential inflow	$Nu_d=0.24Re^{0.78}Sc^{1/3}(d_e/L)^{1/2}(A/A_i)^{1/3}$ $Re=Qd_e/\nu A$	$48<Re<500$ $1.3<L/d_e<12$ $18.7<Q<47.5$	r_i=inner radius r_o=outer radius L=length Q=volume flow rate $A=\pi(r_o^2-r_i^2)$ A_i=cross-section flow entrance $d_e=2(r_o-r_i)$	$Fe(CN)_6^{4-}$	Regner, Rousar[86]

(continued on p. 56)

$$Gr_{\delta} = \frac{g\alpha\Delta c d L}{\nu \bar{u}} \gtrless 920 \qquad (1.30)$$

If this number was smaller than 920, mass transfer could be represented by the forced convection correlation, otherwise by the free convection correlation of Fenech and Tobias.[11] They also inferred the existence of cellular vortex flow near the electrode from deposition patterns; the induction length for this deposition pattern agreed with the criterion (30).

In studies such as these it is convenient and, as can be proven experimentally, necessary for the accuracy of limiting current measurements, that the electrode is divided in several insulated sections. A limiting current curve is obtained for each of these. This technique, first introduced by Fenech and Tobias,[11] requires that the potential be kept the same on the various sections as the limiting current is approached. Some complications associated with this condition will be discussed in Chapter 5.

1.8. Restricted cells with agitation*

Under this heading a number of investigations are grouped in which the electrolyte is stirred by movement of the electrode, or where this stirring (or circulation) is accomplished independently. In principle the boundary with the laminar flows discussed earlier is not sharp. Complications arise in the first place because of secondary flows in restricted cells. An example is the enclosed rotating disk mentioned above. Furthermore boundary-layers on the stirring electrodes may become detached. Local turbulence can be generated near electrodes or inert stirrers. Of interest is the mass-transfer to the stirrer, as

*Numbers 38 through 45 in Table 1.3.

well as to selected points of the cell. The first aspect has been investigated more frequently, but with a refined technique the second could give valuable information about convection patterns in stirred tanks. Stirring by gas-evolution is considered separately in the next section.

An example of agitation by a free rotating cylinder is the work of Krishna and Jagannadharaju,[40] who measured mass transfer at a cylindrical rotor, as well as at ring electrodes inserted concentrically in the bottom of the cell. An impeller attached to the free end of the rotor did not change the current. The clearance between rotor and ring-electrodes was varied. They found that mass transfer to the rings was maximal for those rings having the same diameter as the rotor (or impeller).

Flow in stirred vessels was also investigated by Holmes a.o.[21] who simulated the mass transfer in a diaphragm diffusion cell stirred by magnetic stirrer bars. This is a good example of a model study with a direct practical purpose. A minimum stirring speed in such cells is necessary to avoid appreciable errors in the cell constant. The experiment permits this stirring speed to be related to the solution properties.

Mass transfer in a pulsating flow perpendicular to a stationary plate[57] could be correlated by a laminar-type mass transfer expression at low frequencies, and a turbulent one at higher frequencies. The pulsating flow is generated by a vibrating diaphragm, which forms the bottom of a cylindrical cell of 20 cm diameter, with an open upper end. The mass transfer to the horizontal disk electrode is not dependent on distance to the diaphragm, if above 17.5 cm, nor on free liquid height.

Raju, Rao, and co-workers,[33,71] also investigated mass transfer at vibrating electrodes, for low frequencies (higher frequencies would cause cavitation). Mass transfer follows a laminar type correlation for transverse vibration of a vertical cylinder, and for a vertical plate vibrating parallel to the face. The Reynolds number in the case of the plate is based on the width, indicating predominance of form drag. For vibrations perpendicular to the thickness, skin friction predominates and the Reynolds number is preferably based on the equivalent diameter (total surface area divided by transverse perimeter).

Rotte and Noordsij[53] studied a vibrating sphere, i.e., a sphere kept in oscillating motion by means of an attached rod held by a spring against an eccentric wheel. The results showed considerable spread and are approximately represented by a $Pe^{1/2}$ dependence, with a constant term (due to pure diffusion) of correct magnitude. Experiments with the same sphere in rotating motion showed less spread but a higher intercept, possibly due to secondary flow generated by free convection or temperature differences (cell dimension was only 6 times sphere diameter). Local mass transfer measurements on rotating and vibrating spheres should be of interest from a hydrodynamic point of view.

An interesting modification of coaxial flow in annular cells was studied by Regner and Rousar,[86] who created swirling flow by means of a tangential inlet. The mass transfer correlation combines features of the boundary layer correlations (dependence on $L^{-1/2}$) with those of turbulent flow between rotating cylinders (dependence on $Re^{0.78}$), although the Reynolds numbers do not reach the range where concentric flow is turbulent (29 or Table 1.3). Related is the flow in a hydrocyclone investigated by Ravoo.[80]

1.9. Cells with gas-evolution

Electrolytic gas-evolution has been used as a means of generating convection in heat transfer experiments,[92] where the primary purpose was to gain an understanding of the subcooled-boiling mechanism. Only more recently has it been realized that electrochemical mass transfer itself can serve as a convenient model for heat transfer in the neighborhood of an "active," bubble-generating point. Weder[54] measured limiting currents of ferricyanide reduction at concentric horizontal ring electrodes surrounding a single orifice from which gas was bubbled. A dependence on $Q^{0.30}$ (where Q is the gas volume flow rate) was found, in excellent agreement with earlier heat transfer results.

Earlier, Venczel[14] had made measurements of limiting currents of ferric and ceric ions at a cathode where hydrogen was simultaneously evolved. The bulk solution was titrated after the experiment to establish the partial current due to hydrogen ion reduction. The electrode was oriented vertically. In this more complicated situation two effects can be expected to occur at the same time: convection of the solution due to the rising bubbles; and turbulent mixing near the cathode after detachment of a single bubble. The experimental dependence of mass transfer rate on $v^{0.525}$ (where v is the gas volume evolution rate per cm^2 electrode) shows that the second effect is predominant. Ibl[102] proposed a modified "surface renewal" theory to explain this dependence, where at least on copper electrodes fair agreement was found with experiment.

Table 1.3. (continued from p. 51)

	System	Correlation	Range	Parameters	Electrolyte	Authors
46	Flow at the wall of a hydrocyclone	$Nu_d=14.1Re_c^{2/3}Sc^{1/3}G$ $Re_c=\Phi_v/\nu d$ $G=(d-2h\tan\theta/d)^{2/3}(d/d_i)^{1/6}(\tan\theta)^{4/3}$ if $\theta>13°$ $G=0.14(d-0.46h/d)^{2/3}(d/d_i)^{1/6}$ if $0\leq\theta\leq13°$	$Re_c>20$	L=length d=diameter cyclone d_i=diameter inlet h=electrode distance from inlet θ=half apex angle Φ_v=volume flow rate	$Fe(CN)_6^{3-}$	Ravoo[80]
47	Mass transfer to a small plate immersed in fluidized bed	$\varepsilon j_D=0.027Re_p^{-0.375}Sc^{0.292}(1-\varepsilon)^{0.15}\varepsilon^{-1.25}$ $j_D=(k/\bar{u})Sc^{2/3}, Re_p=\bar{u}d_p/(1-\varepsilon)\nu$		$\bar{u}$=superficial velocity ε=porosity d_p=particle diameter (or char.dimension)	$Fe(CN)_6^{3-}$	Jottrand, Grunchard[18]
48a	Mass transfer to the wall in packed bed	$\varepsilon j_D=0.43Re_p^{-0.38}$	$200<Re_p<23,000$		$Fe(CN)_6^{4-}$	Jagannadharaju Rao[39] Krishna, et al.[45] Krishna[94]
b	Mass transfer to a screen supporting a packed bed	$j_D=0.822Re_p^{-0.38}$			$Fe(CN)_6^{4-}$	Krishna[94]

(continued on p. 57)

Table 1.3. (continued from p. 56)

	System	Correlation	Range	Parameters	Electrolyte	Authors
49	Mass transfer to a single sphere in a packed bed	(a)$35<Re_d<140$: $Nu=1.44Re^{0.58}Sc^{1/3}$ (b)$Re_d>140$: $Nu=1.59Re^{0.56}Sc^{1/3}$ $Nu=kd/D$; $Re=d_p\bar{u}/\nu$	d=1cm 6<Re<1500 1580<Sc<1890	d=sphere diameter $\bar{u}$=superficial velocity	$Fe(CN)_6^{3-}$	Jolls, Hanratty[72]
50	Mass transfer in a packed bed, or a channel with turbulence promoters	$j_D=0.121Re_m^{-0.49}$ $j_D=(k/\bar{u})Sc^{2/3}$; $Re_m=\bar{u}s/(va\epsilon)$; see eq. (1.37) text.	Sc=2500 $60<Re_m<500$		$Fe(CN)_6^{3-}$	Hicks, Mandersloot[62]

1.10. Particulate flow systems.*

Recently the limiting current method has been increasingly used for studies in packed and fludized beds.

In 1962 Jottrand and Grunchard[18] reported on mass transfer to a small rectangular nickel plate immersed in a liquid fluidized bed of sand particles. Mass transfer rates were 5 to 10 times those measured in an open pipe flow, and a maximum rate was measured at a bed porosity of 0.58. Vergnes, Le Goff a.o. showed later that this maximum is directly related to a maximum in the average kinetic energy of the fluidized particles per unit bed volume.[70]

Measurements at the wall of fluidized beds were made by Krishna, Raju and Rao,[45] who used an annular cell, with varying radial ratios, to test the influence that an inner tube has on the fluidization. Only at low r_i/r_o values is the inner wall coefficient appreciably higher than the outer wall coefficient, which is itself somewhat lower than in a pipe bed of the same radius.[55] Raju and Rao[39] made measurements in an annular packed bed, with the inner wall as the measuring electrode (anode). These measurements were later extended to both walls.[45] The correlation employs the conventional dimensionless quantities:

$$j_D = \frac{k}{\bar{v}} Sc^{2/3} \quad , \text{ and} \tag{1.31}$$

$$Re_p = \frac{\bar{v} d_p}{(1-\varepsilon)\nu} \quad . \tag{1.32}$$

---

*Numbers 47 through 50 of Table 1.3.

In these wall transfer measurements stagnant liquid regions may play an important part (Kramers-Thoenes theory). It is interesting to observe the differences obtained by measurements in different places of the bed. A beginning was already made by Krishna and Raju,[58] who measured at ring electrodes embedded in the perforated plates between which the packed bed was contained. They obtained virtually the same dependence:

$$j_D \sim Re_p^{-0.38} \tag{1.33}$$

found earlier for the wall mass transfer.[93]

Very refined measurements in various places of the bed were made by Jolls and Hanratty,[72] who used an electrode sphere in a packed bed of 1 inch spheres. The over-all mass transfer data suggest a dependence

$$j_D \sim Re_d^{-0.42} \text{(turbulent) or } \sim Re_d^{-0.44} \tag{1.34}$$

outside the low laminar flow region ($Re_p < 35$), where the flow rate dependence is uncertain. A transition to turbulence occurred between Re_d=110 and 150, but no conspicuous change in the mass transfer ensues because large flow fluctuations occur over the whole range.

The rate expressions 49 of Table 1.3 are valid only for a single active sphere in a bed of inert spheres. In a bed of active spheres the spheres are bathed in the detached difusion layers of other spheres and the rates are lower. This is, of course, a general objection to the study of single activated elements of a particulate system. Nevertheless, such a study can yield valuable information about flow patterns, and variations throughout the system.

Hicks and Mandersloot[62] investigated flow systems with turbulence promoters, where the orientation of the promoters (or packed irregular particles) is an important parameter. In such systems the Reynolds number $d_p G/(1-\varepsilon)\mu$ used for packed beds of spheroid particles is not effective. Instead, they correlated their data with the "viscous part" of the pressure drop, based on the consideration that the average transfer rate in turbulent flow over a flat plate is proportional to the square root of the shear stress (analogous to expression 2 of Table 1.5).

The modified Reynolds number therefore is based on the void velocity $\bar{v}/\varepsilon$, the kinematic viscosity ν, and an equivalent diameter s/a where s is total area per unit volume and a a dimensional coefficient derived from pressure drop data:

$$\frac{\Delta P}{L} = a\mu\bar{v} + b\rho\bar{v}^2 \qquad (1.35)$$

Then:

$$Re_m = \frac{s\bar{v}}{a\varepsilon\nu} \quad , \qquad (1.36)$$

and the expected mass transfer correlation is:

$$j_D = \text{const } Re_m^{-1/2} \quad . \qquad (1.37)$$

This expectation is very satisfactorily borne out by limiting current measurements.

The application of a fluidized bed of conducting particles as a statistically continuous electrode has been discussed by Le Goff a.o.[70] Interesting similarities with heat transfer in fluidized beds could be exploited in this way.

1.11 Electrochemiluminescence

An interesting variant of the usual limiting current method is the technique of electrochemiluminescence,[43,44] where a blue glow appears on the anode when a potential is applied between platinum electrodes immersed in a solution containing H_2O_2 and luminol* in very small amounts. The intensity of the glow can be measured by a photomultiplier and is, in laminar flows, proportional to the mass transfer rate of H_2O_2 to the anode, where it activates the reaction. The proportionality constant has to be derived from calibration in known transfer geometries. Likewise for the correlation of mass transfer rates the diffusivity of H_2O_2 is necessary and was obtained by Springer a.o.[44] from measurements of luminescence on a flat plate anode in laminar flow. The technique appears to be especially suitable for flow visualization.[43]

1.12. Conclusions

It is clear from the enumerative review presented here that the limiting current method has established itself as a powerful tool in the study of mass transfer rates in chemical engineering operations.

In the ease and accuracy with which currents at electrodes can be measured it compares favorably with heat transfer techniques used to establish rate correlations. One should realize, however, that the conditions during the measurement are different. Heat transfer is most readily measured with a uniform flux generated at the surface. In electrochemical measurements also it is very easy to impose a constant current at the electrode. There is, however,

---

*Eastman Kodak Co. Luminol = 5-amino-2,3-dihydrol-1,4-phthalazinedione

no assurance that the current distribution will be uniform unless it is imposed (by means of separate, insulated sections). The interplay of concentration overpotential, kinetic effects and ohmic potential drop between the electrodes can give rise to complicated current distributions. Even if a uniform distribution is externally imposed, the overpotential measured at the electrode is not simply related to the concentration at the electrode. Only in the limiting current condition, where the overpotential is predominantly concentration overpotential, does one have assurance that, at the electrode surface everywhere, the concentration is zero, or effectively zero.

The limiting current method in mass transfer and the usual heat transfer techniques are therefore in a sense complementary, since they correspond to different boundary conditions.

Over the most popular non-electrochemical technique of measuring mass transfer, by dissolution, the limiting current method has the advantage of keeping the transfer surface unchanged, at least in the redox reactions. This is of great importance, e.g., in work on turbulent mass transfer. Furthermore, instantaneous flux measurement is possible so that various flow conditions can be tested in one experiment.

On the other hand, the method is restricted to electrolytic solutions, which have a high Schmidt number. Mass transfer in gases, e.g., differs significantly from that in electrolytic solutions, in particular for turbulent flow, and is closely analogous to heat transfer. However, many mass transfer situations are more readily analyzed for the condition of a high Schmidt number, so that the limiting current method has a considerable value for comparison of theory and experiment.

It is of interest also to compare optical techniques, in particular interferometry at an electrode, with the limiting current method. Measurement of interference fringes allows us to observe mass transport below the limiting current. Also, since it directly visualizes the diffusion layer, it is helpful in correlating theory and experiment (as, e.g., in the turbulent mass transfer work of Lin a.o.[4]), and in establishing the onset of secondary convection patterns, boundary layer separation, etc.

However, the disadvantages are considerable:

1. For a cell of finite thickness refraction of the beam (into regions of higher refractive index) causes serious difficulties of interpretation. Thin cells, on the other hand, influence profoundly the flow profile.

2. Interference fringes are crowded into the region of greatest interest, near the electrode. The reading of the slope at the electrode becomes almost impossible at high current densities, e.g., at or near the limiting current, where this would be of great interest. Even the position of the electrode surface on the interferogram depends on the setting of the focal plane.[115]

3. A parallel plate channel geometry is practically the only configuration that the method allows.

There is no question of the more general applicability of the limiting current technique. Interferometry may serve in discrete instances as complementary to the limiting current technique.

This review of experimental work has brought to light several aspects of the method that are in need of further clarification.

1. The use of correct and precise diffusivities is decisive for its accuracy if one wants to derive mass transfer correlations. In particular for the copper deposition reaction accurate diffusivities are not available over the whole range of Cu^{2+}-concentrations. The diaphragm-cell diffusivities used in free-convection work[11] are significantly higher than the effective diffusivities for solutions dilute in Cu^{2+}, as measured by Arvia[17] and successfully used by Wragg[63] to correlate laminar mass transfer in annular flow.

2. At electrodes where the current-distribution at the limiting current is non-uniform, the limiting current plateau is often of a poor quality. It appears that, in such cases, sectioning the cathode and reading separate sectional limiting currents markedly improves the quality of the curves. It is desirable to understand whether this is a typical characteristic of extended electrodes, or somehow connected with the particular system (Cu^{2+}) and geometry (parallel plate channel) used. In other words, what factors determining the shape of a limiting current curve can be controlled, and which other ones are inherent in the reaction, or the geometry?

3. In free-convection experiments with very dilute solutions the attainment of steady state is so slow that often no definite limiting current can be read. If, on the other hand, the limiting current is approached too slowly surface roughness, or depletion of the bulk solution, may create an unsteady state of a different kind. What are reasonable approach times to be used in forced and free convection limiting current experiments?

These three questions will be taken up in Chapters 3 and 4 after a discussion of some fundamental concepts in the next chapter.

Chapter 2 VALIDITY OF THE LIMITING CURRENT METHOD

Part I. Basic concepts of electrochemical mass transfer.

2.1. Introduction.

In the first part of this chapter the concepts of migration, electrode polarization, and current distribution are briefly reviewed since they are, at least as far as their quantitative aspect is concerned, less familiar to chemical engineers than to electrochemists. More detailed expositions of the fundamentals of electrochemical mass transfer, from a physico-mathematical viewpoint, can be found in the recent literature.[103,109] The material brought together in the next sections is aimed at a quantitative understanding of what factors determine, in the steady state, the limiting current level and in what sense the mass transfer process, in that condition, is different from that below the limiting current. The electric field is found to influence the limiting current level and this effect can be expressed in terms of electrolyte composition. The results are relevant to the interpretation of limiting currents, i.e., in particular, to the diffusivities used in the correlation of mass transfer rates calculated from limiting currents. (Chapter 3) However, the electric field also is the cause of dissimilarity between the current distribution at the limiting current and that prevailing below the limiting current. Some results discussed in Chapter 4 can be understood in terms of this dissimilarity, interacting with unsteady-state mass transfer.

The concepts discussed in the first part of this chapter allow us to define an ideal limiting current measurement or, rather, to perceive what inherent limitations of a given electrode-reaction cause it to produce a

poorly defined limiting current plateau. Part 2 of this chapter defines in a more general way the conditions for valid measurement and interpretation of limiting currents, taking into account that the measurement is by nature an unsteady-state phenomenon.

2.2. Migration and diffusion

When a potential is applied between conducting surfaces submerged in an electrolytic solution, a surface reaction will take place at each electrode. A general expression for this electrode reaction, which may be a deposition or dissolution reaction, or a redox reaction involving only species in the solution, is:

$$\sum_i s_i M_i^{z_i} \rightarrow n e^- \quad . \tag{2.1}$$

The current density by stoichiometry is proportional to the reacting ion flux (or fluxes, in the case of a redox reaction):

$$s_i \underline{i} = -nF\underline{N}_i \quad . \tag{2.2}$$

If the current measured serves to evaluate the mass transfer rate due to convective diffusion, it is desirable that the electric field make a negligible contribution to the flux of reactant species at the electrode. Since the electric field can never be completely suppressed, it would be preferable to know its contribution to the flux exactly, so that it could be accounted for.

The migration contribution could be determined experimentally for any combination of reacting and inert ions, if the reacting ion diffusivity (D_R)

would remain constant upon addition of varying amounts of supporting electrolyte. The migration contribution to the current would then simply be:

$$i_L - i_D$$

where i_L is the measured limiting current and i_D the limiting diffusion current, i.e., the limiting current measured with the same reactant concentration but enough supporting electrolyte to suppress the electric field completely. In the acidified cupric sulfate solution this condition is:

$$r = c_{H_2SO_4}/(c_{H_2SO_4}+c_{CuSO_4}) = 1 \quad . \qquad (2.3)$$

Although this condition can obviously not be realized, the value of i_D could be extrapolated from the behavior of i_L/i_D near r=1.

However, in the first place the behavior of ionic diffusivities with concentration variation of the supporting electrolyte is *a priori* unknown. Furthermore, the migration contribution would not necessarily be the same in various flow geometries. It is, therefore, important to gain whatever insight we can from theoretical calculations based on assumptions that are not unduly restrictive.

For dilute solutions the contributions to the flux of the ionic species i are:

$$\underline{N}_i = -D_i \nabla c_i - c_i z_i u_i F \nabla \Phi + \underline{v} c_i \quad . \qquad (2.4)$$

The second term represents the migration in a field of strength $\underline{E} = -\nabla\Phi$. The mobility u_i is the average velocity due to a unit force per mole

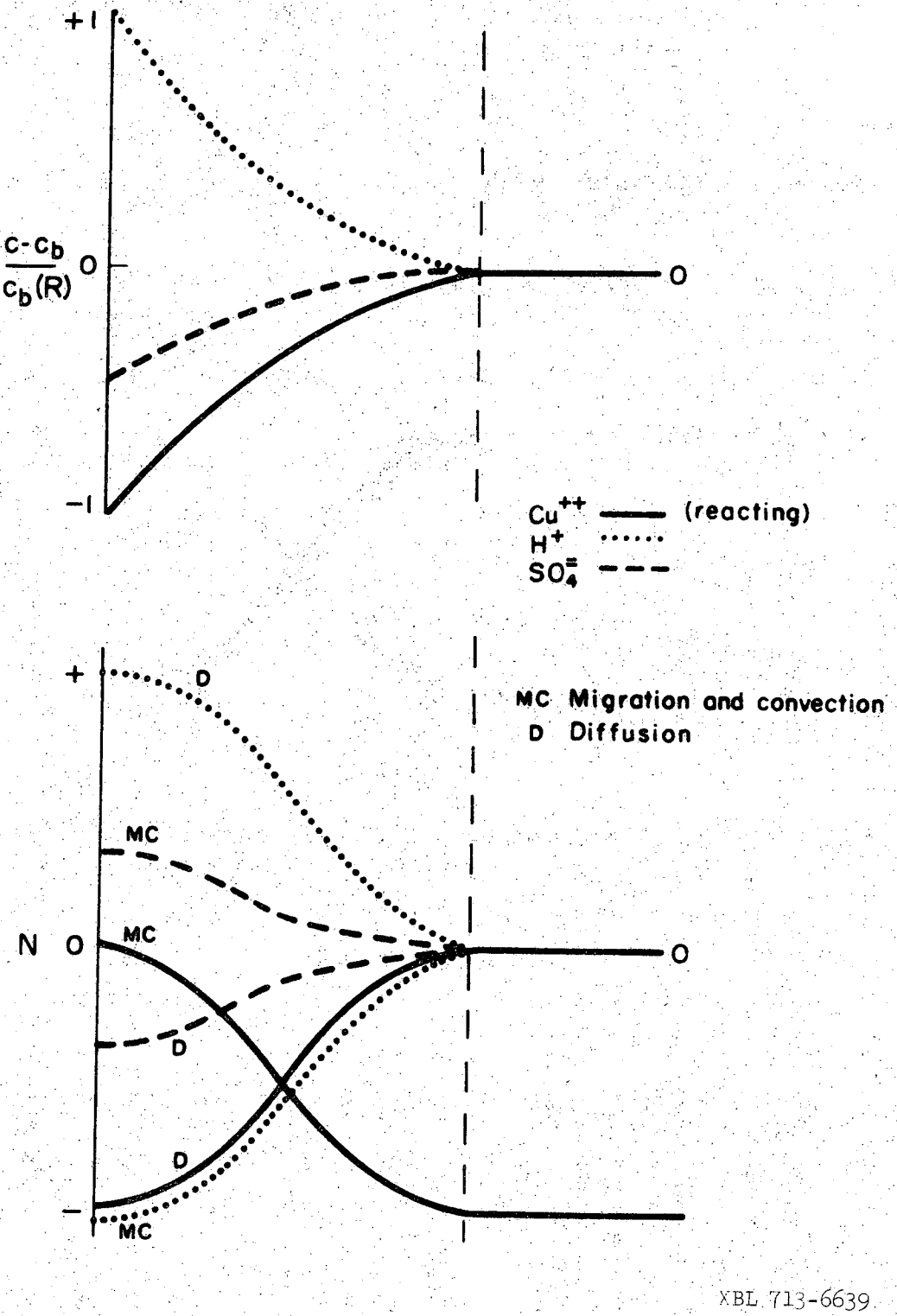

XBL 713-6639

Fig. 2.1. Concentration profiles and component fluxes in a cathodic diffusion layer (schematic).

(e.g., expressed in cm^2mole/Jsec). It is related to the ionic diffusivity D_i by the Nernst-Einstein equation:

$$D_i = R_o T u_i \quad , \tag{2.5}$$

valid in the limit of infinite dilution.

In the limiting current method the reacting ion concentration at the electrode is made vanishingly small by applying a large negative, or positive, potential. Even though, according to (4) the direct migration contribution to the reactant flux at the electrode vanishes (except in the case of a binary electrolyte), there will be an indirect contribution of the electric field because it affects the concentration profiles of reacting and inert ions. The species conservation equations:

$$\frac{\partial c_i}{\partial t} = - \nabla \cdot \underline{N}_i \tag{2.6}$$

are interdependent because electroneutrality is preserved everywhere in the solution, except in a very thin double charge layer near the electrodes. Therefore,

$$\sum_i z_i c_i = 0 \quad . \tag{2.7}$$

Since the current density in the solution is defined as:

$$\underline{i} = F \sum_i Z_i \underline{N}_i \quad , \tag{2.8}$$

the electroneutrality condition implies that:

$$\nabla \cdot \underline{i} = 0 \quad . \tag{2.9}$$

In the bulk solution the net transport of charge takes place by migration only. Near the electrode concentration gradients develop and diffusive transport occurs. For each inert ion convective diffusion and convective migration cancel each other in the diffusion layer, since the total flux toward the electrode must be zero according to (2). For the reacting ion, on the other hand, a shift occurs in the relative contributions of diffusion and migration to the reacting ion flux, which is constant throughout the diffusion layer. Figure 2.1 shows this schematically for the system: Cu^{++} (reacting cathodically), H^+, SO_4^{--}. A common diffusion layer thickness has been assumed for all three ions. In reality H^+, having the highest mobility and diffusivity, spreads out farther into the bulk solution than Cu^{++} and SO_4^{--}. In certain cases of free convection, namely, when the density difference at the limiting current is relatively small, e.g., in the ferricyanide-ferrocyanide redox reaction, a large excess of highly mobile supporting ion, in this case OH^-, tends to make the velocity profile unstable.[113]

The diffusivities and mobilities of the inert ions influence the concentration profiles directly and indirectly. The migration flux in (4) is proportional to the ionic mobility and concentration, but also to the field strength and, therefore, indirectly dependent on the total concentration and the mobilities of the other ions. Thus the migration contribution in acidified cupric sulfate solution can be expected to be lower if H_2SO_4 is completely dissociated to SO_4^{--} and two highly mobile H^+, than if the dissociation is only partial, with one H^+ ion present for each HSO_4^- ion.

For a binary solution, i.e., an unsupported solution (r=0), the migration contribution can be calculated directly if the ionic mobilities and diffusivities of the two ions are known. In such a solution the equations (6) for both species can be combined to one equation:

$$-D_s \nabla^2 c_s + \underline{v} \cdot \nabla c_s = 0 \quad , \tag{2.10}$$

where D_s and c_s now refer to the molecular diffusivity and concentration. Equation 10 is the analogue of the equation

$$-D_i \nabla^2 c_i + \underline{v} \cdot \nabla c_i = 0 \quad , \tag{2.11}$$

for the reacting species i in the presence of an excess of supporting electrolyte, such that the electric field is virtually suppressed. In dilute solutions the binary diffusivity D_s is related to the ionic diffusivities by

$$D_s = \frac{z_+ u_+ D_- + z_- u_- D_+}{z_+ u_+ - z_- u_-} = \frac{(z_+ - z_-) D_+ D_-}{z_+ D_+ - z_- D_-} \tag{2.12}$$

One can now express the limiting current i_L as a multiple of the limiting diffusion current i_D; for laminar forced convection i is proportional to $D^{1/3}$ so that in a cupric sulfate solution, e.g.,

$$i_L / i_D = \frac{D_s^{2/3}}{(1-t_R) D_R^{2/3}} = 1.883 \quad , \tag{2.13}$$

based on the mobility ratio $u_{SO_4^{--}} / u_{Cu^{++}} = 1.493$.

From (12) it is evident that binary diffusivities are, in principle, not appropriate for the correlation of mass transfer rates calculated from limiting currents. The binary diffusivity of $CuSO_4$, e.g., is approximately

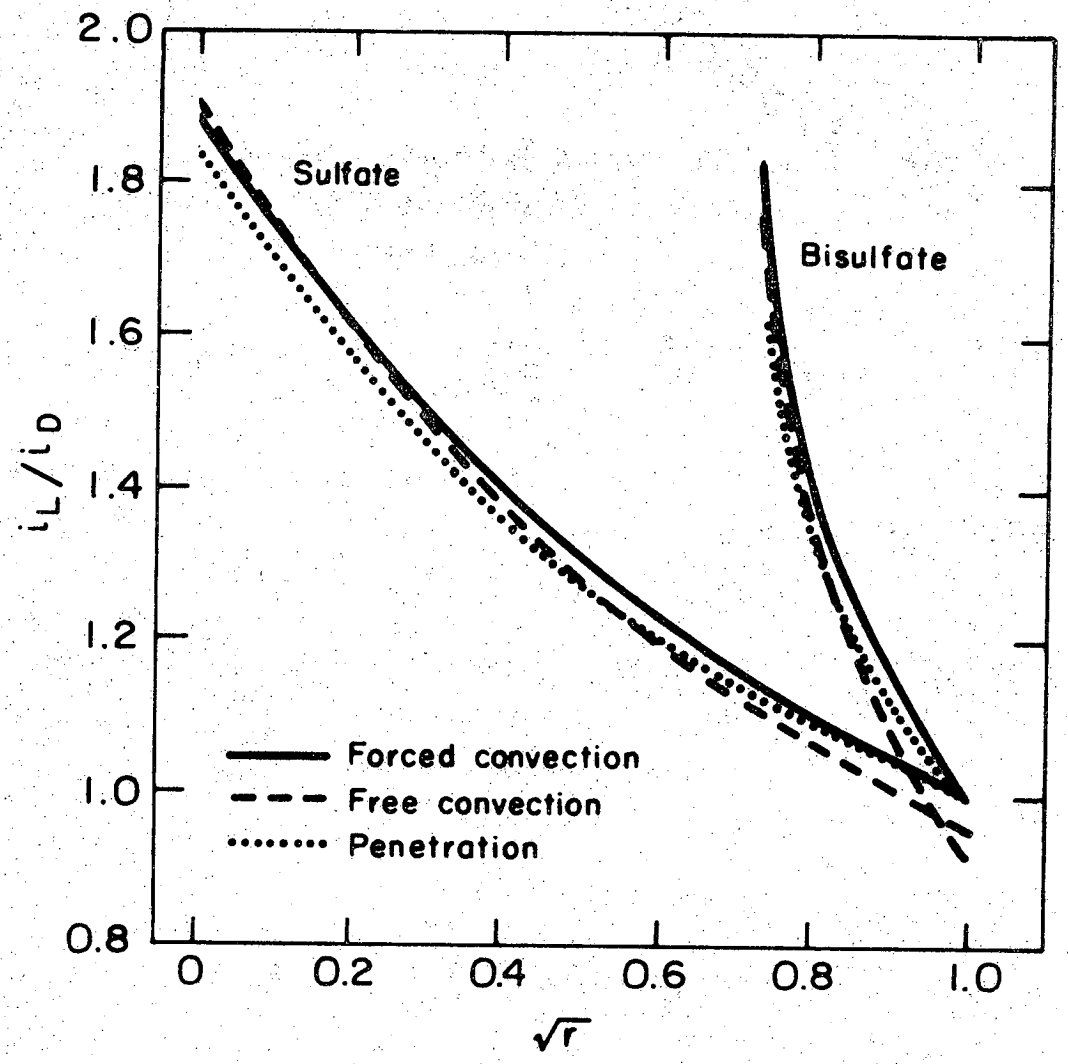

Fig. 2.2. Migration contribution to the limiting current in acidified cupric sulfate solutions (from ref. 113, 123)

$$r = c_{H_2SO_4}/(c_{H_2SO_4} + c_{CuSO_4}).$$

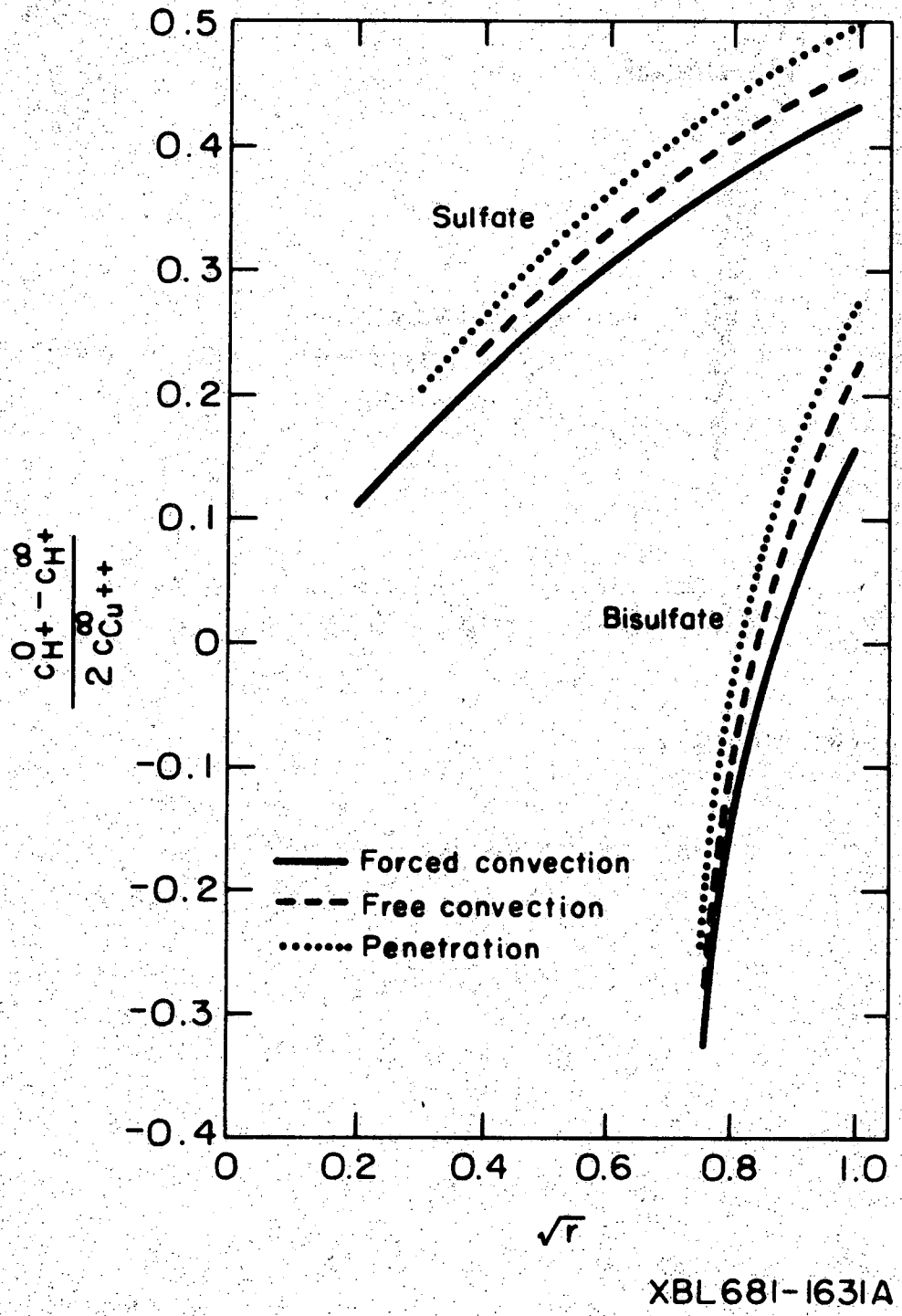

Fig. 2.3. Accumulation of H_2SO_4 at the cathode, due to migration in acidified cupric sulfate solution, at the limiting current. (from ref. 113, 123).

20% higher than the ionic diffusivity of Cu^{++} (both at infinite dilution); this is due to the higher mobility of the SO_4^{--} ion, compared to Cu^{++}.

For solutions with composition intermediate between a binary solution (r=0) and a well-supported solution (r=1), the migration contribution has to be calculated numerically. The equations of convective diffusion for all species:

$$\nabla \cdot \underline{N}_i = -D_i \nabla^2 c_i - z_i u_i F \nabla \cdot (c_i \nabla \Phi) + \underline{v} \cdot \nabla c_i = 0 \qquad (2.14)$$

are solved together with the equation of electroneutrality (7) and appropriate boundary conditions. The results of interest are the ratio i_L/i_D and the inert ion concentrations at the electrode, as a function of bulk composition varying from r=0 to r=1. For a specific ternary ion combination the parameters appearing in the problem are the ratios of the inert ion mobilities to the reacting ion mobility, and similar ratios for the diffusivities. If the Nernst-Einstein equation (5) is applied to the extent that diffusivity ratios will be equal to mobility ratios, also in more concentrated solutions, the only two parameters (mobility ratios) remain. This constant-ratio assumption is plausible for solutions dilute in the reacting ion but concentrated in supporting electrolyte. The more complicated case where the reacting ion concentration is also high, is not properly represented anyway by the constant-property equations (14).

For a number of frequently used ionic combinations Newman[123] and coworkers[113] have solved the migration equations (14), using infinite-dilution mobility ratios as parameters. Figure 2.2 shows the function i_L/i_D as a function of r(3) for the acidified cupric sulfate solution, assuming

either complete dissociation to SO_4^{--} or partial dissociation to HSO_4^- only. The calculations were made for three different kinds of diffusion layer: laminar forced convective; laminar free convective; and penetration-type diffusion layers. The last type includes time-dependent pure diffusion in a capillary cell and at a growing mercury drop. Laminar forced convective diffusion layers include those at a rotating disk and in Lévêque-type mass transfer. Figure 2.2 shows that the migration effect in free convection as $r \to 1$ is anomalous; this has been discussed elsewhere.[113]

The most conspicuous feature of these results is the dependence of the migration contribution on the degree of dissociation of the HSO_4^- ion, rather than on the kind of diffusion layer. This is also shown strikingly by Figure 2.3, which presents the solution composition at the electrode in terms of the relative acid accumulation:

$$(c_{H_2SO_4,\text{cathode}} - c_{H_2SO_4,\text{bulk}})/c_{CuSO_4,\text{bulk}} \qquad (2.15)$$

The composition of the solution near the electrode has long been of interest to investigators of the copper electrorefining process, which is traditionally conducted in free convection. By pinhole sampling[168] and by freezing[126] of the diffusion layer it was found that H_2SO_4 is present in the cathode layer in concentrations exceeding that of the bulk by approximately 0.5 to 0.7 times the bulk $CuSO_4$ concentration. From Figure 2.3. one can see that this would correspond to complete dissociation of HSO_4^-. This appears to be at variance with the rather small dissociation constant (0.0103 at 25°C) reported for bisulfate ion in very dilute solutions. Recently, however, Hsueh and Newman[125] have

employed results of Raman spectrum measurements in aqueous H_2SO_4 solutions to calculate the stoichiometric dissociation constant of HSO_4^- ; they found an increase by three orders of magnitude as the acid concentration increases from very dilute to 3 molar.

Optical measurements at a capillary cell cathode[125] confirmed the high values for the relative accumulation indicated by earlier, primitive methods. The evidence, however, is not yet conclusive. An accurate determination of the composition of the solution at the cathode is especially desirable in free convection since the driving force, i.e., the density difference with respect to the bulk, is affected strongly by the degree of dissociation. Also the excess current due to migration increases sharply with a small deviation from complete dissociation. This will be of importance in the interpretation of rotating disk integral diffusivities reported in Chapter 3, since these diffusivities include a migration effect. An accurate assessment of the effect will be attempted by computation along the lines indicated by Newman and Hsueh.

2.3. Polarization

The limiting current reveals itself as a plateau or inflection point in the plot of current vs. electrode potential. The potential of the electrode is measured most conveniently as the "overpotential" with respect to an identical reference electrode, i.e., a piece of the same metal as used for the working electrode, immersed in the bulk solution. (Figure 3.2). An arrangement which uses a liquid bridge, is quite common where one does not want to disturb the flow in the main cell. In any

case the essential condition is that a negligible current is flowing between the reference electrode and the working electrode.

The potential measured between these electrodes can be thought to represent the sum of two components. One of these would be measured between the reference-electrode and a second, imaginary, reference-electrode in the liquid adjacent to the working electrode (but just outside the double layer). The second component is then the potential difference between the imaginary reference electrode and the working electrode; following Newman,[124] it will be called the surface overpotential (η_s). It is dependent on the reaction rate and the concentrations at the electrode. It can also be identified as the potential drop over the double layer at the electrode.

The first component of the overpotential is interpreted, in the most general approach, in terms of electrochemical potentials of the ions in equilibrium with the reference electrode. The potential of a movable reference electrode, with respect to a fixed one, is

$$-nF\nabla E_r = \sum_i s_i \nabla \mu_i \qquad (2.16)$$

where μ_i is the electrochemical potential of species i.

For dilute solutions this can be written:

$$\nabla E_r = \nabla \Phi - \sum_i \frac{s_i R_o T}{nF} \nabla \ln c_i \qquad (2.17)$$

where $-\nabla\Phi$ is the electrostatic field strength in the solution. In the absence of concentration gradients two reference electrodes measure the ohmic potential drop in the solution, since:

$$\nabla\Phi = -\frac{i}{\kappa} + \frac{F}{\kappa}\sum_i z_i D_i \nabla c_i \quad , \tag{2.18}$$

where:

$$\kappa = F^2 \sum_i z_i^2 u_i c_i \quad . \tag{2.19}$$

If no current is passed an electric field may still exist if there are concentration gradients; this so-called diffusion potential is caused by unequal ionic diffusivities.

One generally distinguishes three contributions to the overpotential, besides the surface overpotential: an ohmic potential drop; a diffusion potential, caused by the concentration gradients in the diffusion layer; and a "Nernst" potential difference which is identical with the thermodynamic EMF of a concentration cell having the two reference electrodes as poles:

$$\Delta E_{\text{conc.cell}} = \frac{R_o T}{nF} \ln \frac{c_1}{c_2} \quad . \tag{2.20}$$

In reality the EMF of the concentration cell is lower by the magnitude of the diffusion potential. (Corresponding to the classical "cell with transference")

Two half-cells cannot be combined without creating a concentration gradient which gives rise to an electric field opposing the over-all potential gradient. For this reason the diffusion potential and the thermodynamic potential are jointly designated as concentration overpotential. (η_c). The complete expression for the concentration

overpotential includes an ohmic contribution due to the variation of conductivity in the diffusion layer:

$$\eta_c = i_{y=0} \int_0^b \left(\frac{1}{\kappa} - \frac{1}{\kappa_b}\right) dy + \sum_i \frac{s_i R_o T}{\kappa F} \ln \frac{c_{i\infty}}{c_{i0}} + F \int_0^b \left[\sum_i \frac{z_i D_i}{\kappa} \frac{\partial c_i}{\partial y}\right] dy \quad , \tag{2.21}$$

where subscripts 0 and b. stand for, respectively, electrode surface and bulk.

This expression can be simplified considerably for the case of a binary electrolyte and for a minor reacting species in excess supporting electrolyte. For metal deposition from a binary electrolyte the concentration overpotential reduces, after application of (4), to:

$$\eta_c = \frac{R_o T}{F} \left(\frac{1}{z_-} - \frac{1}{z_+}\right) \left[\ln \frac{c_b}{c_o} - t_+ \left(1 - \frac{c_0}{c_b}\right)\right] \tag{2.22}$$

The second term in the brackets is not negligible except at the limiting current the concentration overpotential in a symmetric binary electrolyte is twice that obtained with excess supporting electrolyte.

In the case of a minor reacting species with excess supporting electrolyte, the conductivity of the solution in the diffusion layer makes the first and third term in (21) negligibly small compared to the thermodynamic overpotential so that:

$$\eta_c = \sum_i \frac{s_i R_o T}{nF} \ln \frac{c_{ib}}{c_{i0}} \quad . \tag{2.23}$$

Summarizing, the overpotential measured with respect to an identical reference electrode may be represented as the sum of three contributions:

$$\eta = \eta_s + \eta_c + \Delta\Phi_\Omega \quad . \tag{2.24}$$

The ohmic contribution:

$$\Delta\Phi_\Omega = \int_0^{\underline{r}} \frac{\underline{i}\cdot d\underline{r}}{\kappa_b} \quad , \tag{2.25}$$

of equation 2.30, depends on the position ($\underline{r}$) of the reference electrode. In a situation where the other contributions are absent, it can be calculated by solving Laplace's equation for the geometry in question, with cathode and anode being equipotential surfaces. Characteristically the ohmic drop depends only on the geometric parameters of the cell configuration, and, of course, on the conductivity of the solution.

For example, for a disk electrode embedded in an inert plane the ohmic drop from an equipotential disk to an infinitely far removed counter-electrode is given by

$$IR_{total} = \frac{I}{4r_o\kappa} = \frac{\pi i r_o}{4\kappa} \quad . \tag{2.26}$$

Figure 2.7 shows the equipotential lines and current flow lines near a disk electrode. One notes from this that the placement of a reference electrode tip near the edge of the inert disk, where it cannot disturb the flow toward the disk (in rotation), includes almost 90% of the ohmic drop between cathode and anode. If the reference electrode is placed in the plane of the disk, at a distance r, the exact value is:

$$\frac{\Delta\Phi_\Omega(r)}{IR_{total}} = \frac{2\tan^{-1}\left(\frac{r^2}{r_o^2} - 1\right)^{1/2}}{\pi} \quad . \tag{2.27}$$

To exclude the ohmic drop from the overpotential measured by the reference electrode, one resorts to the use of backside-capillaries, i.e., capillaries connected from behind to an orifice in the electrode surface, small enough not to disturb the boundary layer at the electrode. The orifice should have insulated walls, since otherwise it would act as a pore electrode.

If a suitable expression is available for the surface overpotential, one can construct a theoretical polarization curve, i.e., a limiting current curve. Since the concentration overpotential as well as the surface overpotential depends on the reactant concentration at the electrode, this concentration has to be assumed. A reasonable assumption is that the Nernst diffusion layer thickness is not very dependent on the current level. Then one can write for cathodic currents:

$$\frac{i}{i_L} = \frac{c_b - c_o}{c_b} \quad . \tag{2.28}$$

If constant physical properties are assumed, this expression is obviously valid. A theoretical test assuming variable physical properties has, so far, only been made for a binary electrolytic solution ($CuSO_4$) at a rotating disk. Hsueh and Newman[98] showed that (28) is a good approximation; the largest deviation, occurring at $i/i_L = 0.5$ is 6-8% for 0.1 - 0.5 M $CuSO_4$.

The surface overpotential η_s can be related to the current density and the surface concentration by the Volmer-Butler expression:

$$i = j_o\{\exp(\alpha\eta_s ZF/R_oT) - \exp(-\beta\eta_s ZF/R_oT)\} \tag{2.29}$$

where j_o is the concentration-dependent exchange current density, α and β are anodic and cathodic transfer coefficients. Z is the electron transfer number:

$$Z = -z_+ z_- / (z_+ - z_-) \text{ for a binary solution;} \qquad (2.29a)$$

$$Z = -n \text{ for a solution with excess supporting electrolyte.} \qquad (2.29b)$$

Equation (29) is here used as a functional relation, without regard to its implications for the reaction mechanism. One may consider j_o dependent on a power of the reactant concentration:

$$j_o = i_o (c_o / c_b)^{\gamma} \quad , \qquad (2.30)$$

where i_o is taken at the bulk concentration. Equation 29 is then an expression for η_s with four adjustable parameters. At large negative potentials only i_o, β and γ are effective.

The steady-state relation between i and η can now be obtained by solving the set of equations 21-30 for a given electrode reaction in a given electrode configuration, where i_L is known. To write these equations in a concise form adopt the definitions:

$$f = i/i_L \quad , \quad \phi = \frac{\eta Z F}{R_o T} \quad . \qquad (2.31)$$

Then: $$\phi = \phi_c + \phi_s + \phi_\Omega \text{ , and} \qquad (2.32)$$

$$\phi_c = \ell n(1-f) + t_+ f \qquad (2.33)$$

(with excess supporting electrolyte t_+ is zero.).

From (29) and (30) then:

$$-Mf = (1-f)^{\gamma-\alpha} e^{\alpha(\phi-\phi_\Omega-t_+f)} - (1-f)^{\gamma+\beta} e^{-\beta(\phi-\phi_\Omega-t_+f)} , \qquad (2.34)$$

where:

$$M \equiv |i_{lim}|/i_o \qquad (2.35)$$

The value of ϕ_Ω depends on the electrode configuration. For example, for a rotating disk at uniform current density one can use the potential difference between the center of the disk and a remote counter-electrode:

$$\Delta\Phi_\Omega = \frac{1.273I}{4\kappa_b r_o} = \frac{1.273\pi i r_o}{4\kappa_b}$$

This ohmic contribution can then be expressed as:

$$\phi_\Omega /ZF = \frac{1.273\pi r_o i_L}{4\kappa_b} f \qquad . \qquad (2.37)$$

The level of the current therefore affects the polarization curve through M, and by way of the parameter

$$N' = \frac{1.273\pi r_o |i_L| ZF}{4\kappa_b R_o T} \qquad . \qquad (2.38)$$

The solution of (32-34) is very simple if surface-overpotential can be neglected ($M \to \infty$). Then:

$$\phi = \ell n(1-f) + t_+ f - N'f \qquad (2.39)$$

Figure 4a shows this (i-η)curve for a solution of 0.1 M $CuSO_4$ at 300 rpm, and the same if 1 M H_2SO_4 is added as supporting electrolyte. In the latter case the ohmic contribution is negligible ($N' \approx 1$).

For the reactions most frequently used in limiting current studies the surface over potential is not necessarily small. For the reduction of ferricyanide at a nickel or platinum electrode the surface overpotential is indeed very small.[167] At a Pt electrode in excess KCl solution the rate constant:

$$k = \frac{i_o}{c_b nF} \quad , \tag{2.40}$$

has values of the order of 10^{-1} cm/sec. i^o, the "standard exchange current density," i.e., i_o for a (hypothetical) 1 M solution, is 10 A/cm^2.

However, for the copper deposition reaction the surface overpotential is not negligible. Mattson and Bockris[134] found values of i_o of the order of 1-10 ma/cm^2 in highly purified solutions of $CuSO_4$ in 0.5 M H_2SO_4 (see Figure 2.5). It is likely that in the solutions used for mass-transfer experiments, which because of their bulk cannot easily be kept free of organic contaminants, i_o is even lower.

The complete equations (32-34) including surface overpotential can be solved by means of a Newton-Raphson root finding iteration for given values of f. The program is reproduced in Appendix A. Figure 4b shows the results for the 0.1 M $CuSO_4$ solution at 300 rpm, with and without supporting electrolyte. The kinetic parameters adopted are those of Mattson and Bockris:[134] $\alpha Z = 1.50$, $\beta Z = 0.50$, $\gamma = 0.42$,* i_o(at 0.1 M $CuSO_4$) = 4.2 ma/cm^2.

Fig. 2.4. (over)

Calculated limiting current curves for 0.1 M $CuSO_4$ at a rotating disk (r_o=0.2 cm, ω = 300 rpm, 25°C).

(a) No surface overpotential assumed;
(b) Surface overpotential included.

Data unsupported solution: i_{lim} = 79.2 ma/cm^2,
Z = 1, κ_b = 0.00872 Ω^{-1}cm^{-1}, t_+ = 0.363.
Data supported solution (1 M H_2SO_4): i_{lim} = 46.0 ma/cm^2,
Z = 2, κ_b = 0.387 Ω^{-1}cm^{-1}, t_+ = 0.
Kinetic parameters: i_o = 4.2 ma/cm^2; αZ = 1.50, βZ = 0.50, γ = 0.42

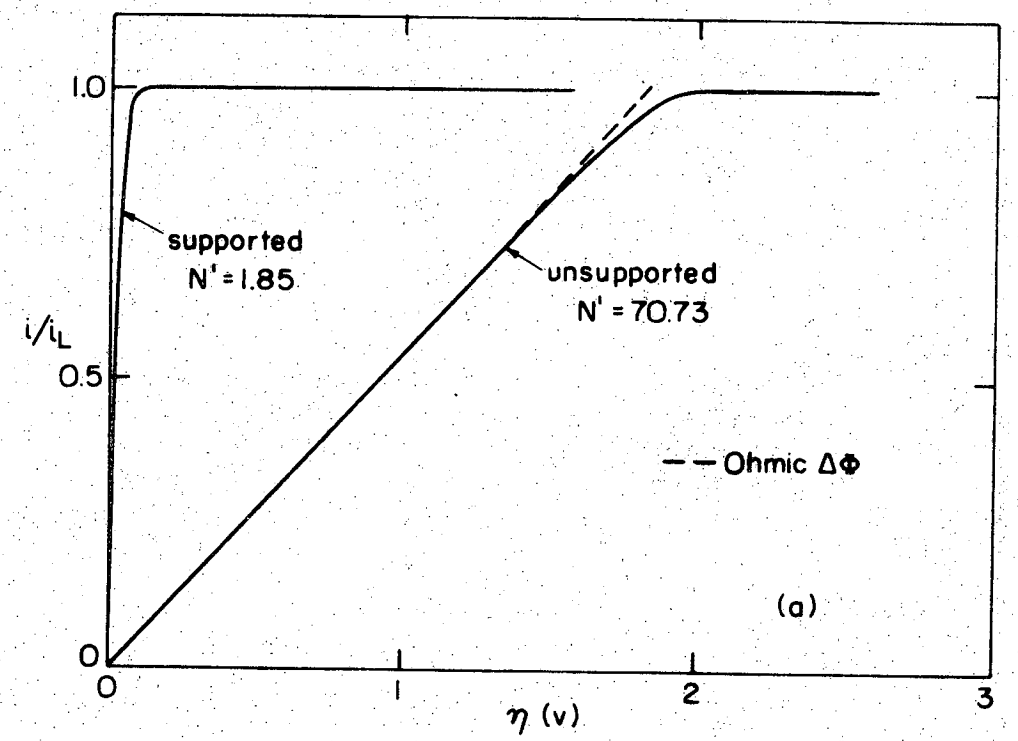
1.0
0.5
0
i/i_L
supported
N' = 1.85
unsupported
N' = 70.73
Ohmic ΔΦ
(a)
0
1
2
3
η (v)

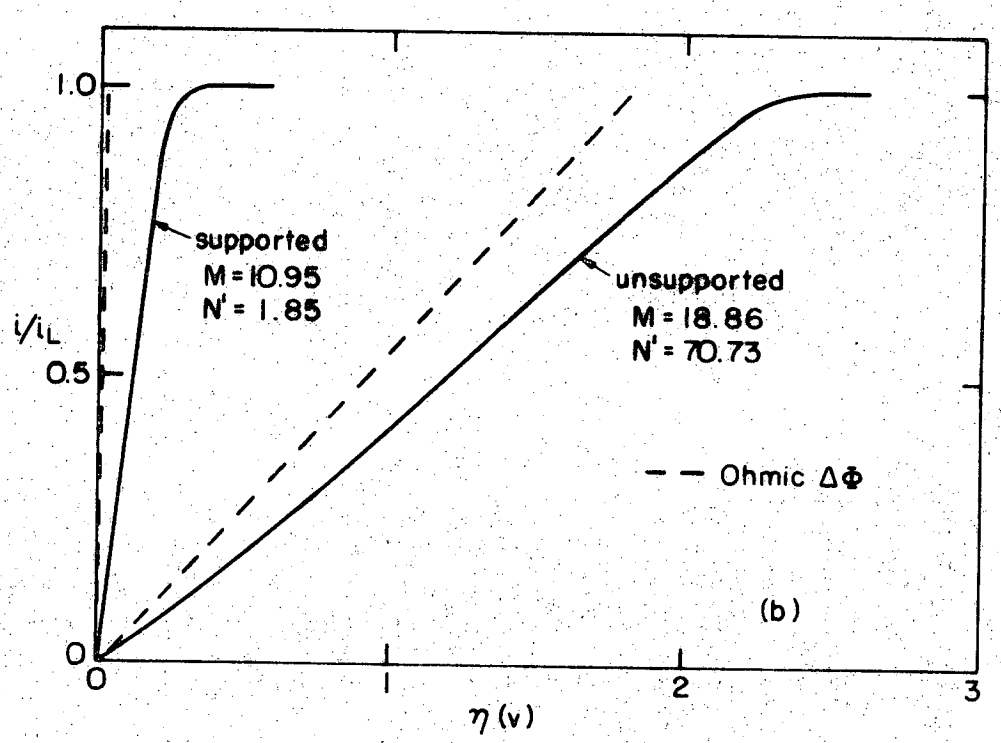
1.0
0.5
0
i/i_L
supported
M = 10.95
N' = 1.85
unsupported
M = 18.86
N' = 70.73
Ohmic ΔΦ
(b)
0
1
2
3
η (v)

XBL 715-6771

If the ohmic contribution is negligible, as with excess supporting electrolyte, the (f-η) curve depends only on M and the exponential coefficients α, β, γ. Figure 6 shows the dependence on M for the same α, β, γ values used in Figure 4. The value of η at $i/i_L = 0.5$ shifts to more negative values as the exchange current density decreases. In accordance with Tafel's law the shift for every decade increase in M has a constant value if $i_{lim} >> i_o$ ($M \geq 10$). At 25°C:

$$(\Delta\eta)_{f=0.5} = -\frac{25.679}{2}\left(\frac{\ell n\ 10}{\beta}\right) = -118.3 \text{ mv} \qquad (2.41)$$

The value of this "half-limiting potential" is given, for large η ($\phi > 7$, i.e., $\eta > 90$ mv) by

$$-\eta = \frac{29.58}{\beta}\ \{\log M - 0.3010\ (1-\gamma-\beta)\} \qquad (2.42)$$

The assumption that the ohmic contribution is negligible reduces to the criterion

$$\frac{r_o i_L}{\kappa_b} << \frac{60}{\beta} \log M \qquad (2.43)$$

For a disk of $r_o = 0.2$ cm and a solution of more than 0.5 M H_2SO_4 strength, this is equivalent to $i_L << 400$ ma/cm^2. The supported solution of Figure 2.4 has an $i_L = 46$ ma/cm^2 at 300 rpm. For more dilute solutions the criterion 43 is certainly fulfilled.

Therefore, equation 42 might be used to estimate kinetic parameters from the measured limiting current curves. But (42) contains three such

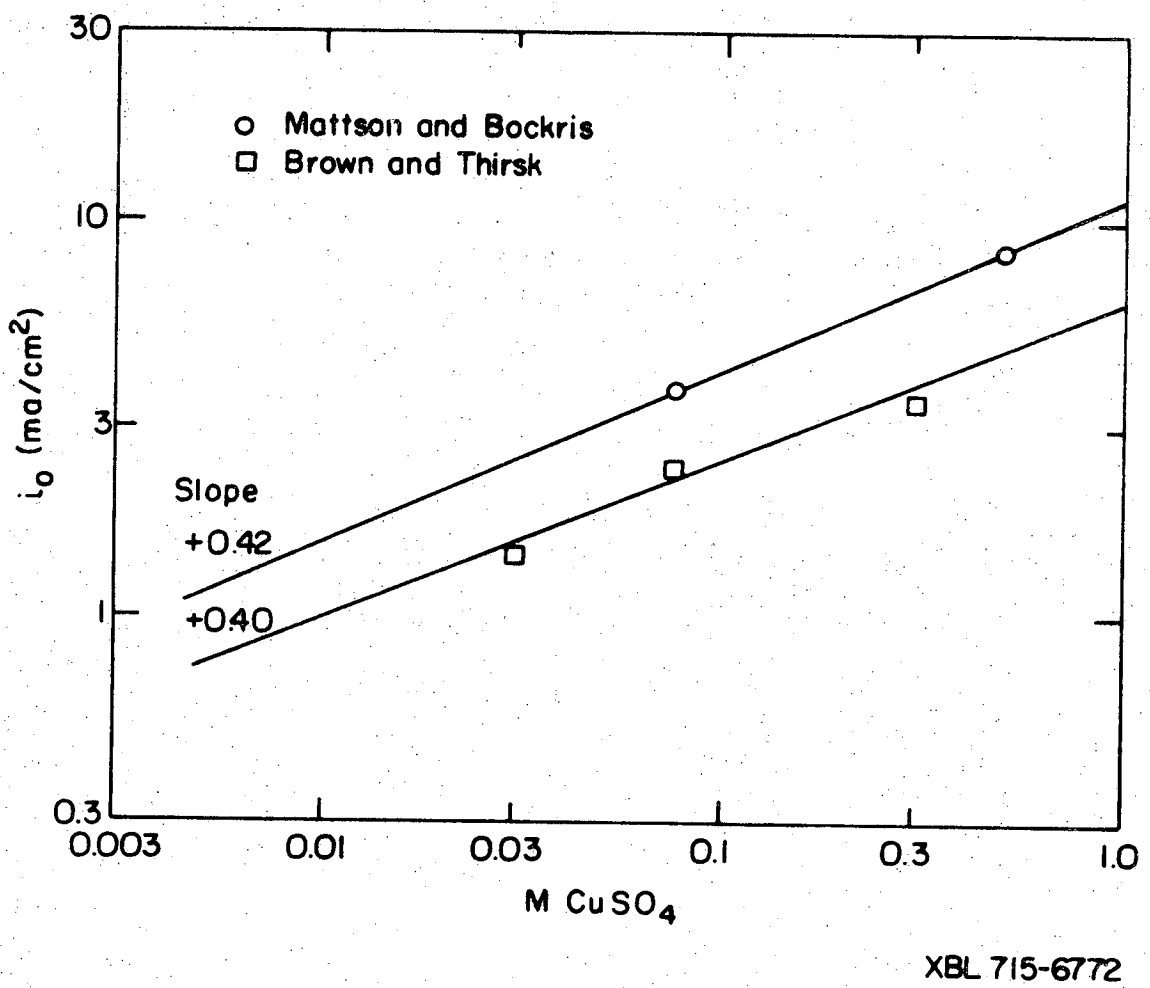

Fig. 2.5. Exchange current density in acidified cupric sulfate solutions, according to Matison and Bockris[134] (cathodic i_o for electrodeposited electrodes used only), and Brown and Thirsk.[138]

parameters; therefore more information is needed. Significant for the relative magnitude of the exponential coefficients, β and γ, is the slope $df/d\phi$ of the curve at the "half-limiting" potential:

$$\left(\frac{df}{d\phi}\right)_{f=0.5} = \frac{-\beta}{2(1+\gamma+\beta)} \quad . \tag{2.44}$$

The third relation between β and γ could be derived by making certain assumptions about the reaction mechanism. Mattson and Bockris,[134] e.g., proposed that, at higher current densities than those corresponding to the linear polarization region, the mechanism of the copper deposition reaction is

$$Cu^{++} + e \xrightarrow{slow} Cu^{+} \tag{2.45a}$$

$$Cu^{+} + e \xrightarrow{fast} Cu \quad , \tag{2.45b}$$

and the reverse for dissolution. In that case β would very likely be 0.25, a value found by the authors in extremely pure solutions and by many other investigators in solutions of various degrees of purification.

For γ Mattson and Bockris[134] deduced the relationship

$$\gamma = 1-\beta \quad . \tag{2.46}$$

However, from experiments in extremely pure solutions γ is found to be approximately 0.4 (Figure 2.5).

In solutions which are not carefully purified, such as commonly used in limiting current studies, organic contaminants occur. These may decrease the exchange current densities considerably, as can be inferred from studies by Karasyk and Linford.[170]

Therefore, it appears advisable to assume $\beta = 0.25$ and to derive values of γ and M from equations 42 and 44. This is the course adopted in the next chapter, where steady state limiting currents for various rotation rates need to be constructed. From a curve for a relatively low current level, where surface roughness effects are presumably not very important, values of γ and M can be derived which serve to construct an "ideal" limiting current curve for high current levels.

2.4. Current and potential distribution.

The general definition of the overpotential with respect to a reference electrode can be applied to the anode as well as to the cathode. If these two overpotentials, and the ohmic potential drop between cathode and anode (for uniform, i.e., bulk, concentration), are added together, the applied cell potential is obtained:

$$\Delta E = \eta_{cathode} + \eta_{anode} + \Delta\Phi_{bulk} \qquad (2.47)$$

In the calculations of Figure 2.4 the reference electrode was taken to be the anode. This implies that the dependence of overpotential on current density of the anode is negligible, which is usually ensured by making the anode area 100 - 1000 times as large as the cathode area.

In any electrode configuration where cathode and anode are of equal area, e.g., in the important case of parallel plate electrodes, the limiting current should be measured against a reference electrode. If the applied voltage were taken as the potential indicator, the plateau would be obscurred by the nonsimultaneous occurrence of diffusion

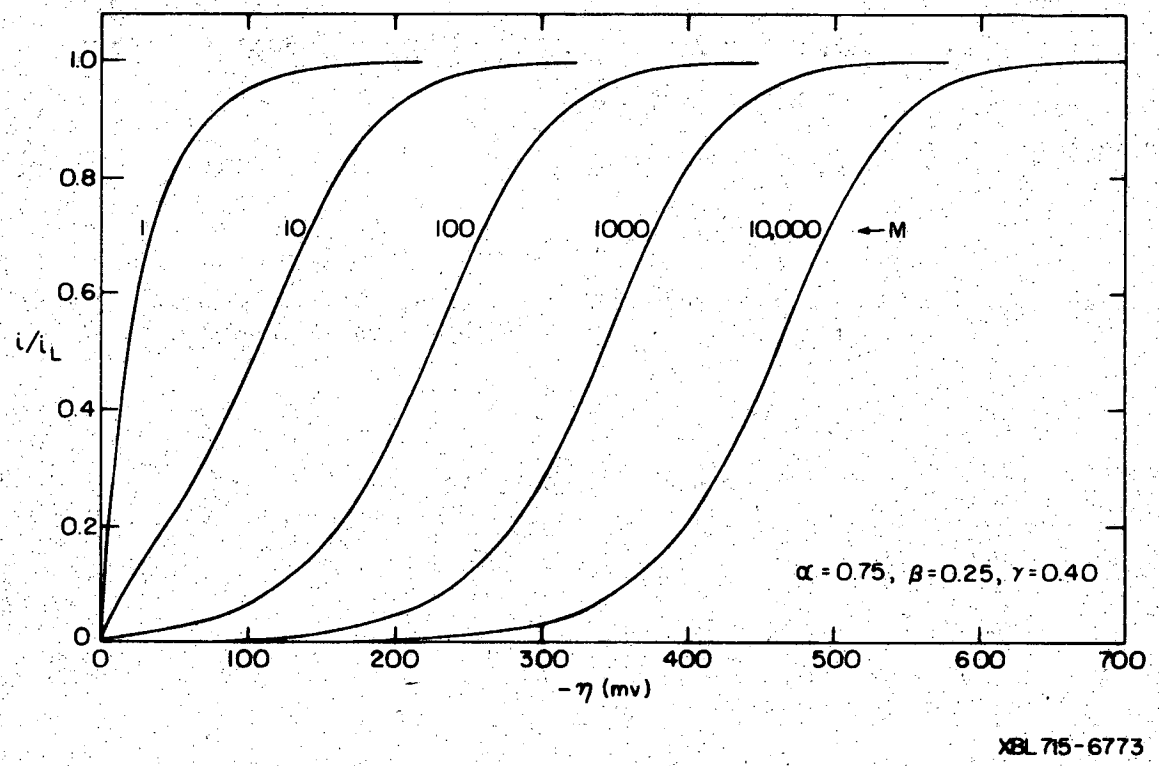

Fig. 2.6. Limiting current curves calculated on the assumption that ohmic resistance is negligible ($N \to 0$). $M = i_{lim}/i_o$.

limitation at the anode as well as the cathode. If also convection and mass transfer are interdependent, as in free convection between parallel plates, this can lead to problems which are best avoided by separating anolyte and catholyte by means of a diaphragm.

In equimolar solutions of ferri- and ferrocyanide between parallel electrodes the limiting current is reached first on the anodic side since the diffusivity of ferrocyanide is less than that of ferricyanide (see Table 1.4). Boëffard[46] has performed calculations to obtain the minimum ferrocyanide concentration, at a given ferricyanide concentration, necessary to obtain equal limiting currents at both electrodes in free convection.

Apart from the complications caused by the existence of anodic current limitations, there is good reason to question whether it is possible to reach a virtual zero concentration at every point of the cathode simultaneously. This will be considered in detail in Chapter 4. In order to clarify what occurs during a slow (quasi-static) passage to the limiting current, we discuss here what factors determine the current distribution below the limiting current and to what degree it is different from that at the limiting current.

In the limiting current condition, i.e., with c_o virtually zero everywhere, the current distribution is characterized by the predominance of concentration overpotential. Practically the entire applied voltage is used up in maintaining the concentration gradient at the electrode. The ohmic drop $\Delta\Phi_{bulk}$ is unimportant and, consequently, so is the location of the counter-electrode. The concentration gradient is determined by the hydrodynamics of the electrode flow cell.

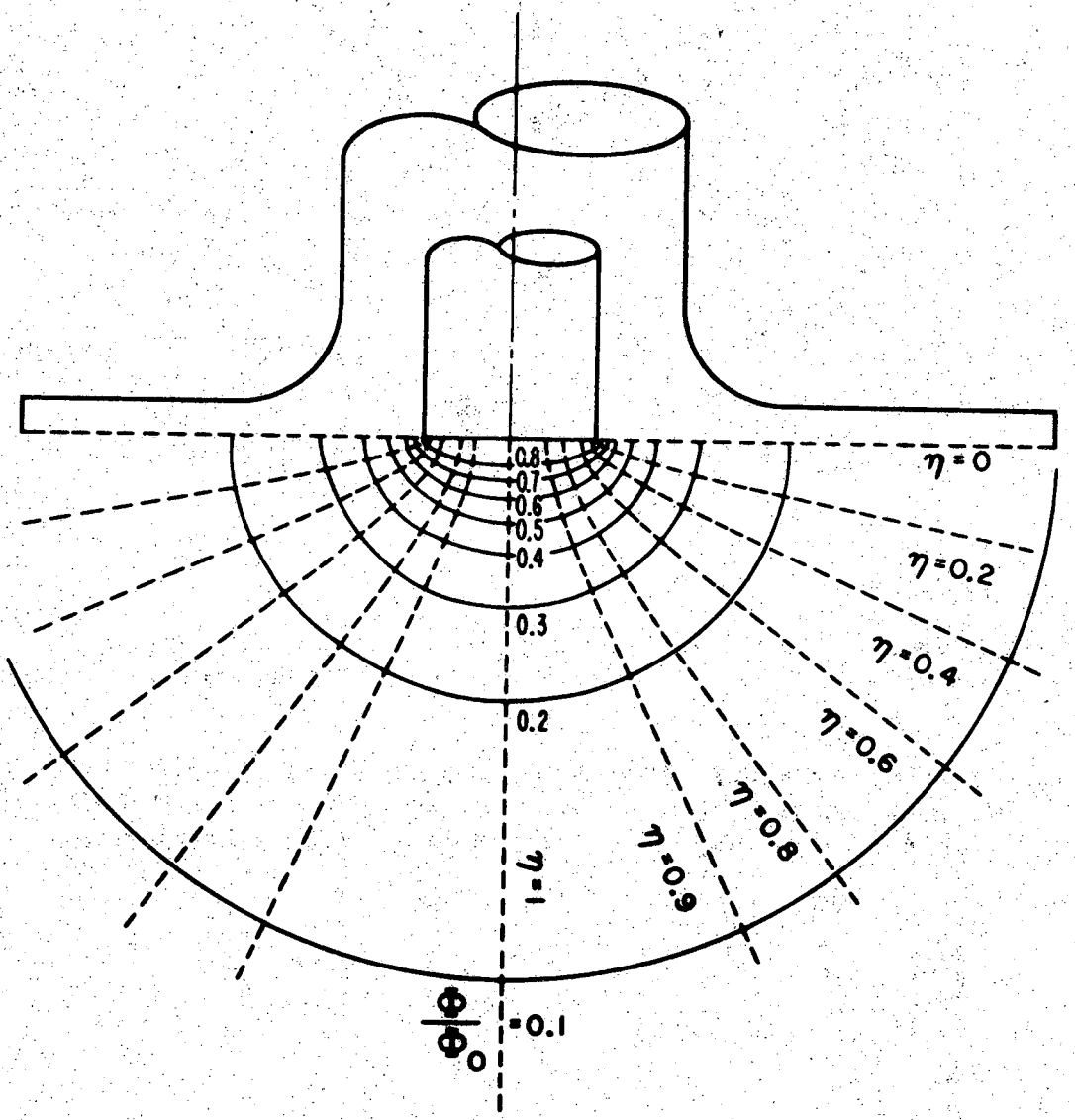

Fig. 2.7. Equipotential lines (solid) and current flow lines (dashed) between a disk electrode embedded in an insulating plane and an infinitely remote counter-electrode. From Ref. 139.

Thus, certain limiting current distributions are uniform, e.g., at a rotating disk of infinite extent; most, however, are nonuniform, e.g., the Lévêque-type distribution for developing mass transfer where the velocity profile is linear. In the absence of surface and concentration overpotential the current distribution is determined exclusively by the geometrical characteristics of the electrode configuration. In the absence of concentration gradients the conductivity is uniform everywhere and the Laplace equation describes the electric field:

$$\nabla^2\Phi = 0 \quad , \tag{2.48}$$

with the boundary conditions:

$$\Phi = \text{constant} \qquad \text{at electrode surfaces} \tag{2.49a}$$

$$\underline{i} = \kappa\nabla\Phi$$

$$\nabla\Phi = 0 \qquad \text{at insulating surface} \tag{2.49b}$$

Figure 2.7 shows current and potential lines between a disk electrode embedded in an insulating surface, and a hemispherical counter-electrode at infinite distance, for such a hypothetical primary current distribution. Characteristic for the primary current distribution is the infinite current density at the edge of an embedded electrode (unless the insulating wall is perpendicular to the electrode).

Since uniform current density at a rotating disk is reached, only at the limiting current, one can expect that below the limiting current the non-uniformity caused by the electric field will persist to some extent.

Also, one can expect that at the limiting current the potential drop $\Delta\Phi$, from a reference-electrode to various points near the disk but

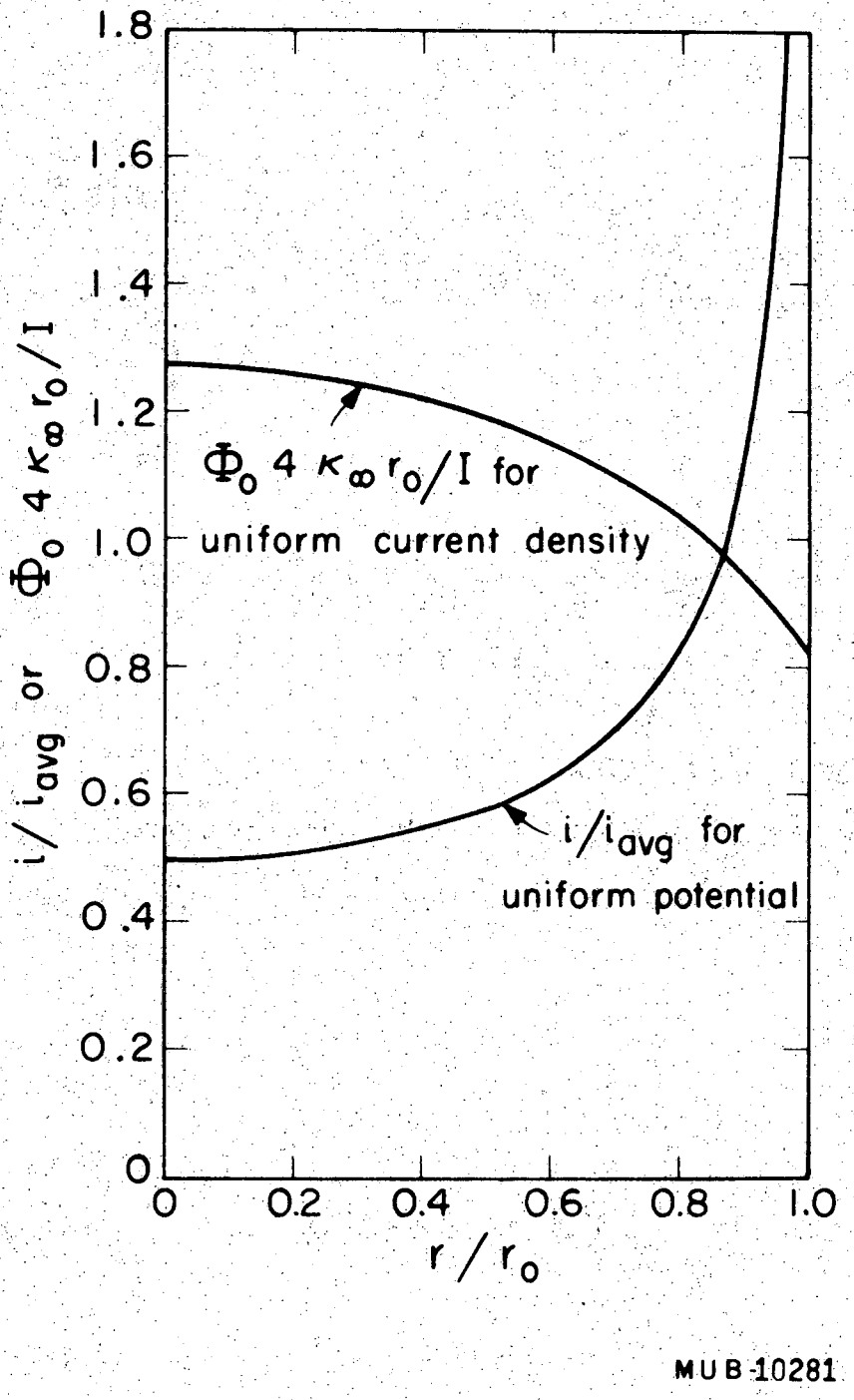

Fig. 2.8. Current distribution at an equipotential disk (primary current distribution), and potential distribution at a disk with uniform (limiting) current density. From Ref. 135.

just outside the diffusion layer, will be non-uniform. The highest bulk solution potential will exist at the center of the disk, in order to maintain there a current density that is two times as large as that at an equipotential disk for the same total current.

Figure 2.8, which illustrates this, is taken from Newman,[135] who calculated the potential difference between the bulk solution at the center and at the edge of the disk:

$$\Delta\Phi = 0.3634 \frac{r_o|i_L|}{\kappa_b} \quad \text{volt} \quad , \tag{2.50}$$

or, expressed in the dimensionless potential (31)

$$\Delta\phi = 0.3635\ N' = 0.3635\ \phi_{\Omega,\text{lim}} \tag{2.51}$$

The connection with the parameter N' (38) implies that the potential variation <u>across</u> the disk is, at the limiting current, a fixed fraction of the ohmic drop <u>between electrodes</u>, where the latter is taken to mean: between the center of the disk and the equipotential counter-electrode.

The dimensionless quantity N' obviously plays an important role in characterizing the non-uniform current distribution below the limiting current, where concentration and surface overpotential are not negligible. A similar quantity can be defined for other geometries. In particular, for a plane electrode of length L

$$N' = \frac{L|i_L|ZF}{\kappa_b R_o T} \tag{2.52}$$

Figure 2.10 shows the primary and limiting current distributions

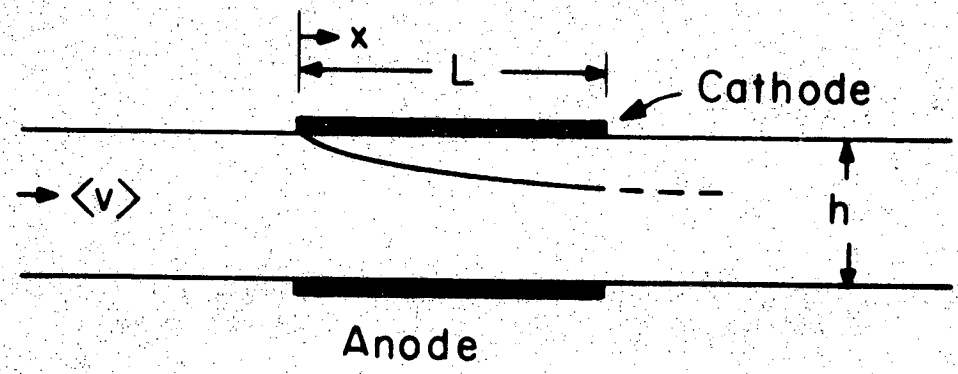

Plane electrodes in the walls of a flow channel

XBL673-2382A

Fig. 2.9. Plane electrodes in the wall of a flow channel. The diffusion layer on the cathode is indicated schematically.

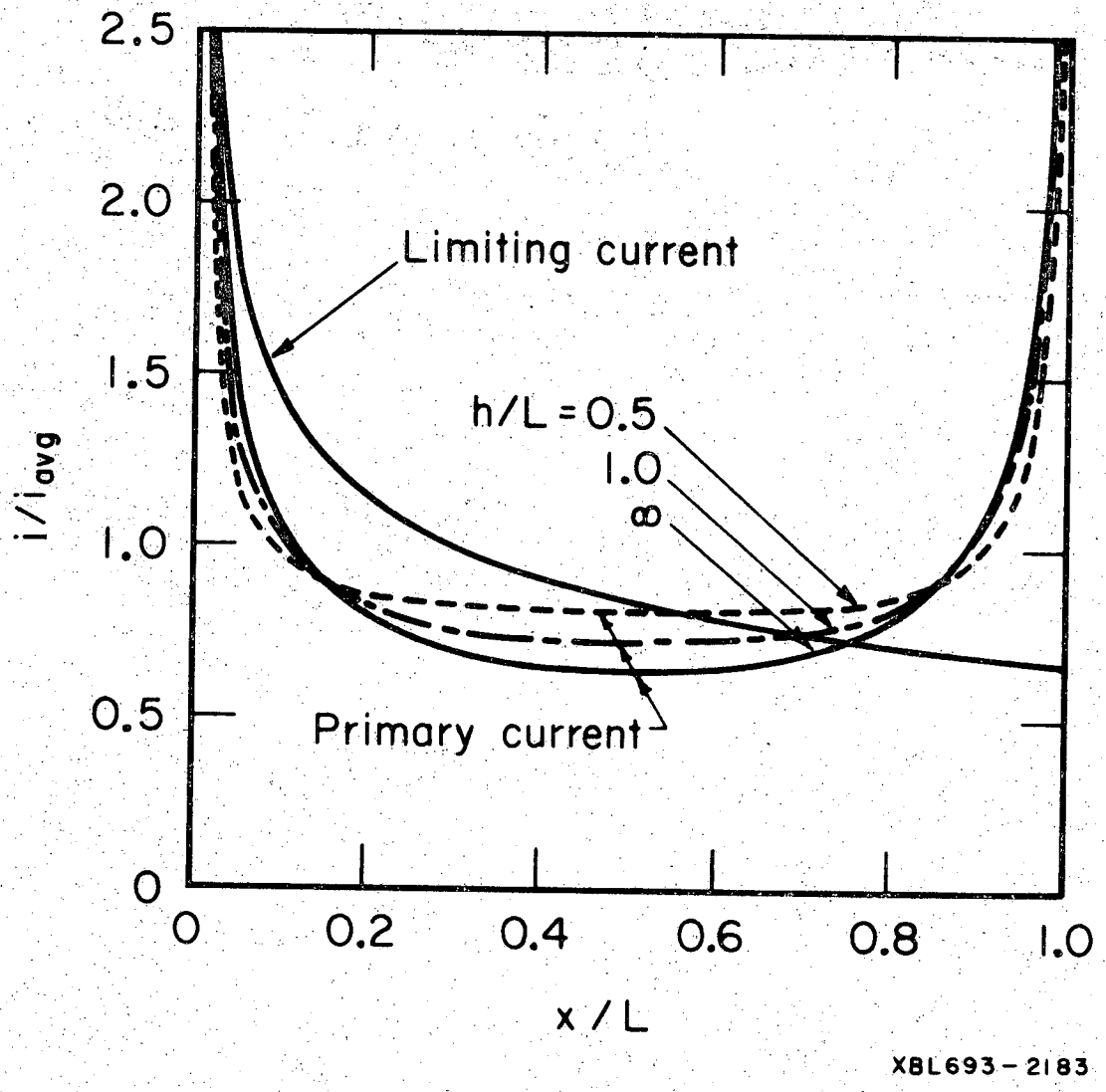

Fig. 2.10 Primary and limiting current distribution for parallel plane electrodes at finite distance h. From ref. 137.

for such a plate, with the counter-electrode at distance h (Figure 2.9). If the distance h is small the primary current distribution depends on the parameter h/L; it is more uniform at small h, the edge effect being confined to areas of approximate length h/2.

At low current levels, where concentration polarization is not important, the current distribution is not identical with the primary distribution because the very high edge currents automatically cause a non-negligible surface overpotential, even if no concentration gradients would develop at the edges. The so-called secondary current distribution corresponds to this combination of kinetic resistance and ohmic resistance of the electrolyte, in the absence of concentration gradients.

Secondary current distributions have been calculated mostly for two simplifications of (29). One is linear polarization:

$$i = i_o(\alpha+\beta)\frac{ZF}{R_oT}\eta_s \quad , \tag{2.53}$$

valid for $|i| >> i_o$; the other Tafel polarization:

$$\eta_s = -\frac{1}{\beta}\frac{R_oT}{ZF}(\ell n|i| - \ell n\, i_o) \quad , \tag{2.54}$$

valid for $|i| >> i_o$.

The expression (53); used instead of (49a) as a boundary condition for solving the Laplace equation, introduces the dimensionless parameter

$$J = \frac{i_o LZF}{\kappa_b R_o b} \tag{2.55}$$

for a planar electrode. The current distribution (i/i_{avg}) is not dependent on the current level, only on $(\alpha+\beta)J$. The case $J \to \infty$ corresponds to the primary current distribution.

At higher currents the current level becomes important. If (54) can be applied, the value of i_o is irrelevant in the solution of Laplace's equation. The current distribution, i/i_{avg}, is determined completely by:

$$\frac{\beta|i|ZFL}{R_o T \kappa_b} \quad \text{or} \quad \beta f N' \tag{2.56}$$

These secondary current distributions can be calculated by classical analytic techniques only in the most simple configurations. Numerical solution is often more convenient.

Obviously a solution including the effect of concentration overpotential presents even greater difficulties, Newman[135] has provided such a solution for the rotating disk electrode, and (with Parrish)[136,137] for plane plate electrodes with parallel flow. In the latter case solutions were obtained only for distances $h \geq 0.5$ L.

Figures 2.11a and b show the current distributions at a planar cathode at four intermediate values of the average current level, according to Newman and Parrish.[137] The parameters employed are: J(55); N, which related to N'(52) by

$$N' = 0.5384\ N \quad ; \tag{2.57}$$

The transference number t, as well as α, β, and γ (equation 29) which have been given arbitrary values. The parameter J is 0, indicating Tafel polarization.

A very important conclusion to be drawn from Figure 2.11a is that the current distribution approaches the limiting current distribution only at current levels very close to the limiting current. The degree to which

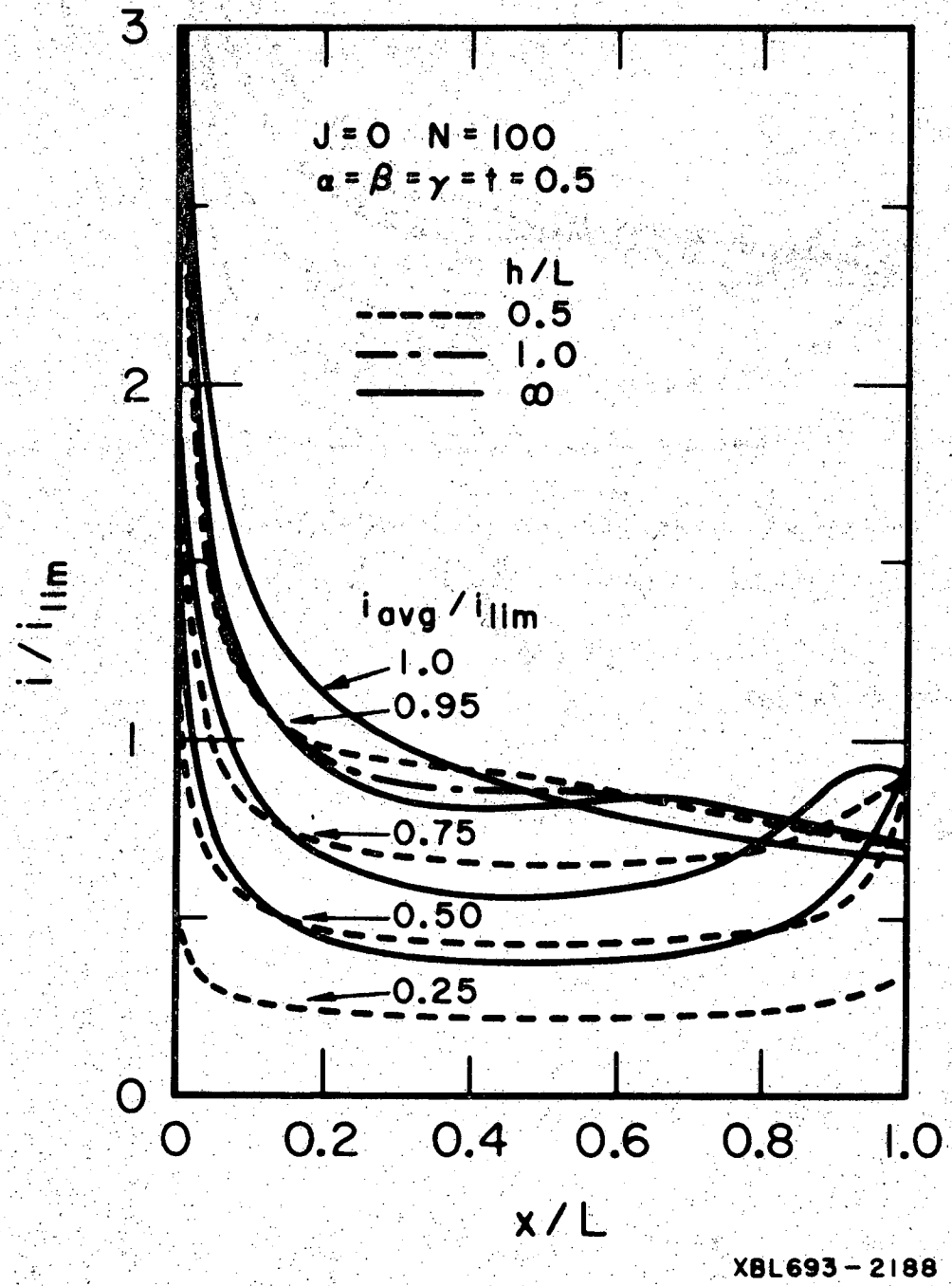

Fig. 2.14. Current distribution at a plane cathode with parallel counter-electrode at distance h. From Ref. 137.

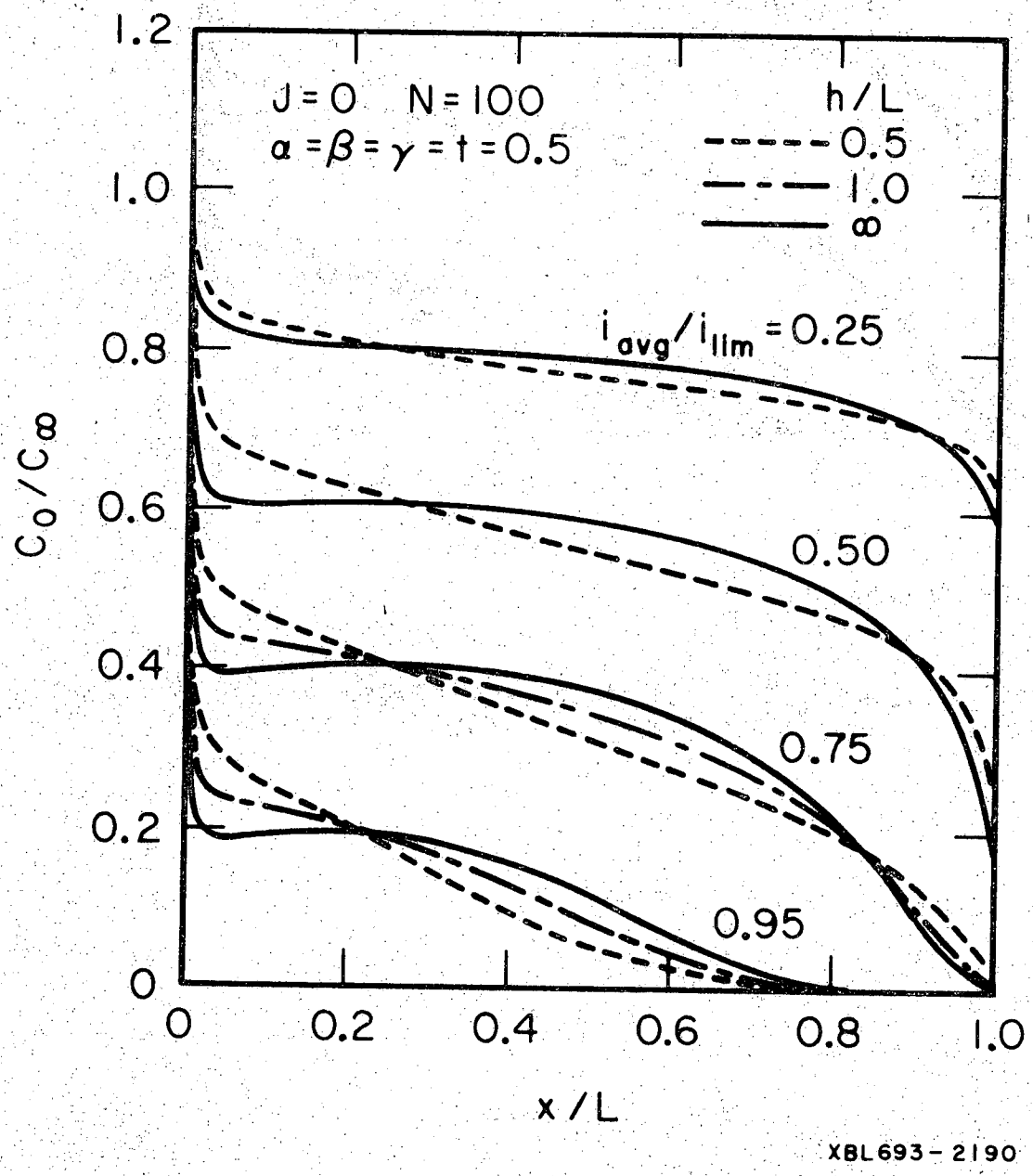

Fig. 2.15. Concentration variation at the surface of a plane cathode with parallel counter-electrode at distance h. From Ref. 137.

the current distribution retains non-limiting character close to the limiting current, depends on the parameter N and on h/L. For high values of N and h/L the current distribution exhibits a local maximum near the trailing edge, at current levels above 50% of the limiting current.

Figure 2.11b helps to explain the origin of these local maxima. At low current levels the current density at the edge tends to be high; it may exceed the eventual limiting current. At higher current levels the reactant supply at the electrode is a limiting factor and the increase of overpotential toward the edge does not increase the current density any further. The reactant concentration at the electrode has reached a virtual zero level near the trailing end of the plate, while the average current is only 95% of the limiting current.

It should be noted, however, that these calculated distributions are steady-state distributions. A slow enough transition from one intermediate current level to the next, should still lead to a simultaneous limiting current condition, i.e., a uniform overpotential along the plate. How slow this transition has to be, one cannot infer from the information presented here.

Earlier experiments in this laboratory have shown that in copper deposition on planar electrodes the limiting current is invariably reached first at an edge: at both edges in free convection (Fenech;[11a] increase of applied potential), and at the trailing edge in forced convection (Hickman;[156] increase of applied current). This was first established by observing the hydrogen evolution on the electrode; later, also by sectional limiting current measurements. The nonsimultaneous limiting current condition along the electrode obscured the plateau if the total current was being

recorded; consequently, a sectioned electrode

with separate reference electrodes for each segment has been used in later work.

In Chapter 4 the rationale for adopting such a painstaking procedure will be re-considered in the light of the current distribution below the limiting current, as discussed above, and in conjunction with purely convective unsteady-state mass transfer.

Part II. Conditions for validity.

2.4. Definition of the limiting current plateau.

It is useful to distinguish three determinants in the definition of a limiting current plateau:

1. The approach to the limiting current, which would be steep, i.e., complete within approximately 200 mv, if it were not for kinetic and ohmic contributions to the overpotential (section 2.3);

2. the termination of the plateau, by a follow-up reaction (mostly hydrogen evolution) at a potential determined by the composition of the electrolyte (pH) and the state of the electrode surface;

3.6 the inclination of the plateau, which is ideally zero but may reach considerable proportions due to surface area increase (in metal deposition, in particular of Cu) or, less commonly, due to changes in the bulk concentration.

2.5. Conditions for valid measurement

For a valid limiting current measurement it is obviously desirable that the plateau should be well-defined. From the foregoing it is clear that this can not always be achieved; in particular,

1. The model reaction may be characterized by slow electrode kinetics.

Compare, e.g., figures 3.3 and 4.5 for, resp., copper deposition and ferricyanide reduction at a rotating disk.

2. The model reaction may change the surface area. This is particularly obvious in copper deposition and leads to poor plateaux at high limiting current levels (Figure 3.6). In Chapter 3 methods will be sought to avoid this effect; but it is not likely that it can be completely eliminated at high concentrations of $CuSO_4$.

3. The bulk concentration of reactant may be low and will become depleted in lengthy experiments, e.g., in free convection measurements (to be discussed in Chapter 4).

On the other hand, certain conditions can be avoided:

1. Unsuitable placement of the reference electrode, such that a high ohmic contribution is included in the overpotential (Figure 2.4b).

2. Changes in bulk reactant concentration due to variations in gas pressure (O_2 reduction) or, worse, presence of other species reducible at the limiting current potential (O_2 in I_3^- reduction; O_2 in Cu^{++} reduction at low bulk concentration).

3. Unsteady-state mass transfer caused by excessively fast current ramps or potential scans. This is the subject of Chapter 4. Here it should be noted, however, that in certain conditions where transition-times to the steady-state are long, an actual steady-state may never be reached due to continual change of surface area, or depletion of the bulk concentration.

2.6. Conditions for valid interpretation.

1. Incorrect values for mass transfer rates are obtained if migration in the electric field contributes more than a negligible fraction of the

total limiting current. (section 2.2) For several types of diffusion layer and for specific ion combinations this contribution has been calculated and can therefore be subtracted. In the practically important case of acidified cupric sulfate the migration effect is strongly dependent on the dissociation of bisulfate ion. This dissociation appears to be complete, but the experimental evidence is not conclusive.

2. Mass transfer rates from limiting current measurements in well-supported solutions should be correlated with ionic, not molecular, diffusivities. These can be calculated from limiting current measurements, e.g., at a rotating disk electrode. In Chapter 3 this will be done for Cu^{++} ion in $CuSO_4$ - H_2SO_4 - H_2O. For diffusivities of $Fe(CN)_6^{4-}$ and $Fe(CN)_6^{3-}$ with various supporting electrolytes, see Table 1.4.

The diffusivities thus obtained are necessarily effective diffusivities since 1) they reflect a migration contribution which is not always negligible; 2) they contain the effect of variable properties in the diffusion layer, not accounted for by the well-known solutions to constant-property equations. In the case of Cu^{++} ion diffusivities they may also reflect the effect of surface area increase during the approach to limiting current.

Chapter 3. ROTATING DISK INTEGRAL DIFFUSIVITIES OF Cu^{2+} IN $CuSO_4$-H_2SO_4-H_2O.

3.1. Introduction.

In many investigations of mass transfer at electrodes by the limiting current method, use is made of the copper deposition reaction in acidified $CuSO_4$ solution. To correlate the results in terms of dimensionless numbers. (Re, Sc, Gr, Nu) the diffusivity of the reacting ion has to be known. From an analysis of the electrochemical mass transfer process in well-supported solutions, it becomes evident that the use of the molecular diffusivity (of $CuSO_4$) is not appropriate. On the other hand the ionic (Cu^{2+}) diffusivity cannot be determined from molecular diffusivities; it is only known, in the limit of infinite dilution, from the Nernst-Einstein equation. In such solutions, one can calculate, the ionic diffusivity of Cu^{2+} is approximately 20% lower than the molecular diffusivity of $CuSO_4$. Confronted with these unattractive alternatives, many investigators have used the molecular diffusivities measured by Cole and Gordon[141] for $CuSO_4$ in the ternary system $CuSO_4$-H_2SO_4-H_2O. Their measurements were carried out in diaphragm cells, mostly at 18°C. These diffusivities have been correlated by Fenech[11] using the Stokes-Einstein equation:

$$\mu D/T = (2.495 + 0.0173\ c_{H_2SO_4} + 0.0692\ c_{CuSO_4}) \times 10^{-10}\ \text{dyne/°K} \qquad (3.1)$$

This expression, originally given for 22°C, has been used extensively in later work.

The validity of (1) for correlations of limiting current measurements was first questioned by Arvía, Bazán and Carrozza,[142] and later by Wragg and Ross.[63] The latter found that limiting currents in an annular flow cell could be correlated in better agreement with the Lévêque mass transfer theory if a lower mobility (Stokes-Einstein) product was employed:

$$\mu D/T = 2.09 \times 10^{-10} \text{ dyne/°K} \qquad (3\text{-}2)$$

This value is based on ionic diffusivities calculated from limiting current measurements at a rotating disk electrode by Arvía, Bazán and Carrozza.

Effective ionic diffusivities at a rotating disk electrode are calculated from the Levich equation (valid for constant physical properties) by inverting it:

$$D = \nu(0.6205\ c_\infty ZF\ \sqrt{\nu\omega}/i_{lim})^{-3/2} \qquad (3.3)$$

This has been done earlier for ferri- and ferrocyanide ions in excess NaOH (or KOH).[47,51]

The values of D on which (2) is based, were measured by Arvía c.s. in four solutions, of concentrations lower than 0.1 M in $CuSO_4$. Practical conditions, e.g., copper refining or winning, often require higher Cu^{2+} and H^+ concentrations. The present work is intended to make available diffusivity values for a larger range of $CuSO_4$ and H_2SO_4.

3.2. Experimental procedure:

A. Equipment

The disk electrodes used in this work had the dimensions and shape recommended by Riddiford[110] (Figure 3.1). The central part was machined from OFHC copper to a tolerance of less than .001 inch, then embedded in epoxy resin and machined to the specified flare shape. The electrode diameter was 0.3 cm or 0.4 cm, and was measured from an average of 4 readings by means of a Nikon projection table. The uncertainty in the electrode area, due to deviations from circularity and to variations depending on the surface preparation, was estimated at $\pm$ 2%.

The disk was attached to a spindle which was fitted tightly in two 7/8 inch O.D. bearings, mounted in a heavy brass case. In the galvanostatic series of experiments the spindle and disk were driven by a variable speed motor (Bodine Electric Co., Type NSE 11R, gear ratio 10 to 1). The motor was connected to an adjustable d.c. voltage supply (Power Designs Inc., Model 5015A). For reasons of practical convenience rotation rates were limited to 120-400 rpm. The rotation rate was measured by a Strobotac (General Radio Co., Type 631-BL).

In the potentiostatic experiments, the spindle and disk were connected by a rubber coupling to the shaft of a Servotek Control Motor with Precision Adjustable-Speed Drive (Series 500). The experimental range of rotation rates was 600-1500 rpm. The speed settings were calibrated with a Strobotac, accuracy $\pm$ 1%.

The alignment of the disks was ensured by means of a flat annular interface and a screw fitting. The excentricity of the electrode center with respect to the spindle axis was less than 1 micron.

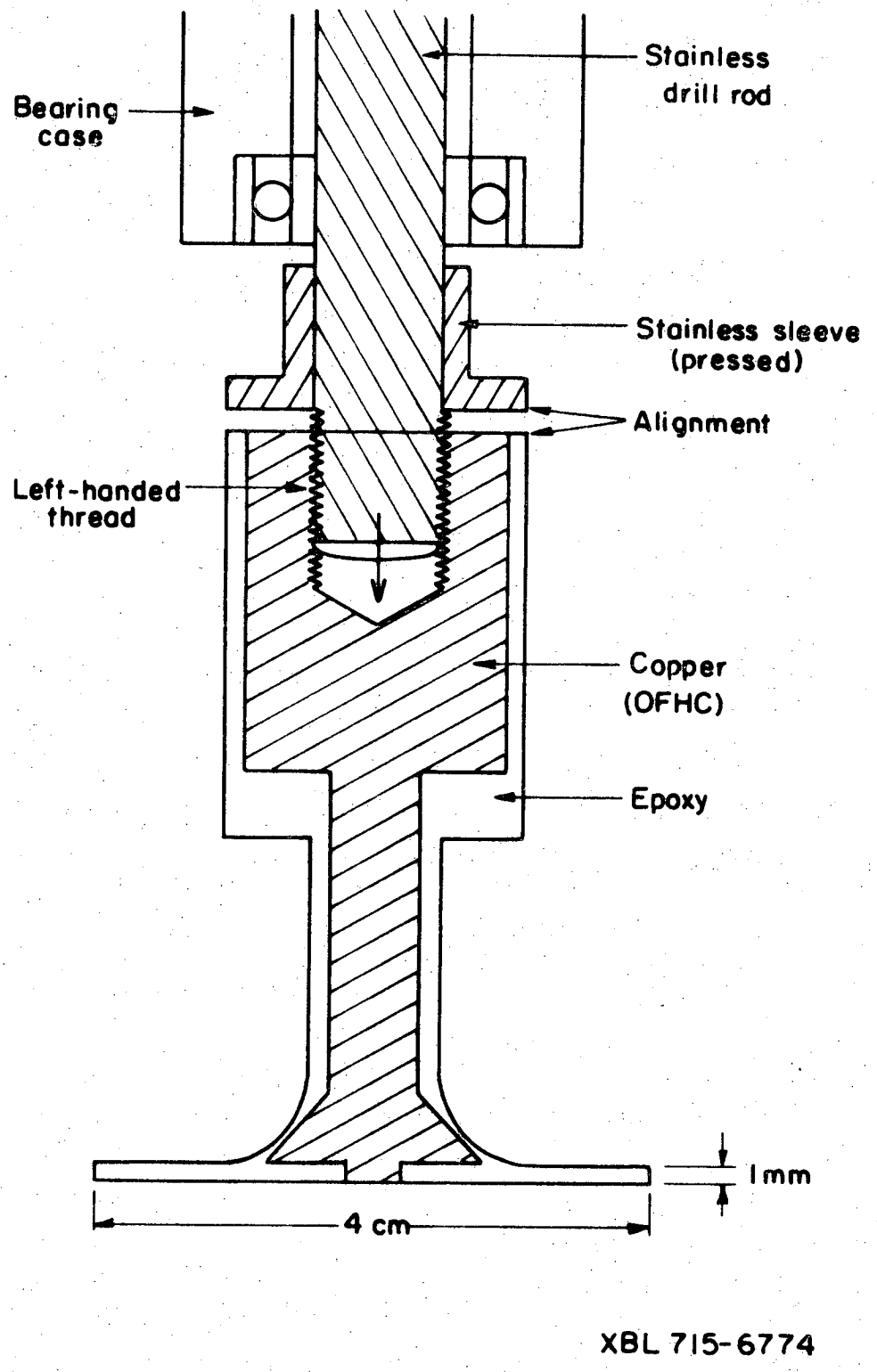

Fig. 3.1. Rotating disk and lower end of spindle assembly.

The disk was polished by hand before each measurement, either on a glass plate or on a polishing wheel. A slight deviation from perpendicularity between disk surface and spindle axis usually developed in the course of time. When this deviation was larger than approximately 1° the limiting current curves would be severely affected, giving irreproducible and usually too high results. The disk was then machined down and re-cast. The conical shape of the copper rod near the disk surface (Figure 3.1) was found to help maintain perpendicularity since it stiffens the epoxy disk and acts as a heat sink in wheel polishing.

As shown in Figure 3.2, the disk was submerged in approximately 1.25 ℓ of solution contained in a cylindrical cell of lucite. The bottom of the cell accomodated a circular copper anode of 7.5 cm diameter. The reference electrode of copper (OFHC) was inserted in a glass compartment connected by capillary to the main cell. The capillary emerged in the bulk solution 0.5 cm from the outer edge of the disk, in the plane of the disk.

The cell was submerged in a constant temperature bath kept at 25.0 $\pm$ 0.1°C. Temperature variations in the cell were occasionally larger, due to frequent exchanging of the disk. All recorded currents were corrected for deviations from 25.0°C, by a temperature coefficient $(di/dT)/i = +0.02°C^{-1}$.

B. Electrical circuit

In the galvanostatic series of measurements the current source was a model 28 Lambda Electronics Corp. regulated power supply. A Keithley Electrometer (model 610R) was used to measure the current, in conjunction with an x-y recorder (F. L. Moseley Co. model 4B) to plot

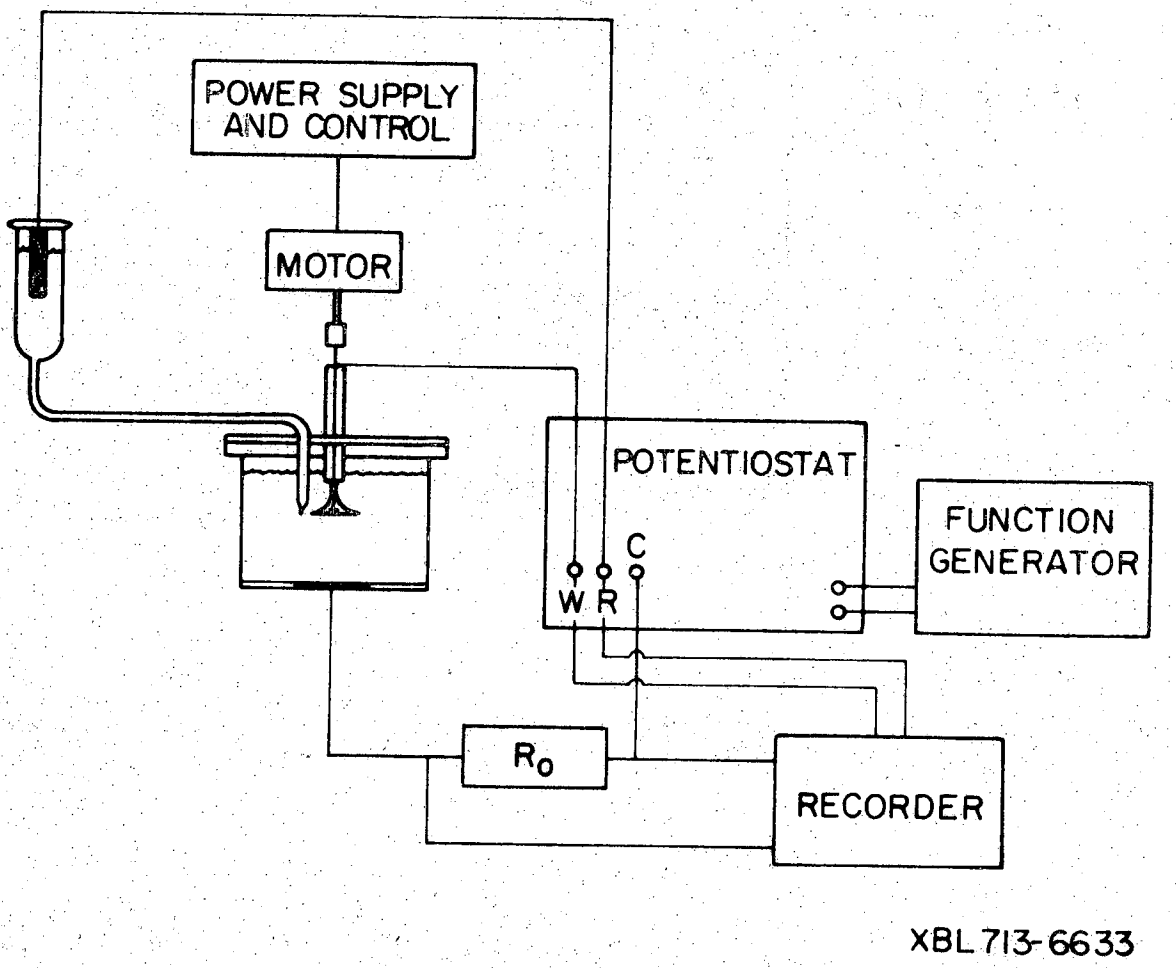

Fig. 3.2. Schematic of the rotating disk apparatus and associated equipment.

current vs. overpotential. In the potentiostatic series of measurements a Wenking 61 RH potentiostat was used and the current was recorded as a potential difference over a known resistance R_o (Figure 3.2), by a Brown-Honeywell Electronik 19 Recorder.

Potential control was manual or by means of a digital function generator designed to give a signal of up to 6 v in 4095 steps (or a binary fraction), in a total time variable between 1/128 sec and 12,800 sec. The time-scale of the strip-chart recorder was calibrated so that potentials could be read in slow scans. The electrical connection to the rotating disk electrode was accomplished by means of a mercury well. The resistance between the cathode surface and the terminal of the potentiostat was less than .5Ω.

C. Analysis and physical properties of the solutions

Solutions were prepared using A.R. $CuSO_4 \cdot 5H_2O$ and H_2SO_4. $CuSO_4$ concentration was varied from 0.01 to 0.64 M; H_2SO_4 concentration from 0.3 to 2.5 M. Oxygen was excluded from the solutions by purging with nitrogen. Particular care was taken with solutions very dilute in $CuSO_4$.

The $CuSO_4$ concentration was analyzed by electrogravimetry, using platinum gauze electrodes, or by titration with EDTA, using murexide as an indicator. The acid was titrated with NaOH potentiometrically (end-point pH 4.5 to 5.5). Characteristic aspects of the titration curve have been discussed elsewhere.[155]

The density and kinematic viscosity of all solutions were determined by standard methods, using bulb pycnometers and Ubbelohde type viscometers. The refractive index for sodium d-light (5893 Å) was also measured, by means of an Abbe refractometer.

The experimental accuracy of these measurements is estimated to be:

density $\pm$ 0.0002 g/ml

kinematic viscosity $\pm$ 0.002 cst

refractive index $\pm$ 0.0001

$CuSO_4$ concentration $\pm$ 0.001 M

H_2SO_4 concentration $\pm$ 0.01 M

D. Surface treatment

Near the limiting current the copper deposit is characterized by local dendritic growth and creates a very rough surface (see below for some qualitative observations). Therefore, as a rule, the disk was removed after each measurement, or series of measurements, at one rotation speed. The disk was then polished with increasingly fine grades of silicon carbide or emery paper until all traces of the previous deposit, which often persisted as a waviness resembling the texture of orange skin, had disappeared. The disk was then further polished on a glass plate or on a polishing wheel, using lens powder (0.3 μ grain aluminum oxide) or diamond paste (1 μ grain). The maximum scratch on the surface was then 1 μ or less. The disk was next thoroughly washed with carbon tetrachloride or ethanol.

After rinsing with distilled water and with acidified cupric sulfate solution, the disk was immediately screwed on to the spindle shaft and submerged in the solution. The shaft was kept running during this operation to prevent air bubbles from sticking to the disk, although an occasional small bubble at the electrode did not seem to lower the limiting current significantly.

The reference electrode and the anode were etched briefly in nitric acid, then rinsed with distilled water and acidified cupric sulfate solution before being inserted.

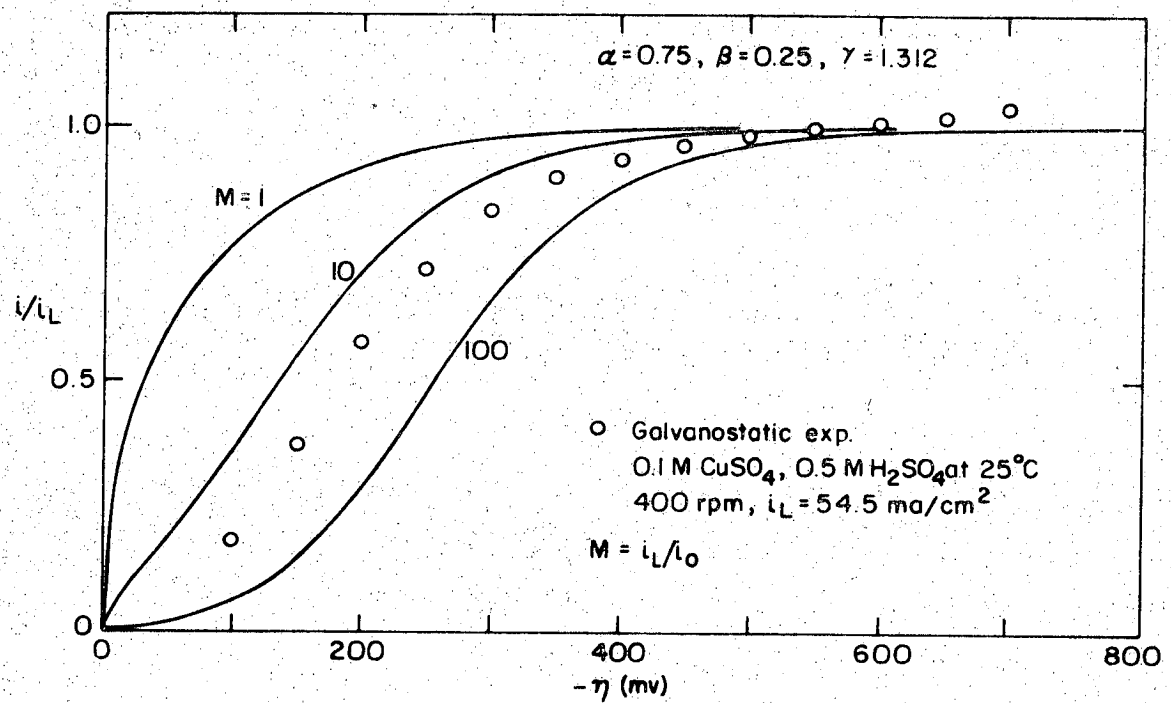

Fig. 3.3. Typical galvanostatic limiting current curve (circles). Solid curves are calculated using $\alpha = 0.75$, $\beta = 0.25$, $\gamma = 1.312$, $N' = 0$, M as indicated.

3.3 Results

A. Galvanostatic measurements

In a first series of measurements the limiting current was approached galvanostatically. The current was increased in steps, the increments being initially large but decreasing after the overpotential reaches 300 to 400 mv. The time allowed after each step for the potential to reach a steady value was approximately 5 seconds or longer. The total time to reach the limiting current was approximately 60 sec. Figure 3.3 shows an example of a galvanostatic curve (dots).

The limiting current was taken to be the current value at the inflection point, which occurred between -500 and -700 mv overpotential. In particular for rotation rates above 300 rpm and for solutions more concentrated than 0.1 M $CuSO_4$, the limiting current plateau was only distinguishable as an inflection point.

The linear dependence of the limiting current on the square root of the rotation rate is shown, for a number of solutions, in Figure 3.4. Multiple points at one speed represent measurements in which the electrode was not re-polished. In such cases care was taken not to exceed the limiting current by more than one or two percent. As expected the change in limiting current value compared to the first measurement is cumulative and depends strongly on the level of the limiting current. In concentrated solutions and at high rotation rates the passage to the limiting current was therefore made as quickly as compatible with potential equilibrium after every step. The shortest total time was 12 seconds. A marked

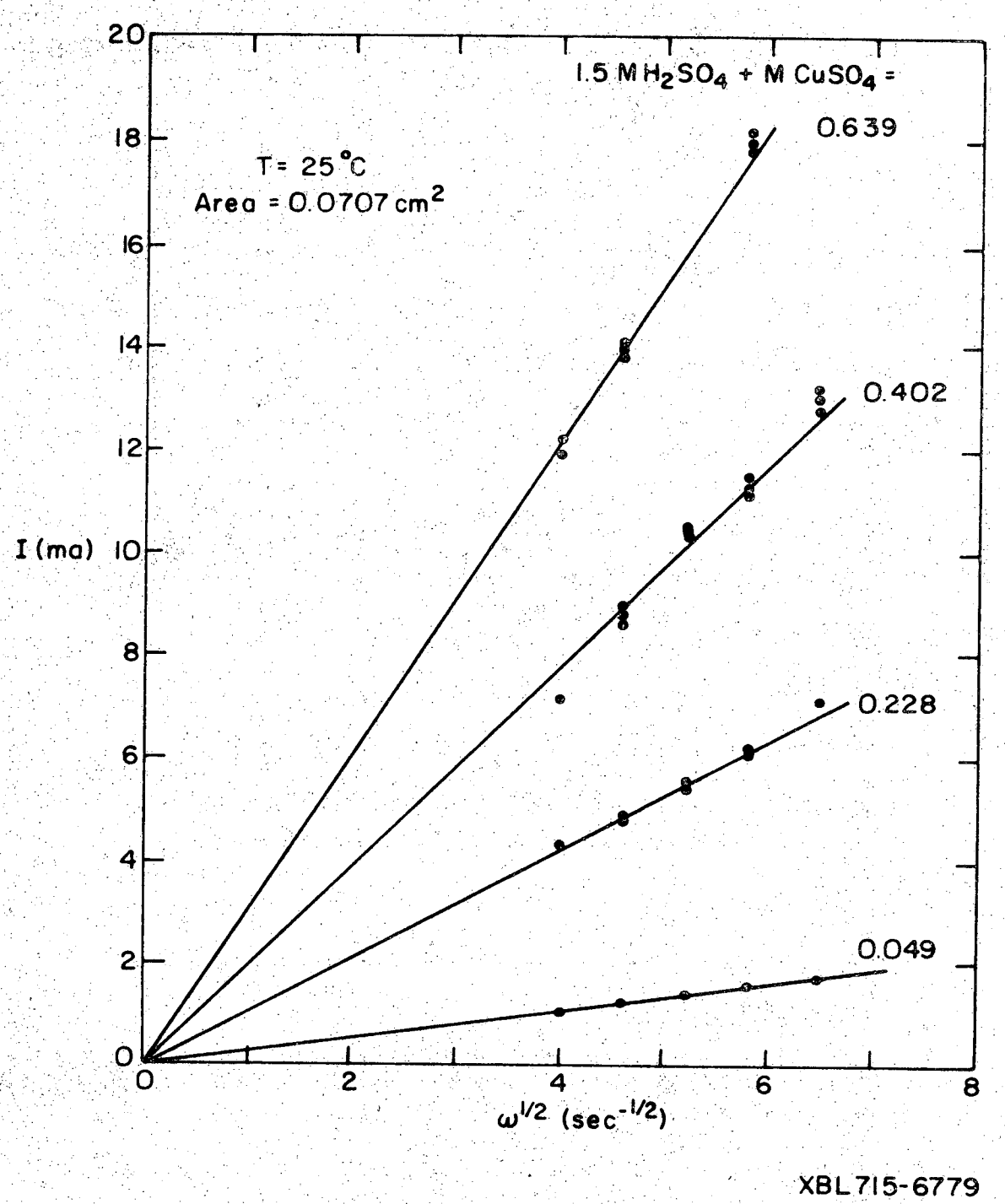

Fig. 3.4. Dependence of limiting current on square root of rotation rate, for selected galvanostatic measurements.

improvement in the quality of the plateau was observed when the passage to the limiting current was shortened.

The least squares slope through the origin was obtained for all solutions using the first, or the first 2, measurements at each speed. The diffusivities calculated according to (3) are collected in Table 3.1, together with the other physical properties.

As can be inferred from Figure 3.4, the spread of the data for one particular solution was rather large and the standard error of the slope through the origin is of the order of 2-3 %. The uncertainty in D is then of the order of 5%.

Further, it appeared that even though the passage to the limiting current was fairly rapid in the concentrated solutions, the limiting current level was still affected by the deposit. Lease-squares slopes, if not forced through the origin, show a negative intercept. As mentioned above, at high limiting current levels the plateau is only preserved if the time of passage is short. If the deposit roughness, though barely visible at 10 x magnification, does affect these galvanostatic measurements, a marked dependence on the $CuSO_4$ bulk concentration should exist.

Figure 3.5 shows that this is indeed the case. The mobility product $\mu D/T$ depends much more strongly on the $CuSO_4$ concentration than on the H_2SO_4 concentration. For comparison some diaphragm cell diffusivities of Cole and Gordon are also shown, as well as the values predicted by Fenech's correlation (1). The weak concentration dependence of the latter is in agreement with expectations (see Discussion, section 3.4), but it is clear that, at least for those solutions that are $\leq$ 0.1 M in

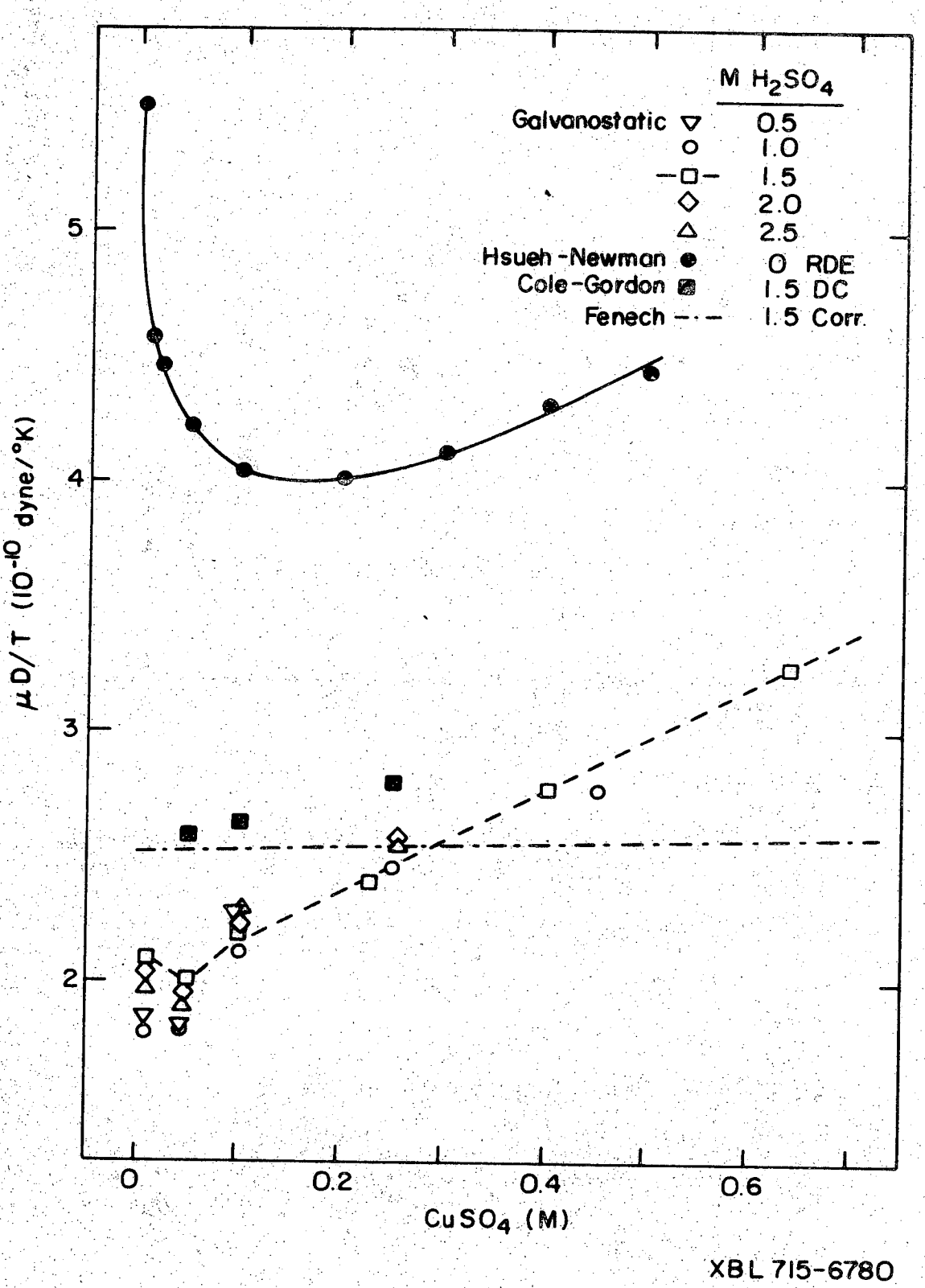

Fig. 3.5. Dependence of Cu^{++} diffusivity (from galvanostatic limiting current measurements) on $CuSO_4$ concentration.

Table 3.1. Rotating disk integral diffusivities of Cu^{2+}-ion (from galvanostatic measurements) and other physical properties of $CuSO_4$-H_2SO_4-H_2O at 25°C.

#	$CuSO_4$	H_2SO_4	ρ	$\nu x10^2$	$Dx10^6$	$i_{lim}/\sqrt{\omega}$	$\mu Dx10^{10}/T$	n_D
	M	(M)	(g/ml)	(cm^2/sec)	(cm^2/sec)	($masec^{1/2}/cm^2$)	(dyne/°K)	
A9	0.0093	0.476	1.0298	0.954	5.61	0.766	1.848	
A2	0.00956	0.980	1.0612	1.018	4.98	0.718	1.804	
A4	0.00976	1.469	1.0917	1.086	5.21	0.747	2.072	
A11	0.00947	1.946	1.157	1.157	4.67	0.666	2.030	
A13	0.00943	2.434	1.1489	1.238	4.11	0.602	1.960	
A10	0.0460	0.492	1.0361	0.968	5.42	3.68	1.823	
A3	0.0461	0.991	1.0670	1.032	4.86	3.39	1.820	
A5	0.0488	1.463	1.0968	1.098	4.93	3.59	1.991	
A12	0.0462	1.936	1.1252	1.172	4.41	3.12	1.951	
A14	0.0466	2.420	1.1547	1.264	3.88	2.86	1.869	
A39	0.0967	0.500	1.0438	0.987	6.56	8.77	2.269	1.3413
A15	0.1017	1.003	1.0760	1.070	5.48	8.06	2.115	1.3461
A40	0.0997	1.253	1.0892	1.084	5.68	8.09	2.248	1.3488
A16	0.1031	1.514	1.1086	1.134	5.16	7.78	2.175	1.3513

Table 3.1. (continued)

#	$CuSO_4$	H_2SO_4		$\nu x10^2$	$Dx10^6$	$i_{lim}/\sqrt{\omega}$	$\mu Dx10^{10}/T$	n_D
	M	(M)	(g/ml)	(cm^2/sec)	(cm^2/sec)	($masec^{1/2}/cm^2$)	(dyne/°K)	
A41	0.1001	1.769	1.1201	1.164	5.04	7.40	2.203	1.3537
A17	0.1024	2.013	1.1378	1.210	4.82	7.31	2.226	1.3592
A42	0.1015	2.551	1.1658	1.296	4.52	6.85	2.291	1.3610
A6	0.2273	1.457	1.1227	1.115	5.38	17.5	2.384	
A18	0.2520	0.995	1.0973	1.177	5.98	21.0	2.455	1.3493
A19	0.2565	2.006	1.1585	1.285	5.14	18.9	2.569	1.3593
A20	0.2561	2.535	1.1900	1.390	4.59	17.3	2.546	1.3654
A7	0.4018	1.464	1.1486	1.266	5.66	31.7	2.760	
A21	0.4536	0.988	1.1271	1.212	6.03	37.5	2.763	1.3554
A8	0.6394	1.468	1.1835	1.408	5.81	50.4	3.246	

Table 3.2.A. Rotating disk integral diffusivities of $CuSO_4$ in H_2O, at 25°C.

$CuSO_4$ (M)	ρ** (g/ml)	μ*** (cp)	$Dx10^6$ (cm^2/sec)	$i_{lim}/\omega^{1/2}$ * ($masec^{1/2}/cm^2$)	$\mu Dx10^{10}/T$ dyne/°K
0	0.997	0.890	18.45		5.50
0.00998	0.999	0.898	15.19	1.608	4.58
0.01986	1.0007	0.902	14.75	3.135	4.46
0.04969	1.0055	0.920	13.68	7.443	4.22
0.1000	1.0135	0.955	12.63	14.13	4.04
0.2000	1.0290	1.02	11.72	26.66	4.01
0.2985	1.0444	1.09	11.23	38.34	4.11
0.4000	1.0602	1.16	11.06	50.47	4.30
0.4989	1.0756	1.24	10.67	61.07	4.44

*from Ref. 96 (Table 2.3)

**from Ref. 139 (Figure 2.3)

***from Ref. 140

B. Diaphragm cell diffusivities of $CuSO_4$ in $CuSO_4$-H_2SO_4-H_2O, at 18°C. (after Cole and Gordon[141]).

$CuSO_4$ (M)	H_2SO_4 (M)	μ* (cp)	$Dx10^{6**}$ (cm^2/sec)	$\mu Dx10^{10}/T$ dyne/°K
0.05	1.5	1.44	5.21	2.58
0.10		1.48	5.15	2.63
0.25		1.61	5.02	2.78

*from Ref. 97.

**from Fig. 8 of Ref. 141.

$CuSO_4$, the predicted values are too high by as much as 20%. This is in agreement with the conclusions of Wragg and Ross.[63]

The values of the binary $CuSO_4$ diffusivities are also shown, but as integral diffusivities according to (3) where i_{lim} includes the migration contribution (Table 3.2).

The migration contribution to the limiting current is at least partly responsible for the dependence of $\mu D/T$ on the $CuSO_4$ concentration. This will be considered below in more detail. To investigate whether the deposit effect could be eliminated more completely, a second series of measurements were made, using potentiostatic current control.

An interesting observation made during the galvanostatic measurements was that the building up of the deposit does not always lead to an increased limiting currents. When measurements at one particular speed were repeated without re-polishing the disk, the limiting current in concentrated solutions ($\geq$ 0.25 M) would usually increase; in solutions of $\geq$ 0.05 M $CuSO_4$ a slight decrease (approximately 1%) was observed in the next two or three measurements. Eventually the electrode surface becomes very rough and the current increases again.

B. Potentiostatic measurements: potential scan

In these measurements the limiting current was at first approached by potential scanning. The potential scan rate was -32 or -40 mv/sec. The limiting current was thus reached in 20 to 25 seconds. This rate was chosen after preliminary experiments with various rates, in order to minimize non-stationary mass transfer effects (see Chapter 4). Typical limiting current curves are shown in Figure 3.6. The rotation rates were varied over a larger range, from 60 to 1200 rpm. The solutions employed

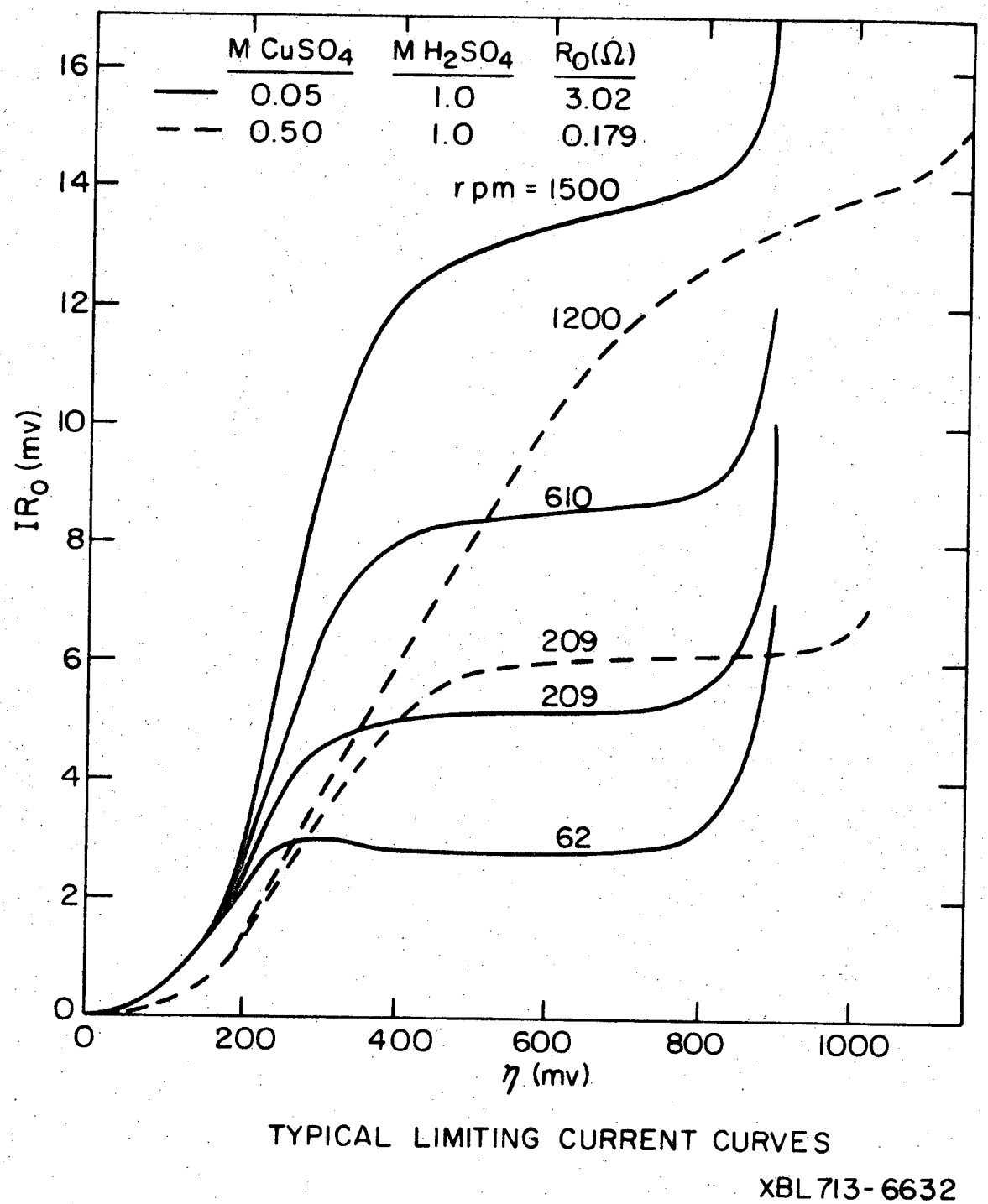

Fig. 3.6. Typical potentiostatic limiting current curves. (R_o = resistance of measuring resistor).

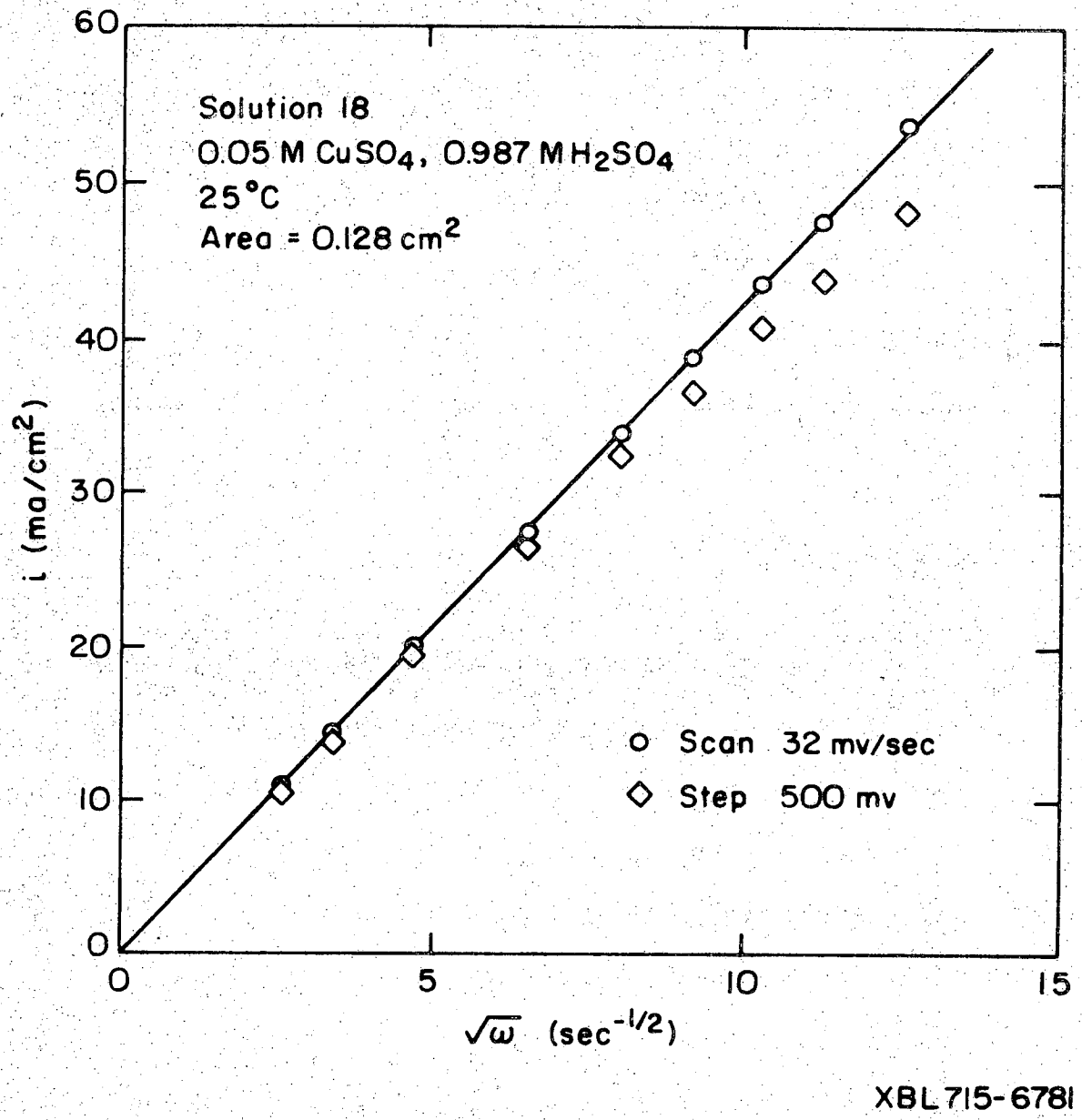

Fig. 3.7. Dependence of limiting current on square root of rotation rate, for a typical potentiostatic measurement. Dots indicate current at the inflection point, diamonds current after transition-time (3.6) to steady-state, following a potential step to-500 mv.

were not identical with those of part A. They were generally of a higher $CuSO_4$ concentration, so that the deposit and migration effect would be more prominent.

The potentiostatic curves show a plateau only at low current levels. At higher current levels the plateau appears to become shorter and increasingly tilted, but the potential at which hydrogen ion reduction starts to increase the current, is still recognizable. The potential of this inflection point depends of course on the acidity of the solution, but it also appeared to depend on the rotation speed and on the $CuSO_4$ concentration of the solution, i.e., on the amount of deposit (Table 3.3). This behavior had already been found in the galvanostatic measurements, but there the inflection potentials were, in general, less negative than in the present measurements.

It was also clear from visual inspection that at the potentiostatic inflection point the copper deposit had become quite rough (dendritic), while in the galvanostatic measurements the surface is still relatively smooth if the current passage is terminated at the point of inflection.

Therefore, although the currents at the inflection point were surprisingly linear with the square root of the speed (Figure 3.7), they were not limiting currents corresponding to the smooth electrode area. This was also obvious from a comparison with galvanostatic limiting currents (Table 3.3). The difference in current level at the inflection point appeared to be related to the amount by which the potential was more negative at the potentiostatic inflection points.

Table 3.3. Potentials and currents at the inflection point in acidified 0.05 M $CuSO_4$ solutions.

	inflection point potential (mv)				Ratio of
	(A) potential scan			(B) galvanostatic	currents
rpm	200	600	1200	260	A/B
M H_2SO_4					
0.5	760	780	810	660	1.20
1.0	700	750	775	660	1.16
1.5	650	675	750	650	1.03
2.0	600	650	725	600	1.06
2.5				580	

C. Potentiostatic measurements: potential step

To avoid the effect of deposit roughness on the limiting current, a potential step to the limiting current would be most effective. Two difficulties are associated with this procedure: 1. the potential necessary to reach the limiting current depends on the rotation speed; 2. a certain transition time has to elapse to avoid unsteady-state mass transfer. These points will be considered in more detail.

Ad 1. Potential range of the limiting current.

From galvanostatic as well as potential-scan curves it is evident that the limiting current plateau shifts to higher potentials as the limiting current level becomes higher. This is an indication that the reaction kinetics of the copper deposition reaction contribute an appreciable surface overpotential to the total overpotential. The approach to the limiting current plateau is thereby made more gradual. Under certain simplifying assumptions the steady-state limiting current curve can be constructed (see Chapter 2.2), and in particular it can be shown that for well-conducting solutions the approach to the plateau depends on two parameters: the relative magnitude of limiting current and exchange current density ($M = i_{lim}/i_o$), and the cathodic transfer coefficient β (Figure 2.6)

The potential step to be applied was therefore based on the expectations according to this model. The exchange current density was estimated from some of the galvanostatic curves (e.g., Figure 3.3), by means of the potential at half the limiting current (equation 2.42). If the value of β was assumed to be 0.25, the average i_o was approximately 2 ma/cm^2 for a solution of 0.1 M $CuSO_4$. This is somewhat below the values found in

electrode-kinetic studies using extremely pure solutions.[134,138]

Since the parameter M varied between 10 and 500 for the range of concentrations (0.05-0.5 M $CuSO_4$) and rotation rates (100-1200 rpm) in this work, the potential step was set at -500 mv. This is large enough to ensure a near-limiting current even in the most concentrated solutions, and is below the minimum potential for hydrogen evolution even at the lowest current levels.

Ad 2. Mass-transfer transition time.

A large enough potential step applied to a cathode would cause the initial current to be infinite if the reactant concentration at the electrode were to become instantaneously zero at the electrode. Actually the current excursion is limited because the measured over-potential contains an ohmic contribution and a surface overpotential. Both of these retard the initial concentration drop at the electrode.

On the other hand, the time necessary to reach steady-state conditions is determined primarily by the diffusion mechanism. It may, however, be dependent on the level of the initial current, i.e., on reaction kinetics and ohmic resistance.

At a rotating disk electrode convection reinforces the diffusion process. A complete solution of the current response to a potential step at the surface would therefore be quite complicated.

Since we are here only interested in the duration of the non-stationary process, let us assume that it is determined only by the convective-diffusion process. This is the case if the time-period during which the reactant concentration at the electrode has not yet reached a virtual zero value, is very short compared to the total transition time.

For a large potential step (to $\phi = -\phi ZF/RT$) at a cathode in a stagnant medium, Gerischer and Vielstich[143] give the characteristic time-period:

$$t_1 = \frac{Dc_\infty^2 n^2 F^2}{i_o^2 e^{-2\beta\phi}} = \frac{De^{2\beta\phi}}{k^2} \qquad (3.4)$$

At times $>> t_1$ the current is the same as if the concentration at the electrode had been zero from the beginning. For the copper deposition reaction and a potential step to -500 mv, t_1 has a value of the order of 10^{-5} sec.

On the other hand, it can be expected that at very short times the concentration transients at a rotating disk electrode approach those in a stagnant solution, since the concentration change takes place so close to the surface. A numerical solution for the case of a high Schmidt number shows that, up to a characteristic time-period

$$t_2 = 0.16\ Sc^{1/3}\ \omega^{-1} \quad , \qquad (3.5)$$

the flux response to a concentration step at the disk surface is, within 1%, identical with that in a stagnant medium. (See Appendix B and Figure B.1)

The period t_2, for solutions of Sc ~ 2000 and rotation rates between 200 and 1200 rpm, is of the order of 10^{-1} sec or higher. We can therefore safely use the convective-diffusion transition times to a flux within 1% of the steady-state value. According to the numerical solution given in Appendix B, this transition time is:

Table 3.4. Transition times for mass-transfer at a rotating disk (in sec).

ω	conc. step[7]		current step[2]	
(rpm)	Sc	Sc	Sc	Sc
	2000	5000	2000	5000
50	4.94	8.45	13.16	22.50
100	2.47	4.23	6.58	11.25
400	0.62	1.05	1.64	2.81
1600	0.15	0.26	0.41	0.70

1 $\tau = \omega t/Sc^{1/3} = 2.05$ at $i/i_{ss} = 1.01$ (eq. 6)

2 $\tau = \omega t/Sc^{1/3} = 5.46$ at $(c_{el}-c_b)/(c_{el,ss}-c_b) = 0.99$

(Ref. 154)

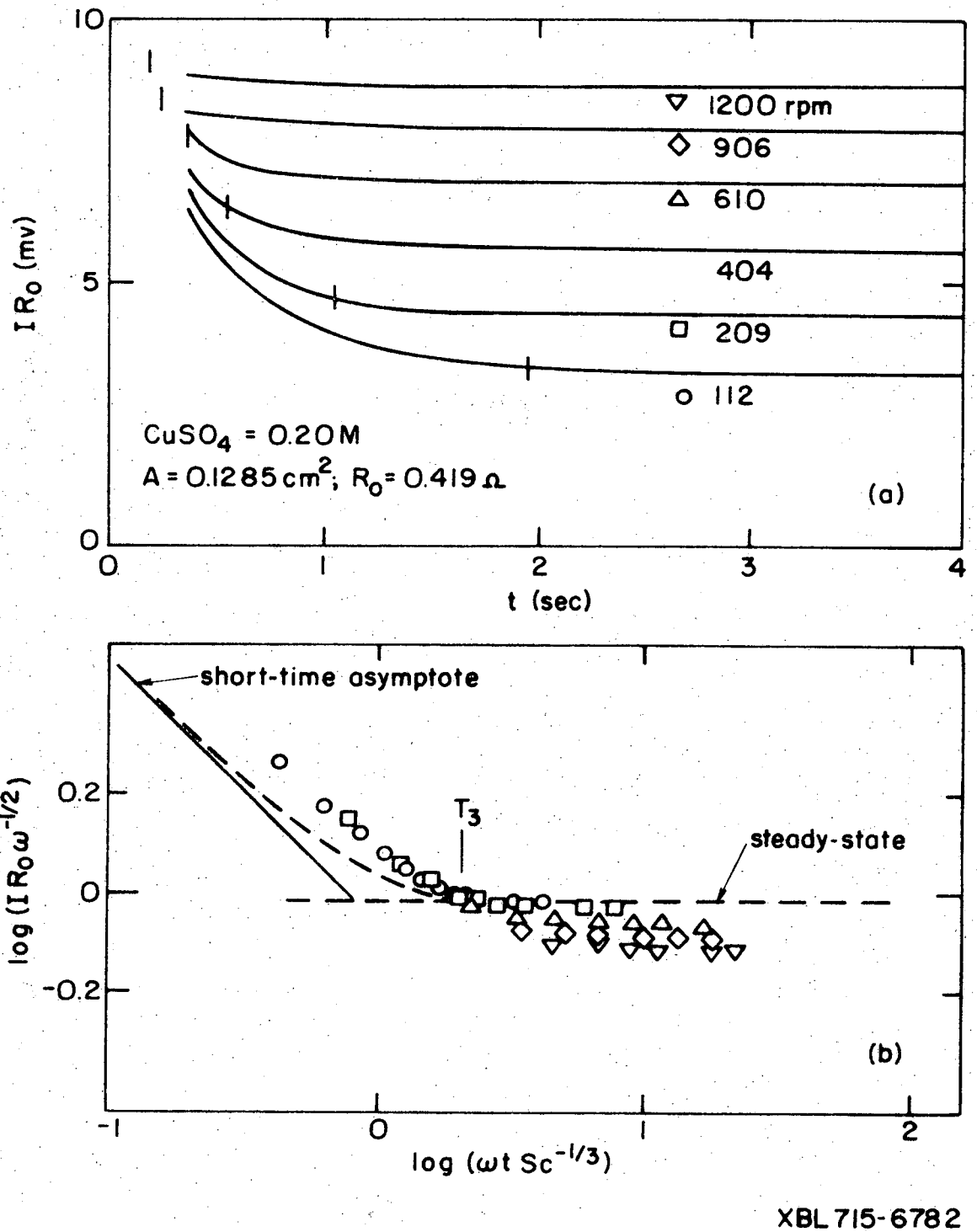

Fig. 3.8. Transition following a potential step to-500 mv, for various rotation rates as indicated (part a). In part (b) the various curves are combined into one, using $i\omega^{-1/2}$ and a dimensionless time τ. R_o=value (Ω) of precision resistance (Fig. 3.2) vertical marks in (a) correspond to $\tau_3(3.6)$.

$$t_3 = 2.05\ Sc^{1/3}\ \omega^{-1} \quad . \qquad (3.6)$$

The Sc number necessarily has to be estimated a priori, but t_3 is not very sensitive to its value.

Using a potential step to -500 mv and observing a transition time according to (6), the current was now measured again for all solutions, at various rotation rates. Before the potential step was applied, the disk electrode was plated at 200 rpm and at a constant current of approximately 10%, or less, of the limiting current (50 ma-min/cm^2, i.e., approximately 1 μ thickness).

The currents were satisfactorily linear with the square root of rotation speed, except above 600 rpm where they appeared to be low (Figure 3.7). From Figure 3.8 it can be seen that this is due to 1. The limited response-time of the recorder; 2. the fact that the current does not reach a steady value after the transition time (6), but keeps decreasing for several more seconds (apparently depending on the current level). For dilute solutions a fairly steady value establishes itself, while in concentrated solutions the current starts to increase again, apparently due to roughness. Ibl and Schadegg[150] have observed a similar behavior: even at 2000 rpm the current decrease lasts for approximately 30 sec. From impedance measurements they concluded that at currents close to, but below, the limiting current a surface smoothing or re-crystallization takes place during several minutes. The consequences of this extended transition-time will be discussed below. For the calculation of diffusivities it is assumed that the currents measured after

Table 3.5. Rotating disk integral diffusivities of Cu^{2+}-ion (from potentiostatic measurements) and other physical properties at 25°C.

#	$CuSO_4$ (M)	H_2SO_4 (M)	ρ (g/ml)	$\nu x10^2$ (cm^2/sec)	$Dx10^6$ (cm^2/sec)	$i_{lim}/\sqrt{\omega}$ ($masec^{1/2}/cm^2$)	$\mu Dx10^{10}/T$ (dn/°K)	n_D
B11	0.0500	0.492	1.0358	0.968	6.71	4.62	2.259	1.3391
B18	0.0498	0.987	1.0651	1.024	5.57	4.021	2.040	1.3443
B13	0.0499	1.493	1.0957	1.095	4.74	3.578	1.907	1.3492
B12	0.0502	2.013	1.1261	1.171	4.61	3.494	2.038	1.3543
B8	0.0992	0.496	1.0435	0.988	6.98	9.365	2.413	1.3404
B5	0.1017	1.008	1.0744	1.052	6.07	8.656	2.300	1.3457
B6B	0.2043	0.498	1.0594	1.022	7.34	19.79	2.657	1.3432
B4	0.2005	0.992	1.0882	1.091	5.67	16.21	2.256	1.3481
B10	0.2956	0.295	1.0619	1.041	7.33	28.58	2.715	1.3435
B7	0.2998	0.494	1.0737	1.064	8.01	30.64	3.068	1.3455
B2A	0.3158	1.011	1.1062	1.141	6.10	26.61	2.581	1.3509
B14	0.2950	1.492	1.1318	1.204	6.66	26.12	3.044	1.3549
B15	0.2990	2.020	1.1625	1.299	6.02	24.44	3.048	1.3599
B16	0.4002	0.991	1.1178	1.177	6.71	35.74	2.961	1.3527
B1	0.5001	0.997	1.1320	1.235	7.25	46.65	3.398	1.3550

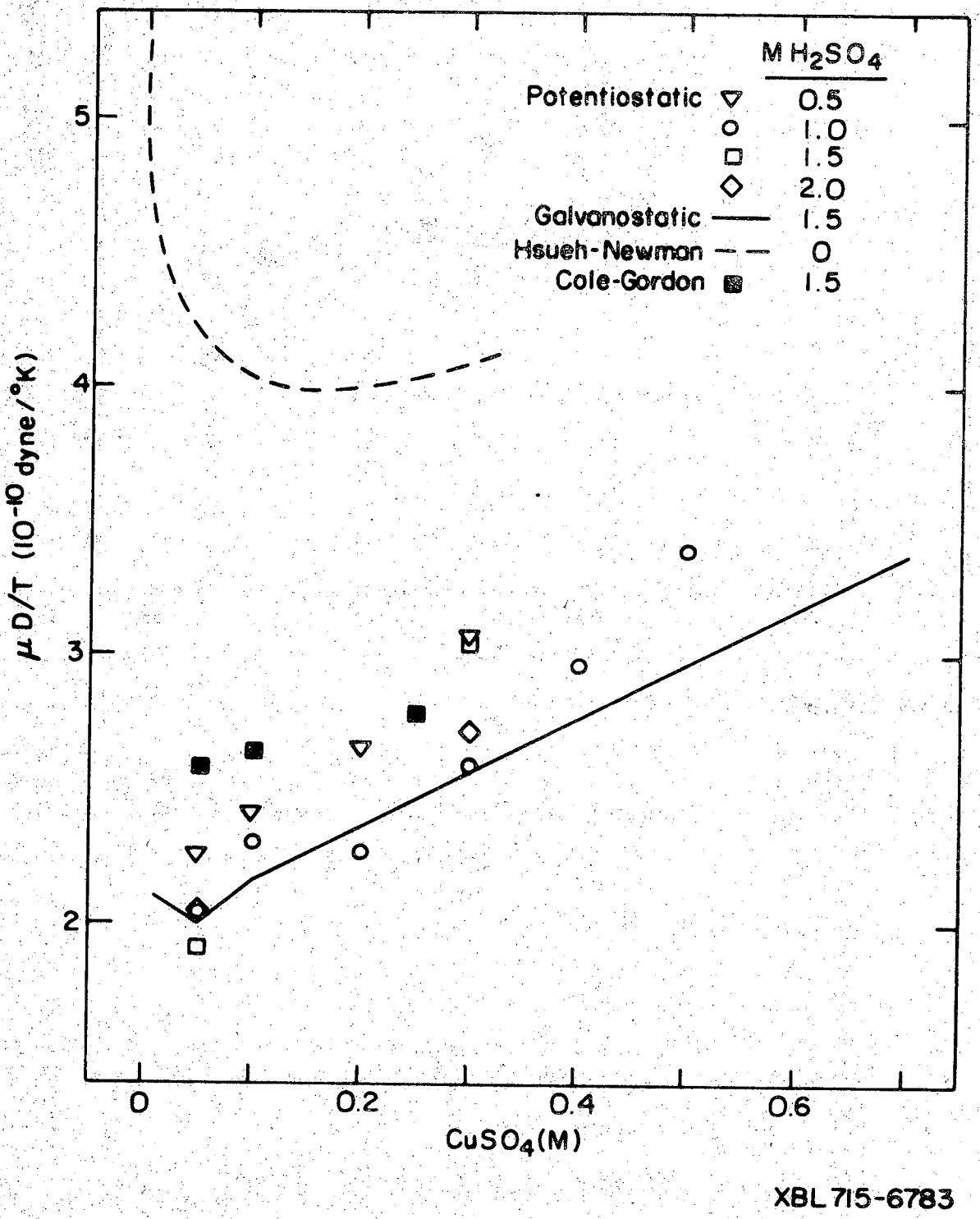

Fig. 3.9. Dependence of Cu^{++} diffusivity (from potentiostatic limiting current measurements) on $CuSO_4$ concentration.

the transition time (6) are actual limiting currents corresponding to the measured surface area.

Table 3.5 gives the integral diffusivities from these potential-step measurements. In Figure 3.9 the mobility product is plotted against the $CuSO_4$ concentration. The dependence on this concentration is comparable to that in the galvanostatic measurements, although the values themselves are generally higher. Also, the spread in the data is larger.

3.4. Discussion: Migration Effect

The diffusivities calculated from the galvanostatic and potentiostatic measurements can be corrected for the effect of migration if some assumptions are made concerning the degree of dissociation of HSO_4^- ions. The few experimental data available concerning the composition of the electrolyte at the cathode, in free convection and in pure diffusion, suggest that the HSO_4^- ion is almost completely dissociated. Since the dissociation constant of HSO_4^- ion in very dilute solutions is small (K_B = 0.0104 at 25°C), the apparently almost complete dissociation in concentrated solutions is due to the low activity coefficient of H^+ and $SO_4^=$ ions:

$$K_B' = K_B f_{HSO_4^-} / f_{H^+} f_{SO_4^=} \qquad (3.7)$$

where K_B' is the stoichiometric dissociation "constant" and K_B the thermodynamic (true) constant. From spectroscopic data on H_2SO_4 solutions it is known that K_B' varies by 3 orders of magnitude as the concentration increases from 0 to 3 M.

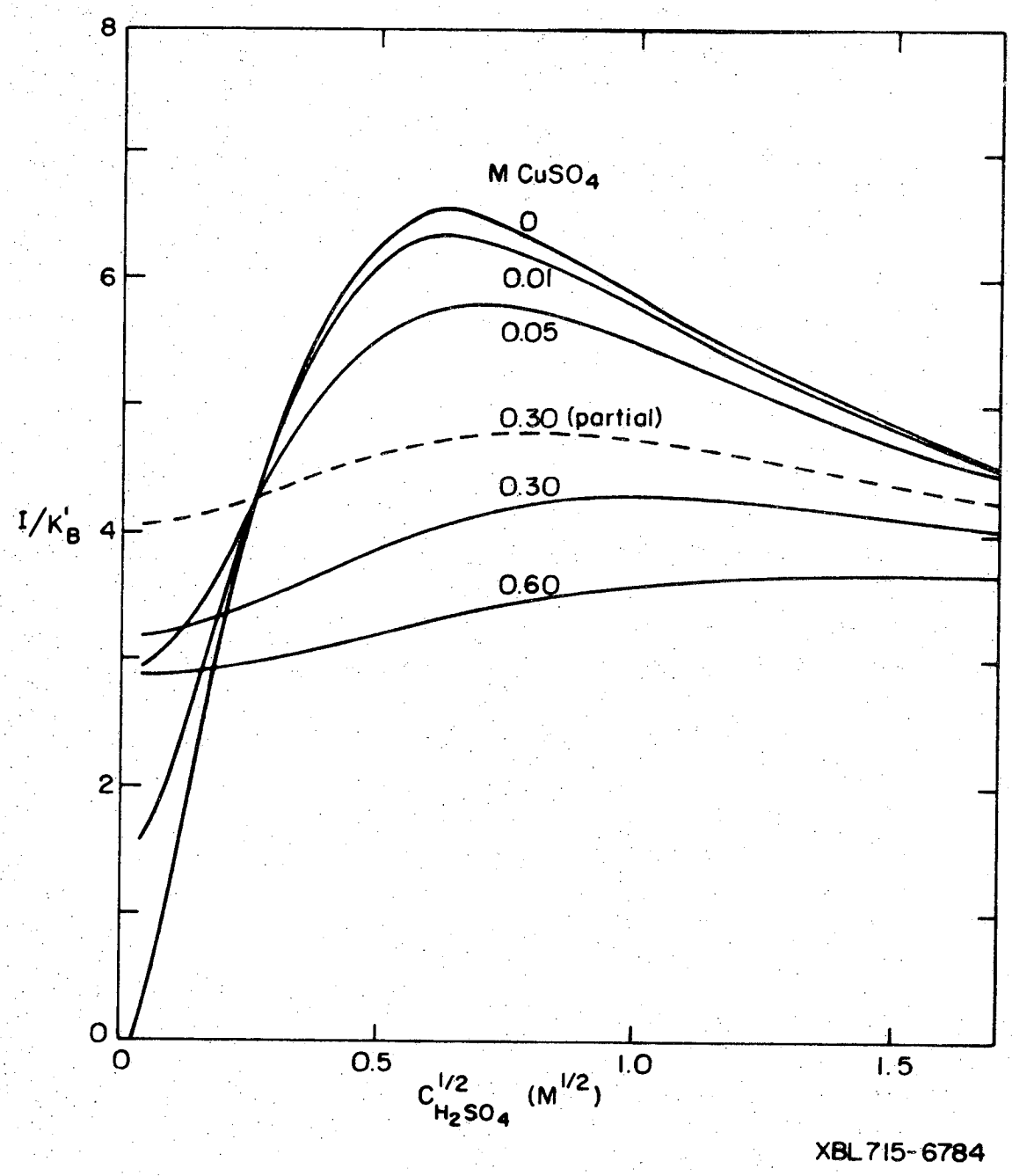

Fig. 3.10. Degree of dissociation of HSO_4^- ion (expressed as I/K'_B) as a function of H_2SO_4 concentration, for various $CuSO_4$ concentrations. Complete dissociation of $CuSO_4$ is assumed, except for 0.30 M (dashed line) where the effect of partial association is also shown.

Since the presence of bisulfate ions, even in small amount, increases the migration current of Cu^{2+} ions considerably, it is important to establish the degree of dissociation of the bisulfate ions more accurately. Hsueh and Newman have correlated the results of spectroscopic investigations of dissociation in aqueous H_2SO_4 solutions as follows:

$$\ell n(K_B'/0.0104) = \frac{5.29\sqrt{I_r}}{1 + 0.56\sqrt{I_r}} \quad , \qquad (3.8)$$

where I_r is the true ionic strength (in mole/ℓ).

Assuming that this relationship holds also in solutions containing $CuSO_4$ in addition to H_2SO_4, the degree of dissociation can be calculated and expressed in terms of the parameter I/K_B', which is dimensionless (I is the stoichiometric ionic strength). The method of calculation is given in Appendix C. Figure 3.10 presents I/K_B' as a function of $CuSO_4$ and H_2SO_4 concentration. The value of I/K_B' is close to 5 for the range of compositions (0-0.5 M $CuSO_4$, 0.5 - 3 M H_2SO_4) used in limiting current experiments.

The contribution which migration makes to the limiting current at a rotating disk has been computed by Newman and Hsueh for I/K_B' values of 0 (complete dissociation of HSO_4^-), 10,100 and ∞ (HSO_4^- undissociated). Additional computations have been made for $I/K_B' = 5$; for the details see Appendix D. Figure 3.11 shows the ratio of limiting current to limiting diffusion current vs. the ratio of H_2SO_4 to total electrolyte concentration. The migration contribution is approximately two times that in the case of complete dissociation of HSO_4^- (Table 3.6).

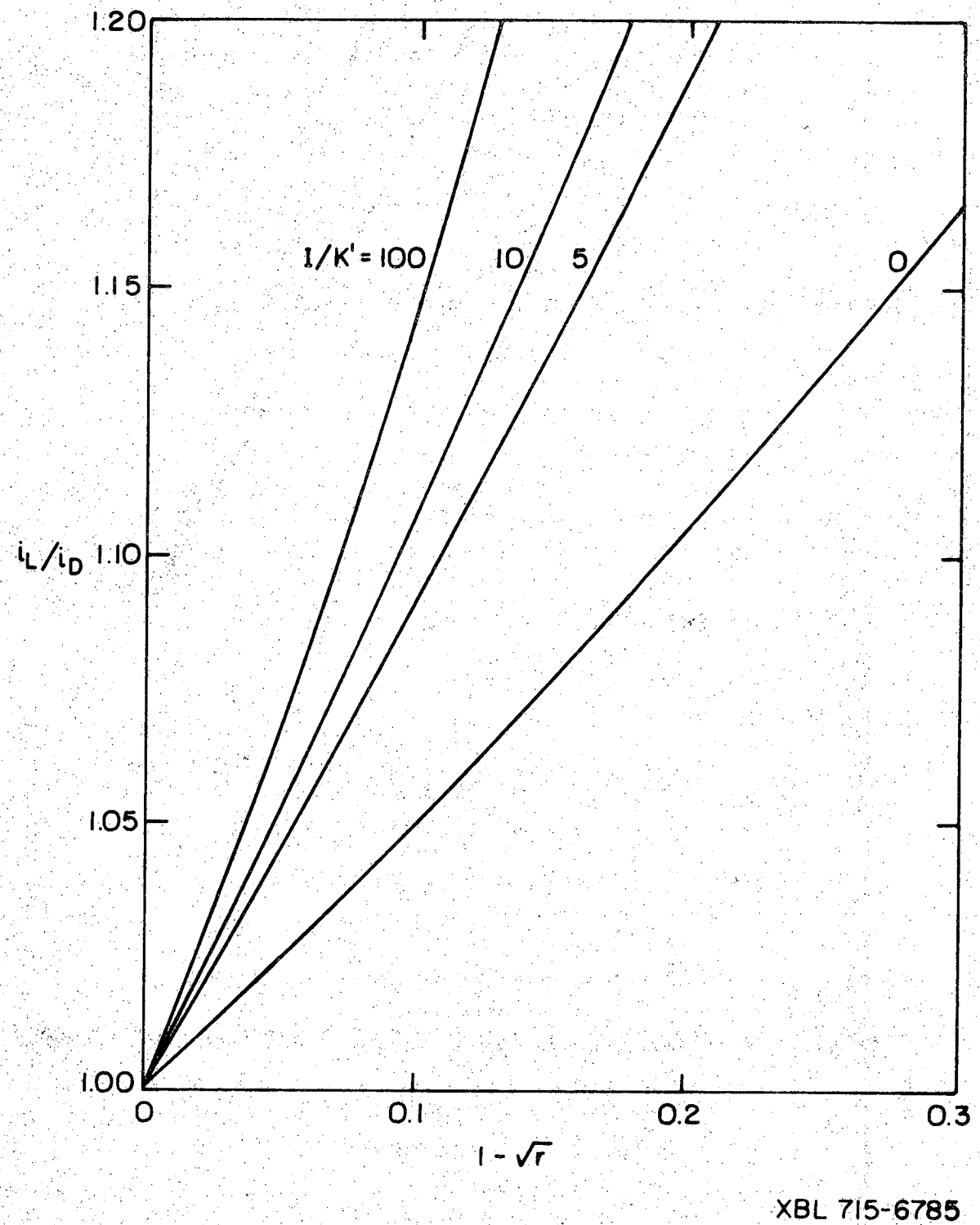

Fig. 3.11. Migration contribution to the limiting current at a rotating disk, for various values of the HSO_4^- dissociation parameter I/K'_B. $r = c_{H_2SO_4}/(c_{H_2SO_4}+c_{CuSO_4})$.

Table 3.6. Corrected diffusivities and true ionic strength (present work and literature data).

	$CuSO_4$ (M)	H_2SO_4 (M)	I_r (M)	$\mu D \times 10^{10}/T$,corr. (dyne/°K)
A9	0.0093	0.476	0.764	1.825
A2	0.00956	0.980	1.573	1.795
A4	0.00976	1.469	2.388	2.067
A11	0.00947	1.946	3.196	2.025
A13	0.00943	2.434	4.032	1.957
A10	0.0460	0.492	0.925	1.719
A3	0.0461	0.991	1.727	1.768
A5	0.0488	1.463	2.526	1.948
A12	0.0462	1.936	3.327	1.921
A14	0.0466	2.420	4.158	1.845
A39	0.0967	0.500	1.125	2.029
A15	0.1017	1.003	1.959	1.987
A40	0.0997	1.253	1.652	2.138
A16	0.1031	1.514	2.820	2.082
A41	0.1001	1.769	3.245	2.124
A17	0.1024	2.013	3.671	2.155
A42	0.1015	2.551	4.600	2.234
A6	0.2273	1.457	3.203	2.172
A18	0.2520	0.995	2.536	2.131
A19	0.2565	2.006	4.260	2.376
A20	0.2561	2.535	5.200	2.355
A7	0.4018	1.464	3.926	2.374
A21	0.4536	0.988	3.341	2.204

Table 3.6. (continued)

	$CuSO_4$ (M)	H_2SO_4 (M)	I_r (M)	$\mu D \times 10^{10}/T$,corr. (dyne/°K)
A8	0.6394	1.468	4.883	2.613
B11	0.0500	0.492	0.941	2.033
B18	0.0498	0.987	1.736	1.976
B13	0.0499	1.493	2.582	1.866
B12	0.0502	2.013	3.468	2.005
B8	0.0992	0.496	1.129	2.150
B5	0.1017	1.008	1.967	2.160
B68	0.2043	0.498	1.545	2.156
B4	0.2005	0.992	2.326	2.007
B10	0.2956	0.295	2.067	1.864
B7	0.2998	0.494	1.912	2.291
B2A	0.3158	1.011	2.810	2.184
B14	0.295	1.492	3.539	2.716
B15	0.299	2.020	4.456	2.786
B16	0.4002	0.991	3.117	2.411
B9	0.5001	0.9968	3.525	2.671

Table 3.6 (continued)

Arvía, Bazán, and Carrozza[142]:

T (°C)	$CuSO_4$ (M)	H_2SO_4 (M)	I_r (M)	$\mu Dx10^{10}/T$ (dyne/°K)	$\mu Dx10^{10}/T$, corr. (dyne/°K)
24.6	0.011	0.715	1.15	2.026	2.005
18.0	0.025	1.693	2.82	2.094	2.072
25.0	"	"	"	2.070	2.048
24.9	0.048	1.382	2.41	2.200	2.150
30.4	"	"	"	2.026	1.980
35.0	"	"	"	2.118	2.070
41.8	"	"	"	2.214	2.163
18.0	0.077	1.752	3.11	2.011	1.955
24.7	"	"	"	2.067	2.010

Capillary cell diffusivities (Hsueh[96])*:

$CuSO_4$ (M)	H_2SO_4 (M)	I_r (M)	$\mu Dx10^{10}/T$ (dyne/°K)	$\mu Dx10^{10}/T$, corr. (dyne/°K)
0.1024	0.810	1.62	1.970	1.793
0.1008	0.888	1.76	1.970	1.811
0.0986	0.998	1.95	2.00	1.856
0.1005	1.085	2.09	2.02	1.882
0.1006	1.195	2.27	2.02	1.897
0.1006	1.295	2.44	2.03	1.913
0.0999	1.375	2.57	2.05	1.940
0.0999	1.473	2.74	2.06	1.957

*only the data for (H_2SO_4) > 0.5 M are included.

The integral diffusivities, thus corrected for the migration contribution:

$$D_{corr}/D = (i_D/i_L)^{3/2} \quad , \tag{3.9}$$

are shown in Figure 3.12 versus the true ionic strength (calculated as in Appendix C). Table 3.6 contains all the data shown in Figure 3.12, including the data of Arvía a.o., and the capillary cell diffusivities measured by Hsueh. The latter have been corrected for the migration effect in stagnant diffusion, as computed by Hsueh and Newman.

In spite of the migration correction a marked dependence on the ionic strength persists. This dependence is only partly due to ionic concentration effects. From Table 3.6 the dependence due to concentration effects can be estimated by considering sets of results for fixed $CuSO_4$ concentrations; on the average:

$$d(\mu D x 10^{10}/T)_{corr}/dI_r = 0.05 \tag{3.10}$$

whereas for the entire set of rotating disk diffusivities:

$$(\mu D x 10^{10}/T)_{corr} = 1.792 + 0.119\ I_r \tag{3.11}$$

This outspoken dependence on the $CuSO_4$ concentration is also evident in Figure 3.12, where the open symbols represent $CuSO_4$ concentrations > 0.1 M. The average of the data given solid circles and triangles is:

$$(\mu D/T)_{corr} = (2.01 \pm 0.13) \times 10^{-10}\ (dyne/°K)\ , \tag{3.12}$$

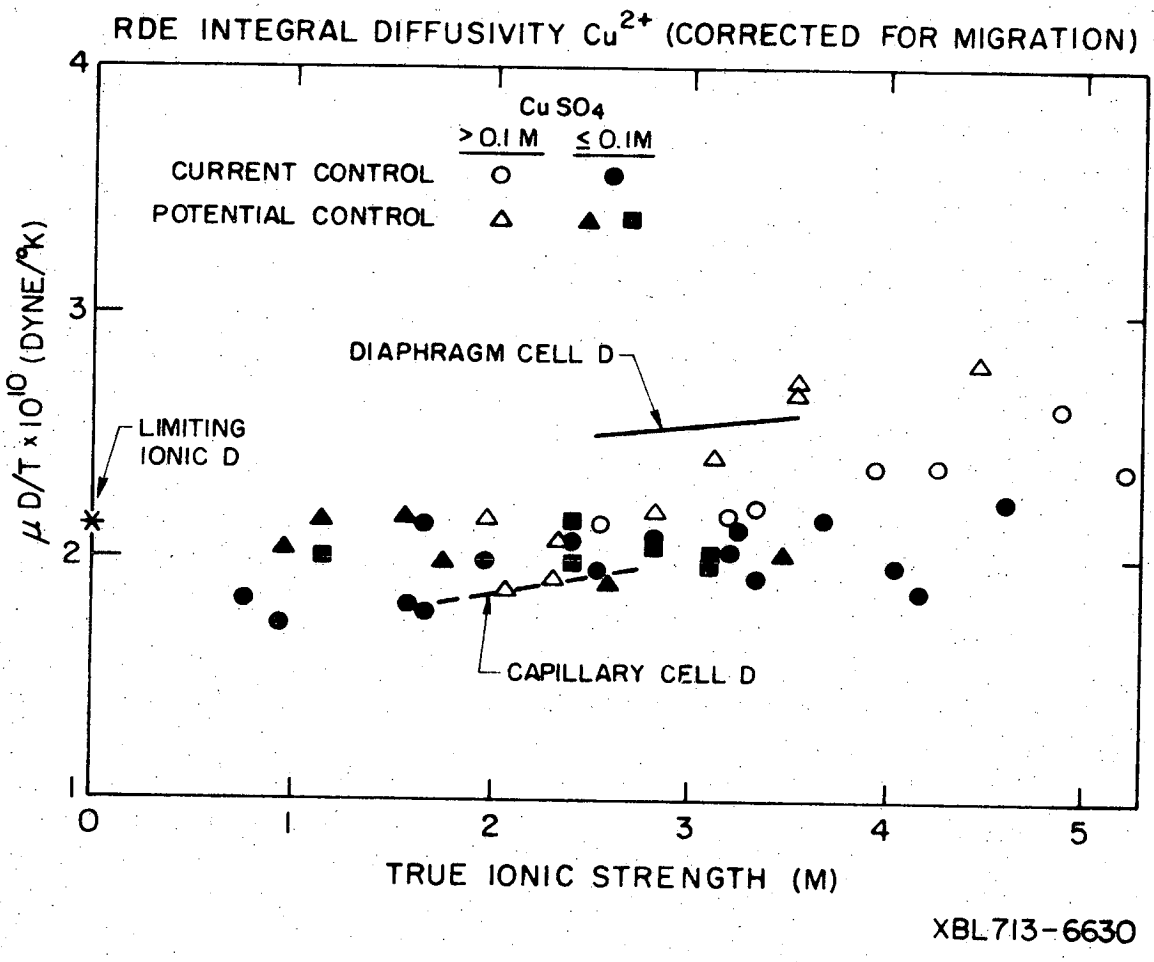

Fig. 3.12. Integral diffusivities of Cu^{++}, corrected for migration effect, as a function of true ionic strength, I_r. Circles and triangles indicate values reported in this work, squares indicate results of Arvía c.s.[142] Diaphragm cell diffusivities according to Fenech,[11] and capillary cell diffusivities according to Hsueh[96] are also shown.

i.e., very close to the average of Arvia's data (solid squares): 2.05×10^{-10} dyne/°K. The average of data for 0.1 M $CuSO_4$: 2.11×10^{-10} dyne/°K is significantly higher than that of the capillary cell data for the same concentration, 1.88×10^{-10} dyne/°K. The average of data for > 0.1 M $CuSO_4$ is 2.33×10^{-10} dyne/°K, and significantly higher than that of the data for $CuSO_4$ concentrations $\leq$ 0.1 M. Note that these values for the averages, and for the concentration dependence, refer to the corrected diffusivities and that the migration correction is by no means unambiguously established. In the concluding section average values and other expressions for the diffusivity will be given which are practically more useful.

Although the possibility is not excluded that the migration current is actually larger than predicted (see Appendix D), it is likely that the particular dependence on $CuSO_4$ concentration reflects an increase in area due to deposit roughness. Thus, in spite of the precautions taken in the potentiostatic experiments, the influence of deposit roughness seems to be present. The following section will be devoted to this aspect of the measurements.

3.5. Discussion: deposit roughness

The effect of deposit roughness has been found, in the course of this work, to be quite important except in solutions with low $CuSO_4$ content (< 0.1 M). Several observations have been made:

1. In potentiostatic scanning and in galvanostatic stepped current increase the limiting currents are apparently high due to an increase in effective area; however, much more so in potentiostatic scanning than in the galvanostatic stepped increase.

2. If the mobility product $\mu D/T$ is in reality independent of the ionic strength, then the increase in effective area is from 0 to 15% in the galvanostatic method, and up to 30% in the potentiostatic scan method.

3. The potential step method gives values that are comparable to the galvanostatic stepped increase method, in spite of the much shorter time for roughness to form.

4. The higher the values observed, the more spread (irreproducibility) in the data.

5. In the galvanostatic technique, repeated measurements with the same disk may initially lead to lower values.

Of these observations (1) and (4) are readily explained. In potentiostatic scanning approximately 1/2 of the total scan time is passed in the neighborhood of the limiting current (see figure 3.6), while in the current stepping experiments this time was usually 1/3 or less. Galvanostatic scans could possibly reduce it even more. Ibl and Schadegg,[150] and earlier Emelyanenko and Baibarova,[152] have observed similar differences between potentiostatic and galvanostatic limiting currents. The poor reproducibility of the potentiostatic limiting currents is due to the rough deposit, and is reinforced by the current fluctuations characteristic for potentiostatic control in the limiting current range. The reproducibility is best on predeposited electrodes and worst on those that are merely polished and cleaned.

Observation (3) is least expected and suggests that a rough deposit is formed in the initial unsteady-state period, followed by re-arrangement whereby the surface becomes more smooth, as mentioned before (see Figure

3.8a). Figure 3.8b shows the transients for various speeds compared in one graph with the theoretical transient current (Appendix B). This, too, suggests that the steady-state limiting current (dashed line) as well as the unsteady-state current, is too high; rearrangement appears to take place faster, the higher the deposition rate.

It would then appear to be preferable to take the second, surface-rearrangement, transition time as the period after which a valid limiting current value is recorded, instead of the time t_3 (equation 6). However, there is no assurance that the surface is really smooth; at most a certain minimum effective area may be reached before new roughness formation (of a dendritic kind) starts.

Two experiments made in the course of the potentiostatic experiments are of interest since they tend to confirm the fairly high effective-area estimates of observation (2).

1. In several measurements the potentiostatic step to -500 mv was followed up with a slow scan at the rate of -20 mv/sec, through the limiting current range. It can be assumed that the current increase measured during this scan reflects the increase in effective surface. The current increase was of the order of 10 to 15% for a 10 second period, in 0.05 M $CuSO_4$ solutions (compare Table 3.3). In these experiments it was found that, except for the most concentrated solutions (in $CuSO_4$), the current increase was proportional to the rotation speed. Figure 3.13 shows this for the case of solutions B11 (0.05 M $CuSO_4$) and B14 (0.3 M $CuSO_4$).

This result implies that the increase in effective surface is proportional to the square of the "smooth" limiting current. Such a relationship can be made plausible from a microscopic model of preferential growth.

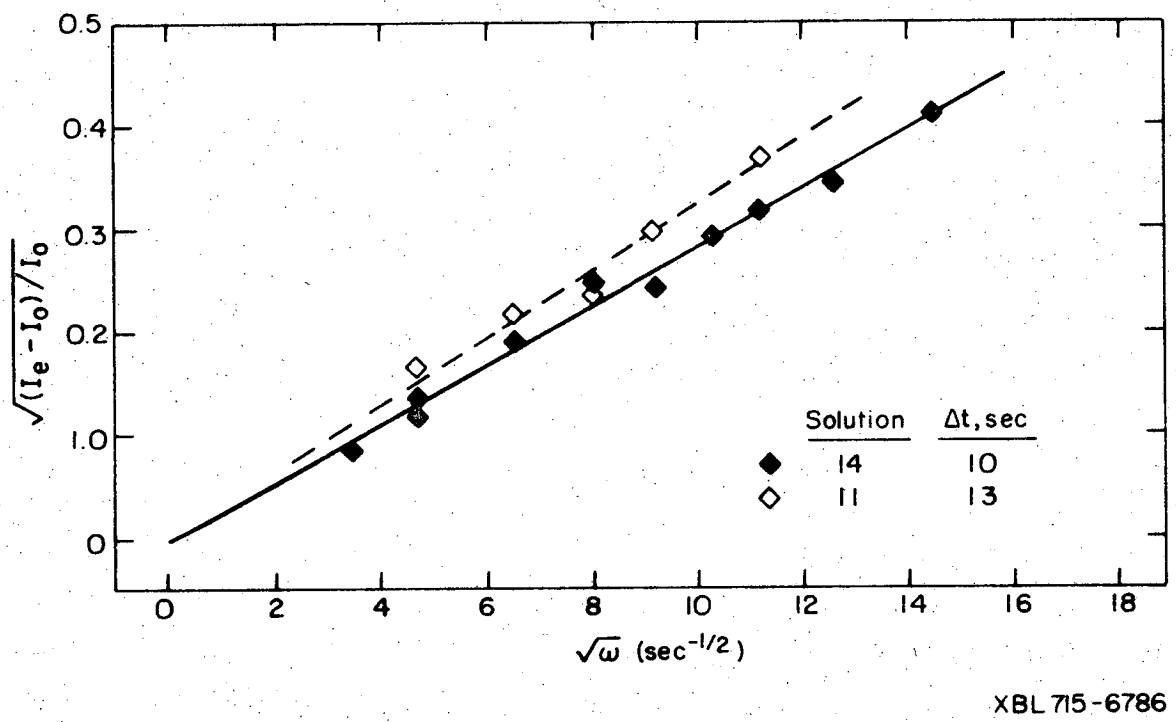

Fig. 3.13. Effect of rotation rate on the increase in current, between -500 mv potential and the inflection point, for a slow potential scan (20 mv/sec) during the time interval Δt indicated. I_o = current at -500 mv potential, I_e = current after time Δt.

In a very simplified model of roughness formation, spheres of diameter a grow preferentially on a fixed number of sites, n. Deposition on the smooth surface goes on side by side with that on the protuberant spheres, but the spheres present a growing surface. Assume that each sphere contributes an extra area πa^2 to the mass transfer surface. This implies that the diffusion layer is not disturbed; it is equivalent to assuming a local current increase by a factor of approximately 5.

The fraction covered by dendrites, θ_d, is then related to the effective current I_e by

$$\theta_d = 0.25\ (I_e - I_o)/I_o = 0.25\ \Delta A/A_o \quad , \tag{3.14}$$

where I_o is the "smooth" current, A_o the smooth area, and ΔA the increase in area. If a ring adjacent to the edge of the disk would be occupied, then $A/A_o = 0.20$ would correspond to a "solid" ring with inner radius 0.975 times the disk radius.

The growth equation of the protuberant spheres is now:

$$\frac{d}{dt}\left(\frac{n\pi a^3}{6}\right) = \frac{(63.54)i(\theta_d A_o + \Delta A)}{(2)(8.96)F} \tag{3.15}$$

Since $\theta_d A_o = n\pi a^2/4$ and $\Delta A = n\pi a^2$, this yields

$$a = 9.2 \times 10^{-8}\ \ i\ dt\ (cm) \tag{3.16}$$

where i expressed in ma/cm^2, and t in sec. If the current is a constant

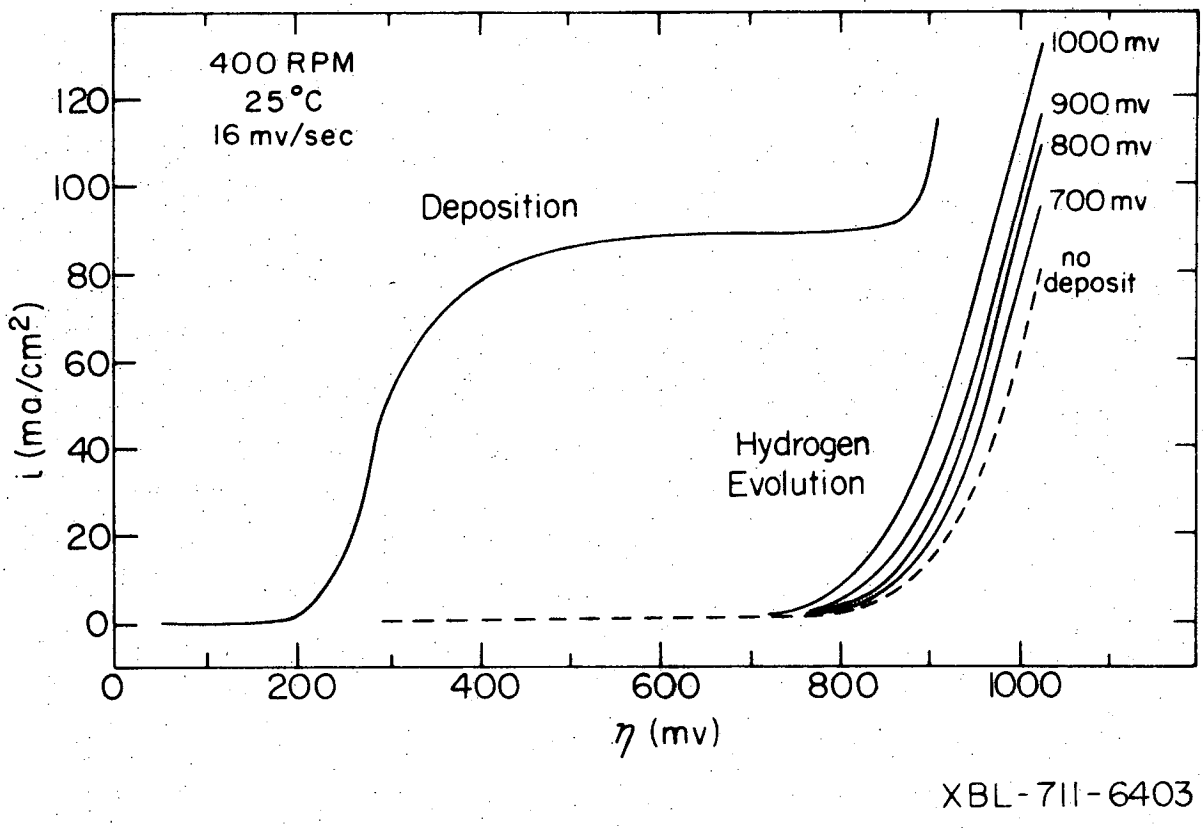

Fig. 3.14. Hydrogen evolution on a rotating disk previously plated by negative potential scanning to the terminal potentials indicated. $CuSO_4$ concentration of plating solution 0.3 M; H_2SO_4 concentration 1 M (during plating as well as hydrogen evolution).

limiting current density, one has after 10 sec, for solution B14 0.84 μ (at 62 rpm) or 3.0 μ(at 1500 rpm). The latter dimension is still less than 1/4 of the diffusion-layer thickness at that speed (13 μ).

Equation 16 shows that the effective increase of surface is proportional to the square of the limiting current, as long as no disturbance of the diffusion layer takes place. This condition obviously limits the validity of the model, in particular at high deposition rates. There are also other objections, in particular that it does not account for non-uniform dendritic growth, which is always observed starting at the edge. This is probably due to non-uniform current distribution on the disk, not to nonuniform availability of nuclei for dendritic growth. The density of nuclei calculated from the slope of Figure 3.13 (sol. B14) is of the order of 0.1 - 1 per square micron. Nevertheless, the model shows in semi-quantitative terms how the preferential sites may lead to a very large increase in effective area, without any hydrodynamic effects such as local turbulence (which becomes effective only at local Re numbers above 10, i.e., several orders of magnitude larger than the dimensions calculated above).

2. To determine the influence of the deposit on the hydrogen evolution reaction, a potential scan was made at a copper disk electrode rotating in an aqueous solution of H_2SO_4 of the same concentration as in the acidified cupric sulfate solution in which the disk electrode had previously been plated. The disk electrode had previously been plated by potential scanning (at the same rate) down to various terminal potentials (see Figure 3.14). The disk was always kept in contact with solution.

Scans were also made with the disk freshly pre-deposited (at 10% of the limiting current), and after mere polishing and cleaning.

Figure 3.14 shows that the rough surface created above 600 mv leads to an earlier hydrogen breakthrough. The most straightforward explanation of this phenomenon is the increase in effective surface area. If the small residual limiting current of Cu^{2+} ions (due to spilling during transfer, and to diffusion from the reference electrode compartment) is subtracted, the hydrogen evolution currents yield Tafel-plots* (Figure 3.15) with an average slope

$$\beta = -\frac{2F}{R_o T}\frac{d\ell n_i}{d\eta} = 0.585 \quad , \qquad (3.17)$$

somewhat higher than the value $\beta = 0.5$ generally accepted for hydrogen evolution. Using this β value for all recorded curves, an apparent exchange current density can be found as given in Table 3.7.

The values of i_o suggest that already at 700 mv the increase in surface area due to current passage (from 500 - 700 mv in 12.5 sec) is more than 30%. It is not surprising that this is higher than suggested by the current increase in the potentiostatic copper deposition. The current distribution for the hydrogen evolution reaction can be expected to be much more non-uniform than for the copper-deposition reaction. The hydrogen reaction is very far below its (hypothetical) limiting current but into the Tafel region, so that the appropriate current distribution

---

*To convert to hydrogen overpotential, use is made of:

$E(Cu/Cu^{++}) = 0.289$ v for 0.3 M $CuSO_4$ (stoichiometric activity-coefficient 0.08)

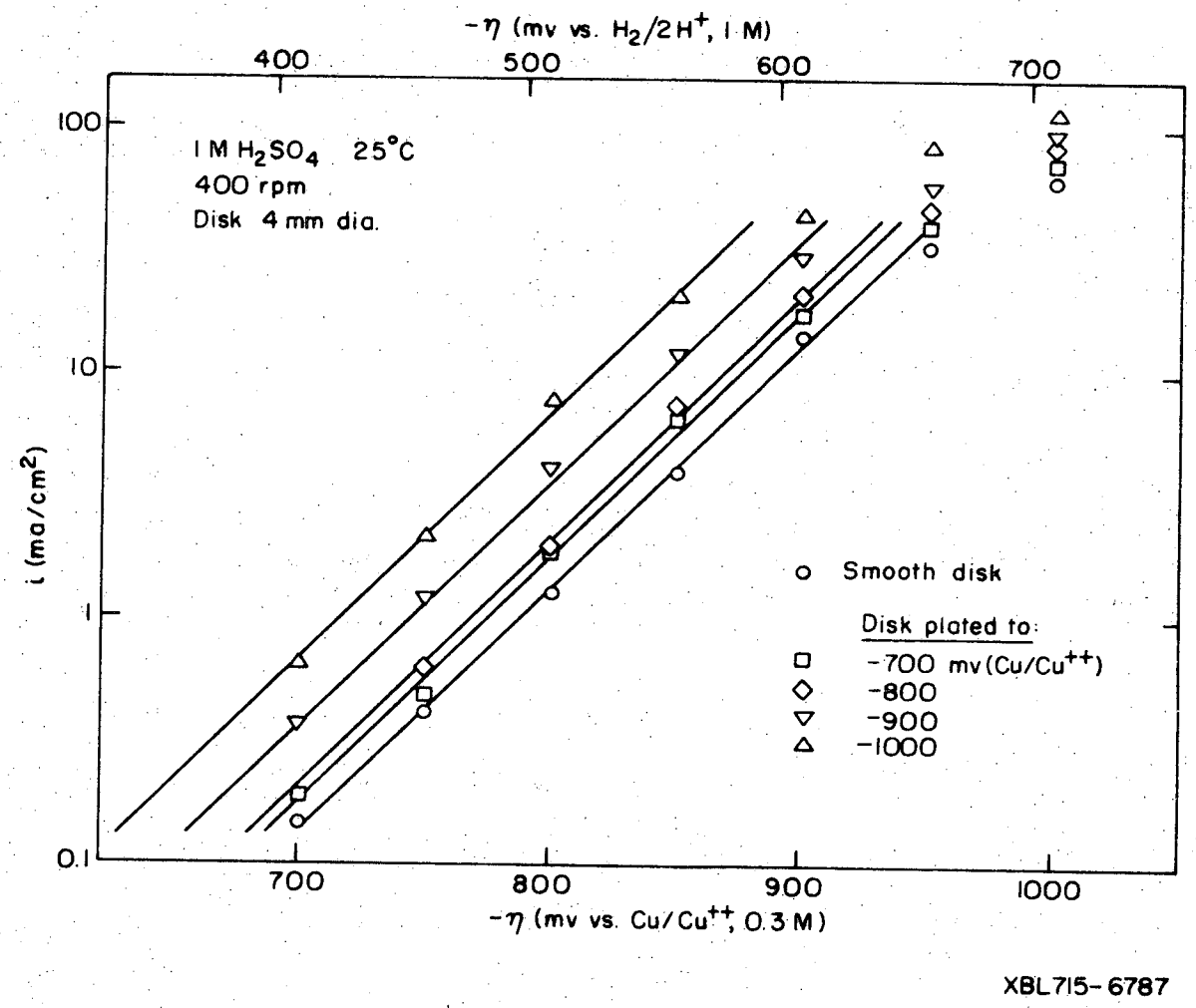

Fig. 3.15. Tafel plot of hydrogen ion reduction current on a smooth disk electrode and for electrodes previously plated to various terminal potentials (Fig. 3.14).

Table 3.7. Apparent exchange current density of cathodic hydrogen evolution on polished and pre-deposited copper electrodes.

condition	β	i_o, apparent ($ma/cm^2 \times 10^5$) based on β = 0.585
polished	0.578	1.185
pre-deposited	0.536	1.200
pre-deposited with potential scanning to:		
-700 mv	0.618	1.607
-800 mv	0.608	1.873
-900 mv	0.572	3.245
-1000 mv	0.597	6.183
avg β	0.585	

parameter is

$$\frac{\beta i r_o Z F}{R_o T n_\infty} \approx 1.5 \qquad (3.18)$$

and a fairly non-uniform current-distribution exists. As a result, the region near the edge of the disk where the dendrites predominate, has a higher weight in determining the effective area for hydrogen evolution.

The lowering of the breakthrough potential of hydrogen evolution suggests an explanation for the slightly lower limiting currents observed when galvanostatic measurements were repeated with the same disk. As the current is forced up, at fairly low potentials an appreciable fraction of the current will be due to the hydrogen reaction; due to the larger effective surface the original limiting current will not be a limiting current any more, and this, too, will depress the potential. As a result, the inflection point which was originally the end of the plateau, shifts to the onset of the plateau and, thereby, to slightly lower current levels.

3.5. Conclusions

1. In solutions which are sufficiently dilute in $CuSO_4$ so that migration and surface roughness effects can be ignored, the rotating disk ionic diffusivity is not significantly dependent on the ionic strength and can be represented by:

$$\mu D/T = (2.01 \pm 0.13) \times 10^{-10} \text{ dyne/°K} \qquad (3.20)$$

This is based on 23 diffusivity data for the condition $c_{CuSO_4} < 0.1$ M and $c_{H_2SO_4} > 10\ c_{CuSO_4}$. Included are 14 data obtained by galvanostatic

and potentiostatic techniques in the present study, as well as 9 data points of Arvía c.s.[142] It should be noted that the latter authors[142] found that addition of glycerol apparently increases the $\mu D/T$ product of solutions dilute in $CuSO_4$. (See Figure 3.17)

2. In limiting current measurements using solutions concentrated in $CuSO_4$, the galvanostatic approach to the limiting current is preferable; potentiostatic techniques lead to higher levels of surface roughness.

3. In solutions of concentration $\geq$ 0.1 M $CuSO_4$ diffusivities obtained by the galvanostatic approach are not significantly dependent on the H_2SO_4 concentration, and can be expressed with sufficient accuracy by:

$$\mu D/T = (2.03 + 1.82\, c_{CuSO_4}) \times 10^{-10} \text{ dyne/°K} , \quad (3.21)$$

This expression, based on 14 galvanostatic data of this work is believed to represent the integral diffusivity in more concentrated solutions with an accuracy of $\pm$ 10%, taking into account migration and minimal surface roughness effect.

4. The diffusivities found for dilute solutions of $CuSO_4$, of up to 0.1 M concentration, lie appreciably below the diaphragm-cell diffusivities of Cole and Gordon, and the correlation based thereon by Fenech. In the range of concentrations 0.2 to 0.5 M $CuSO_4$, frequently used in free convection studies, the agreement is somewhat better, especially if migration is corrected for. This may explain why these diaphragm-cell diffusivities could be used successfully in certain

free-convective mass-transfer studies.*

5. The rotating disk ionic diffusivities reported in this work appear to be somewhat higher than the stagnant diffusion (capillary) ionic diffusivities reported by Hsueh,[96] for the same $CuSO_4$ concentration (0.1 M). Considering capillary diffusivities in solutions with $c_{H_2SO_4} > 0.5$ M, and correcting for migration, the average rotating disk diffusivity is approximately 12% higher than the average of the capillary diffusivities, i.e., significantly different at the 99% probability level.

---

*It should be noted that the values reported by Cole and Gordon for the diffusivity of $CuSO_4$ in absence of H_2SO_4, at 18°C, are suspiciously high. With a temperature coefficient $D^{-1}\ dD/dT = 0.03$, they would translate to values at 25°C which are 20% higher than those measured in recent work (see e.g., ref. 139).

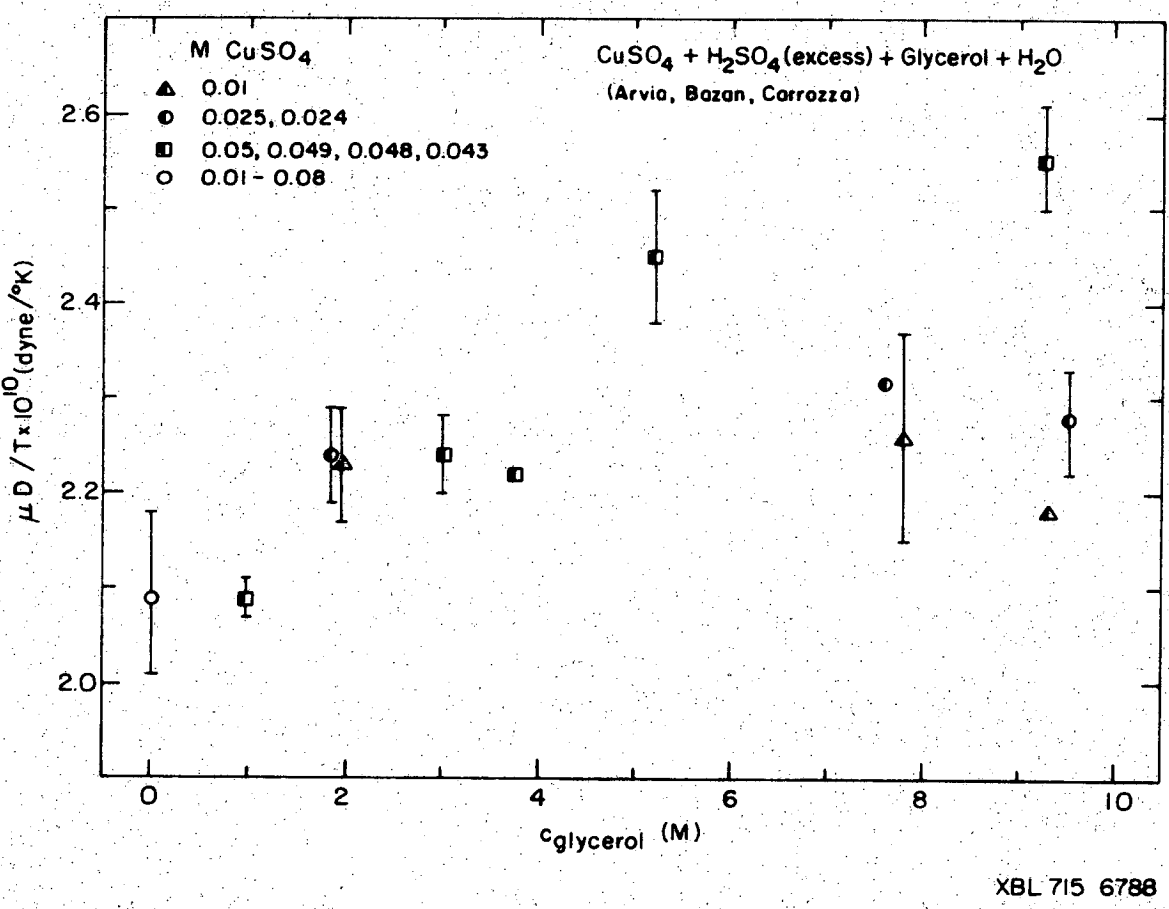

Fig. 3.16. Diffusivity of Cu^{2+} in $CuSO_4$-H_2SO_4 (excess) - glycerol according to Arvia c.s.[142] The spread in the data (obtained at various temperatures, 10-40°C) is indicated.

Chapter 4. UNSTEADY-STATE EFFECTS IN LIMITING CURRENT MEASUREMENT

Part I. Review

4.1. Introduction

Previous investigations carried out in this laboratory[11a,156] on mass transfer rates along planar electrodes, revealed that the length of time in which the limiting current was attained influenced the limiting current curve. This unsteady-state effect was noticeable both in the definition (or lack of definition) of the plateau, and in the current value read from it (or from the inflection point).

The effect has been most prominent in free convection but, as will be shown in the section 3 , it can be quite important in forced convection also. A comparison of theoretical information about transients in convective diffusion with selected experimental data available in the literature, shows that convective transients, in particular on elongated electrodes, are complicated considerably by the presence of an electric field. Besides this interaction there is often the possibility of an unsteady state due to surface area or bulk concentration changes.

For a situation where these complicating effects are not important, namely for a redox reaction at a rotating disk electrode, some experiments are reported in Part II. The purpose of these experiments is to establish the minimum time required to reach a steady-state limiting current in a representative case of forced convection.

4.2. Free convection

Figure 4.1 shows limiting current curves recorded by Hickman[156] at a horizontal cathode facing upward, in free convection. The apparent limiting current value is definitely dependent on the time passed to reach the limiting current; it increases 80% as the current increase rate is varied from 0.25 to 20 $ma/cm^2 min$.

Figure 4.2 shows that the relative increase in the apparent limiting current is even more important in pure diffusion, i.e., where the cathode plate faces downward. In this case the expectation is that the apparent limiting current will drop to lower and lower values as the current application rate, di/dt,is made smaller. If it were not for edge effects (advection) at the embedded plate, no steady limiting current could be expected.

In the case of free convection, the apparent limiting current will not drop below the steady-state value as the rate, di/dt, is decreased. Hickman, in experiments on free convection at horizontal electrodes, found that a time

$$t_{ss} = i_L / \frac{di}{dt} \geq 8 \text{ min} \qquad (4.1)$$

would be sufficient to guarantee steady-state limiting current values.

Earlier, Fenech[11] had produced limiting currents in the same free-convection system by means of linear increase of the applied potential (cell voltage). Using concentrated solutions, he found that the limiting current value is essentially independent of the initial voltage applied,

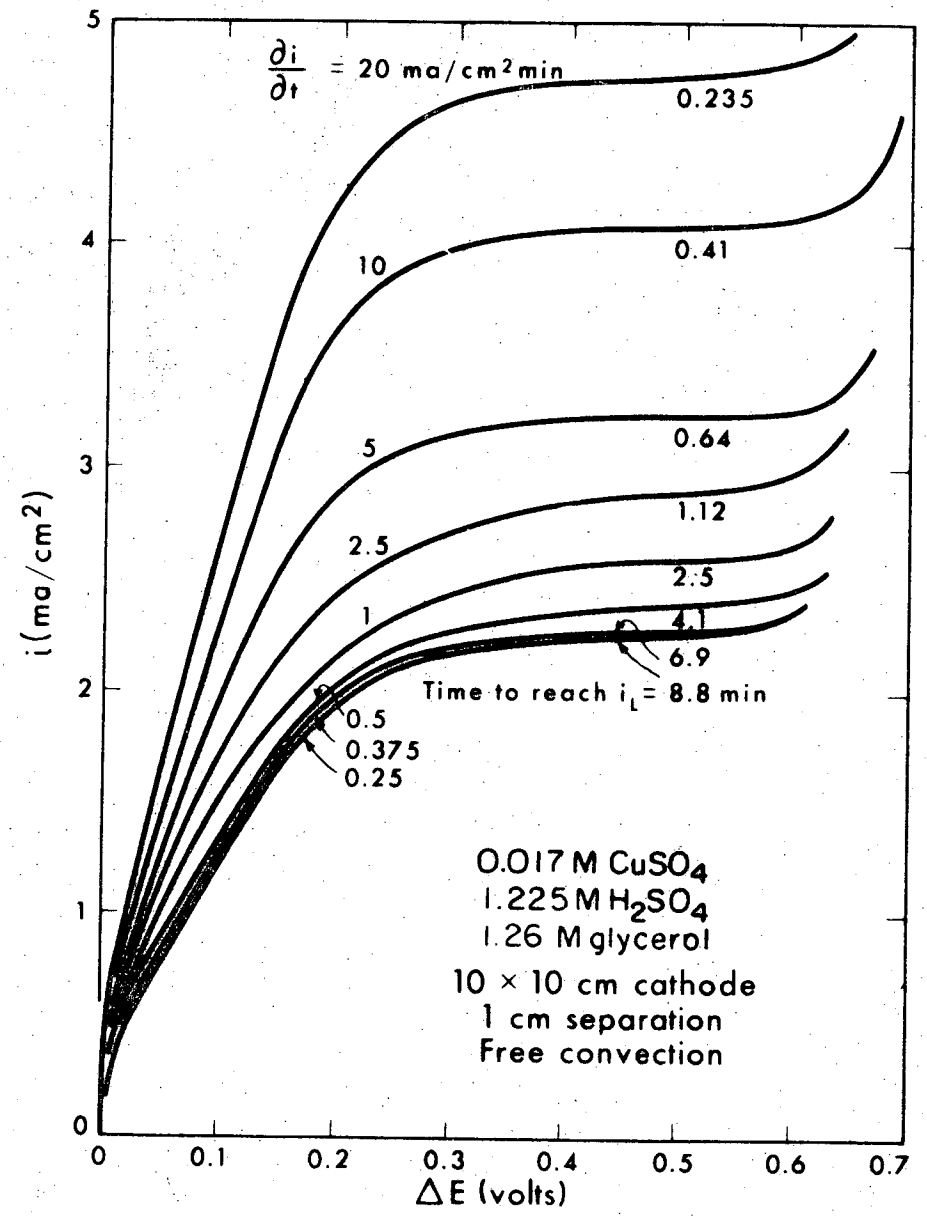

XBL 698-1210 A

Fig. 4.1. Limiting current curves recorded for various current application rates in free convection at a horizontal electrode (from Ref. 156).

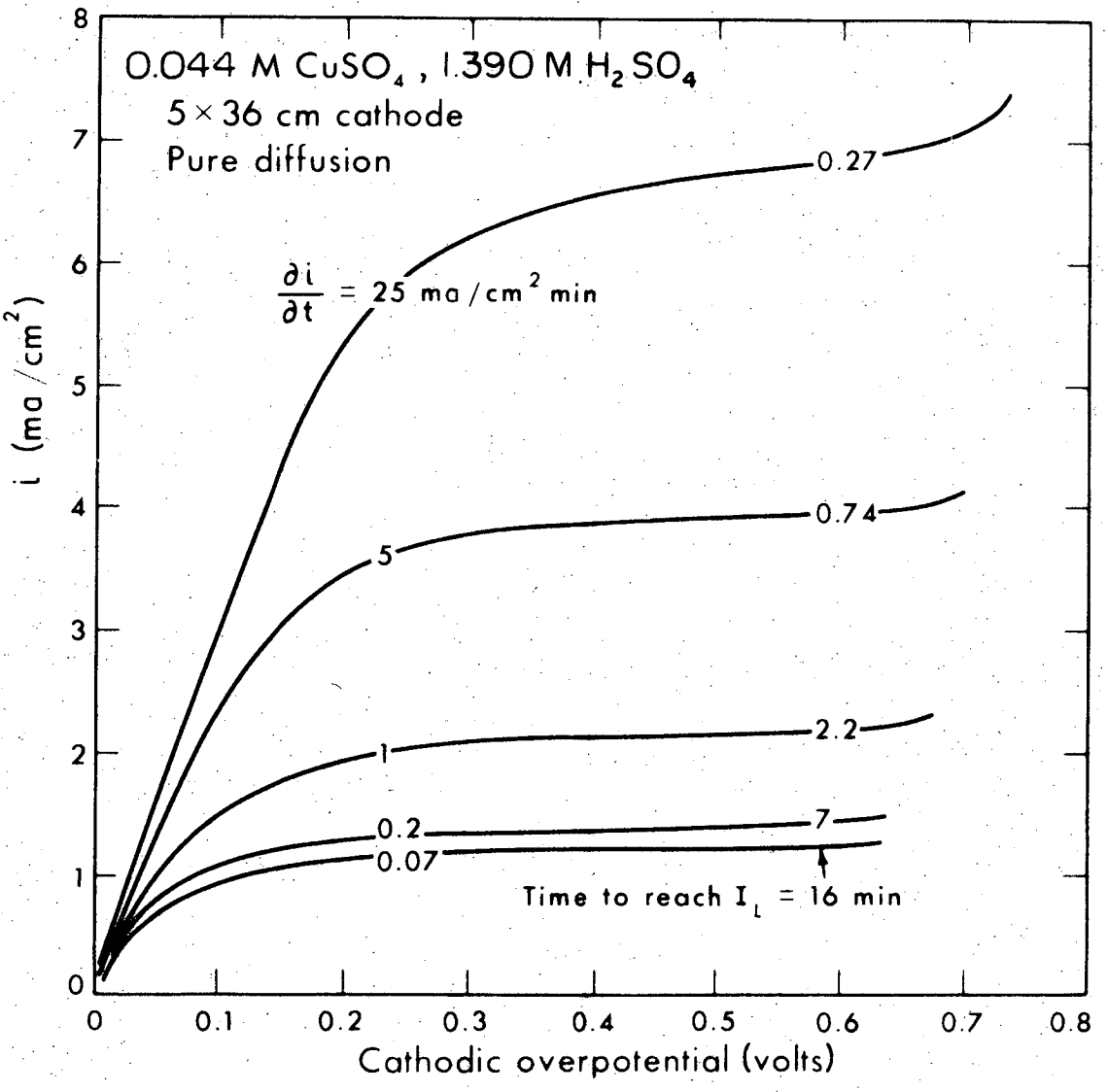

Fig. 4.2. Limiting current curves recorded for various current application rates in pure diffusion at a horizontal electrode (from Ref. 156).

provided the same rate of increase is used. Starting with ΔE = 200 mv, steady reproducible limiting currents were obtained if

$$t_{ss} = 500 \text{ mv} \Big/ \frac{d(\Delta E)}{dt} \geq 3 \text{ min} \qquad (4.2)$$

This time is considerably shorter than the galvanostatic minimum time (1). Since a theoretical analysis of this type of unsteady-state free convection offers severe difficulties, there is no way to confirm this difference except by controlled experiments of the kind undertaken, on a limited scale, by Hickman and Fenech.

Even in the classical example of laminar free convection, namely, at a vertical plate, the analysis of unsteady-state transport is very complicated. Only fairly recently have approximate and numerical solutions been given for the two basic unsteady-state boundary conditions: a concentration (temperature) step, or a flux step, applied at the plate surface. In Appendix E these solutions, insofar relevant for the case of electrolytic solutions (Sc >> 1), are reviewed and compared with those few transition times reported in work on laminar free convection.

Table 4.1 lists some transition times calculated for this kind of free convection, following a concentration step in 0.05 M $CuSO_4$ solution. It can be seen that the transition time (to a flux 1% in excess of steady state) varies along the plate. Of course, in free convection the transition time is also dependent on the density difference generated at the plate. The dimensionless time variable in the transient process is:

$$\tau_{\text{free conv.}} = t \left(\frac{Dg\Delta\rho}{\mu x} \right)^{1/2} \qquad (4.3)$$

Table 4.1. Transition times (in seconds) in laminar free and forced convection along a planar electrode, for a solution of 0.05 M $CuSO_4$, 1.5 M H_2SO_4 at 25°C. Current densities indicated between parentheses (in ma/cm^2).

Distance from leading edge (cm)	0.5	1	5	10	40
Free convection at vertical plate	42	60	133	189	377
	(2.84)	(2.40)	(1.61)	(1.35)	(0.95)
Forced convection between parallel plates (1 cm distance)					
Re = 10	95	151	444	707	1777
	(1.31)	(1.04)	(0.61)	(0.48)	(0.30)
100	21	33	96	151	382
	(2.82)	(2.24)	(1.31)	(1.04)	(0.65)
1000	4.4	7.1	21	33	83
	(6.08)	(4.83)	(2.82)	(2.24)	(1.41)
2000	2.8	4.4	13	21	52
	(7.66)	(6.08)	(3.56)	(2.82)	(1.78)

The transition times in very dilute solutions, e.g., $\leq$ 0.01 M $CuSO_4$, therefore become so long that serious difficulty is encountered in obtaining any steady-state value at all. It appears (see Appendix E) that this is particularly so where the transport process takes place in a restricted space, but provides the driving force for a secondary convection pattern extending over larger distances. Examples are high-Sc free convection at a horizontal plate,[11] and laminar free convection in a narrow vertical slit which, at the top and the bottom, is open to a large reservoir of solution.[48]

Figure 4.3 shows an unusual limiting current curve obtained by Fenech[11a] in 0.01 M $CuSO_4$ solution at a horizontal electrode. The current maximum could be made smaller by applying a lower rate $d(\Delta E)/dt$ (2), but could not be made to disappear altogether. It is likely that the maximum is caused by the unsteady-state diffusion process close to the plate while the free convection pattern at larger distances is slowly being established. However, in laminar free convection at vertical plates the existence of such an "overshoot", at least in high-Sc liquids, is dubious; if it exists, it is inconspicuous.[157,158]

The risk inherent in long transition times, such as are characteristic of free convection with a feeble driving force, is two-fold:

1. The bulk solution may become depleted. In free-convection experiments the cathode and anode compartment are often separated by a diaphragm to prevent mutual interaction of the convection patterns; replenishment of the catholyte does not take place. Examples of sagging limiting current plateaux due to bulk depletion can be found in the work of Boëffard[46] with ferri-/ferrocyanide in free convection at horizontal electrodes.

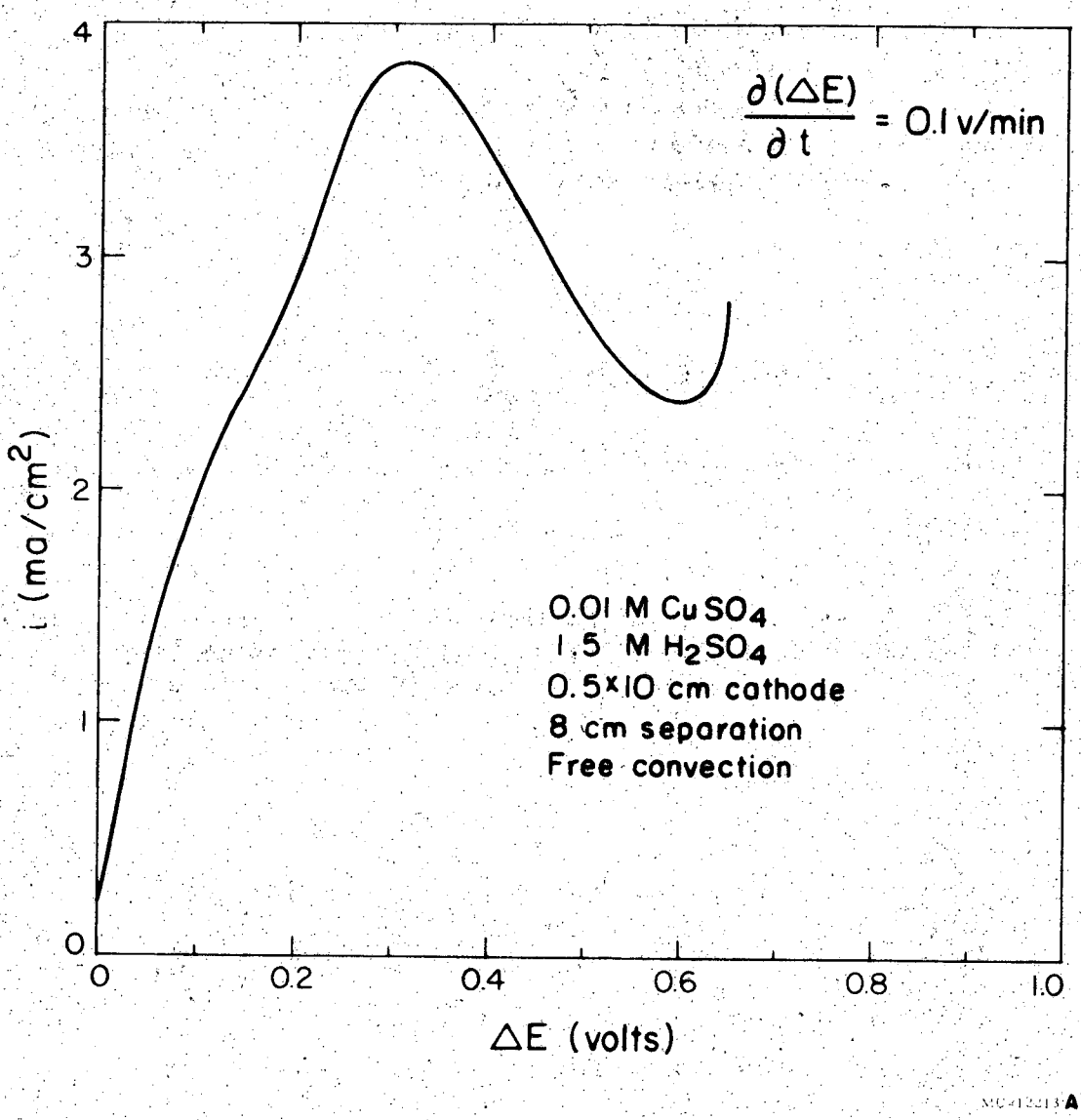

Fig. 4.3. Limiting current curve for low concentration of the reacting ion in free convection at a horizontal electrode, recorded by linear increase of applied potential (from Ref. 11a).

2. In copper deposition surface roughness may lead to an increase in the apparent limiting current. This is particularly serious in potentiostatic current control, whether through the applied potential or the working electrode potential. In free convection experiments, in particular, it is convenient to apply a large negative potential and let the current come to its steady state value. As demonstrated in chapter 3, however, this may lead to a more serious roughness formation than if a series of current steps are taken. It is reasonable to believe that this finding is valid for free convective as well as forced convective mass transfer.

The second consideration is complicated by the fact that those solutions which have the smallest driving force and, therefore, the longest transition times, also have the lowest limiting current levels.

The surface roughness problem in free convection, therefore, can only be resolved by extensive experimental investigation. It is very probable that for any well-defined type of free convection there is a minimal surface roughness effect associated with each $CuSO_4$ concentration. This effect could be incorporated in an effective diffusivity of the same kind as those determined in chapter 3 for the rotating disk electrode. These diffusivities would then reflect a compromise between high apparent limiting currents due to unsteady-state free convection, and high apparent limiting currents due to surface roughness formation.

4.3. Forced convection

Although the scarce experimental data mostly refer to unsteady-state effects in free convection, one should not infer from this that in forced

convection transition times are negligible. Recently solutions have been obtained for the flux response to a concentration step at a plate in parallel flow[159] and in boundary layer flow[160,161] (Appendix E). A solution for the analogous transient at a rotating disk has been given in Appendix B.

Table 4.1 presents theoretical transition times following a concentration step at the wall in laminar flow between parallel plates (Lévêque mass transfer). Clearly, in slow laminar flow (Re $\lesssim$ 100 or lower) transition times are comparable to those in free convection. Here, however, they are but weakly dependent on the concentration, through the diffusivity; the dimensionless time-variable in unsteady-state mass transfer of the Lévêque type is:

$$\tau_{\text{forced conv.}} = t\left(\frac{S^2 D}{x^2}\right)^{1/3} \tag{4.4}$$

where S is the velocity gradient at the wall.

The transition time is, however, more strongly dependent on the distance from the leading edge (x) than in free convection at a vertical plate.

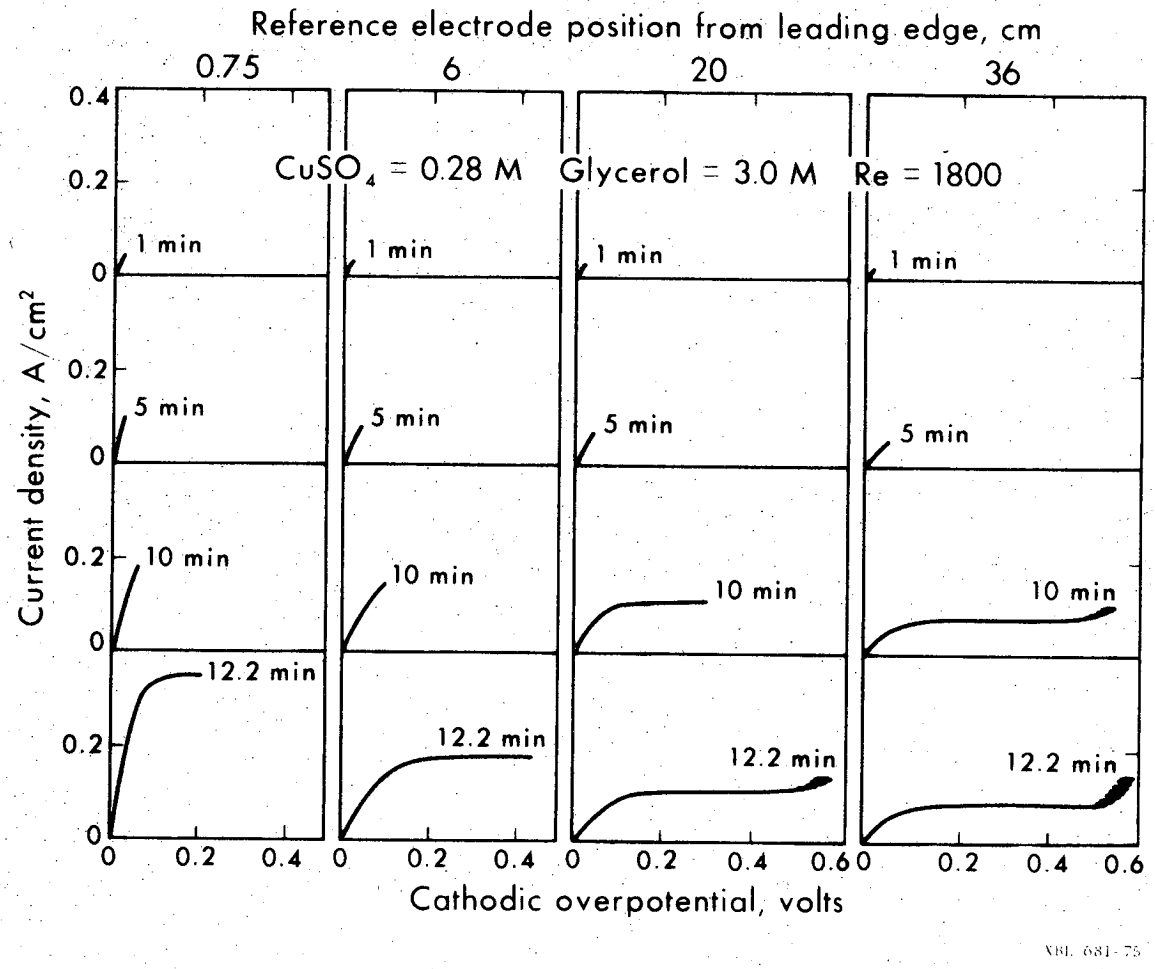

Fig. 4.4. The development of local cathodic overpotentials at a segmented horizontal plate electrode in forced convection (from Ref. 156).

4.4. Interaction with the potential distribution at elongated electrodes

Two factors restrict the usefulness of the step-response transient solutions reviewed so far:

1. In most electrochemical measurements the limiting current is not imposed abruptly but approached gradually, controlling either the current or the electrode potential. Since the unsteady-state transport equation for forced convection is a linear equation, it is in principle possible to derive solutions for more complicated time-dependent boundary conditions from the step-response solution, by application of the superposition (Duhamel) theorem.

If the response to a uniform step in the concentration, c_o, at the electrode is $i = i^*(x,t)$, then in general:

$$i(x,t) = \int_0^t dt_1 \int_0^x dx_1 \frac{\partial^2 c_o}{\partial t_1 \partial x_1}(x_1,t_1) i^*(x-x_1,t-t_1) \qquad (4.5)$$

Conversely, if the response to a uniform step in the current is $c = c_o^*(x,t)$, then:

$$c(x,t) = \int_0^t dt_1 \int_0^x dx_1 \frac{\partial^2 i}{\partial t_1 \partial x_1}(x,t_1) c_o^*(x-x_1,t-t_1) \qquad (4.6)$$

Suppose the imposed boundary condition is simply a linear increase, st, of the current density, which is taken to be uniform everywhere, then the equation to be solved is:

$$c(x,t) = S \int_0^t dt_1 c_o^* \frac{D^{1/3} S^{2/3} (t-t_1)}{(x-x_1)^{2/3}} \qquad (4.7)$$

where the function $c_0^*(x,t)$ is a rather involved analytic expression, given by Soliman and Chambré.[159] Note, however, that (7) implies that the current density is at all times uniformly distributed; this is obviously in

contradiction with the limiting current distribution which one would like to reach eventually.

In any case, for an application of the superposition theorem to mass transfer at electrodes with a non-uniform limiting current distribution, it is necessary that the applied local current density is known throughout the approach to the limiting current.

2. Mass transfer is not the only process controlling the unsteady-state behavior of electrode potential in response to an imposed current, or vice versa. In particular in the copper deposition reaction an equation such as (6) cannot be used to represent the total imposed electrode potential in terms of concentrations.

The implications of this are illustrated by Figure 4.4, which shows the development of sectional limiting current curves recorded by Hickman[156] at a horizontal plate electrode in laminar forced convection. Here the total current is increased linearly with time, and the potential of selected electrode segments is recorded. The limiting current plateau is reached first at the trailing edge of the plate, then in the center, and finally at the leading edge. The time-difference is on the order of 4 minutes i.e., approximately 1/3 of the time required to reach i_L everywhere. It is clear that if sectional limiting currents had been read with respect to the central overpotential, inaccurate local current values would have resulted for the edge segments. If the total current had been recorded against the central overpotential, the correct total i_L might have been read (due to compensating errors), but the plateau would not be well-defined.

Figure 4.4, therefore, illustrates the practical importance of sectional measurements on extended electrodes, as first systematically applied by Fenech.[11a] However, from the viewpoint of unsteady-state mass transfer the phenomenon observed raises several questions.

1. The time in which the limiting current is approached (8-12 minutes) was selected by Hickman after preliminary experiments to establish a maximum rate of current increase beyond which the apparent limiting current would reflect unsteady-state effects. Therefore, one would expect the measurement to be quasi-static, i.e., deviations from the steady state are insignificant during the passage to the limiting current. Nevertheless, the limiting current is reached nonsimultaneously. The order in which the apparent limiting currents are attained agrees, at least qualitatively, with the distribution of transition-times which follows from (4). In the unsteady state caused by a forced current increase, an apparent limiting current due to depletion at the electrode is reached first where the time to reach the steady-state concentration profile is longest.

2. The time in which the limiting current is reached, i.e., the minimal time to obtain steady-state, is an order of magnitude larger than the transition times listed in Table 4.1 for Re = 2000. A comparison can be made in terms of the dimensionless time τ (4), substituting for t the minimum time to reach steady-state,

$$t_{ss} = i_L/(di/dt) \quad ,$$

for the trailing segment. This yields $\tau = 2.7$. The transition time τ

following a step in the flux at a surface in Lévêque type mass-transfer is not exactly known; it is probably no more than three times the transition time following a concentration step,which is 0.239 (Appendix E). The time of passage observed in the experiment of Figure 4.4 is an order of magnitude larger.

To explain, first, the order in which the sectional limiting currents are reached, one has to take into account that the applied current is neither distributed uniformly at all times (equation 7), nor similar to the limiting current distribution. If the steady-state is essentially maintained during the transition, the trailing edge will have a fairly high current density throughout (see Figure 2.14). This will lower the minimum time required to establish a steady-state limiting current, compared to the values suggested by Table 4.1. The distribution of this minimum time along the plate will probably be more uniform than $x^{2/3}$ as required by (4). Nevertheless, it is likely that in the final stage of the passage to limiting current, where mass transfer dominates the potential distribution, each small increase of the current (now distributed approximately as $x^{-1/3}$) will require a local transition time distributed as $x^{+2/3}$. At the same time, as Figure 2.14 shows, the steady-state reactant concentration can reach a virtual zero level near the trailing edge of the plate before the limiting current is reached. Therefore, even if, for the plate as a whole, the passage to the limiting current is quasi-static until very close to the limiting current (e.g., 95%), the attainment of the limiting current condition, i.e., $c_R \to 0$, is very likely to be non-stationary and, therefore, nonsimultaneous.

If this explanation is correct, sectional limiting currents near the trailing edge of the plate will tend to be somewhat higher than expected unless the passage to the limiting current is made very slowly, in particular near the limiting current. Note that no consideration is given to surface roughness formation and hydrogen development, which may reinforce the tendency to unsteady state.

Clearly it would be a formidable problem to obtain a quantitative picture of the transient current distribution corresponding to a certain rate of approach to the limiting current. For the present, it is sufficient to conclude that the minimum time allowable to reach steady-state limiting current by applying a current ramp, should be equal to, or greater than, that required for the trailing section.

At this point the second question raised by Figure 4.4 needs an answer. The minimum time of passage to the limiting current, according to Figure 4.4 and equation 1, is an order of magnitude larger than the transition time following a step change in concentration or flux.

It was thought desirable to check experimentally in a simpler situation whether this particular relationship between minimum time of passage and step transition time is a general feature of forced convective diffusion. The hydrodynamic model selected was the rotating disk; for this case numerical solutions are available both for a concentration step and for a flux step instantaneously applied.

The transition following a concentration step is relevant for potential scanning. This was investigated as an alternative way to approach the limiting current, closely related to linear increase of applied

potential in well-supported solutions. To avoid interference of electrode kinetics with the transient mass transfer, the electrode reaction was reduction of ferricyanide at a nickel electrode in equimolar $K_3Fe(CN)_6$ + $K_4Fe(CN)_6$ solution with excess NaOH.

From the few investigations[162,163] available in the literature one can conclude that the minimum scan period necessary to reach a steady-state limiting current is of the same order of magnitude as the step transition time.

There appears to be, therefore, a significant difference between the passage to limiting current potentiostatically as opposed to galvanostatically. This should be observed most clearly at a rotating disk electrode, where the limiting current distribution and the transition time are not distance dependent.

Part II. Unsteady-state mass transfer at a rotating disk electrode

4.5. Experimental

The experimental equipment is essentially the same as that described in chapter 3 for the potentiostatic measurement of rotating disk diffusivities. The Wenking potentiostat was used both in the potentiostatic and galvanostatic experiments; in the latter the potential drop over a fixed resistance was controlled.

Current and electrode potential were recorded by a Vidar 12289 Low-Level Data Logging System, consisting of a idar 510 Integrating Digital voltmeter, Vidar 12029 scanner, Vidar 625 Digital clock, Franklin 1040 High-Speed Printer, and vidar 650-8 Coupler. The data in digital form were

Table 4.2. Experimental solutions.

$c_{K_3Fe(CN)_6} = c_{K_4Fe(CN)_6}$; $c_{NaOH} = 0.4$ M

A. Galvanostatic measurements.

$c_{Fe(CN)_6^{3-}} = 0.0184$ M

$\rho = 1.022$ g/ml

$\mu = 0.985$ cp

$D = 7.88 \times 10^{-6}$ cm^2/sec

Sc = 1223 ; $\mu D/T = 2.60 \times 10^{-10}$ dyne/°K

B. Potentiostatic measurements.

$c_{Fe(CN)_6^{3-}} = 0.0143$ M

$\rho = 1.021$ g/ml

$\mu = 0.984$ cp

$D = 7.89 \times 10^{-6}$ cm^{2}sec

Sc = 1222 ; $\mu D/T = 2.60 \times 10^{-10}$ dyne/°K

Note 1. D calculated from the limiting current by means of the Levich equation.

2. According to Gordon, Newman and Tobias[47] $\mu D/T = 2.35 \times 10^{-10}$dyne/°K; according to Arvía, Marchiano and Podestá[51] 2.52×10^{-10}dyne/°K.

either printed out directly, or stored on magnetic tape and processed by computer. The highest scanning speed was 30 signals per second.

The rotating disks employed were of the design shown in Figure 3.1, with an embedded nickel electrode. Before each series of experiments the disk surface was pre-treated by cathodic hydrogen evolution in 5% NaOH solution at a current density of 20 ma/cm^2 for 10 to 15 minutes, to obtain a stabilized surface. The nickel reference electrode was given the same treatment.

The electrolyte was an equimolar solution of $K_3Fe(CN)_6$ and $K_4Fe(CN)_6$ prepared from reagent grade chemicals, with NaOH added as supporting electrolyte. The concentration of $K_3Fe(CN)_6$ was approximately 0.02M, that of NaOH 0.4 M. The exact reactant concentrations and physical properties for the two series of measurements are given in Table 4.2. The ferrocyanide and NaOH concentration were made up to the indicated values but not analyzed. Experiments were conducted at 25.0 $\pm$ 0.1 °C.

4.6. Results

A. Galvanostatic current ramps.

At two different rotation speeds (115 and 491 rpm) a series of current ramps were applied, with di/dt ranging from 0.005 to 12 ma/cm^{2}sec. Figures 4.5 to 4.7 illustrate the curves obtained. The individual points are overpotential readings taken at 60 msec intervals. The limiting current plateau gradually takes the character of an inflection, as di/dt is increased. The apparent limiting current was taken to be the value at the inflection point; this was located at approximately -900 mv overpotential except at the highest increase rates, where it tended to shift to higher potentials, up to-1200 mv.

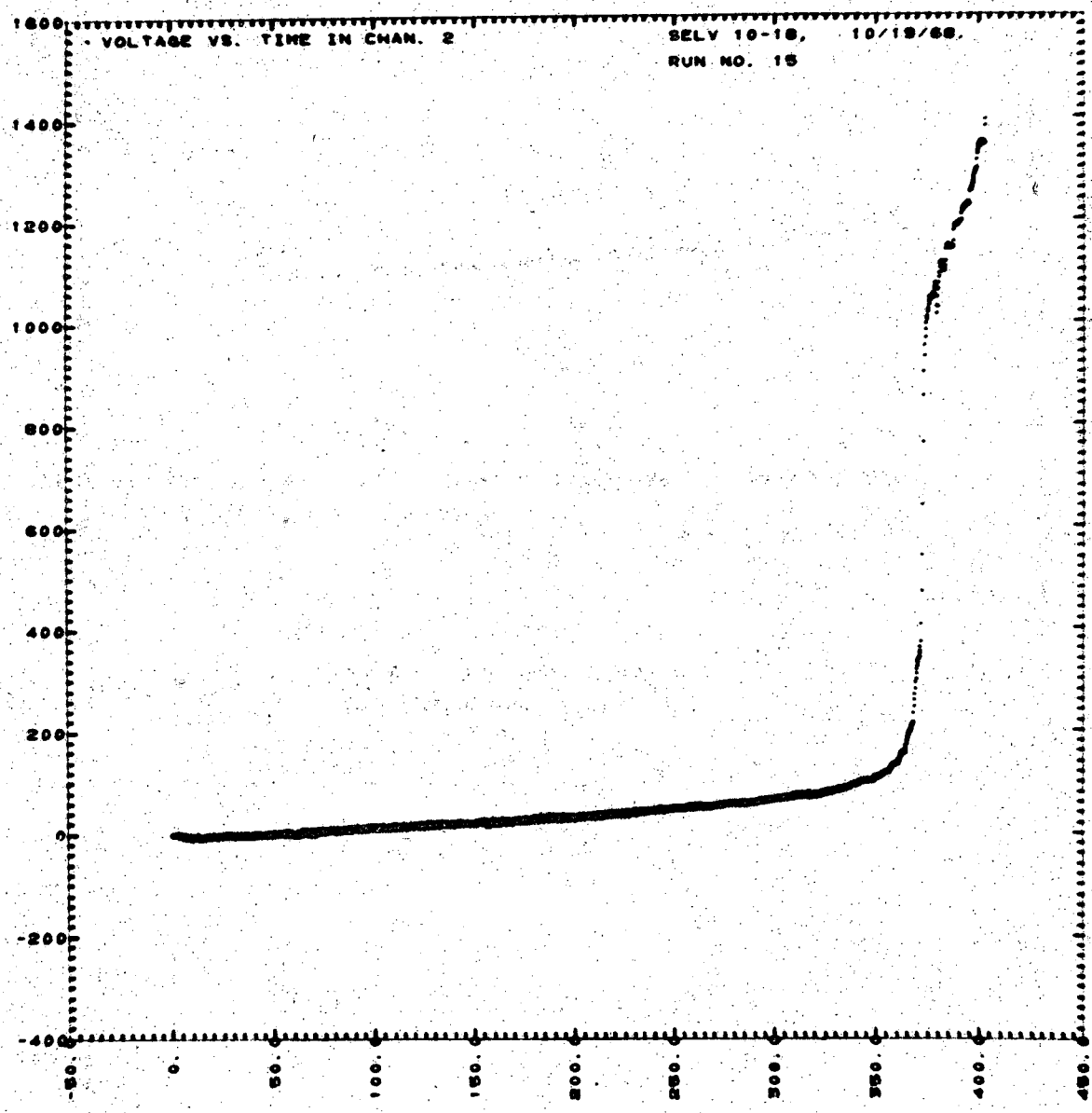

XBL 716-6882

Fig. 4.5. Overpotential (mv) vs time (sec) for a current application rate of 0.0104 ma/cm^{2}sec at 115 rpm (exp. 14).

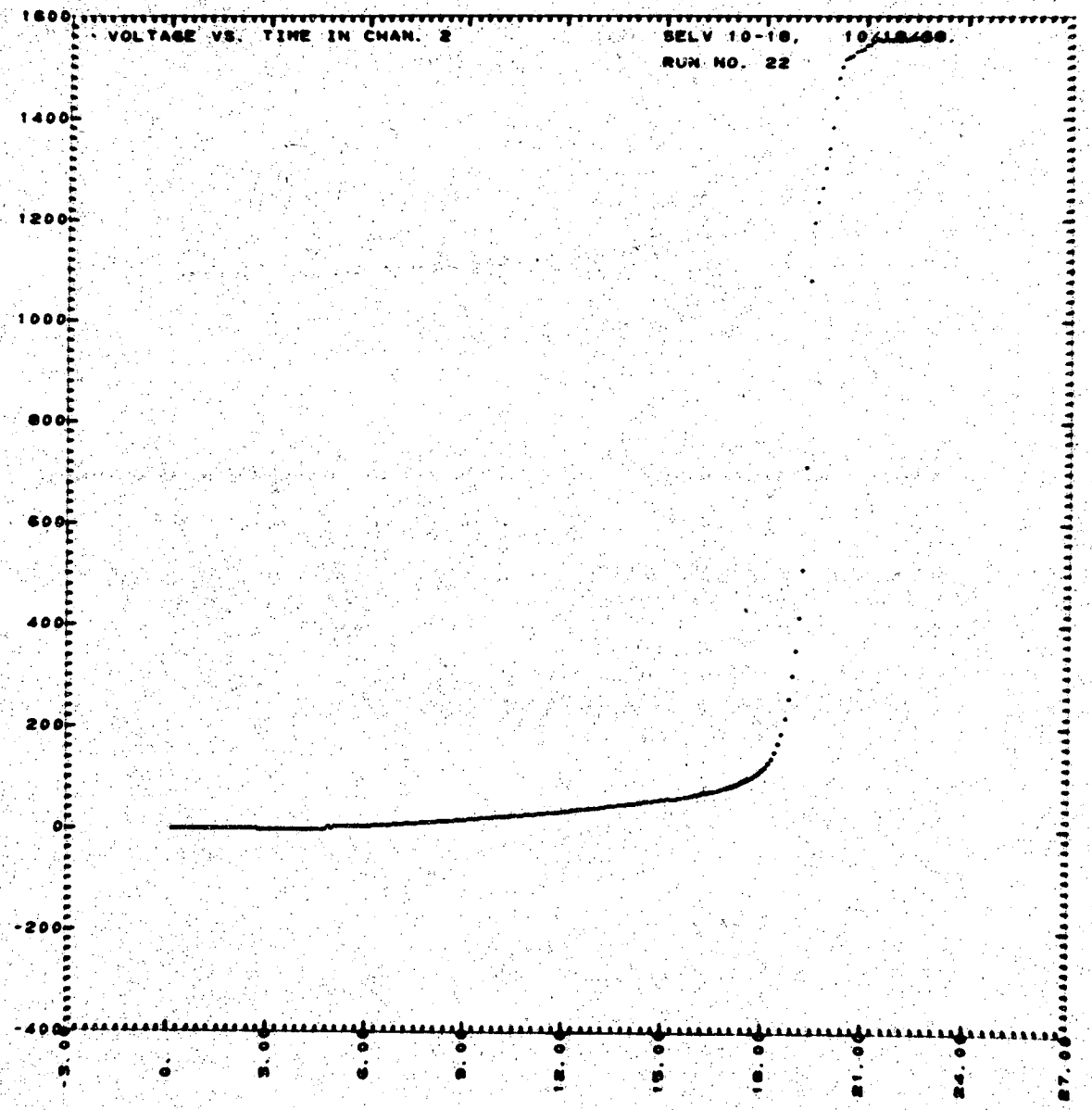

XBL 716-6883

Fig. 4.6. Overpotential (mv) vs time (sec) for a current application rate of 0.266 ma/cm$^2\sqrt{\text{sec}}$ (exp. 21).

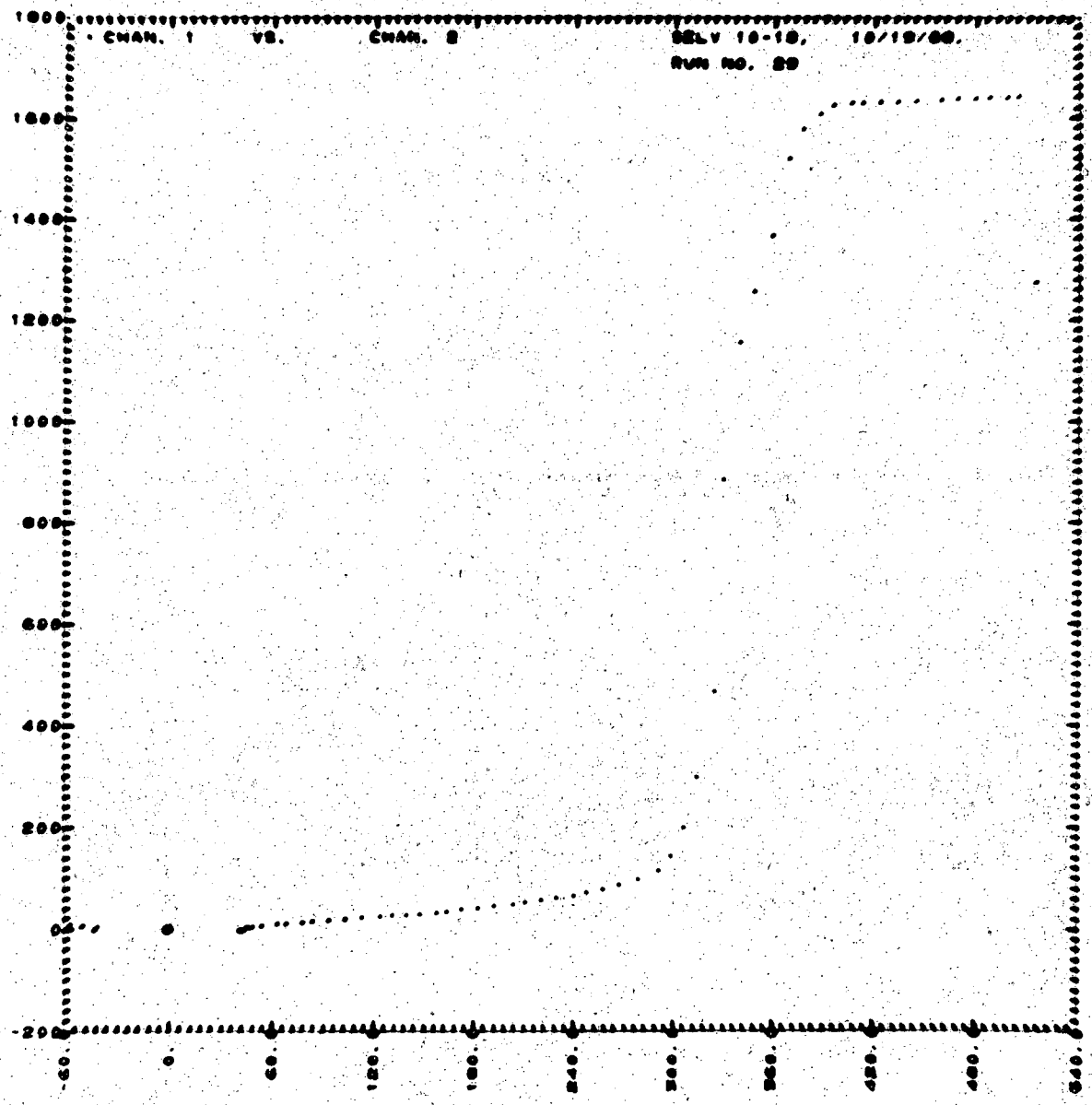

XBL 716-6884

Fig. 4.7. Overpotential (mv) vs current x 500 Ω(mv) for a current application rate of 2.04 ma/cm^2sec at 115 rpm (exp. 28).

Table 4.3 lists the results and gives also the values of dimensionless quantities, in terms of which the results at different speeds can be compared. The time in which the limiting current is reached, $i_\infty/(di/dt)$, is represented as a Fourier number with respect to the diffusion layer thickness:

$$\tau = Dt/\delta^2 \sim \omega t D^{1/3}/\nu^{1/3} = \frac{\omega i_\infty Sc^{-1/3}}{di/dt} \quad . \qquad (4.8)$$

This dimensionless time is the same one used to describe the decay of the flux following a concentration step at the rotating disk surface, or the concentration response to a constant flux instantaneously applied at the surface. (Appendix B and E use $\tau = 0.307\ \omega t\ Sc^{-1/3}$).

The minimum time to obtain steady-state limiting currents by means of a current ramp is apparently an order of magnitude larger than

$$\tau = \omega t\ Sc^{-1/3} = 5.46 \quad , \qquad (4.9)$$

i.e., the time in which the steady-state concentration is established (to within 1%) following a current step at the disk.

Figure 4.8 shows the results in a double-logarithmic plot of apparent limiting currents, relative to the steady-state value, against dimensionless time (8). At short times the apparent limiting current appears to tend toward a cube root dependence on time.

The steady-state limiting current values at the two speeds were in good agreement with the values for integral diffusivities of ferricyanide reported by Arvía a.o.[47] (Table 4.2).

Table 4.3. Apparent limiting current values obtained by linear current increase.

A. 115 rpm.

#	$di/dt \times 10^3$ (ma/cm^{2}sec)	i_L (ma/cm^2)	$i_\infty \omega Sc^{-1/3}/(di/dt)$	i_L/i_∞
16	5.03	3.18	723	0.985
15	5.43	3.16	670	0.978
13	10.3	3.23	353	1.000
14	10.4	3.23	350	1.000
9	21.7	3.23	168	1.000
17	81.6	3.37	44.6	1.043
20	163	3.56	22.3	1.102
18	172	3.38	21.1	1.046
22	261	3.60	13.9	1.115
21	266	3.62	13.7	1.121
24	494	4.00	7.36	1.238
23	506	4.03	7.19	1.248
26	1063	4.57	3.42	1.415
25	1150	4.62	3.16	1.430
28	2040	5.23	1.78	1.619
27	2140	5.35	1.70	1.656
29	4360	6.42	0.834	1.988
30	4680	6.48	0.777	2.006
31	6975	7.66	0.522	2.372
32	7040	7.62	0.517	2.359

Table 4.3. (continued)

B. 491 rpm

#	$di/dt \times 10^3$ (ma/cm^{2}sec)	i (ma/cm^2)	$i\,\omega Sc^{-1/3}/(di/dt)$	i_L/i
30	130	5.19	192	1
34	133	5.19	188	1
36	258	5.20	96.7	1.002
35	260	5.24	95.9	1.010
37	414	5.31	60.2	1.023
38	421	5.31	59.3	1.023
39	835	5.53	29.9	1.065
40	857	5.48	29.1	1.056
41	1700	5.96	14.7	1.148
42	1760	5.71	14.2	1.100
43	3370	6.35	7.41	1.223
44	3400	6.29	7.34	1.212
45	6660	7.30	3.75	1.407
46	6700	7.42	3.73	1.430
47	11620	8.34	2.15	1.607
48	11620	8.42	2.15	1.622

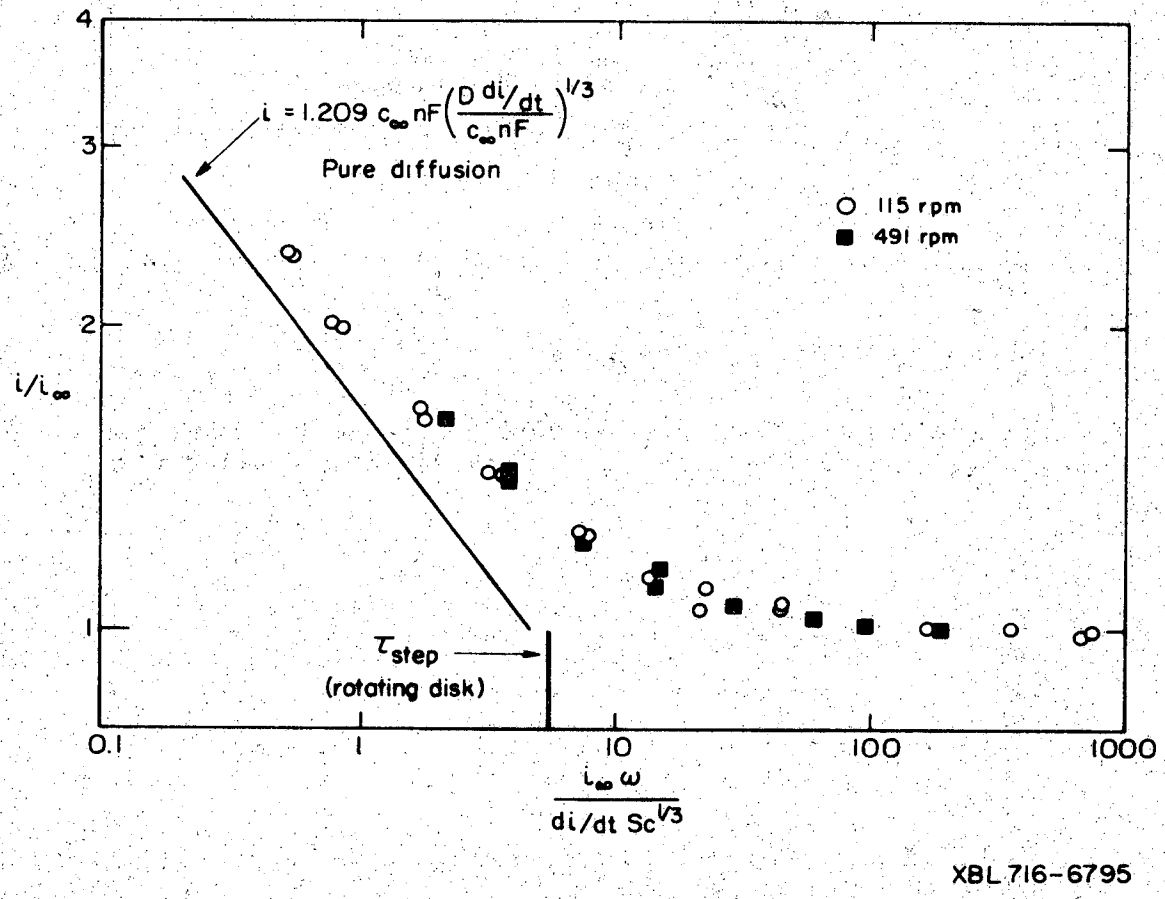

Fig. 4.8. Logarithmic plot of apparent limiting current against dimensionless current increase rate, i_∞ = steady-state limiting current.

B. Potentiostatic current increase

A series of potential scans were applied at 490 rpm, ranging from $d\eta/dt$ = 5 mv/sec to 2 v/sec. Figures 4.9 to 4.12 illustrate the curves obtained. Note that the potential scan did not start from exactly zero mv overpotential but from a small negative bias potential, so that the current shows a step at time zero. Characteristic for potential control in the limiting current region are the current fluctuations ($\pm$ 1% standard deviation) with a frequency somewhat higher than 1 sec^{-1}. The limiting current value was determined by averaging over the plateau, which here extended from 400-800 mv.

At higher scan rates the plateau is reached at lower values (< 200 mv); this is apparently due to a current maximum at low potentials, which at the highest scan rates can be clearly recognized as such. Where the current peak is higher than the plateau, the latter tends to be in unsteady-state, i.e., its current value is higher than the steady-state limiting current. At the highest scan rates a saddle-type curve is formed (Fig. 4.12).

Table 4.4 lists the peak and plateau currents, and the potential scan times. The latter can be expressed as

$$\tau = \omega t \; Sc^{-1/3} = \frac{\omega \; Sc^{-1/3}}{d\phi/dt} = \frac{\omega \; Sc^{-1/3} \; R \; T}{(d\eta/dt) \; nF} \quad . \qquad (4.10)$$

The time of passage necessary to obtain steady-state limiting currents by potential scanning is apparently of the same order of magnitude as the transition time (to within 1% of steady state) following a concentration step:

$$\tau = \omega t \; Sc^{-1/3} = 2.05 \qquad (4.11)$$

(see Appendix B)

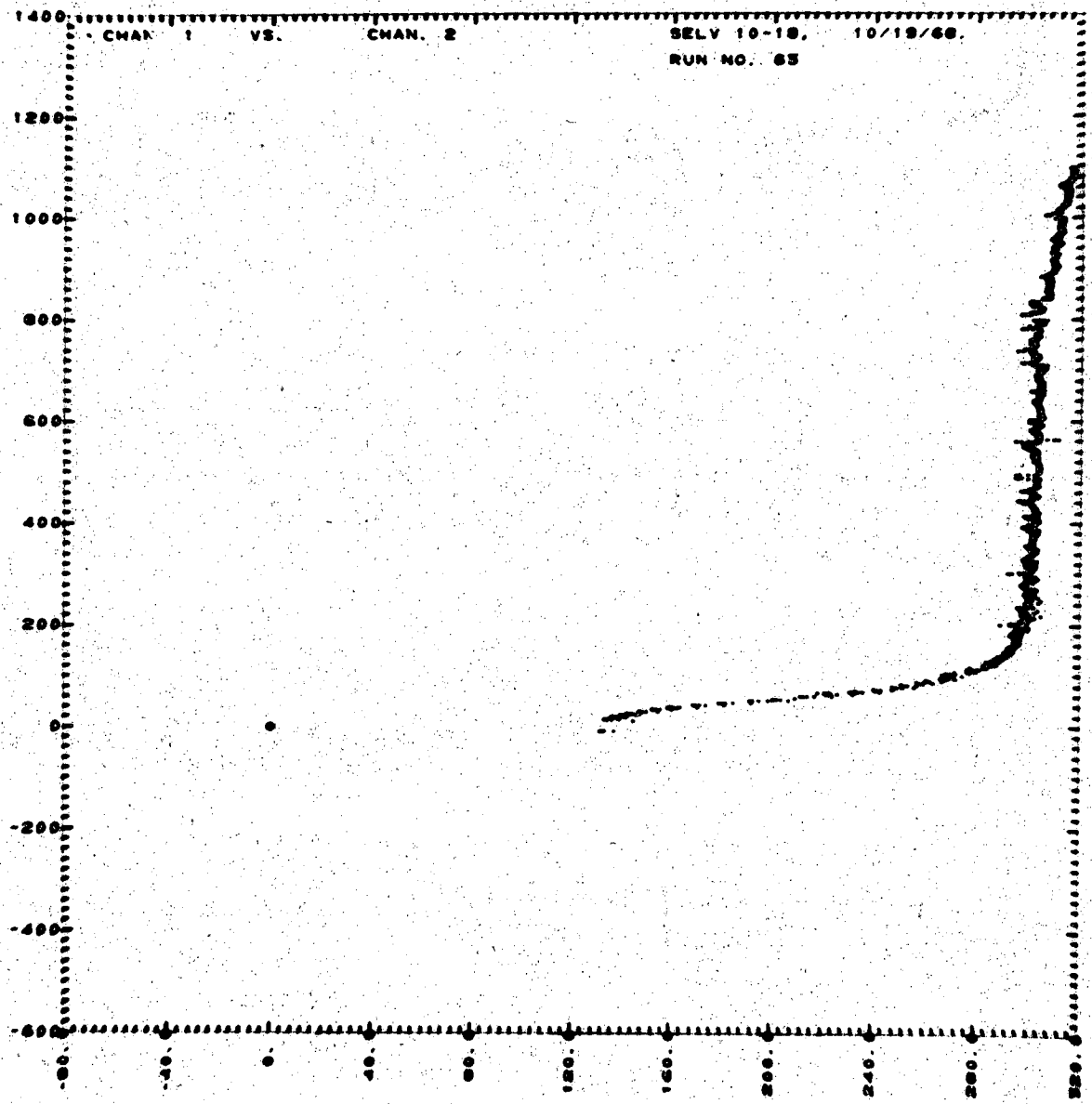

XBL 716-6885

Fig. 4.9. Overpotential (mv) vs current (max 500 Ω) for a potential scan rate of 8.77 mv/sec at 490 rpm (exp. 59).

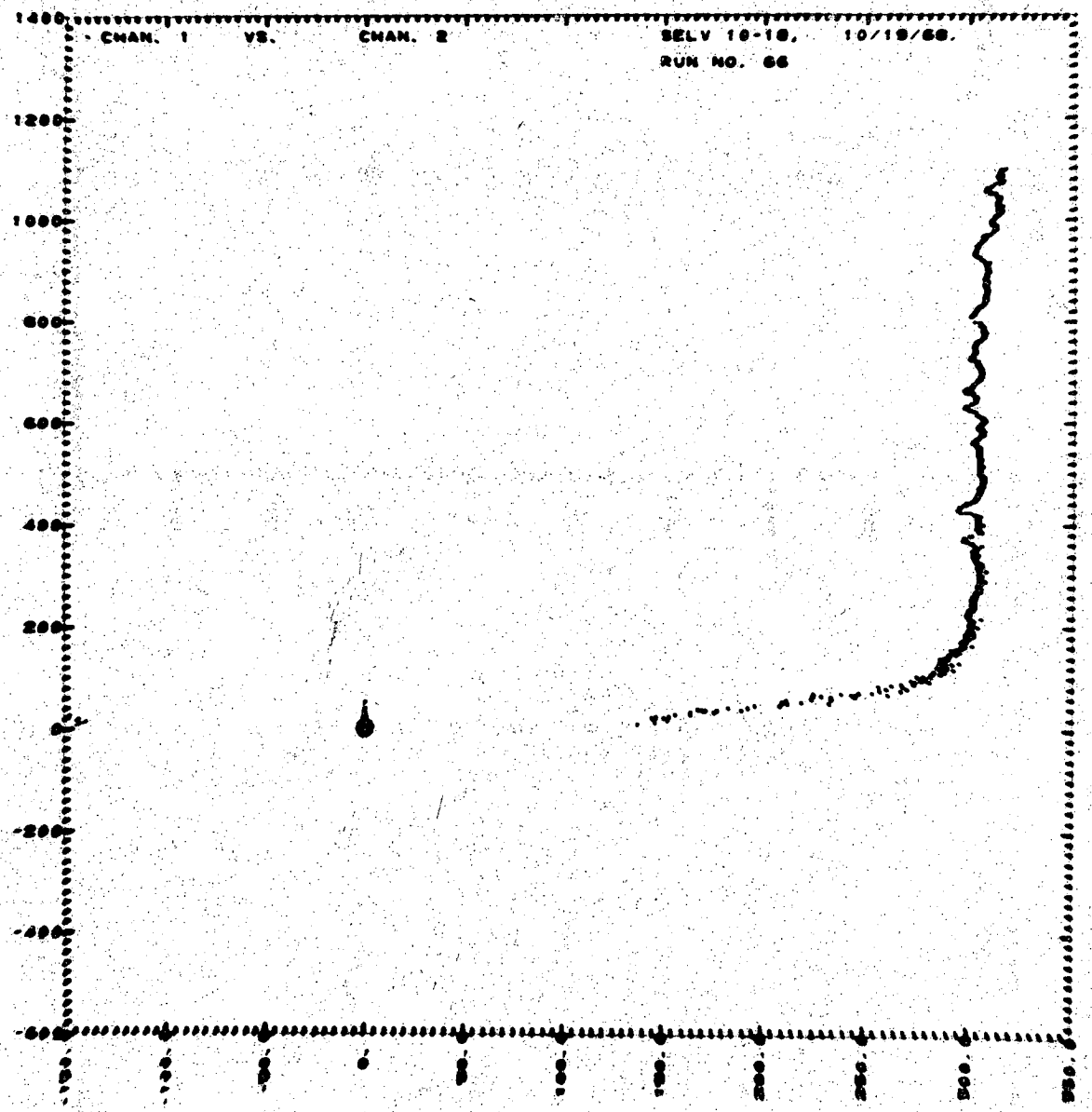

XBL 716-6886

Fig. 4.10. Overpotential (mv) vs current (ma x 500 Ω) for a potential scan rate of 27.9 mv/sec at 490 rpm (exp. 62).

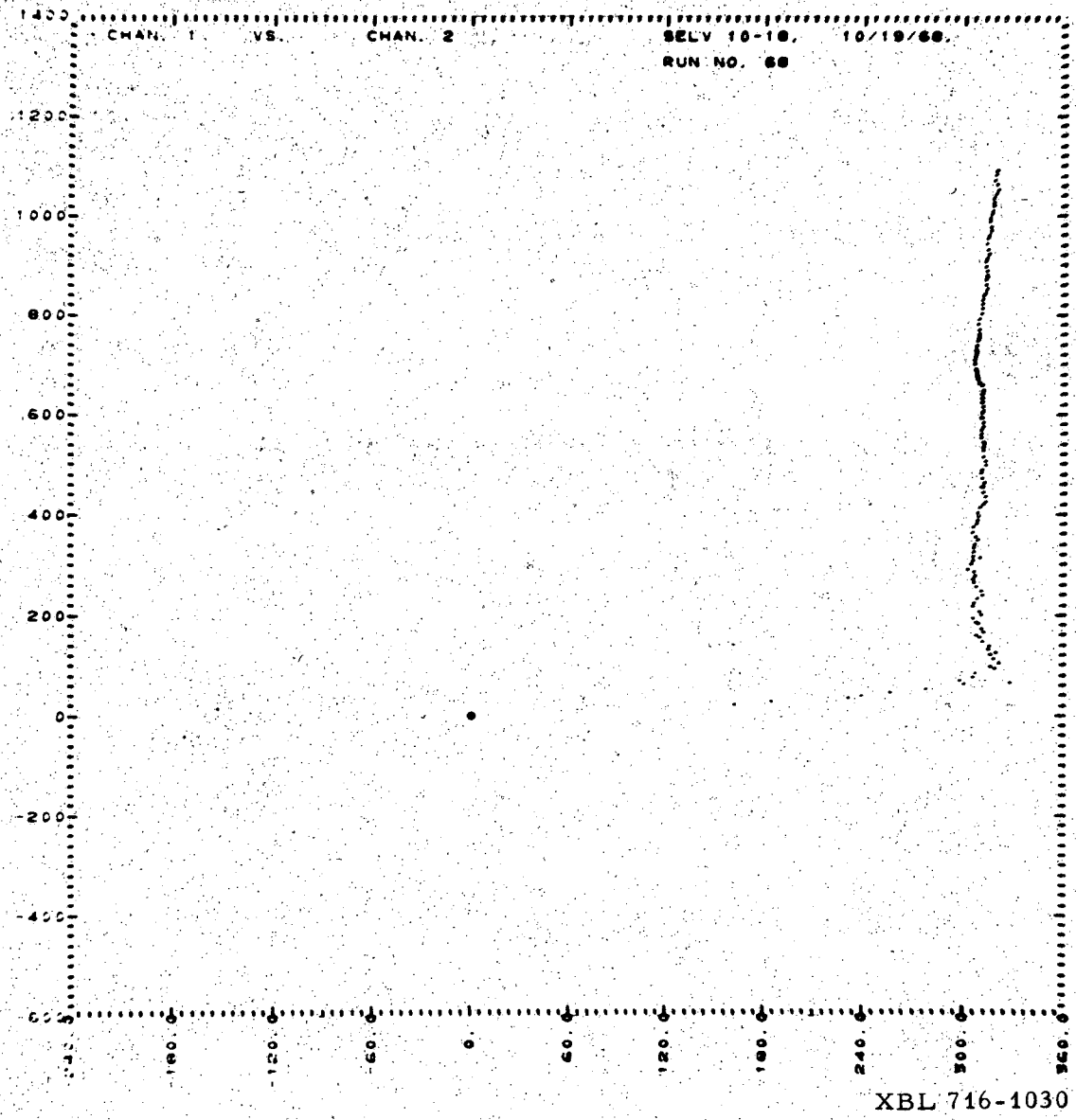

XBL 716-1030

Fig. 4.11. Overpotential (mv) vs current (max500 Ω) for a potential scan rate of 114 mv/sec at 490 rpm (exp 64).

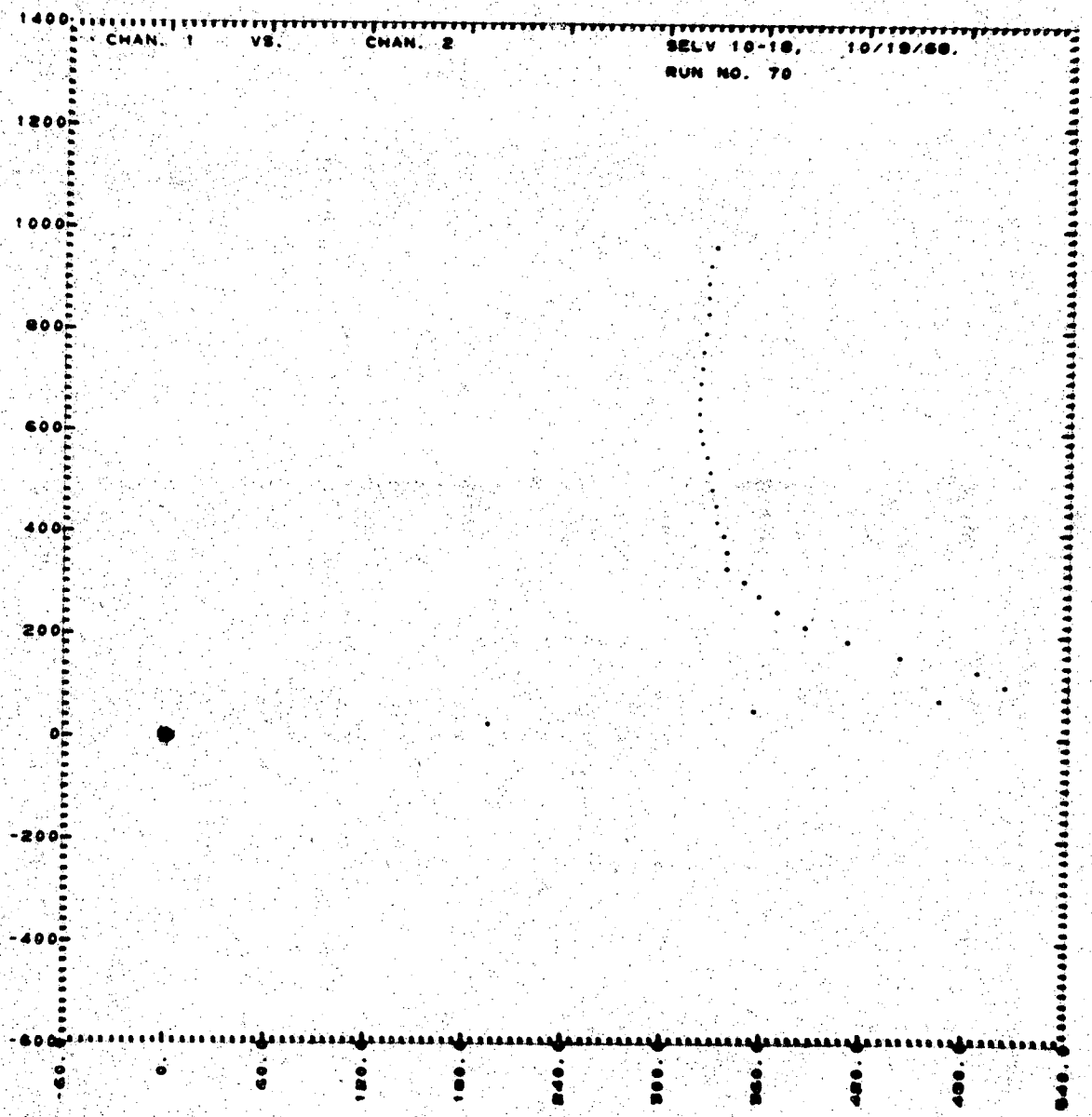

XBL 716-6887

Fig. 4.12. Overpotential (mv) vs current (ma x 500 Ω) for a potential scan rate of 436 mv/sec at 490 rpm (exp. 66).

Table 4.4. Apparent limiting current values obtained by linear potential decrease. (490 rpm)

#	$d\eta/dt$ (mv/sec)	i_L (ma/cm^2)	i_{max} (ma/cm^2)	$\omega Sc^{-1/3}(d\phi/dt)$	i_L/i_∞	i_{max}/i_∞
58	4.55	4.76	-	26.50	0.996	-
59	8.77	4.78	-	13.75	1	-
60	17.6	4.79	-	6.85	1.002	-
61	27.9	4.79	-	4.33	1.002	-
62	27.9	4.80	-	4.33	1.004	-
63	54.7	4.84	-	2.21	1.013	-
64	114	4.89	5.16	1.05	1.023	1.079
65	221	5.01	5.95	0.546	1.048	1.245
66	433	5.14	8.30	0.279	1.075	1.732
67	436	5.13	8.28	0.277	1.073	1.736
68	633	5.46	9.48	0.919	1.142	1.983
69	920	5.70	11.05	0.131	1.192	2.312
70	2165	8.06	16.5	0.0557	1.686	3.46
71	2097	8.06	16.5	0.0575	1.686	3.46

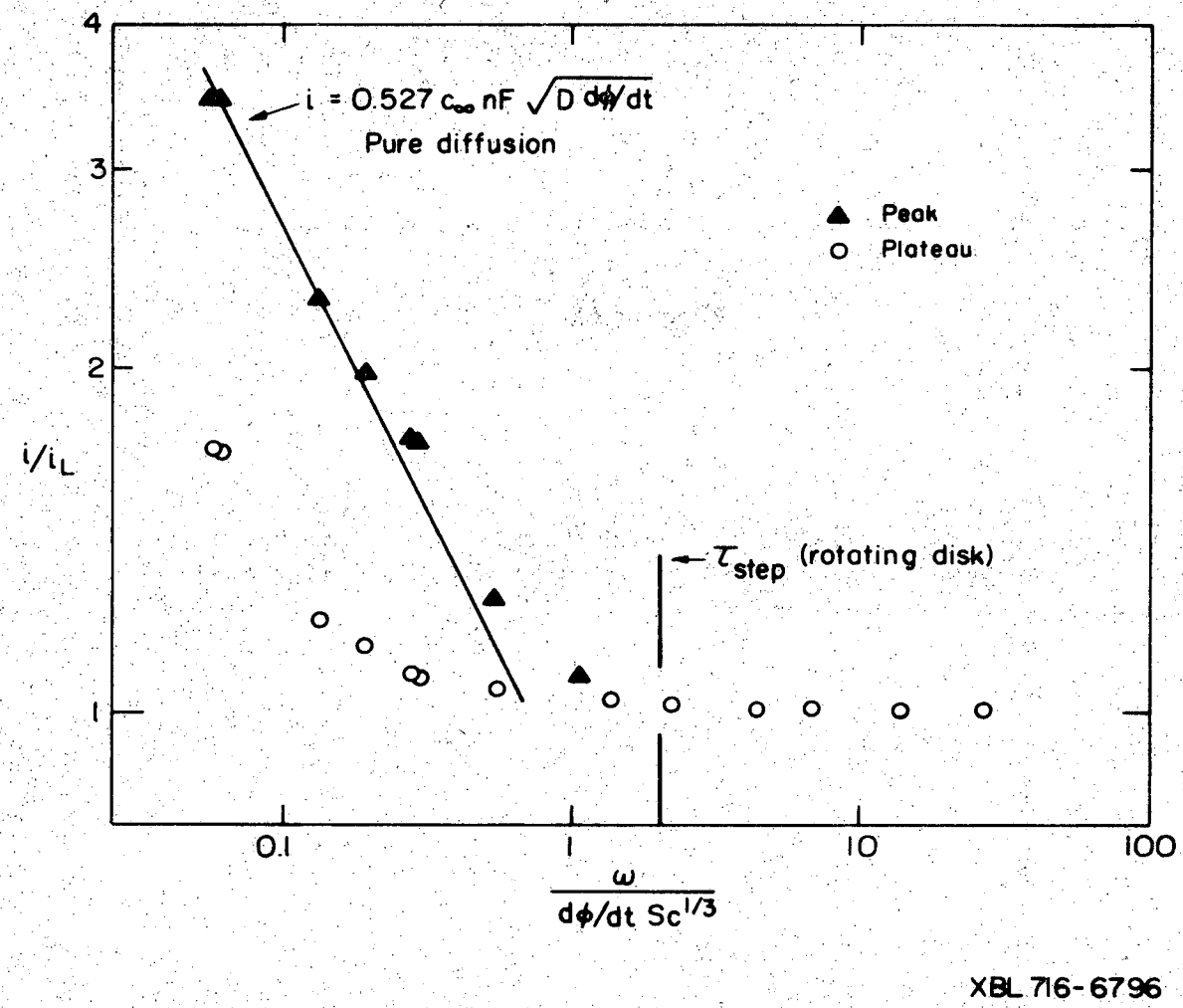

Fig. 4.13. Logarithmic plot of apparent limiting currents against dimensionless potential scan rate. i_L = steady-state limiting current.

Figure 4.13 shows the results in a double-logarithmic plot of apparent limiting currents (plateaux) and peak currents, relative to the steady-state limiting current, against the dimensionless time(10). At short times the apparent limiting current appears to depend inversely on the square root of the dimensionless time.

The steady-state limiting current was again as expected on the basis of diffusivities given by Arvía a.o.[51] (Table 4.2).

4.7. Discussion

The results of both galvanostatic and potentiostatic unsteady-state experiments may be interpreted in terms of a pure-diffusion model which is the more valid as the current or potential increase rate is higher. Near the disk surface the convection velocity toward the disk is

$$v_y = -\alpha y^2 \omega^{3/2} \nu^{-1/2} \qquad (4.12)$$

where $\alpha = 0.51023$. The convective term in the equation of convective diffusion is very small if

$$\frac{v_y y}{D} << 1 \rightarrow y << \left(\frac{\nu}{\omega}\right)^{1/2} Sc^{-1/3} \qquad (4.13)$$

i.e., an order of magnitude smaller than the steady-state diffusion layer.

In very fast transients the limiting current condition ($c \approx 0$), or a current maximum, is reached before the diffusion-layer thickness has grown enough to make convective transport important. This is evident in particular from the potentiostatic experiments, where the purely diffusive phase distinctly precedes the convective-diffusion.

phase if the scan rate is fast enough.

In the following analysis, to facilitate interpretation, the pure diffusion model is first applied to a deposition reaction. The results are then reconsidered for a redox reaction.

A. Galvanostatic experiments

The response of the concentration at the electrode, c_o, to a linearly increasing flux:

$$N = -D\left(\frac{\partial c}{\partial y}\right)_9 = +c_\infty st \qquad (4.14)$$

is[164]:

$$\frac{c_o - c_b}{c_b} = \frac{4st^{3/2}}{3(\pi D)^{1/2}} \qquad (4.15)$$

If the flux is toward the electrode ($N < 0$) and

$$s = \frac{|dN/dt|}{c_b} \quad , \qquad (4.16)$$

zero concentration at the electrode is reached in a time

$$t = \left(\frac{9\pi D}{16\ s^2}\right) \quad , \qquad (4.17)$$

and the flux will be $1.209\ c_b(sD)^{1/3}$.

Therefore, at high current increase rates the apparent limiting current should be proportional to $(di/dt)^{1/3}$. In terms of the dimensionless variables of Figure 4.8:

$$i_L/i_\infty = 1.662 \left(\frac{i_\infty \omega \, Sc^{-1/3}}{di/dt} \right)^{-1/3} \qquad (4.18)$$

This equation is shown as a solid line in Figure 4.8; the experimental values are definitely higher but tend toward the theoretical line at higher values of di/dt (or w).

It is easy to see that the deviation from (18) can not be ascribed to the fact that a redox reaction is involved. Since the flux is controlled, equations 14-17 are valid for the oxidized species, i.e., the ferricyanide ion (ox); the accumulation of the reduced species (red) at the cathode will be according to (15) but with D_{red} substituted for D_{ox}, and s_{red} equal to s_{ox} in an equimolar solution.

Calling

$$\tau_g = t \left(\frac{16 \, s_{ox}^2}{9\pi D_{ox}} \right)^{1/3} , \qquad (4.19)$$

one has for the concentration overpotential:

$$\eta = \frac{R_o T}{F} \ln \frac{1-\tau_g^{3/2}}{1+R\tau_g^{3/2}} , \qquad (4.20)$$

where

$$R = (c_{ox,b} D_{ox}^{1/2})/(c_{red,b} D_{red}^{1/2}) , \qquad (4.21)$$

For the present solution R = 1.1. From (20) it is clear that the time passed until the potential is sufficiently negative for hydrogen ion reduction, will be less than the theoretical time (17), i.e., $\tau_g = 1$. The limiting current then ought to be less than (18). A similar reasoning

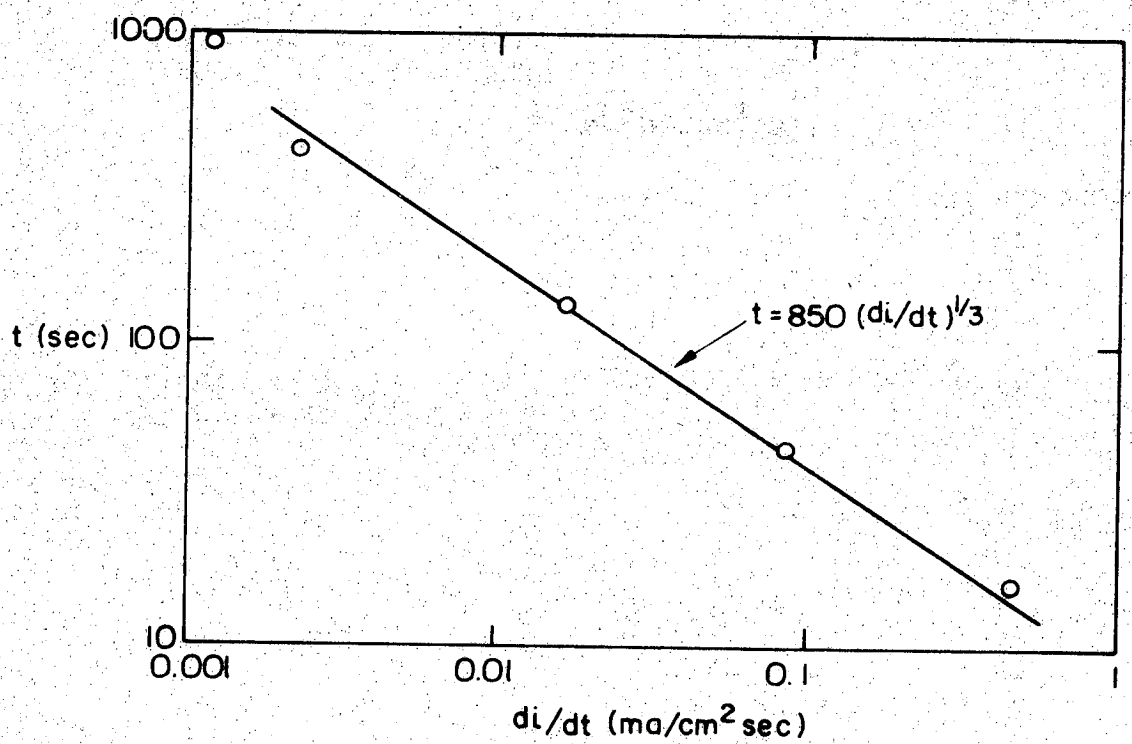

Fig. 4.14. Interpretation of the data of Fig. 4.2 in terms of non-stationary diffusion (equation 4-17).

shows that charge transfer overpotential, if influential, would lead to a lower limiting current.

The higher limiting current value, therefore, should be ascribed to convection. In the final phase of the transition, where the concentration of reactant at the electrode is exponentially decreasing, convection becomes important and prolongs the transition, thereby increasing the current.

It is of interest to compare the unsteady state currents found by Hickman (Figure 4.2) with equation (17). The proportionality between t and $s^{2/3}$ is very satisfactory (Figure 4.14). The diffusivity of Cu^{++} derived from the slope is $D = 4.73 \times 10^{-6}$ cm^2/sec; this is in good agreement with the values reported in Chapter 3. Note that the point for lowest di/dt deviates most from the least-squares slope through the points of Figure 4.14; this is probably due to secondary convection taking place at the edges of the embedded electrode.

Experiments similar to those of Figure 4.2, but for ferricyanide reduction at a nickel electrode, were reported by Boëffard,[46] who also established the dependence of the apparent limiting current on $(di/dt)^{1/3}$.

B. Potentiostatic experiments

The response of the flux at the electrode, N, to a concentration step, $c_b - c_o$, is well-known:

$$N = -D\left(\frac{\partial c}{\partial y}\right)_o = -(c_b - c_o)\sqrt{\frac{D}{\pi t}} \qquad (4.22)$$

If the surface overpotential or ohmic potential is negligible, one has from the Nernst relation:

$$\eta = \frac{R\,T}{F} \ln \frac{c_o}{c_b} \quad , \tag{4.23}$$

For a linear potential scan the boundary condition is then:

$$t > 0 \, , y = 0 \, , \; c_o = c_b e^{\pm at} \tag{4.24}$$

where

$$a = \frac{d\phi}{dt} = \frac{nF\left|d\eta/dt\right|}{R_o T} \tag{4.25}$$

By application of the superposition integral one derives from (22) and (24) for a negative potential scan:

$$N = - c_b \sqrt{aD} \, \frac{2}{\sqrt{\pi}} \, P(\sqrt{at}) \tag{4.26}$$

where the function

$$P(y) = e^{-y^2} \int_0^y e^{\lambda^2} d\lambda \tag{4.27}$$

is known as Dawson's integral.[165] It has a maximum $P(0.92414) = 0.54104$, and for large $y (y > 10)$ approaches asymptotically $(2y)^{-1}$, as shown in Figure 4.15. The flux at long times approaches that due to a concentration step (22) to $c_o = 0$.

The current maximum in potential scanning accordingly should depend on $(aD)^{1/2}$, i.e., on $(d\eta/dt)^{1/2}$:

$$i_{max} = -0.610503 \, c_b nF\sqrt{aD} \quad , \tag{4.28}$$

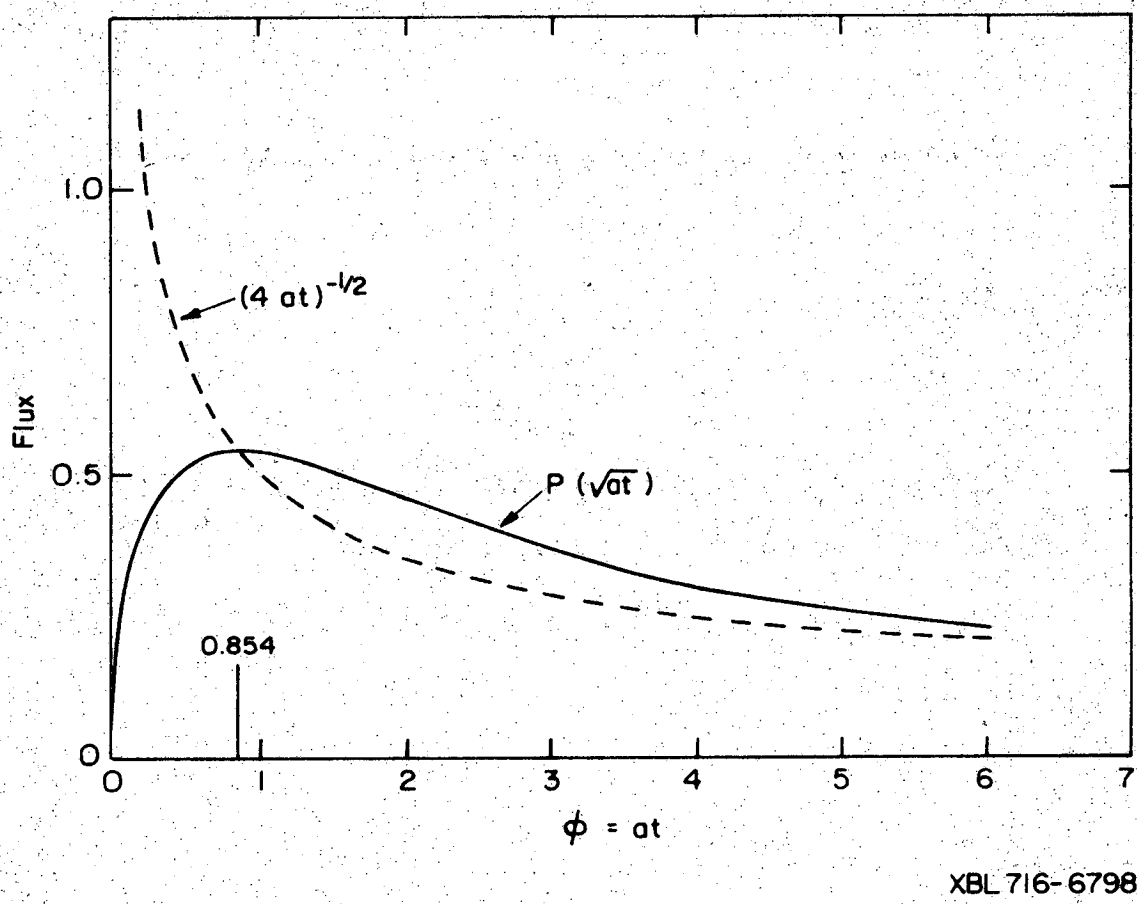

Fig. 4.15. Flux following a concentration step to $c_o = 0$ (dashed) and following a negative exponential concentration decrease (solid). The flux is expressed in units $-2c_b\sqrt{aD/\pi}$ (see equation 26).

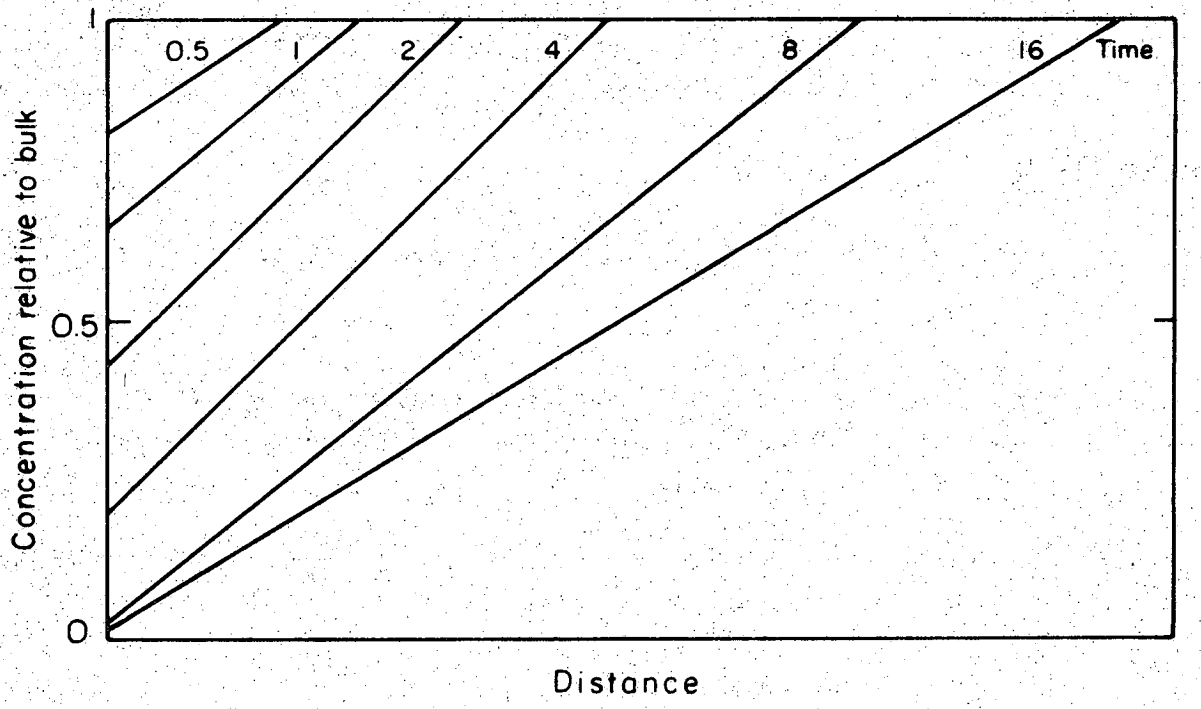

Fig. 4.16. Schematic concentration profiles illustrating the development of a current maximum in linear potential scanning.

while the potential at the peak should be independent of $d\eta/dt$:

$$\eta_{max} = -0.8540\ R_o T \tag{4.29}$$

It is to be noted that the peak current is not a limiting current in the usual sense, since $c_b = 0.426\ c_\infty$. Figure 4.16 illustrates schematically the sequence of concentration profiles, assuming a Nernst layer expanding proportional to $\sqrt{t}$ and the concentration at the electrode decreasing as $(2/3)^t$.

In terms of the dimensionless variables of Figure 4.13 equation 28 is:

$$i_{max}/i_\infty = 0.9838\left(\frac{\omega\, Sc^{-1/3}}{d\phi/dt}\right)^{-1/2} \tag{4.30}$$

When a redox reaction is involved, one should account for the contribution of the product ion (reduced species) to the overpotential. The accumulation of the product ion tends to decrease the potential to more negative values; when the potential is controlled, the result is a lowering of the current. The effect will be negligible in solutions with a small ratio of reactant (ox) to product (red) ion bulk concentration; in that case the conversion rate at the cathode is too small to cause a large shift of the potential with respect to the equilibrium potential. The effect will be large in solutions with an excess of reactant (ox) ion; a mathematical solution is available for this case (Sevcik-Randles equation).

In the present case of an equimolar solution no simplifications are possible. Consequently, a numerical solution had to be obtained using the characteristic diffusion parameter

$$R = \left(\frac{c_{ox,b}}{c_{red,b}}\right)\left(\frac{D_{ox}}{D_{red}}\right)^{1/2} \quad , \qquad (4.33)$$

which for the equimolar ferricyanide-ferrocyanide solution is approximately 1.1. Appendix F gives the details of the numerical solution, which employed a procedure given by Acrivos and Chambré.[169] As a check on the accuracy of the solution, the parameter R was varied from 10^{-3} to 10^{+5} by decades.

Figure 4.17 shows the current, expressed in terms of:

$$I = -\frac{i}{c_{ox,b}nF}\left(\frac{\pi}{aD_{ox}}\right)^{1/2} \quad , \qquad (4.34)$$

against the logarithm of the dimensionless potential $\phi = -\eta nF/(RT)$. Below $R = 10^{-3}$ the current maximum has the value given by (28), as in a deposition reaction, and its potential is given by (29). At high values of R, i.e., for potentials much more positive than the standard redox potential, the current maximum has the value given by the Sevcik-Randles equation

$$i_m/i_\infty = 0.4463\ c_{ox,b}nF\sqrt{aD_{ox}} \quad , \qquad (4.35)$$

where the constant agrees to 3 significant figures with that computed by Nicholson and Shain.[166] The peak potentials are dependent on R, shifting by $-\ell n\ 10$ for every decade increase of R.

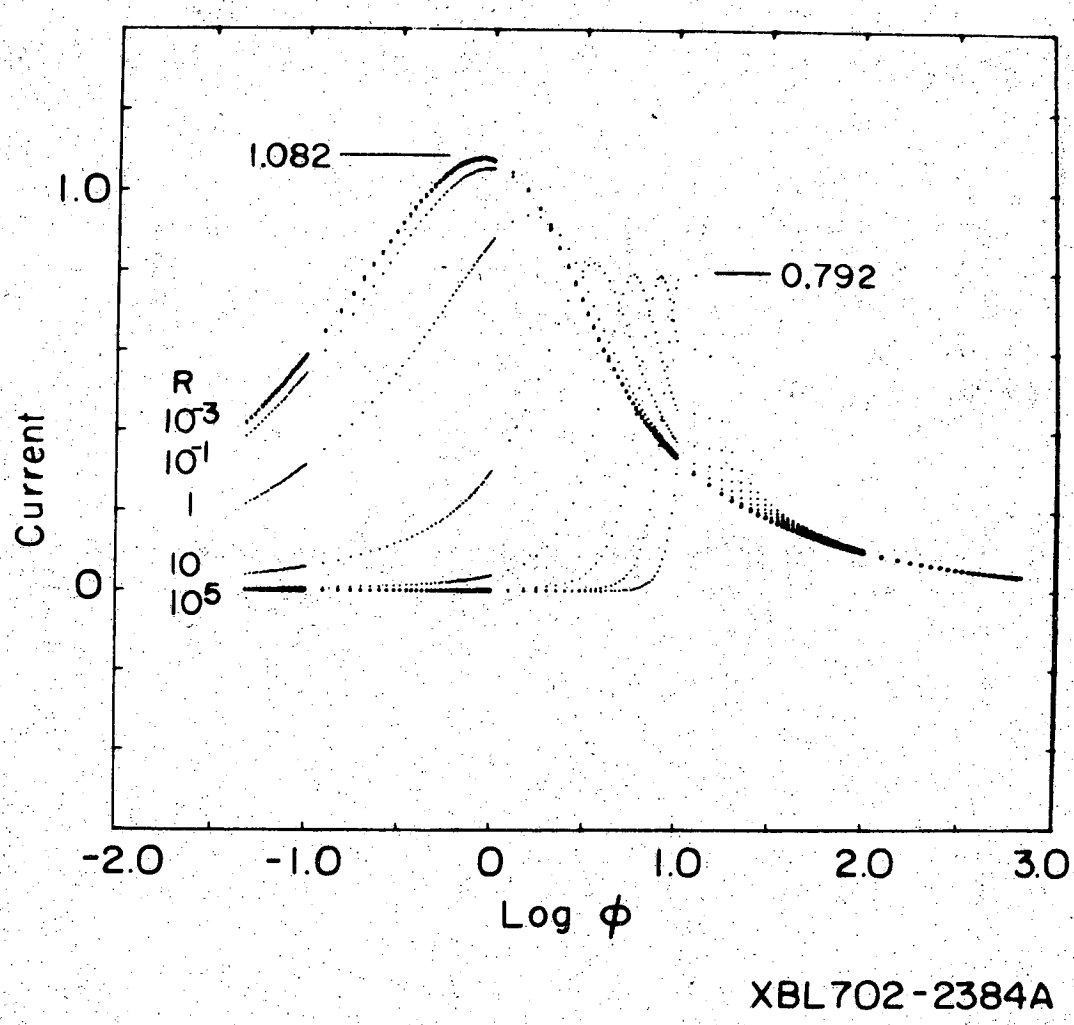

Fig. 4.17. Current response to potential scanning for a redox reaction. $R = (c_{ox,b}/c_{red,b})D_{ox}/D_{red})^{1/2}$. Current expressed in units $-c_{ox,b}nF\sqrt{aD_{ox}/\pi}$.

The current maximum for the equimolar solution is:

$$i_{max} = 0.52738\ c_b nF\sqrt{aD_{ox}} \quad , \tag{4.36}$$

or

$$i_{max}/i_\infty = 0.84995\left(\frac{\omega\ Sc_{ox}^{1/3}}{d\phi/dt}\right)^{-1/2} \tag{4.37}$$

The peak potential is $\phi = 1.6$, or $\eta = -41.1$ mv at 25°C.

Figure 4.13 shows that, for fast scans, (36) predicts the apparent limiting current reasonably well. The minimum scan period to reach steady-state limiting currents, is:

$$\tau = \frac{\omega\ Sc^{-1/3}}{d\phi/dt} = 1.40 \tag{4.38}$$

Note that this is somewhat shorter than the transition time following a concentration step at the rotating disk ($\tau = 2.05$ for $i/i_\infty = 1.01$)

Girina, Filinovskii and Feoktistov[162] measured current maxima for reduction of Tl^+ at copper amalgam, by potential scanning at a rotating disk electrode. They found good agreement with (35), which is the appropriate equation for this reaction. As expected, the minimum scan period is accordingly shorter; the reported value corresponds to $\tau = 0.86$.

The experimental peak potentials were larger than predicted, ranging from 65 to 190 mv, and increasing with the scan rate. The ohmic drop included in the measured overpotential is probably responsible for this shift. The resistance of the solution between cathode and reference electrode was estimated at 15 Ω. At the highest peak currents this leads to an included ohmic drop of 35 mv. It is not unlikely that the inclusion

of ohmic drop in the controlled potential leads to a shift of the peak potentials as large as the one found experimentally. In view of the good agreement between predicted and observed current values this possibility was not explored by further computations

C. Minimum time to reach steady-state limiting current

The minimum time observed in potentiostatic scanning is an order of magnitude smaller than that in galvanostatic passage to the limiting current. This can be explained by comparing the current-time relationship in both. In galvanostatic scanning this is linear. The current during the initial stage of the passage to limiting current is low , while the mass transfer process is still purely diffusive. When convection becomes important and starts to retard the transition to a steady-state concentration profile, the diffusion layer is not very far depleted and, therefore, the retarding influence of convection is effective.

On the other hand, in potentiostatic scanning the initial current is higher. This is indicated schematically in Figure 4.18, where the time is scaled with respect to the minimal time of passage to steady state (t_{ss}). The potentiostatic curve is that given by (30), i.e., for pure diffusion but in a restricted layer (Nernst thickness); the steady-state coincides with the maximum. Here the retarding effect of convection is less since the solution at the electrode has been depleted to a larger extent during the early stages of the transition.

In the pure diffusion model, on which equations (18) and (36) are based, this difference in current profiles leads to a difference in t_{ss}: expressed in the variable $\tau(9)$ the galvanostatic criterion is $\tau_{ss} = 4.59$,

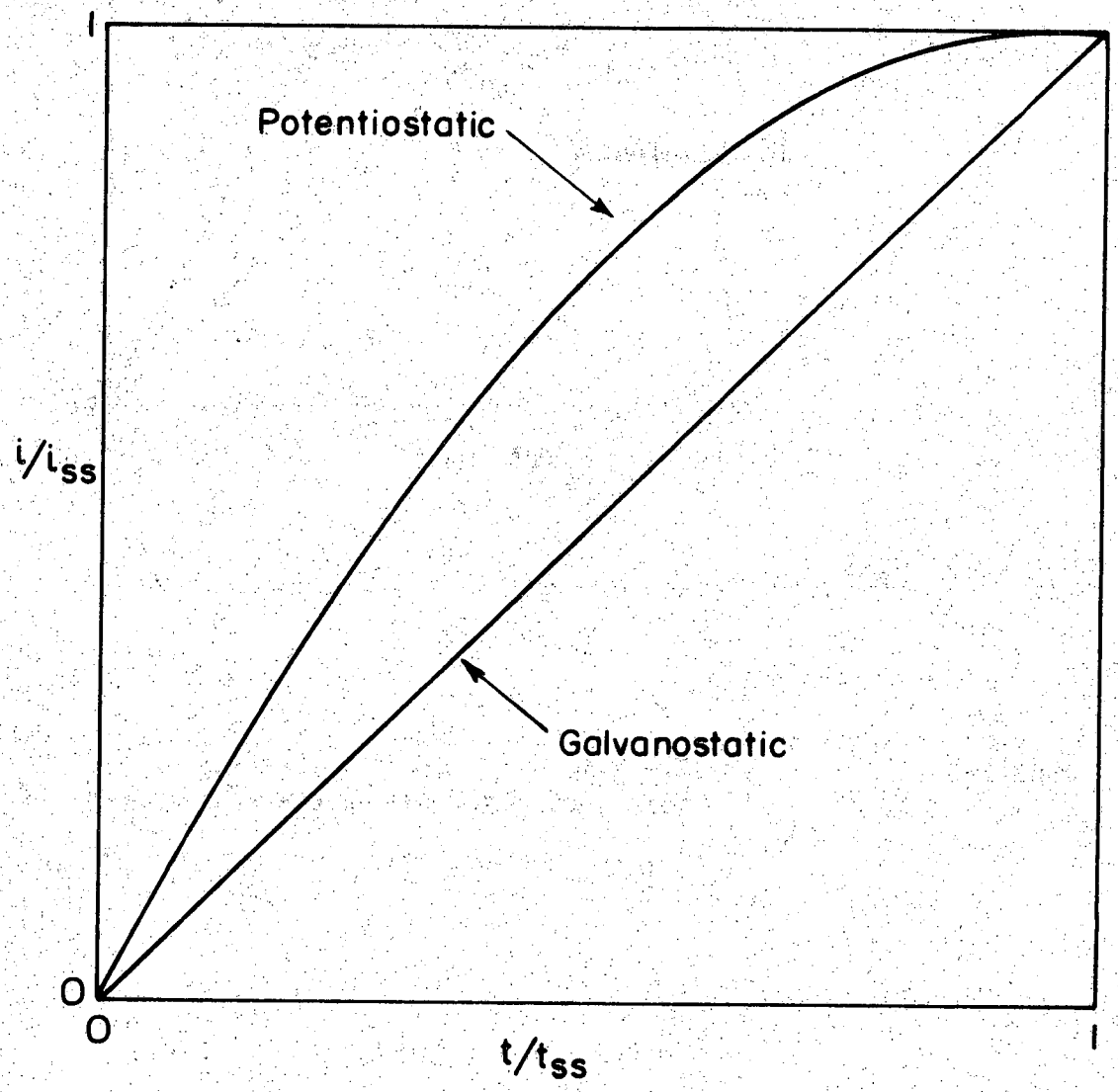

Fig. 4.18. Current vs time in galvanostatic and potentiostatic transition to a steady-state limiting current (schematic). t_{ss} = minimum time of passage to the limiting current.

the potentiostatic one is $\tau_{ss} = 0.85$. When convection enters the picture, the difference is reinforced: according to present results the galvanostatic criterion is $\tau_{ss} \approx 60$, the potentiostatic one $\tau_{ss} \approx 2$.

The minimum potentiostatic scan time is practically the same as the transition time following a concentration step. The minimum galvanostatic scan time is approximately 10 times the transition time following a current step. This last result confirms the conclusion inferred from the experiment of Figure 4.4

4.8. Conclusions

1. Theoretical information about transition times following a concentration or flux step in forced convective diffusion can be used to estimate the minimum time necessary to establish a steady-state limiting current by means of a current ramp or potential scan. In the potentiostatic mode this time is of the same order as the transition time following a concentration step. However, in the galvanostatic mode the minimal time required is an order of magnitude larger than the transition time following a flux step.

2. Experimentally the minimum time to establish steady-state at a rotating disk was found to be $2\ Sc^{1/3}/\omega$ in potentiostatic scanning, and approximately $60\ Sc^{1/3}/\omega$ for current ramps. These values are valid for a redox reaction in equimolar solution, with the assumption of very fast electrode kinetics.

3. The apparent limiting currents generated by fast potential scans or current ramps at a rotating disk electrode can be satisfactorily explained by a pure diffusion model. The agreement is good for the current maxima observed in potential scanning. Qualitative agreement is found for current ramps, where the apparent limiting current is influenced more effectively by convection.

4. At planar electrodes in forced convection the current distribution below the limiting current tends to interact with transient mass transfer to cause nonsimultaneous attainment of the limiting current along the plate. This tendency will be most pronounced very close to the limiting current; it will occur even if the early stages of the passage to the limiting current are quasi-static. Minimum times of passage to the limiting current should be based on experiments with segments at the trailing edge of the plate.

CONCLUSIONS AND RECOMMENDATIONS

1. Properly designed and executed limiting current measurements represent a powerful tool in the study of transport phenomena in forced and free convection at solid-liquid boundaries. This is illustrated by the continually expanding use of the method in chemical engineering, reviewed in Chapter 1.

2. Accurate measurement of limiting currents requires first of all a well-defined limiting current plateau. It has been shown how an ideal plateau for a given model reaction can be constructed. On this basis the limitations inherent in the copper deposition reaction, as compared to the ferricyanide-ferrocyanide redox reaction, can be distinctly recognized.

The slow electrode kinetics lead to a loss in the length of the plateau; the surface area change due to deposit roughness causes an inclination of the plateau when high current levels are involved, or when the steady-state limiting current is attained very slowly. In spite of these shortcomings the copper deposition reaction remains in frequent use, especially in studies of free convection.

3. Correct interpretation of limiting current values requires knowledge of the migration contribution included in the limiting current. For the copper deposition reaction the migration contribution is strongly dependent on the degree to which the HSO_4^- ions in solution are dissociated. Calculations indicate a migration effect roughly twice that for complete dissociation of HSO_4^-.

4. To correlate mass transfer rates from limiting current measurements ionic, not molecular, diffusivities should be used. The effective ionic

diffusivity of Cu^{++} ion in acidified $CuSO_4$ solution at 25°C, determined at a rotating disk electrode, can be expressed as

$$\mu D/T = (2.01 \pm 0.13) \times 10^{-10} \text{dyne}/°K$$

and is not significantly dependent on the ionic strength, at least in solutions sufficiently dilute in $CuSO_4$ (e.g., less than 0.1 M). This is substantially lower than the molecular diffusivities which have long been in use for this system.

5. In more concentrated solutions the ionic diffusivities obtained reflect an increase of effective surface area due to deposit roughness. The product μD is clearly dependent on the $CuSO_4$ concentration when the latter exceeds 0.1 M. The values obtained by a galvanostatic, stepwise, approach to the limiting current are apparently less influenced by this effect than those obtained by potentiostatic measurements, even if a potential-step method is applied.

6. By solving the time-dependent equation of convective diffusion it has been shown that the current following a concentration step at the surface of a rotating disk decays to a value only 1% above the steady-state value within $2.05\ Sc^{1/3}\ \omega^{-1}$ seconds. The transient currents following a potential step to -500 mv at a rotating disk electrode need a time approximately twice as long, probably due to rearrangement of the deposit on the disk.

7. The nonsimultaneous development of local limiting currents at elongated electrodes is difficult to avoid, even if the time to reach the limiting current has been chosen so as to accomodate the most slowly reacting segment, e.g., at the trailing edge of a planar electrode in forced convection.

This is a result of the interaction of transient mass transfer with the current distribution below the limiting current. The latter may, even in the steady-state, create a virtual zero concentration at the last electrode segment.

8. The minimum time to reach a steady-state limiting current is an order of magnitude longer in a galvanostatic approach than in a potentiostatic approach to the limiting current. This was demonstrated in Chapter 4 by measurements at a rotating disk electrode, using a redox reaction.

This conclusion has the interesting implication for the copper deposition reaction that the minimum roughness formation inherent in a galvanostatic approach to the limiting current may not be much less than that in a potentiostatic scan, using the maximum allowable scan rate to reach the steady state limiting current. This could be confirmed by performing experiments of the same kind as those of Chapter 4, using the copper deposition system. A quantitative characterization of the roughness formation by means of impedance measurement would be desirable.

ACKNOWLEDGEMENTS

I would like to express my gratitude to Professor Charles W. Tobias for his personal interest and encouragement throughout the course of this work. Where the thesis tended to become a vast microcosm, his intuition and practical experience were a frequent reminder of the world outside and the road ahead.

I am also very grateful to Professor John Newman for his constant attention and patient help in the analysis and interpretation of many results. His physical insight and critical perception have made it enjoyable to spend so much time in what often appear to be the dry places of the mind.

I am grateful to Professor Douglas Fuerstenau for reviewing this manuscript.

During the course of this work I have had support and sympathy from many individuals. Here I would like to thank in particular Uziel Landau and Samuel Kiprono Arapkoske for their cooperation in the experimental work.

I would like to thank Mrs. Jacqueline Cross for graciously typing the extensive manuscript, and Gloria Pelatowski for the work involved in the drawings.

Financial support was provided by the Atomic Energy Commission, through the Inorganic Materials Research Division of the Lawrence Radiation Laboratory.

Appendix A. Program for calculation of a theoretical limiting current curve.

Input: Z(Z), TP(t_+), XM(M), XNP(N'),

ALPHA(α), BETA(β), GAMMA(γ)

The program puts F(f) = 0.01 and calculates the concentration overpotential ETAC (η_c) according to (2.33), the ohmic contribution PHIOHM ($\Delta\Phi_\Omega$) according to (2.37), and the quantity

$$A \equiv -Mf/(1-f)^{\gamma} \quad .$$

An initial guess for E(ϕ_s) is made, assuming that cathodic surface overpotential constitutes the total η. Then the ϕ_s-dependent part of (2.34):

$$AO \equiv e^{\alpha\phi_s} - e^{-\beta\phi_s}$$

is compared with A, and if they differ by more than 1 in 10^6, a new E is calculated, using $DA \equiv dA_o/d\phi_s$:

$$\phi_s(k+1) = \phi_s(k) - \frac{A-AO(k)}{DA(k)} \quad .$$

After convergence ETAS(η_s), V(total overpotential) and R(η_c/η) are calculated.

```
      PROGRAM LIMCUR(INPUT,OUTPUT)
  101 FORMAT(4F10.6)
  102 FORMAT(3F10.6)
  103 FORMAT(10X,5(F10.6,2X))
  104 FORMAT(10X,5HZ=    ,F10.6,5H,M=    ,F10.6,12H,N-PRIME=     ,F10.6,6H,
     1T=    ,F10.6)
  105 FORMAT(10X,5HALPHA=,F10.6,6H,BETA=,F10.6,7H,GAMMA=,F10.6)
  106 FORMAT(10X,8H  F      ,8H  ETAS  ,8H  ETAC  ,8H PHIOHM ,8H   V    ,
     18H RATIO C)
  107 FORMAT(1H1)
    9 READ 101,Z,TP,XM,XNP
      IF (Z.EQ.0.) STOP
      READ 102,ALPHA,BETA,GAMMA
      PRINT 107
      PRINT 104,Z,XM,XNP,TP
      PRINT 105,ALPHA,BETA,GAMMA
      PRINT 106
      F=0.
      DO 1 I=1,109
      IF (I.LE.99) GO TO 7
      F=F+9./10.**(I-97) $ GO TO 8
    7 F=F+0.01
    8 ETAC=-0.025692/Z*(ALOG(1.-F+TP*F))
      PHIOHM= F*XNP*0.025692/Z
      A=- XM*F/(1.-F)**GAMMA $ E=-ALOG(-A)/BETA
      DO 2 J=1,100 $ A0=EXP(ALPHA*E) - EXP(-BETA*E)
      IF (ABS(A-A0).LT.1.0E-6*ABS(A)) GO TO 3
      DA=ALPHA*EXP(ALPHA*E)+ BETA*EXP(-BETA*E)
    2 E=E+(A-A0)/DA
    3 ETAS=-0.025692*E/Z
      V=ETAS +ETAC +PHIOHM
      R=ETAC/V
    1 PRINT 103,F,ETAS,ETAC,PHIOHM,V,R
      GO TO 9
      STOP
      END
-
+02.000000+00.000000+10.948300+01.849400
+00.750000+00.250000+00.420000
+01.000000+00.363000+18.860000+71.726000
+01.500000+00.500000+00.420000
```

Appendix B. Flux at a rotating disk after a concentration step at the surface, in the limit of high Schmidt numbers.

1. The equation of convective diffusion, including a time-dependent term:

$$\frac{\partial c}{\partial t} + v_y \frac{\partial c}{\partial y} = D \frac{\partial^2 c}{\partial y^2} \quad , \tag{B.1}$$

is to be solved with the boundary-conditions

$$c = 0 \quad , \quad y = 0 \quad , \quad t > 0 \quad ; \tag{B.2a}$$

$$c = 1 \quad , \quad y \to \infty \quad , \quad t > 0 \quad ; \tag{B.2b}$$

and the initial condition:

$$c = 1 \quad , \quad y \geq 0 \quad , \quad t = 0 \quad . \tag{B.2c}$$

In the limit of high Sc numbers the velocity perpendicular to the disk can be set equal to:

$$v_y = -\alpha\omega^{3/2}\nu^{-1/2}y^2 \quad , \quad \alpha = 0.51023 \quad . \tag{B.3}$$

Using the dimensionless variables:*

$$\tau = t\omega(\alpha/3)^{2/3}Sc^{-1/3} \quad ; \tag{B.4a}$$

$$\eta = y\omega^{1/2}\nu^{-1/2}(\alpha/3)^{1/3}Sc^{1/3} \quad ; \tag{B.4b}$$

the equation and boundary conditions can

---

*Note that τ in this Appendix is $(\alpha/3)^{2/3} = 0.307$ times the variable $\tau = \omega t\, Sc^{-1/3}$ used in Chapters 3 and 4.

now be written:

$$\frac{\partial c}{\partial \tau} - 3\eta^2 \frac{\partial c}{\partial \eta} = \frac{\partial^2 c}{\partial \eta^2} \quad ; \tag{B.5}$$

$$c = 0 \quad , \quad \eta = 0 \qquad \tau > 0 \quad ; \tag{B.6a}$$

$$c = 1 \quad , \quad \eta \to \infty \qquad \tau > 0 \quad ; \tag{B.6b}$$

$$c = 1 \quad , \quad \eta \geq 0 \qquad \tau = 0 \quad . \tag{B.6c}$$

The flux at the electrode is:

$$N = -D(\partial c/\partial y)_o = -D(\omega/\nu)^{1/2}(\alpha Sc/3)^{1/3}(\partial c/\partial \eta)_o \tag{B.6d}$$

2. At <u>small times</u> the change in c takes place very close to the disk surface, where the convective term in (5) is negligible. In that case the solution is:

$$c = \mathrm{erf}(\eta/2\tau^{1/2}) \tag{B.7}$$

and the concentration gradient at the electrode is:

$$\left.\frac{\partial c}{\partial \eta}\right|_o = \frac{1}{\sqrt{\pi\tau}} \tag{B.8}$$

At <u>large times</u> the solution of (5) approaches asymptotically the steady-state solution:

$$c = \int_0^{\eta} e^{-\eta^3} d\eta / \int_0^{\infty} e^{-\eta^3} d\eta \quad , \tag{B.9}$$

and the concentration gradient at the electrode to

$$\left.\frac{\partial c}{\partial \eta}\right|_o = 1/\Gamma(4/3) = 1.1198465 \qquad \text{(B.10)}$$

3. Equation (5) can be written in terms of a new variable embodying the short-time asymptotic behavior:

$$Z = \eta/2\tau^{1/2} \quad . \qquad \text{(B.11)}$$

The result is:

$$\frac{\partial c}{\partial \tau} - \left(\frac{Z}{2\tau} + 6Z^2\tau^{1/2}\right)\frac{\partial c}{\partial Z} = \frac{1}{4\tau}\frac{\partial^2 c}{\partial Z^2} \quad , \qquad \text{(B.12)}$$

with the boundary conditions:

$$c = 0 \quad , \quad Z = 0 \quad , \quad \tau > 0 \quad ; \qquad \text{(B.13a)}$$

$$c = 1 \quad , \quad Z \to \infty \quad , \quad \tau \geq 0 \quad . \qquad \text{(B.13b)}$$

The initial condition is now implied in one of the boundary conditions.

A perturbation expansion about the short time solution:

$$c(Z,\tau) = c_o(Z) + \tau^{3/2}c_1(Z) + \tau^3 c_2(Z) + \ldots \quad , \qquad \text{(B.14)}$$

yields for the zero-order term:

$$\frac{1}{4\tau}\left(-2Z\frac{dc_o}{dZ} = \frac{d^2c_o}{dZ^2}\right) \quad , \qquad \text{(B.15)}$$

i.e., $c_o = \text{erf } Z$, in agreement with (7), and next:

$$\frac{\tau^{1/2}}{4}\left\{\frac{d^2c_1}{dZ^2} + 2Z\frac{dc_1}{dZ} - 6c_1 = -24Z^2\frac{dc_o}{dZ}\right\} \quad . \qquad \text{(B.16)}$$

One solution of the homogeneous equation is

$$c_H = Z^3 + \frac{3}{2}Z \quad . \tag{B.17}$$

The complete solution is

$$c_1 = (Z^3 + \frac{3}{2}Z)\ \text{erfc}\ Z + 3\pi^{-1/2}\ Z^2 e^{-Z^2} \quad . \tag{B.18}$$

The second-order term in (14), obtained by solving:

$$\frac{d^2c_2}{dZ^2} + 2Z\frac{dc_2}{dZ} - 12\ c_2 = -24Z^2\ \frac{dc_1}{dZ} \quad , \tag{B.19}$$

is

$$c_2 = -\frac{14}{5}\ Z^6 \text{erfc}\ Z - 3Z^4 \text{erfc}\ Z - \frac{Ze^{-Z^2}}{10\sqrt{\pi}}(52Z^4 - 8Z^2 - 3) \quad . \tag{B.20}$$

For the concentration gradient at the electrode this yields:

$$\left.\frac{\partial c}{\partial Z}\right|_o = \frac{2}{\sqrt{\pi}} + \frac{3}{2}\ \tau^{3/2} + \frac{3\tau^3}{10\sqrt{\pi}} + O(\tau^{9/2}) \quad , \tag{B.21}$$

or

$$\left.\frac{\partial c}{\partial \eta}\right|_o = \frac{1}{\sqrt{\pi\tau}} + \frac{3\tau}{4} + \frac{3\tau^{5/2}}{20\sqrt{\pi}} + O(\tau^4) \tag{B.22}$$

4. A numerical solution of (5) can now be sought using two sets of variables:

A. At times $\tau < 1$ the variables are:

$$T = \tau^{3/2} \quad ; \tag{B.23a}$$

$$Z = \eta/2\tau^{1/2} = \eta/2T^{1/3} \quad ; \tag{B.23b}$$

$$\theta_1(Z,T) = c(Z,T) - \text{erf}(Z) \quad . \tag{B.23c}$$

The equation to be solved (12) is:

$$\frac{\partial\theta_1}{\partial T} = \frac{1}{6T}\left(2Z\,\frac{\partial\theta_1}{\partial Z} + 24\,Z^2T\,\frac{\partial\theta_1}{\partial Z} + \frac{\partial^2\theta_1}{\partial Z^2}\right) + \frac{8}{\sqrt{\pi}}\,Z^2e^{-Z^2} \qquad (B.24)$$

The boundary conditions are:

$$\theta_1 = 0 \quad , \quad Z = 0 \quad , \quad T > 0 \quad ; \qquad (B.25a)$$

$$\theta_1 = 0 \quad , \quad Z \to \infty \quad , \quad T \geq 0 \quad . \qquad (B.25b)$$

B. At times $\tau > 1$ the variables are:

$$T = \tau^{3/2} \quad ;$$

$$\eta \text{ and } \theta_2 = c(\eta,T) - \frac{\int_0^{\eta} e^{-\eta^3}\,d\eta}{\Gamma(4/3)} \qquad (B.25c)$$

The variable T is kept for convenience in numerical integrations, later on. The change to the variables (B) is made most conveniently at $T = 1/8$, since at that time Z and η are numerically equal. The equation to be solved (5) is:

$$\frac{3}{2}\,T^{1/3}\,\frac{\partial\theta_2}{\partial T} = 3\eta^2\,\frac{\partial\theta_2}{\partial\eta} + \frac{\partial^2\theta_2}{\partial\eta^2} \qquad (B.26)$$

The boundary conditions are:

$$\theta_2 = 0 \quad , \quad Z = 0 \quad , \quad T > 0 \qquad (B.27a)$$

$$\theta_2 = 0 \quad , \quad Z \to \infty \quad , \quad T > 0 \qquad (B.27b)$$

5. The numerical procedure is the same for both equations (24) and (26).

Let the concentration (θ_1, resp.θ_2) at step i of T and at step j of the distance (Z, resp. η) be called $c_{i,j}$. The left-hand side of(18), resp. (20), is evaluated as a central difference. The right-hand side, averaged between steps, is the central value of the left-hand side. E.g., for (24):

$$\frac{c_{i+1,j}-c_{i,j}}{\Delta T} = \frac{1}{12T}\left\{\frac{c_{i+1,j+1} + c_{i+1,j-1} - 2c_{i+1,j}}{h^2} + \frac{c_{i,j+1} + c_{i,j-1} - 2c_{i,j}}{h^2}\right\} + \left(\frac{Z_j}{6T} + 2Z_j^2\right)$$

$$\left\{\frac{c_{i+1,j+1} - c_{i+1,j-1}}{2h} + \frac{c_{i,j+1} - c_{i,j-1}}{2h}\right\} + \frac{8}{\sqrt{\pi}} Z_j^2 e^{-Z_j^2} \qquad (B.28)$$

Here $T = \frac{1}{2}(T_i + T_{i+1})$.

This results in a set of equations for the unknown concentrations at time-step i + 1;

$$A_j c_{i+1,j-1} + B_j c_{i+1,j} + D_j c_{i+1,j+1} = G_j \quad . \qquad (B.29)$$

The coefficients for the case of (24) are*:

$$A_j = -\Delta T/12h^2T + Z\Delta T/12hT + Z^2\Delta T/h \quad ; \qquad (B.30a)$$

$$B_j = 1 + \Delta T/6h^2T \quad ; \qquad (B.30b)$$

$$D_j = -\Delta T/12h^2T - Z\Delta T/12hT - Z^2\Delta T/h \qquad (B.30c)$$

---

*The suffix j of Z_j is omitted hereafter.

$$G_j = c_{i,j} + \Delta T(c_{i,j+1} + c_{i,j-1} - 2c_{i,j})/12h^2T$$

$$+ \Delta T(Z/6T + 2Z^2)(c_{i,j+1} - c_{i,j-1})/2h \qquad (B.30d)$$

$$+ \Delta T8Z^2e^{-Z^2}/\sqrt{\pi}$$

Using the relation*

$$c_j = \xi_j + E_j c_{j+1} \quad , \qquad (B.31)$$

we have from (23):

$$A_j\xi_{j-1} + A_jE_{j-1}\xi_j + A_jE_{j-1}E_jc_{j+1}$$

$$+ B_j\xi_j + B_jE_jc_{j+1} + D_jc_{j+1} = G_j \quad , \qquad (B.32)$$

and from this $\xi_j = (G_j - A_j\xi_{j-1})/(B_j + A_jE_{j-1})$; (B.33a)

$$E_j = -D_j/(A_jE_{j-1} + B_j) \quad . \qquad (B.34b)$$

The successive ξ_j, E_j are calculated starting with $\xi_1 = 0$, $E_1 = 0$, i.e., the boundary condition $\theta = 0$. The term G_j for the first time-step is zero. The calculation of c_j is performed in reverse order, starting with $\theta_\infty = 0$.

The derivative at the interface is calculated at every time-step:

$$(4\ c_{i,2} - c_{i,3})/2h + O(h^2) \qquad (B.35)$$

A listing of the program CONST is given at the end of this appendix.

By variation of mesh size (h) at constant number of meshpoints (201)

---

*The suffix i+1 is omitted where the unknown c is meant.

Table B.1. Concentration gradient at the interface: numerical solution* and various approximations.

Part A.

T	τ	$(\frac{\partial\theta}{\partial\eta})_o$	eq. 22		eq. 36	eq. 39	eq. 35
			1 term	2 terms		30 terms	
5×10^{-7}	6.34×10^{-5}	71.0835	71.0834	71.0835	71.0824	54.8483	71.0824
1×10^{-6}	1.00×10^{-4}	56.4190	56.4190	56.4190	56.4190	49.1349	56.4179
5×10^{-6}	2.94×10^{-4}	32.9942	32.9940	32.9942	32.9942	32.6825	32.9931
1×10^{-5}	4.64×10^{-4}	26.1877	26.1874	26.1877	26.1877	26.1593	26.1866
5×10^{-5}	1.36×10^{-3}	15.3155	15.3145	15.3155	15.3155	15.3144	15.3144
1×10^{-4}	2.15×10^{-3}	12.1567	12.1551	12.1567	12.1567	12.1551	12.1556
5×10^{-4}	6.34×10^{-3}	7.1131	7.1083	7.1131	7.1131	7.1083	7.1119
1×10^{-3}	1.00×10^{-2}	5.6494	5.6419	5.6494	5.6494	5.6419	5.64839
5×10^{-3}	2.94×10^{-2}	3.3213	3.2994	3.3213	3.3213	3.2994	3.32038
1×10^{-2}	4.64×10^{-2}	2.6536	2.6187	2.6535	2.6535	2.6187	2.6525
5×10^{-2}	1.357×10^{-1}	1.6335	1.5315	1.6332	1.6323	1.5400	1.6302
1×10^{-1}	2.154×10^{-1}	1.3772	1.2155	1.3771	1.3741	1.2755	1.3684
1.25×10^{-1}	2.500×10^{-1}	1.3155	1.1284	1.3159	1.3115	1.2213	1.3036
2.5×10^{-1}	3.969×10^{-1}	1.1848	0.8956	1.1932	1.1792	1.1363	1.1570
3.75×10^{-1}	5.200×10^{-1}	1.1463	0.7824	1.1724	1.1449	1.1234	1.1057
5×10^{-1}	6.300×10^{-1}	1.1318	0.7108	1.1833	1.1389	1.1208	1.0821

Table B.1. (continued)

Part B

T	τ	$(\frac{\partial\theta}{\partial\eta})_o - (\frac{\partial\theta}{\partial\eta})_{o,\tau\to\infty}$	eq. 30	eq. 39	eq. 35
0.125	0.250	1.957 E-1		1.015 E-1	2.522 E-1
0.250	0.3969	6.506 E-2		1.648 E-2	1.055 E-1
0.375	0.5200	2.654 E-2		3.589 E-3	5.427 E-2
0.5	0.6300	1.198 E-2		9.204 E-4	3.070 E-2
1	1	8.288 E-4		9.44 E-6	4.839 E-3
1.85	1.5070	2.105 E-5		2. E-8	4.055 E-4
2.85	2.0102	5.508 E-7			3.489 E-5

*400 meshpoints, meshwidth = 0.01, initial $\Delta T = 5 \times 10^{-7}$

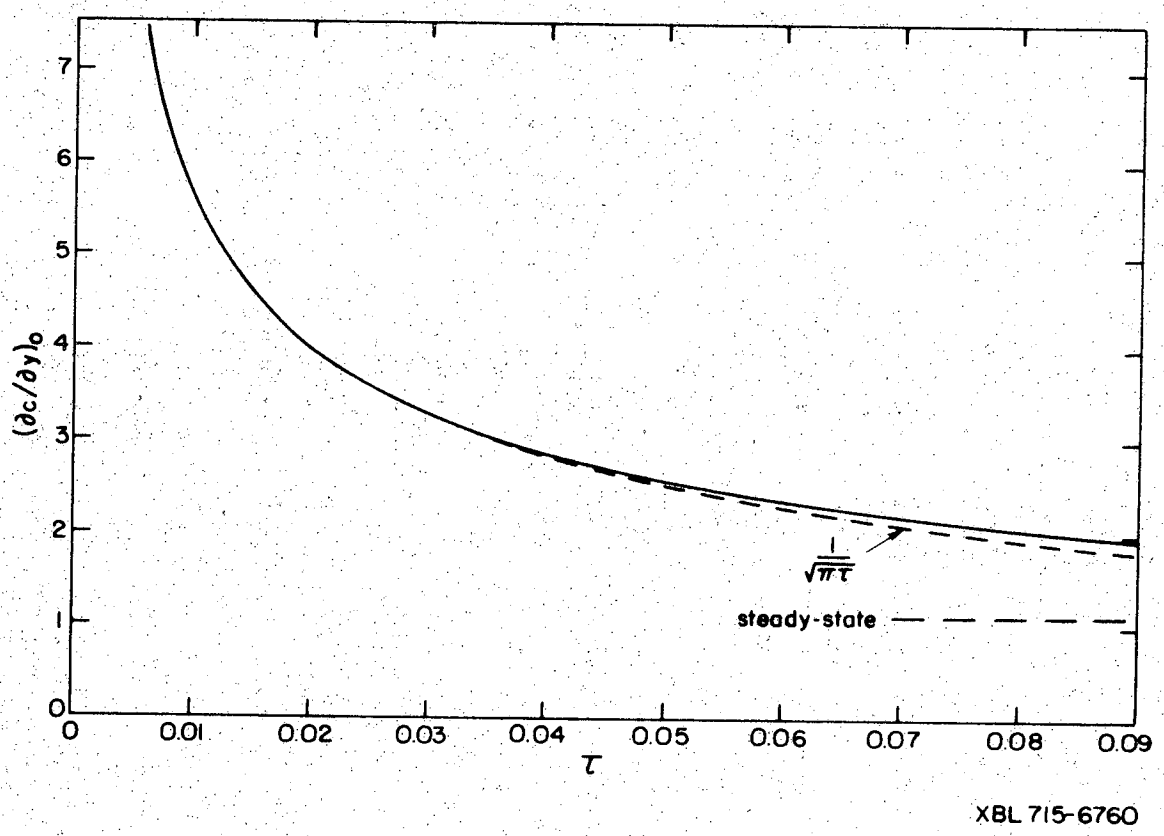

Fig. B.1. Transient flux at a rotating disk for short times after a concentration step at the surface. The approximation (B.8) is shown as a dashed line.

it was found that a field length of 4 is adequate in the first phase of the program. By variation of mesh size at constant field length (4) the accuracy of the procedure was tested at very small times ($T=10^{-3}$). Four-point extrapolation gave the derivative predicted by (21) to 8 decimals. The number of meshpoints (401) used in further calculations limits the accuracy of the results to 5 decimals.

6. The results are given in Table B.1 and in Figures B.1 - B.4. Part A of Table B.1 shows for comparison the concentration gradient predicted by the short-time approximation (22). The pure-diffusion approximation ($1/\sqrt{\pi\tau}$) holds, to within 1% accuracy, if $\tau < 0.04$. Addition of the term in :

$$(\partial c/\partial \eta)_o = 1/\sqrt{\pi\tau} + 3\tau/4 \qquad (B.36)$$

extends the validity (within 1%) to $\tau = 0.43$. The third term in the perturbation expansion does not improve the approximation since it has also a positive sign. (See Figures B.1 and B.2) At $\tau = 0.43$ the flux is 5% higher than the steady-state flux.

Part B of Table B.1 shows, instead of the short-time approximations, the value of $(\partial\theta_2/\partial\eta)_o$, i.e., the deviation from the steady-state flux. This quantity is also plotted in Figure B.4, as a semi-logarithmic plot vs. time. It is seen that for large τ(e.g., $\tau > 0.43$) the flux deviates from the steady-state value as a negative exponential function of time. By correlation of the results of part B, between $\tau = 0.85$ and $\tau = 1$, one obtains

$$\log\left\{\frac{\partial c}{\partial \eta}_o - 1.1198465\right\} = 0.0522 - 3.134\,\tau \qquad (B.37a)$$

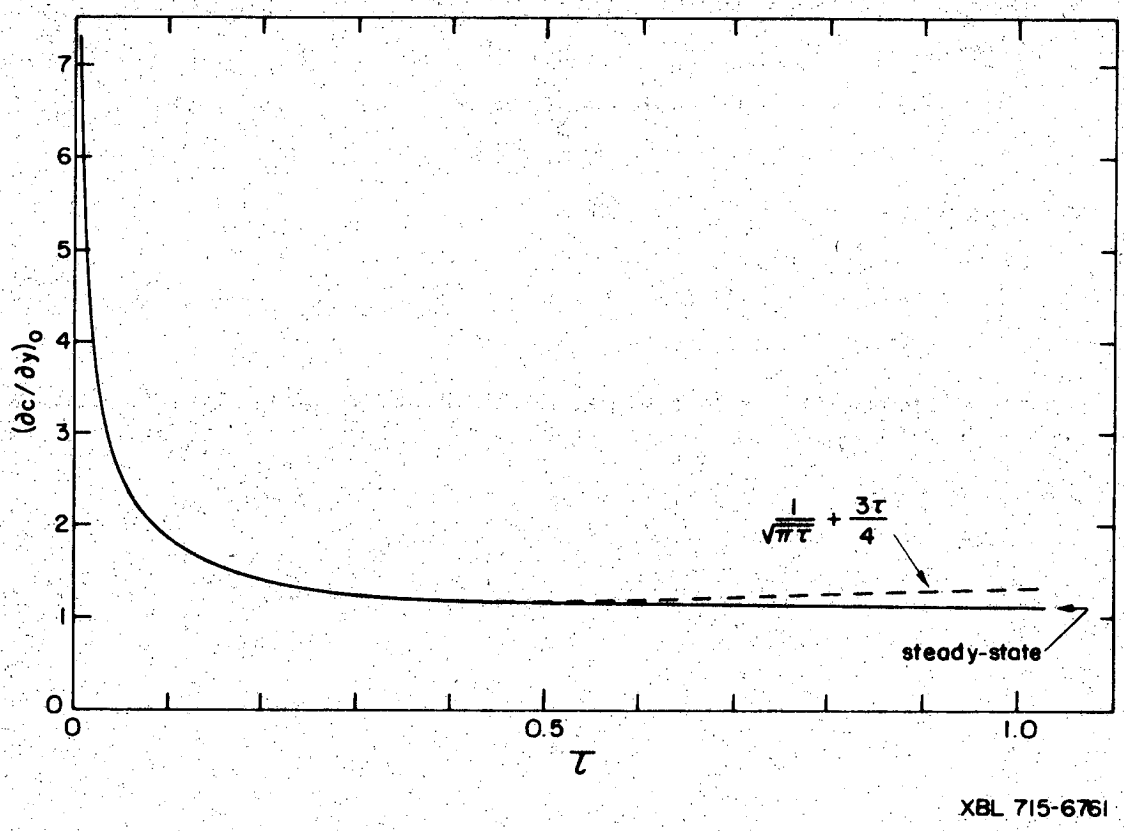

Fig. B.2. Transient flux at a rotating disk, following a concentration step at the surface. The approximation (B.36) is shown as a dashed line.

or

$$\frac{\partial c}{\partial \eta}_{o} - 1.1198465 = 1.1276\ e^{-7.216\ \tau} \qquad \text{(B.37b)}$$

At $\tau = 0.428$ this expression gives $(\partial c/\partial \eta)_o = 1.17123$, i.e., within .05% the exact value (1.17166).

The negative exponential function of time is to be expected since, from (5), the concentration appears to be separable:

$$c = c_\infty(\eta) + A(\tau)C(\eta) \qquad \text{(B.38)}$$

where c_∞ is the steady-state function. For $C(\eta)$ the equation to be solved is:

$$\frac{d^2C}{d\eta^2} + 3\eta^2 \frac{dC}{d\eta} + \lambda^2 C = 0 \qquad \text{(B.39)}$$

At sufficiently long times only the lowest eigenvalue of the continuous set is important. This is:

$$\lambda^2 = 7.216 \qquad \text{(B.40)}$$

according to (37b).

7. The results can be compared with the numerical solution obtained by Olander for $Sc = 10^3$. Olander[144] gives values only up to $\omega t = 5$, i.e., $\tau = 0.1535$. They are slightly lower than the present ones (see Table B.2), in agreement with the trend of Olander's results for increasing Sc number.

An approximate analytic solution of (5) has been given by Filinovskii and Kir'yanov,[146] by Laplace-transformation of (5) and

Table B.2. Gradient at the disk interface at Sc = 10^3 (reference 144).

time		$(\partial c/\partial \eta)_o$	
ωt (Sc = 10^3)	τ	Olander[144]	present work
1	0.0307	3.23	3.243
2	0.0614	2.24	2.322
3	0.0921	1.87	1.928
4	0.1228	1.66	1.702
5	0.1535	1.515	1.555

Note: The values in col. 3 are read from Figure 2 of Ref. 144.

(Nu_{ss} at Sc = 10^3 is 1.08744).

introduction of the auxiliary function:

$$\bar{\psi}(s) = \bar{c}(s)\ \exp(\tfrac{1}{2}\eta^3) \quad . \tag{B.41}$$

This yields:

$$\frac{d^2\bar{\psi}}{d\eta^2} - \bar{\psi}\ (\tfrac{9}{4}\eta^4 + 3\eta + s) = 0 \quad . \tag{B.42}$$

If the term in η^4 is neglected, (42) can be solved. Finally one obtains:

$$(\frac{\partial c}{\partial \eta})_o = \frac{3^{2/3}\Gamma(2/3)}{\Gamma(1/3)} + \sum_{n=1}^{\infty} \frac{3^{1/3}}{c}\, e^{-3^{2/3}c_n\tau} \quad , \tag{B.43}$$

where c_n are the zeros of the Airy function.*

In the limit of short times this approximation leads to:

$$(\frac{\partial c}{\partial \eta})_o = \frac{1}{\sqrt{\pi\tau}} + \frac{3\tau}{4} - \frac{\tau^{5/2}}{4\sqrt{\pi}} + O(\tau^4) \tag{B.44}$$

which is different from (22) only in the third term. Equation (44) is accurate within 1% up to $\tau = 0.667$.

In the limit of long times (43) gives

$$(\frac{\partial c}{\partial \eta})_o = 1.0514127 + 0.616845\ e^{-4.86346t} \quad . \tag{B.45}$$

This shows that the neglect of the term in η^4 in (42) restricts the validity of the approximation to short times. In figure B.4 it is also

*The first seven zeros are given in the second statement (DATA B/) of subroutine APPROX, see end of Appendix. Above n = 6 the asymptotic representation $c_n = (\frac{3\pi}{8}(4n-1))^{2/3}$ is valid to 5 significant figures.

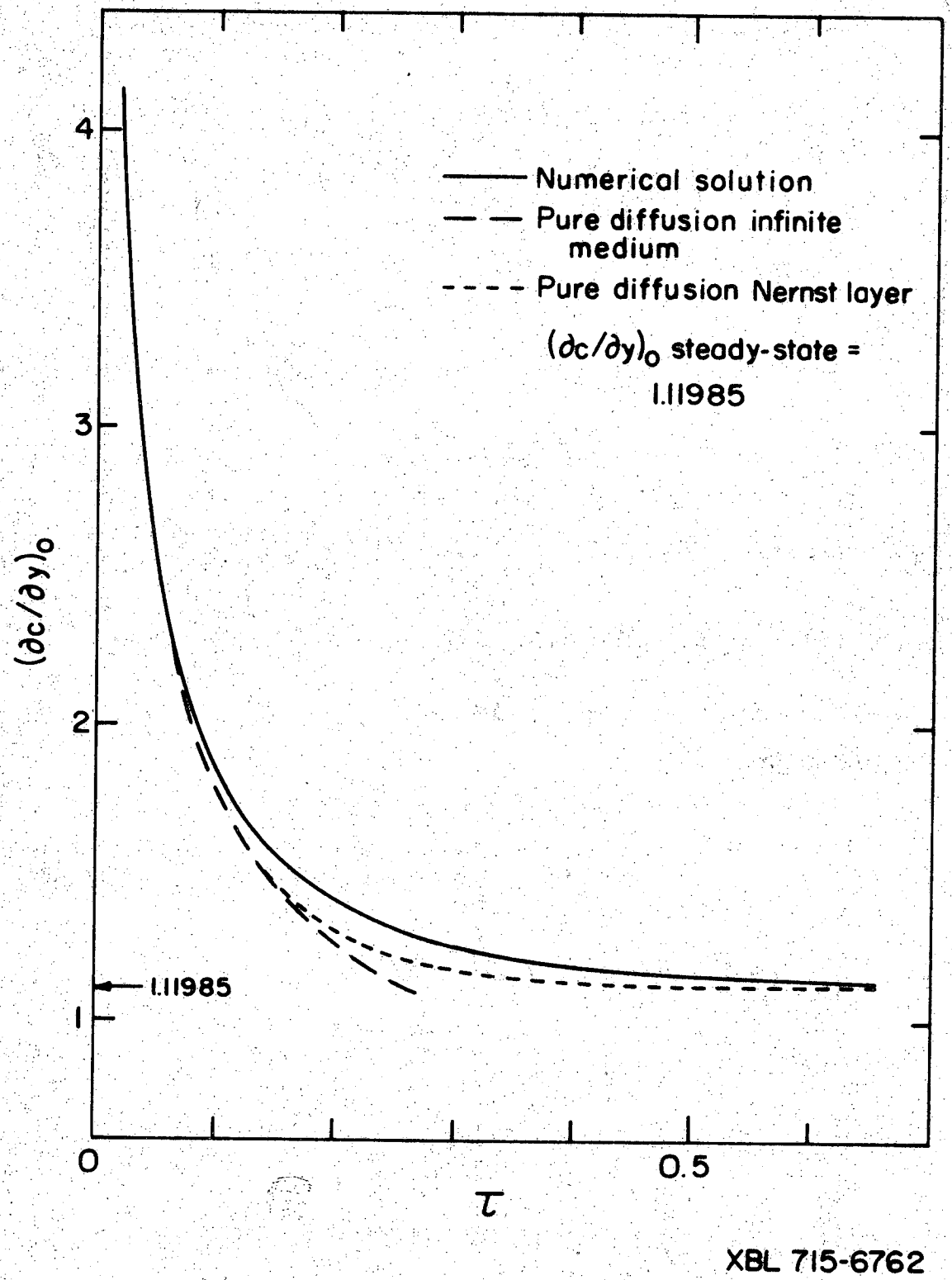

Fig. B.3. Transient flux following a concentration step at the surface. Dashed lines: approximations (B.8) and (B.47).

seen that the transient actually decays faster than in the approximation according to Filinovskii and Kir'yanov.

Finally it is of interest to compare the actual solution with one based on pure diffusion in a restricted domain, namely in the Nernst layer, of thickness

$$\delta_N = \Gamma(4/3)\,(\nu/\omega)^{1/2}\ (\alpha\nu/3D)^{-1/3} \quad , \tag{B.46}$$

i.e., based on the steady-state solution (10). According to Cottrell[147] the solution is, in terms of the variables (4):

$$\left(\frac{\partial c}{\partial \eta}\right) = \frac{1}{\Gamma(4/3)} \left\{1 + 2 \sum_{n=1}^{\infty} e^{-12.377\ n^2\tau}\right\} \tag{B.47}$$

Figure B.3 shows that this solution underestimates the flux considerably in the region $0.2 < \tau < 0.5$. At long times it approaches, of course, to the exact steady-state value, according to

$$\left(\frac{\partial c}{\partial \eta}\right)_o = 1.1198465 + 2e^{-12.3771\ \tau} \quad . \tag{B.48}$$

Figure B.4 shows that this is considerably faster than the actual transient (37).

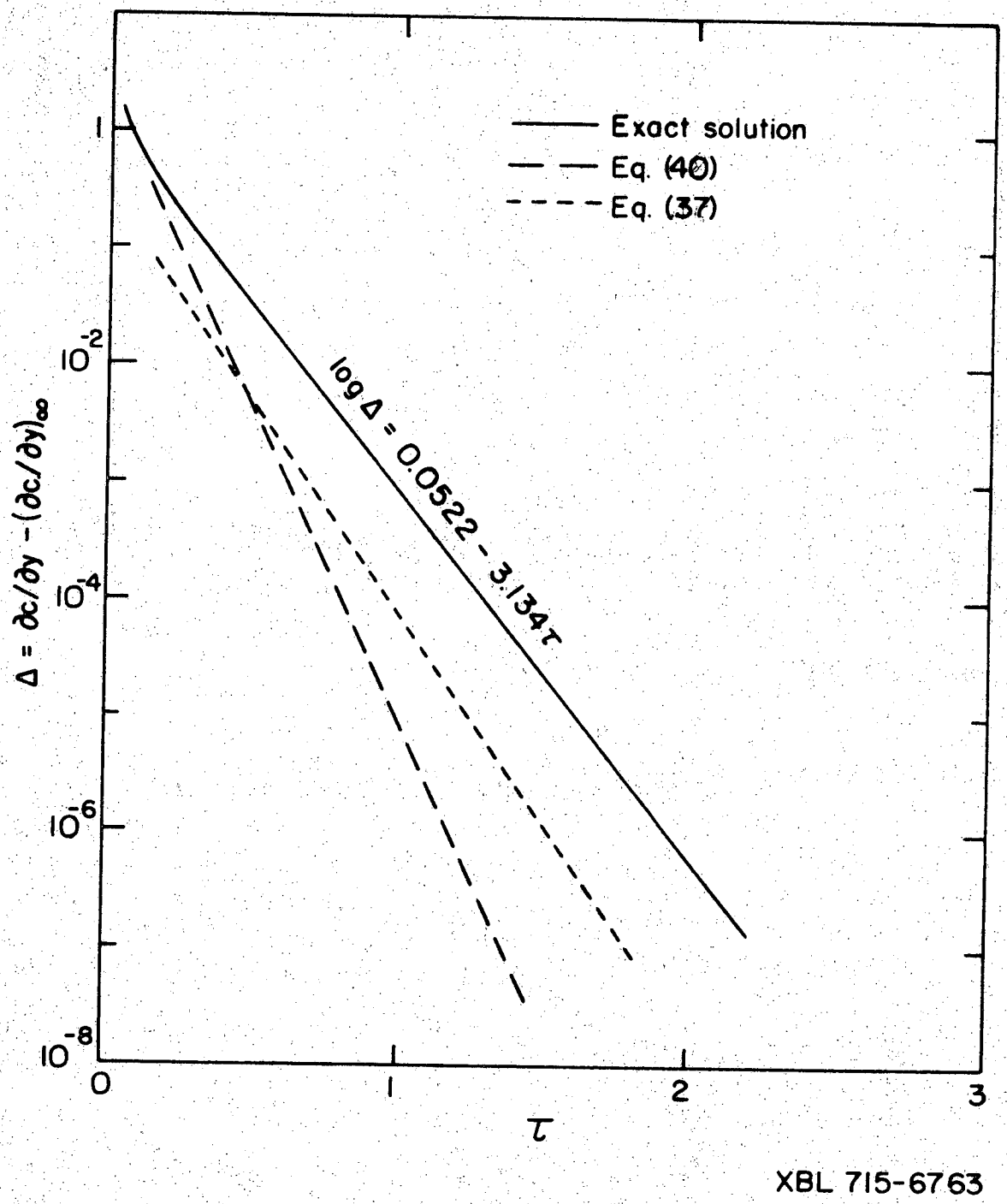

Fig. B.4. Decay of transient flux at a rotating disk, following a concentration step. Also shown are the approximations (B48) and (B45).

```
      PROGRAM CONSTEP(INPUT,OUTPUT)
      DIMENSION C(401),XI(401),E(401),Z(401),CC(401),CD(401)
  101 FORMAT(I4,F6.4,F8.6)
  102 FORMAT(1)(2X,E10.8))
  104 FORMAT(10X,E16.8,3E15.8)
  105 FORMAT(1H1)
  106 FORMAT(10X,4HNJ= ,I4,4H H= ,F6.4,4H DT=,F8.6)
  107 FORMAT( 10X,E15.8)
  108 FORMAT(10X,2E15.8)
  109 FORMAT(5 (2X,E10.6))
  111 FORMAT(1HO)
     1F8.6)
  113 FORMAT(1HO2X,10HCYCLE=     ,I4,6H,DT=  ,F8.6)
  114 FORMAT( 4X,I6,E15.8,2E15.8)
  115 FORMAT(40X,I6,E15.8)
  116 FORMAT(I3)
    8 READ 101, NJ,H
      IF (NJ.EQ.0) STOP
C     READ NUMBER TIME CYCLES, SET INITIAL TIME INCREMENT
      READ 116,KCIN
      DT=5.*10.**(-KCIN)
      KCM2=KCIN-2
      PRINT 105
C     JFLAG=0 PHASE A /  JFLAG=1  PHASE B
      NJM1=NJ-1 $JFLAG=0
C     INITIAL CONC PROFILES/ C(J) = 0 EVERYWHERE / CC(J) REAL PROFILE
      DO 1 J=1,NJ
      Z(J)=H*FLOAT(J-1)
    1 C(J)=0.
      PRINT 106,NJ,H,DT
      DO 30 J=1,NJ
   30 CC(J)=1.-ERFC(Z(J))
      KT=0 $LL=0 $ M=1 $ KC=1
C     START A TIME-CYCLE (180 POINTS, EXCEPT FIRST ONE 200)
    2 KT=KT+1 $ LL= LL+1
      T=-0.5*DT + DT*FLOAT(KT) $ TR=T**(1./3.)
      XI(1)=0. $ E(1)=0.
      DO 3 J=2,NJM1 $ IF (JFLAG.EQ.1) GO TO 17
      A=-DT/12./H/H +DT/12./H*Z(J)*(1.+Z(J)*T*12.)
      B=T+DT/6./H/H
      D=-DT/12./H/H -DT/12./H*Z(J)*(1.+Z(J)*T*12.)
      G=C(J)*T + DT/12./H/H*(C(J+1)+C(J-1)-2.*C(J))+DT/12./H*Z(J)*(1.+12
     1.*Z(J)*T)*(C(J+1)-C(J-1))
     1+8.*Z(J)**2.*T*DT*EXP(-Z(J)**2.)/SQRT(3.1415926534)
      GO TO 20
   17 A=0.50/H/TR*Z(J)**2- 1./3./H/H/TR
      B= 1./DT +2./H/H/3./TR
      D=-0.50/H/TR*Z(J)**2 -1./H/H/3./TR
      G= C(J)/DT+.5/TR/H*Z(J)**2*(C(J+1)-C(J-1)) +(0.5*C(J+1) -C(J) +
     10.5*C(J-1))/H/H*2./3./TR
   20 XI(J)=(G-A*XI(J-1))/(B+A*E(J-1))
    3 E(J)=D/(B+A*E(J-1))
      C(NJ)=0.
      DO 4 JJ=1,NJM1
      J=NJ-JJ
    4 C(J)=XI(J)+E(J)*C(J+1)
      DCDZ= (-C(3)+4.*C(2))/2./H
      T=T+.5*DT
      IF (KT.NE.25) GO TO 34
C     STORE C PROFILE FOR POSSIBLE TRANSITION TO PHASE B
```

```
      DO 31 J=1,NJ
   31 CO(J)=C(J)
   34 ECDZ=1.5*T +3.*T**2.*.1/SQRT(3.141592654)
      PRINT 111
C     PRIMARY OUTPUT AT EVERY TIME-STEP
      PRINT 114,LL,T,DCDZ,ECDZ
      T=(DT*FLOAT(KT))**(2.0/3.0)
C     SHORT-TIME APPROXIMATIONS
      ECDZ=1./SQRT(3.141592654*T)
      GCDZ=ECDZ+0.75*T
      HCDZ=GCDZ-T**2.5/4./SQRT(3.141592654)
C     CO= COTTRELL SOLUTION
      CO=1.
      DO 19 J=1,30
   19 CO    =CO    +2.*EXP(-FLOAT(J)*FLOAT(J)*12.37706549*T)
      CO=CO*1.1198465
C     TSUM= APPROXIMATION OF FILINOVSKII
      CALL APPROX(T,TSUM)
      PRINT 104,T,ECDZ,GCDZ,HCDZ
      PRINT 108,CO,TSUM
      IF (JFLAG.EQ.1) GO TO 21
      DCDY    =(DCDZ    +1.12837917)/T**.5*.5
      EXC     =DCDY     -1.1198465
      GO TO 35
   21 EXC     =DCDZ  $ DCDY    =EXC    +1.1198465
C     FLG = LONG-TIME APPROXIMATION
   35 FLG     =1.1276*EXP(-7.216*T)
      IF (LL.LT.10) GO TO 39
   39 PRINT 104,T,DCDY    ,EXC    ,FLG
      CO=CO-1.1198465
      TSUM=TSUM-1.05141599
      PRINT 108,CO,TSUM
      IF (T.GT.3.0) GO TO 7
      IF (KT.LT.200) GO TO 2
C     IF CYCLE ENDS AND T=1, GO BACK TO T=0.25 AND START PHASE B
      IF (KC.EQ.KCM2.AND.JFLAG.EQ.0) GO TO 14
      PRINT 105
      DT=DT*10.  $ KT=20  $ KC=KC+1 $ IF (KC.EQ.KCIN) GO TO 7
      PRINT 113,KC,DT
      GO TO 2
C     FORM AND PRINT ACTUAL CONC PROFILE AT TRANSITION PHASE A TO B (T=0.25)
   14 DO 15 J=1,NJ
   15 C(J)=CO(J)+1.-ERFC(Z(J))
      PRINT 105
      PRINT 102,(CO(J),J=1,NJ)
C     CALCULATE STEADY-STATE PROFILE BY INTEGRATION
      CO(1)=0. $ DO 32 J=1,NJM1
   32 CO(J+1)=CO(J)+0.5*(EXP(-Z(J+1)**3)+EXP(-Z(J)**3))*H*1.1198465
C     FORM NEW CONC PROFILE BY SUBTRACTING STEADY-STATE PROFILE
      DO 33 J=1,NJ
   33 C(J)=C(J)-CO(J)
      PRINT 111
      PRINT 102,(CO(J),J=1,NJ)
      PRINT 102,(C(J),J=1,NJ)
      KT=25 $ JFLAG=1 $ GO TO 2
    7 CONTINUE
      END
      FUNCTION ERFC(X)
C  ERF=2/SQRT(PI)*INTEGRAL OF EXP(-T*T) FROM 0 TO X.
```

```
C  USING AN APPROXIMATION DUE TO HASTINGS. ABSOLUTE ERROR ABOUT 3E-7
      DIMENSION A(6)
      DATA A/.0000430638,.0002765672,.0001520143,.0092705272,.0422820123
     1,.0705230784 /
      IF(X.GT.2.35)GO TO 1
      T=A(1)*X
      DO 10 I=2,6
   10 T=(T+A(I))*X
      T=1./(T+1.)
      ERFC= T**16 $ RETURN
    1 ERFC=EXP(-X*X)/X/(3.141592654)**0.5*(1.0-0.5/(1.0+X**2)
     1 +0.161/(1.0+X**2)**2)
      RETURN
      END
      SUBROUTINE APPROX(T,TSUM)
      DIMENSION B(7),A(7)
      DATA B/2.33810741,4.08794944,5.52055983,6.78670809,7.94413359,
     19.02265085,10.04017434/
      SUM=1.35411794/2.678938535*3.**(2./3.)
      DO 11 J=1,7
      A(J)=3.**(1./3.)/B(J)*EXP(-3.**(2./3.)*B(J)*T)
   11 SUM=SUM+A(J)
      SUM=SUM-A(7)*.5
      REST=ERFC(3.**(5./3.)*3.141592654**(1./3.)*T**.5*.5)/
     1(T*3.141592654)**.5
      TSUM=SUM+REST
      RETURN
      END
-
+401+.01
+07
```

Appendix C. Degree of dissociation of HSO_4^- ion in the system $CuSO_4$-H_2SO_4 - H_2O.

The dissociation of H_2SO_4 in solutions of 0.1 M to 3 M concentration is virtually complete in the first stage, to HSO_4^- ($K \approx 10^3$ mole/ℓ). In very dilute solutions the second ionization constant

$$K_B = a_{H^+} a_{SO_4^=} / a_{HSO_4^-} \qquad (C.1)$$

is 0.0104 mole/ℓ at 25°C. Except at infinite dilution the bisulfate ions will not be dissociated completely.

The stoichiometric dissociation constant

$$K'_B = c_{H^+} c_{SO_4^=} / c_{HSO_4^-} \quad , \qquad (C.2)$$

varies by three orders of magnitude as the H_2SO_4 concentration increases from 0 to 3 M. The values of K'_B which follow from spectroscopic investigations of aqueous H_2SO_4 solutions,[151] have been correlated[125] with the true ionic strength by the expression:

$$\ell n(K'_B/0.0104) = \frac{5.29\sqrt{I_r}}{1+0.56\sqrt{I_r}} \quad . \qquad (C.3)$$

Equations (2) and (3) can be solved together with the equation of electroneutrality. Figure B.1 shows the true ionic strength, I_r, and figure B.2 the degree of dissociation, α, of HSO_4^- ions in aqueous H_2SO_4 solutions, both as a function of H_2SO_4 molarity. The degree of dissociation of HSO_4^- goes through a minimum (0.268) at 0.4 M, then increases slowly; it is 0.33 at 3 M. The ionic strength in the range of concentrations

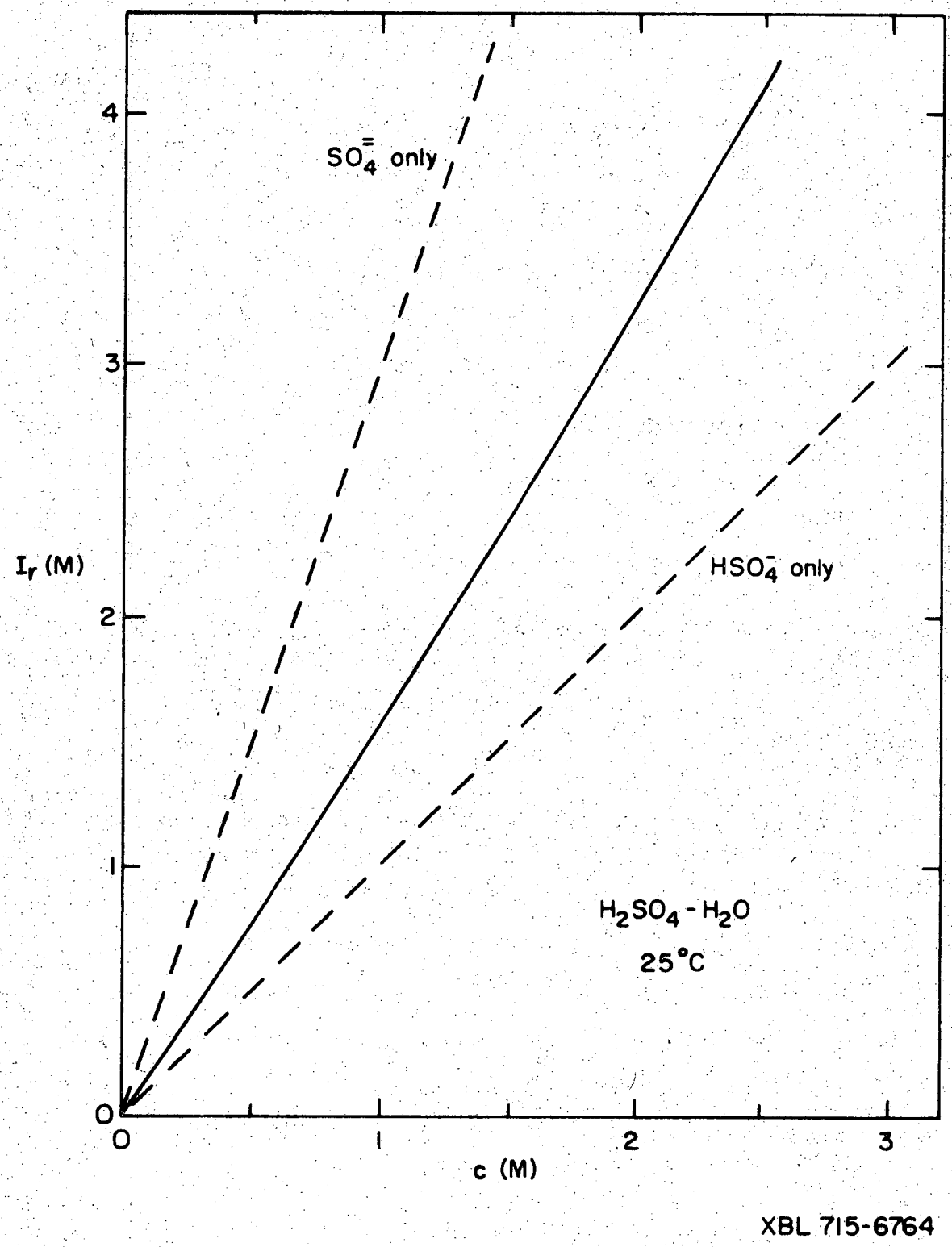

Fig. C.1. True ionic strength of aqueous solutions of sulfuric acid at 25°C.

0.5-3 M is represented fairly accurately by

$$I_r = 1.6\ c \quad . \tag{C.5}$$

The addition of $CuSO_4$ influences the bisulfate-sulfate equilibrium by the increase of ionic strength in general, and by possible inter-ionic effects between Cu^{2+} and SO_4^{2-} or HSO_4^- ions. Neglecting the latter in first approximation, let us assume that $CuSO_4$ is completely dissociated and that the increase in ionic strength affects the bisulfate equilibrium in the same manner as if the solution were H_2SO_4-H_2O only, i.e., according to (3). To find the composition of the solution one needs to solve a set of 4 equations: (2), (3), electroneutrality and a material balance for total sulfate. The equation to be solved, in terms of known H_2SO_4 concentration (4), $CuSO_4$ concentration (C), and unknown HSO_4^- ion concentration (x), is:

$$\ln \frac{(A+C-x)(2A-x)}{0.0104} - \frac{5.29\sqrt{3A+4C-2x}}{1+0.56\sqrt{3A+4C-2x}} = 0 \quad . \tag{C.6}$$

The degree of dissociation is best expressed in terms of I/K'_B, i.e., the stoichiometric ionic strength (based on complete dissociation of HSO_4^- ion), divided by the stoichiometric dissociation constant. Figure 3.10 gives the results. Note that for 0 M $CuSO_4$

$$I/K'_B = \frac{3(1-\alpha)}{\alpha(1+\alpha)} \quad ; \tag{C.7}$$

i.e., a maximum in I/K'_B corresponds to a minimum in α(cf. Fig. B.2). Table C.1 gives the true ionic strength, I_r, for various compositions.

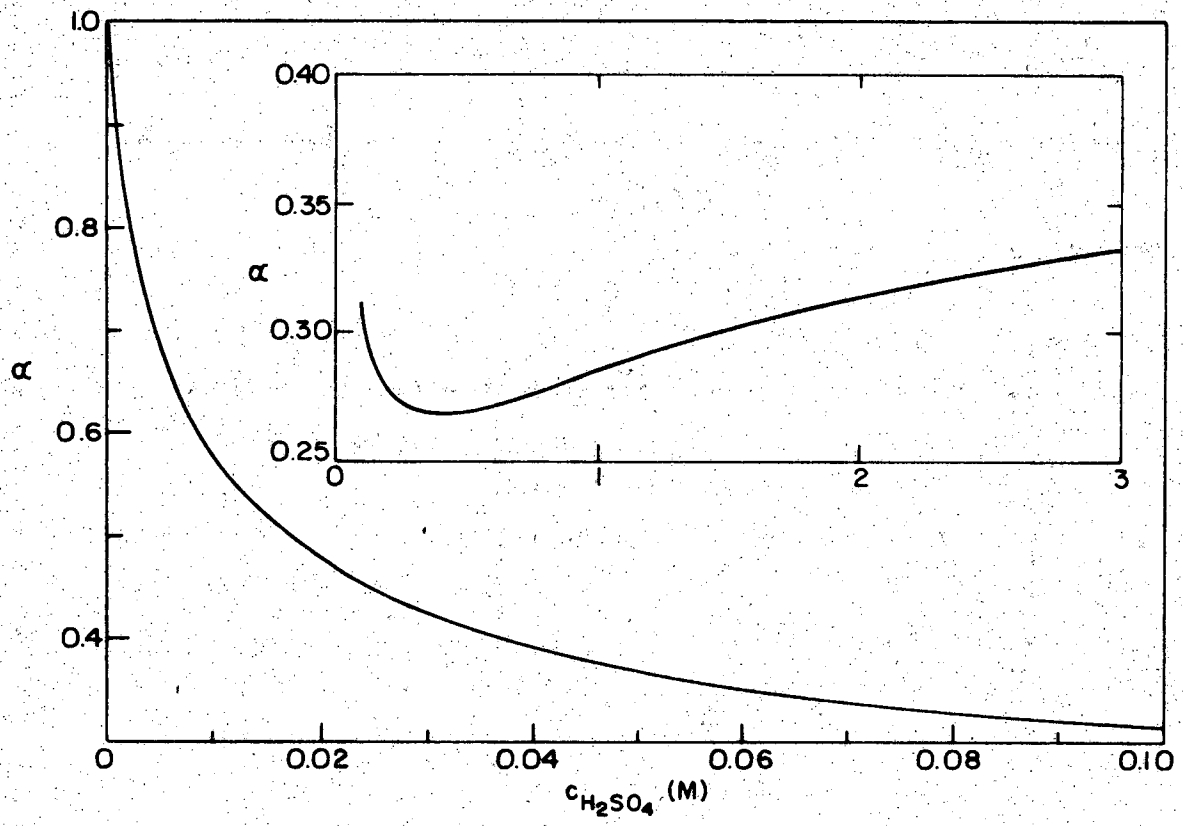

Fig. C.2. Degree of dissociation of HSO_4^- ion in aqueous solutions of H_2SO_4 at 25°C.

Table C.1. True ionic strength (in mole/ℓ) of $CuSO_4$-H_2SO_4 solutions at 25°C. (The values between parentheses are based on partial dissociation of $CuSO_4$ according to eq. 9).

M CuSO4 → / M H_2SO_4 ↓	0	0.01	0.05	0.10	0.30	0.60
0		0.040	0.200	0.400	1.200	2.400
		(0.0281)	(0.118)	(0.222)	(0.678)	(1.153)
0.01	0.021	0.058	0.213	0.412	1.212	2.413
		(0.051	(0.175)	(0.335)	(0.978)	(1.916)
0.05	0.087	0.121	0.269	0.464	1.263	2.467
		(0.115)	(0.235)	(0.392)	(1.033)	(1.972)
0.10	0.162	0.196	0.341	0.523	1.329	2.536
		(0.191)	(0.310)	(0.465)	(1.104)	(2.043)
0.25	0.386	0.421	0.564	0.752	1.542	2.752
		(0.416)	(0.536)	(0.691)	(1.325)	(2.264)
0.50	0.770	0.805	0.950	1.138	1.922	3.131
		(0.799)	(0.923)	(1.078)	(1.710)	(2.645)
1.0	1.569	1.606	1.757	1.948	2.731	3.934
		(1.601)	(1.726)	(1.884)	(2.513)	(3.440)
1.5	2.403	2.439	2.593	2.786	3.571	4.770
		(2.433)	(2.559)	(2.716)	(3.341)	(4.258)
2.0	3.252	3.292	3.446	3.641	4.427	5.622
		(3.284)	(3.410)	(3.566)	(4.185)	(5.090)
2.5	4.117	4.156	4.312	4.507	5.293	6.483
		(4.148)	(4.273)	(4.427)	(5.038)	(5.931)

The program INCOP, which finds x from (6) by Newton-Raphson iteration, is reproduced at the end of this appendix.

Strictly speaking it is also necessary to take into consideration that Cu^{2+} and SO_4^{2-} ions show a strong tendency to association. This is characteristic of bi-bivalent ionic salts (cf. $ZnSO_4$, $MgSO_4$). Spectrophotometric methods have recently been used to determine a dissociation constant in dilute solutions. Earlier methods used conductivity data and cryoscopic measurements.

The association effect can formally be treated as a dissociation, similar to that of HSO_4^-. Spectroscopic data for the whole range of $CuSO_4$ concentrations solutions are not available, but by the use of semi-empirical expressions the "degree of dissociation" has been calculated from conductivity data and molar activity coefficients. Figure C.3 shows the values of θ, the degree of dissociation, given by Fedoroff.[148] From these values the stoichiometric dissociation constant can be calculated

$$K_c' = c_{Cu^{2+}} c_{SO_4^=}/c_{HSO_4^-} = \theta^2 c/(1-\theta) \qquad (C.8)$$

and correlated with the true ionic strength. The expression arrived at is of the same form as (3):

$$\ln(K_c'/K_c) = \frac{15.05\sqrt{I_r}}{1+1.824\sqrt{I_r}} \quad , \qquad (C.9)$$

where K_c is the constant at infinite dilution, 0.00495. Figure C.4 shows the correlation (9).

Equation 9 can now be used to assess the importance of incomplete dissociation of $CuSO_4$ for the ionic strength and for the parameter I/K_B'.

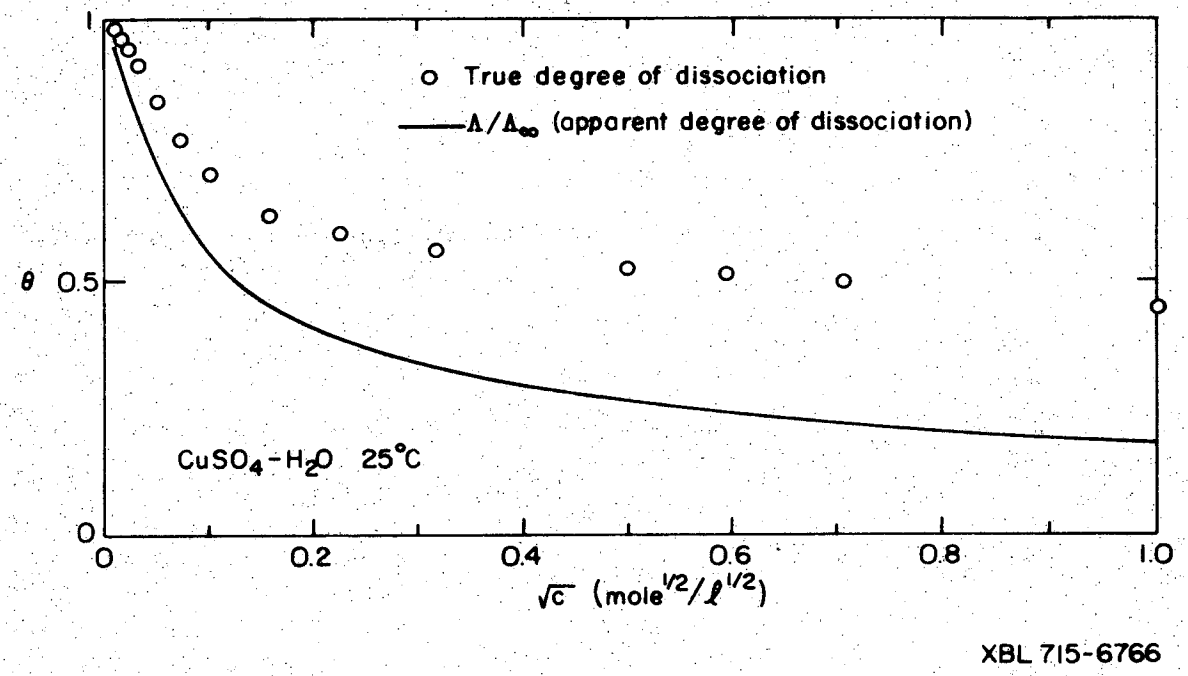

Fig. C.3. Degree of dissociation of $CuSO_4$ in aqueous solutions at 25°C (after Fedoroff[148]).

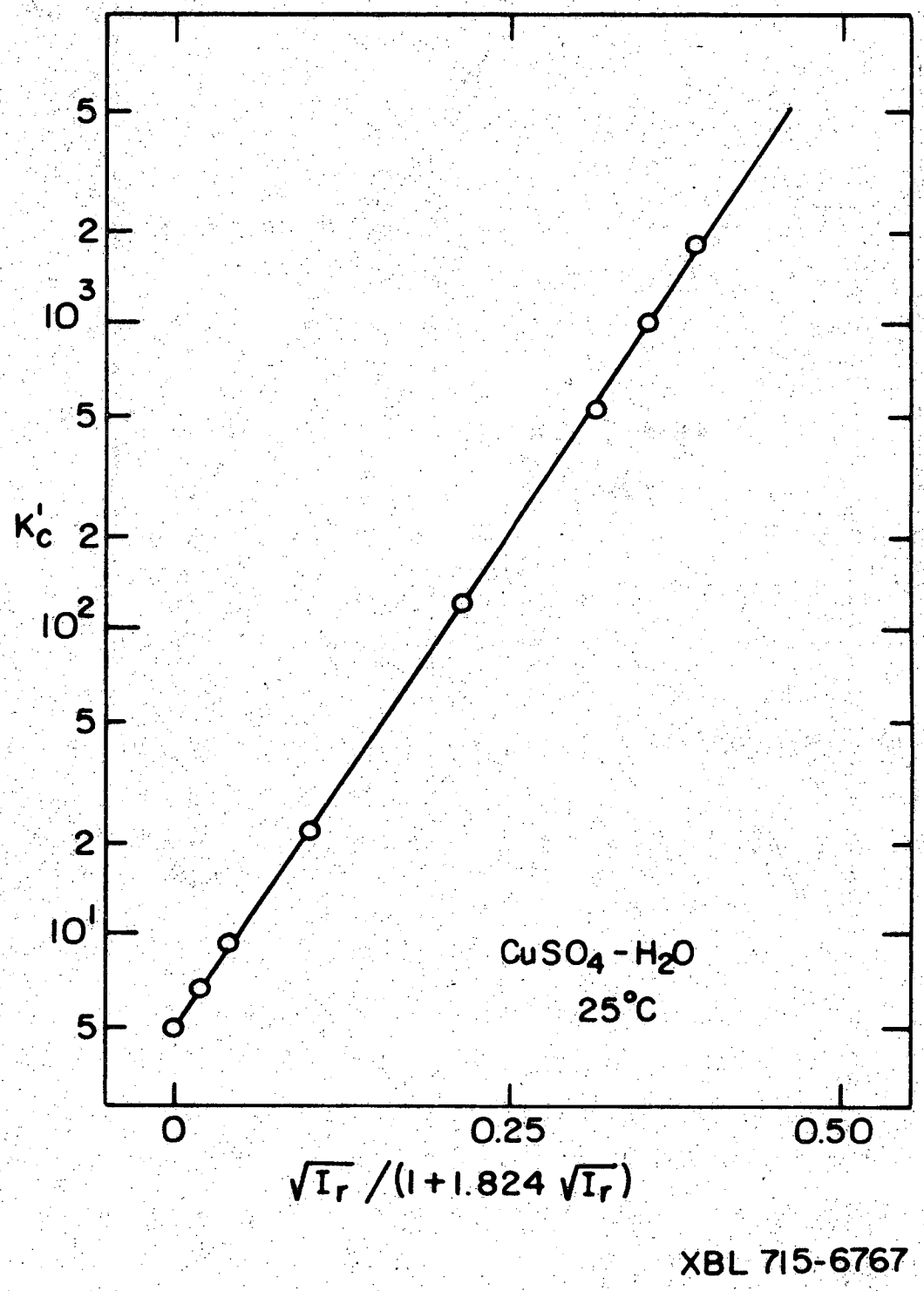

Fig. C.4. Stoichiometric dissociation constant of $CuSO_4$ in aqueous solutions at 25°C, as a function of true ionic strength.

Table C.1 contains in parentheses the values of I_r based on (9). Differences of >10% are found only for the solutions most concentrated in $CuSO_4$ and least in H_2SO_4. Figure 3.10, therefore, shows the effect of incomplete dissociation on I/K'_B only for the case of 0.30 M $CuSO_4$ and variable H_2SO_4 concentration. The effect is to decrease dissociation of HSO_4^-; this implies that the decrease in ionic strength, and consequent increase in the activity coefficients of H^+ and $SO_4^=$ ions, outweighs the effect that the decrease in $SO_4^=$ ion concentration has on the dissociation equilibrium.

Finally, Figure C.5 shows the analogue of I/K'_B for the $CuSO_4$ dissociation (or association) equilibrium. I/K'_c is an index of the degree of dissociation of $CuSO_4$ in acidified solution:

$$I/K'_c = \frac{I(1-\theta)}{\theta c_{SO_4^=}} \quad . \tag{C.10}$$

The addition of 0.5 to 3.0 M H_2SO_4 causes a fairly constant degree of dissociation, $\theta \approx 0.8$, independent of the $CuSO_4$ concentration.

The program INCOP (see below) takes the association of Cu^{2+} and $SO_4^=$ into account after first calculating the ionic strength as if $CuSO_4$ is completely dissociated (from equation 6). Then the bisulfate concentration is treated as a constant and the $CuSO_4$ dissociation is solved for. If y is the concentration of Cu^{2+} ions, the following equation is solved by Newton-Raphson root-finding iterations:

$$\ell n \frac{y(A+y-x)}{(C-y)0.00495} - \frac{15.05\sqrt{3A+4y-2x}}{1+0.56\sqrt{3A+4y-2x}} = 0 \tag{C.11}$$

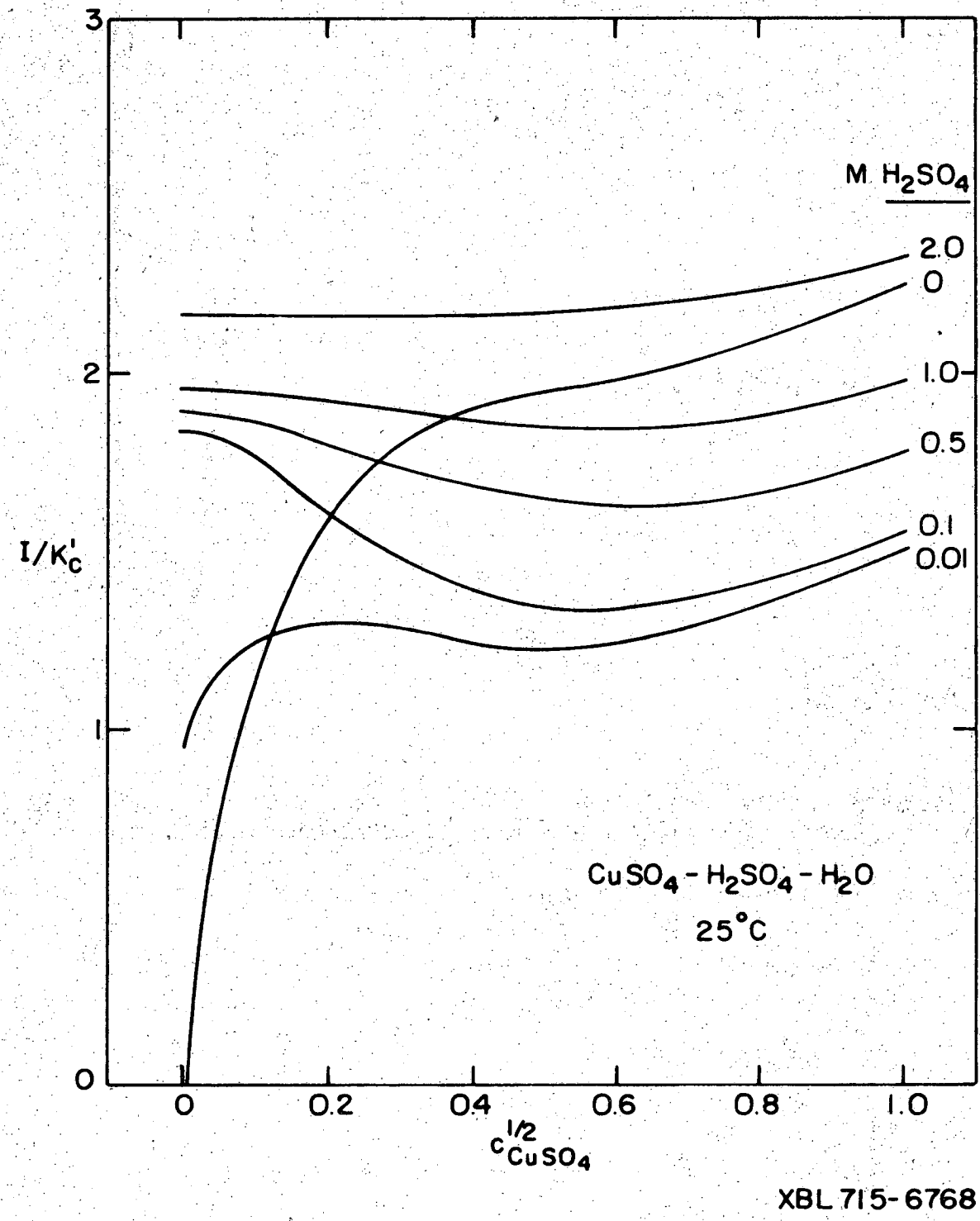

Fig. C.5. Degree of dissociation of $CuSO_4$, expressed as I/K'_c, as a function of $CuSO_4$ concentration, for various H_2SO_4 concentrations.

The new-found y is then substituted for C in equation (6) and a new x is solved for, etc., until the values of x and y do not change any more.

Because of the relative uncertainty of the $CuSO_4$ association data, the "true ionic strength" in Figure 3.12 and Table 3.6 is based on complete dissociation of $CuSO_4$.

```
      PROGRAM COPP(INPUT,OUTPUT)
C     CALCULATES BISULFATE CONCENTRATION (X) AS A FUNCTION OF COPPER SULFATE
C     CONCENTRATION (CC) AND SULFURIC ACID CONCENTRATION (AA), USING EQ.(7) O
C     UCRL-19102 AND NEWTON-RAPHSON ROOT FINDING METHOD.
C     REPEATS CALCULATION TAKING INTO ACCOUNT COPPER SULFATE ASSOCIATION (AP-
C     PENDIX C UCRL-20557)
      DIMENSION R(20),A(20)
    4 FORMAT(1H1)
    7 FORMAT(6X,*THE NEXT CASE DOES NOT CONVERGE*)
    8 FORMAT(6X,*   R     *,*    A    *,*   C     *,* I(APP)  *,
     1*I(TRUE) *,*  K(BIS) *,*I(A)/K(B)*,* A(ACID) *,*H2SO4/ACID*,
     2*CU/COPP  *,*  K(CU)  *,*I(A)/K(C)*)
   16 FORMAT(I5,12F9.6,2I5)
   18 FORMAT(10F8.4)
   19 FORMAT(2I3)
   28 FORMAT(1H0)
      READ 19,KTERM,LTERM
      READ 18,(A(J),J=1,LTERM)
      READ 18,(R(J),J=1,KTERM)
      PRINT 4
      PRINT 8
      KK=0
      DO 21 I=1,KTERM
      DO 21 J=1,LTERM
      PRINT 28
      DEV=0.
      JF=0
      KK=KK+1
      XIL=0. $ LL=1
      AA=A(J)
      CC=R(I)
      RR=AA/(CC+AA)
      AA1=AA $ CC1=CC
C     JF=0 ASSOCIATION CUSO4 NOT TAKEN INTO ACCOUNT
C     JF=1 ASSOCIATION CUSO4 TAKEN INTO ACCOUNT (ITERATION TO FIND Y=COPPER I
   26 IF (JF.NE.1) GO TO 23
      AA=AA1 $ CC=CC1 $ IF(CC.EQ.0.) GO TO 21  $ GO TO 23
C     X=BISULFATE,Y=COPPER ION,XK=CONSTANT BISULFATE,XKK=CONSTANT COPPER SULF
   23 FF=-ALOG(0.0104)
      X=0.5*AA
      GG=-ALOG(0.00495)
      Y=CC $ IF (JF.EQ.1) Y=0.5*CC
C     ITERATE TO FIND X FOR FIXED Y
   12 DO 3 K=1,20
      XIA=3.*AA +4.*CC
      IF (X.GE.(2.*AA)) X=1.999999*AA
      IF (X.GE.(AA+CC)) X=0.99999999*(AA+CC)
      XI = 3.*AA +4.*Y  -2.*X
      F=FF+ALOG((AA+Y -X)*(2.*AA-X)/X)-5.29*SQRT(XI)/(1.+.56*SQRT(XI))
      DFDX=(X**2 -2.*AA**2 -2.*AA*Y )/(AA+Y -X)/(2.*AA-X)/X
     1+5.29/SQRT(XI)/(1.+0.56*SQRT(XI))**2
      XX=X - F/DFDX
      IF (XX.LE.0.) XX=0.000001*AA
      IF (ABS(XX-X).LT..00001) GO TO 2
    3 X=XX
      PRINT 7
    2 X=XX
C     C1=BISULFATE,C2=SULFATE,C3=HYDROGEN,C4=COPPER ION CONCENTRATION
      C1=X
```

```
      C2=AA+Y-X
      C3=2.*AA-X
      XK= C2*C3/C1
      AAA=(C2-Y)/AA $ BBB=C1/AA
      CCC=Y/CC
      XIK=XIA/XK
      IF (JF.NE.1) GO TO 11
      IF (CC.EQ.0.) GO TO 21
C     ITERATE TO FIND Y FOR FIXED X
      DO 10 L=1,20
      XI=3.*AA+4.*Y-2.*X
      G=GG+ALOG (Y*(AA+Y-X)/(CC-Y)) -15.05*SQRT(XI)/(1.+1.824*SQRT(XI))
      DGDY=-((Y**2 -2.*CC*Y +CC*X -AA*CC)/Y/(CC-Y)/(AA+Y-X))
     1-2.*15.05/SQRT(XI)/(1.+1.824*SQRT(XI))**2
      YY=Y-G/DGDY
      IF(YY.LE.0.)YY=.000001*CC
      IF(YY.GE.CC) YY=.99999*CC
      IF(ABS(YY-Y).LT..000001) GO TO 9
   10 Y=YY
      PRINT 7
    9 Y=YY $C4=Y$ C2=AA+Y-X
      AAA=(C2-Y)/AA  $ BBB=C1/AA
      CCC=C4/CC $ XKK=Y*C2/(CC-Y)
      XIKK=XIA/XKK
      IF(ABS(XI-XIL).LT..00001) GO TO 11
      XIL=XI  $ LL=LL+1
      IF(LL.LT.15) GO TO 12
      PRINT 7
   11 PRINT16,KK,RR,AA,CC,XIA,XI,XK,XIK ,AAA,BBB,CCC,XKK,XIKK,LL,K
   27 JF=JF+1 $ IF(JF.EQ.2) GO TO 21 $ GO TO 26
   21 CONTINUE
      STOP
      END
-
+18+18
+00.0001+00.0005+00.0010+00.0050+00.0100+00.0500+00.1000+00.2500+00.3000+00.5
+00.7500+01.0000+01.2500+01.5000+01.7500+02.0000+02.5000+03.0000
+00.0000+00.0001+00.0005+00.0010+00.0050+00.0100+00.0500+00.1000+00.2000+00.2
+00.3000+00.4000+00.4500+00.5000+00.6000+00.7000+00.8000+00.9000+01.00
```

Appendix D. Migration at a rotating disk electrode in acidified solutions of $CuSO_4$ characterized by the bisulfate dissociation parameter $I/K'_B = 5$.

The numerical solution follows the lines indicated by Hsueh and Newman[125] The equations of convective diffusion for the H^+, HSO_4^-, $SO_4^=$ ions now contain a production term involving the parameter I/K'_B (all concentrations being made dimensionless with respect to I). The program MIGR is reproduced at the end of the appendix.

The migration effect on the current is shown in Figures 3.11 and D.1. The results are collected in Table D.1.

Note that the solution pre-supposes (1) constant physical properties; (2) no association of Cu^{2+} and SO_4^{2-} ions. In connection with (2) it is interesting to note that Harned and Hudson,[149] testing the theory of the electrophoretic effect in diffusion of bi-bivalent electrolytes ($ZnSO_4$, $MgSO_4$), obtained good agreement with the theory if a separate mobility was assumed for the ion-pair, approximately 40% higher than that of the dissociated electrolyte. This was explained by loss of water of hydration of the cation. Since migration effects depend on the mobility ratio of reacting ion and supporting ion, $CuSO_4$ association could account for a higher migration contribution to the current than predicted by computations based on complete dissociation of $CuSO_4$ and nearly-complete dissociation ($I/K'_B \approx 5$) of HSO_4^- ions.

Table D1. Migration current and electrolyte composition at the electrode ($I/K'_B = 5$).

A) i_L/i_D

r ↓ / H →	0.020	0.015	0.010	0.005	0.0025	0*
0.99	1.124897	1.124886	1.124878	1.124873	1.124930	1.124872
0.95	1.145449	1.145437	1.145428	1.145423	1.145589	1.145421
0.90	1.172204	1.172189	1.172179	1.172172	1.172495	1.172170
0.85	1.200227	1.200207	1.200193	1.200184	1.200682	1.200181
0.80	1.229608	1.229581	1.229561	1.229550	1.230232	1.229546
0.70	1.292807	1.292752	1.292714	1.292690	1.293731	1.292682
0.60	1.362492	1.362380	1.362300	1.362251	1.363569	1.362235
0.50	1.439323	1.439087	1.438919	1.438818	1.440262	1.438784

B) $\Delta C_{H_2SO_4}/\Delta C_{CuSO_4}$

r ↓						
0.99	0.297586	0.297584	0.297583	0.297582	0.293610	0.29759
0.95	0.289009	0.289008	0.289007	0.289006	0.284910	0.28901
0.90	0.277906	0.277906	0.277907	0.277907	0.273696	0.27791
0.85	0.266385	0.266389	0.266392	0.266394	0.262122	0.26639
0.80	0.254460	0.254471	0.254479	0.254483	0.250211	0.25549
0.70	0.229508	0.229544	0.229570	0.229585	0.225508	0.22959
0.60	0.203365	0.203453	0.203517	0.203555	0.199926	0.20357
0.50	0.176456	0.176659	0.176798	0.176881	0.173900	0.17691

*by three-point extrapolation from H=0.005, 0.010, 0.020.
Number of meshpoints 802. Mobility ratios used: $H^+/Cu^{2+} = 12.95$, $HSO_4^-/Cu^{2+} = 1.852$, $SO_4^=/Cu^{2+} = 1.482$.

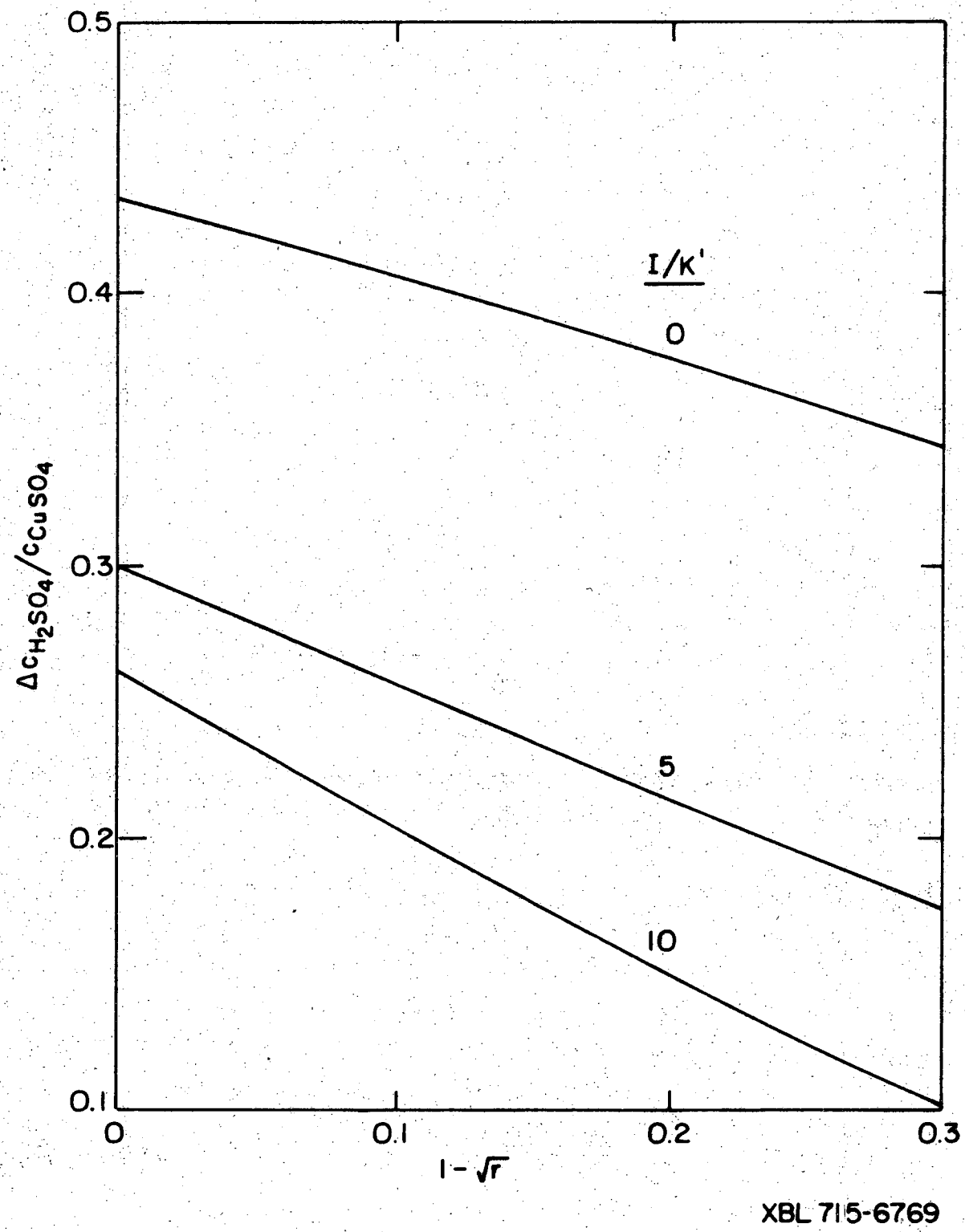

Fig. D.1. Accumulation of H_2SO_4 at a rotating disk cathode, in Cu deposition at the limiting current. $r = c_{H_2SO_4}/(c_{H_2SO_4}+c_{CuSO_4})$.

```
      PROGRAM MIGR(INPUT,OUTPUT)
C     PROGRAM FOR EFFECT OF MIGRATION ON LIMITING CURRENT
C     INCOMPLETE DISSOCIATION
      DIMENSION A(5,5),B(5,5),C(5,802),D(5,11),G(5),X(5,5),Y(5,5),J(5),
     1V(802),DIF(5),Z(5),S(5),CIN(5),REF(5)
      COMMON A,B,C,D,G,X,Y,N,NJ
  101 FORMAT (3I4,F8.4)
  102 FORMAT (4E8.4,A6)
  103 FORMAT (4HONJ=,I4,5H,  H=,F6.4/34HOSPECIES       U       DIF     Z
     1 S/(3X,A6,2F8.5,2F5.1))
  104 FORMAT (32H1NERNST STAGNANT DIFFUSION LAYER)
  105 FORMAT (32H1GROWING DROP OR PLANE ELECTRODE)
  106 FORMAT (14H1ROTATING DISK)
  107 FORMAT (5E8.4)
  108 FORMAT (30HOTHE NEXT RUN DID NOT CONVERGE)
  109 FORMAT (1HO,26X,4E10.6/(3X,A6,2F9.5))
  110 FORMAT (35HOSPECIES      CINF      CZERO      AMP)
   99 READ 101, MODE,NJ,N,H $ IF(MODE.EQ.0) STOP $ GO TO (1,2,3),MODE
    1 H= 1.0/(NJ-2)
      CONST=0.0     $AMPD=1.0             $PRINT 104            $GO TO 4
    2 CONST=2.0     $AMPD=1.12838         $PRINT 105            $GO TO 4
    3 CONST=3.0     $AMPD=1.1198          $PRINT 106
    4 NM1=N-1 $ NM2=N-2 $ CRO=0.0
      READ 102, (U(I),DIF(I),Z(I),S(I),REF(I),I=1,NM1)
      PRINT 103, NJ,H,(REF(I),U(I),DIF(I),Z(I),S(I),I=1,NM1)
      PRINT 110
    5 READ 107,XI,R,AK
                              IF(XI.EQ.0.0) GO TO 99 $ CIN(N)=0.0
      CA=XI*(1.-R)/(4.-R)  $ CB=CA*R/(1.-R)
                         CIN(4)=CA $ R1=SQRT((CB+AK-CA)**2+4.0*(CA+CB)*AK)
      IF(CB+AK.GT.CA) GO TO 31 $ CIN(2)=0.5*(CA-CB-AK+R1) $ GO TO 32
   31 CIN(2)=2.0*AK*(CA+CB)/(R1+CB+AK-CA)
   32 IF(CA+AK.GT.CB) GO TO 33 $ CIN(3)=0.5*(CB-CA-AK+R1) $ GO TO 34
   33 CIN(3)=4.0*CB*AK/(R1+CA+AK-CB)
   34 CIN(1)=CIN(2)*CIN(3)/AK
    6 DO 7 J=1,NJ
      V(J)= CONST*(H*(NJ-J-1))**(MODE-1)*DIF(NM1)
      C(NM1,J)= CRO + (CIN(NM1) - CRO)*(NJ-J-1)/(NJ-2)
      C(N,J)= 0.0
      DO 7 I=1,NM2
    7 C(I,J)= CIN(I) $ JCOUNT=0 $ AMP=0.0
    8 JCOUNT= JCOUNT + 1 $ AMPO=AMP $ J=0
      DO 9 I=1,N $ DO 9 K=1,N $ Y(I,K)=0.0
    9 X(I,K)= 0.0
   10 J= J + 1
      DO 11 I=1,N $ G(I)=0.0 $ DO 11 K=1,N $ A(I,K)=0.0 $ B(I,K)=0.0
   11 D(I,K)=0.0 $ IF(J.GT.1) GO TO 14 $ DO 13 I=1,N $ B(I,I)=1.0
   13 G(I)=CIN(I) $ CALL BAND(J) $ GO TO 10
   14 DO 15 K=1,NM1
   15 B(N,K)=Z(K) $ IF(J.EQ.NJ) GO TO 18 $ DO 17 I=1,NM1
      PP= U(I)/DIF(I)*(C(N,J+1)-C(N,J-1))/2.0
      PPP= U(I)/DIF(I)*(C(N,J+1)+C(N,J-1)-2.0*C(N,J))
      CP= (C(I,J+1) - C(I,J-1))/2.0
      A(I,I)= - 1.0 + PP/2.0 - H*V(J)/2.0/DIF(I)
      B(I,I)= 2.0 - PPP
      D(I,I)= - 1.0 - PP/2.0 + H*V(J)/2.0/DIF(I)
      A(I,N)= U(I)/DIF(I)*(CP/2.0 - C(I,J))
      B(I,N)= 2.0*U(I)/DIF(I)*C(I,J)
      D(I,N)= - U(I)/DIF(I)*(CP/2.0 + C(I,J))
   17 G(I)= - PPP*C(I,J) - PP*CP
```

```
      DO 23 I=2,3 $ A(I,1)=A(1,1) $ B(I,1)=B(1,1) $ D(I,1)=D(1,1)
      A(I,N)=A(I,N)+A(1,N) $B(I,N)=B(I,N)+B(1,N) $ D(I,N)=D(I,N)+D(1,N)
   23 G(I)= G(I) + G(1) $ A(1,1)=0.0 $ B(1,1)=-AK $ D(1,1)=0.0
      A(1,N)= 0.0 $ B(1,N)=0.0 $ D(1,N)=0.0 $ G(1)=C(3,J)*C(2,J)
      B(1,3)= C(2,J) $ B(1,2)=C(3,J) $ CALL BAND(J) $ GO TO 10
   18 DO 19 I=2,NM2
      PP= U(I)/DIF(I)*(C(N,NJ)-C(N,NJ-2))
      Y(I,NM1)= S(I)*DIF(NM1)/S(NM1)/DIF(I)
      Y(I,I)=-1.0 $ A(I,I)=PP $ B(I,I)=1.0 $ B(I,NM1)=-Y(I,NM1)
      Y(I,N)= (S(I)/S(NM1)*U(NM1)*CRO-U(I)*C(I,NJ-1))/DIF(I)
      B(I,N)= - Y(I,N)
   19 G(I)=PP*C(I,NJ-1) $ G(NM1)=CRO $ A(NM1,NM1)=1.0 $ B(1,1)=-AK
      G(1)= C(3,J)*C(2,J) $ B(1,3)=C(2,J) $ B(1,2)=C(3,J) $ CALL BAND(J)
      AMP= (U(NM1)*CRO*(C(N,NJ-2)-C(N,NJ))+DIF(NM1)*(C(NM1,NJ-2)-C(NM1,
     1NJ)))/2.0/H/(CIN(NM1)-CRO)/DIF(NM1)
      DEL=0.5*(C(1,NJ-1)+C(3,NJ-1)-CIN(1)-CIN(3))/CIN(4)
      RAMP=AMP/AMPO $ IF(ABS(AMP-AMPO).LT.ABS(AMP)/1.E5) GO TO 22
      IF(JCOUNT.LE.10) GO TO 8 $ PRINT 108
   22 PRINT 109, AMP,RAMP,AK,DEL,(REF(I),C(I,1),C(I,NJ-1),I=1,NM1)
      GO TO 5 $ END
      SUBROUTINE BAND(J)
      DIMENSION A(5,5),B(5,5),C(5,802),D(5,11),G(5),X(5,5),Y(5,5),
     1E(5,6,802)
      COMMON A,B,C,D,G,X,Y,N,NJ
  101 FORMAT (15HDDETERM=0 AT J=,I4)
      IF(J.GT.1) GO TO 6 $ NP1= N+1 $ DO 2 I=1,N $ D(I,2*N+1)=G(I)
      DO 2 L=1,N $ LPN=L+N
    2 D(I,LPN)=X(I,L) $ CALL MATINV(N,2*N+1,DETERM)
      IF(DETERM.EQ.0.0) PRINT 101, J $ DO 5 K=1,N
      E(K,NP1,1)=D(K,2*N+1) $ DO 5 L=1,N $ E(K,L,1)=-D(K,L) $ LPN=L+N
    5 X(K,L)=-D(K,LPN) $ RETURN
    6 IF(J.GT.2) GO TO 8 $ DO 7 I=1,N $ DO 7 K=1,N $ DO 7 L=1,N
    7 D(I,K)=D(I,K)+A(I,L)*X(L,K)
    8 IF(J.LT.NJ) GO TO 11 $ DO 10 I=1,N $ DO 10 L=1,N
      G(I)=G(I) - Y(I,L)*E(L,NP1,J-2) $ DO 10 M=1,N
   10 A(I,L)=A(I,L) + Y(I,M)*E(M,L,J-2)
   11 DO 12 I=1,N $ D(I,NP1)=-G(I) $ DO 12 L=1,N
      D(I,NP1)=D(I,NP1) + A(I,L)*E(L,NP1,J-1) $ DO 12 K=1,N
   12 B(I,K)=B(I,K) + A(I,L)*E(L,K,J-1) $ CALL MATINV(N,NP1,DETERM)
      IF(DETERM.EQ.0.0) PRINT 101,J $ DO 15 K=1,N $ DO 15 M=1,NP1
   15 E(K,M,J)=-D(K,M) $ IF(J.LT.NJ) RETURN $ DO 17 K=1,N
   17 C(K,J)=E(K,NP1,J) $ DO 18 JJ=2,NJ $ M=NJ-JJ+1 $ DO 18 K=1,N
      C(K,M)=E(K,NP1,M) $ DO 18 L=1,N
   18 C(K,M)=C(K,M) + E(K,L,M)*C(L,M+1) $ DO 19 L=1,N $ DO 19 K=1,N
   19 C(K,1)=C(K,1) + X(K,L)*C(3,L) $ RETURN $ END
      SUBROUTINE MATINV(N,M,DETERM) $ COMMON A,B,C,D
C     MATRIX INVERSION WITH ACCOMPANYING SOLUTION OF LINEAR EQUATIONS.
      DIMENSION A(5,5),B(5,5),C(5,802),D(5,11),ID(5)
      DETERM=1.0 $ DO 1 I=1,N
    1 ID(I)=0.0 $ DO 18 NN=1,N $ BMAX=0.0 $ DO 6 I=1,N
      IF(ID(I).NE.0) GO TO 6 $ DO 5 J=1,N $ IF(ID(J).NE.0) GO TO 5
      IF(ABS(B(I,J)).LT.BMAX) GO TO 5 $ BMAX=ABS(B(I,J)) $ IROW=I$JCOL=J
    5 CONTINUE
    6 CONTINUE
      IF(BMAX) 7,7,8
    7 DETERM=0.0 $ RETURN
    8 ID(JCOL)=1 $ IF(JCOL.EQ.IROW) GO TO 12 $ DO 10 J=1,N
      SAVE=B(IROW,J) $ B(IROW,J)=B(JCOL,J)
   10 B(JCOL,J)=SAVE $ DO 11 K=1,M $ SAVE=D(IROW,K) $D(IROW,K)=D(JCOL,K)
```

```
   11 D(JCOL,K)=SAVE
   12 F=1.0/B(JCOL,JCOL) $ DO 13 J=1,N
   13 B(JCOL,J)=B(JCOL,J)*F $ DO 14 K=1,M
   14 D(JCOL,K)=D(JCOL,K)*F $ DO 18 I=1,N $ IF(I.EQ.JCOL) GO TO 18
      F=B(I,JCOL) $ DO 16 J=1,N
   16 B(I,J)=B(I,J) - F*B(JCOL,J) $ DO 17 K=1,M
   17 D(I,K)=D(I,K) - F*D(JCOL,K)
   18 CONTINUE $ RETURN $ END
-
    3.802    5.22500-2
-50000-1 13310-0-10000-0          HSO4-
-80000-1 10650-0-20000-0           SO4
 34980-0 93130-0 10000-0           H+
 54000-1 71880-1 20000-0 10000-0 CU++
+10000+0+99000-1+20000-1
+10000+0+95000-1+20000-1
+10000+0+90000-1+20000-1
+10000+0+85000-1+20000-1
+10000+0+80000-1+20000-1
+10000+0+70000-1+20000-1
+10000+0+60000-1+20000-1
+10000+0+50000-1+20000-1
```

Appendix E. Theoretical solutions for transient convective diffusion.

The values of transition times in Tables 3.4 and 4.1 are based on the following relations.

1. Free convection at a vertical plate.

Exact, numerical, solutions for a step in concentration at the plate have not been found in the literature. Exact solutions for a step in the flux at the plate have been reported in the heat transfer literature. These will be discussed first.

Gebhart[157] used an integral method to compute solutions for various Pr numbers. He found that there is a rapid initial approach to the steady-state temperature during which the pure-conduction transient is closely approximated until about $T/T_{ss} = 0.75$. The remaining part of the transition is slow and shows a slight (~ 1%) overshoot for small Pr numbers. Expressed in convective diffusion parameters and variables: Sc; $Gr^* = (g\alpha L^4 N)/(\nu^2 D)$; and

$$\tau^* = \frac{Dt}{L^2} (Gr^* Sc)^{2/5} \quad ; \qquad (E.1)$$

the transition times are:

	$\Delta c/\Delta c_{ss} = 0.90$	0.99
Sc = 0.72	$\tau^* = 1.73$	2.73
5	1.36	2.34
1000	1.12	2.13

It is of interest to compare the results for Sc = 1000 with transition times reported by Tvarusko and Watkins[68] from interferometric measurements at a vertical cathode in 0.23 M $CuSO_4$ solution. The transition

times for various current densities as indicated by Fig. 4 of Ref. 68 are:

$i(ma/cm^2)$	t(sec)	τ^*	Gr^*Scx10^{+10}
0.60	80	4.44	0.63
3.92	36	4.24	4.14
23.5	12.0	2.89	24.8
36.9	9.5	2.74	39.0

In the calculation of τ^*, L is taken to be 0.9 cm, $D = 5.4 \times 10^{-6}$ cm^2/sec, $\alpha = 0.15$ ℓ/mole, $\nu = 1.03$ cs, $t_{Cu^{++}} = 0.366$.

The experimental τ^* values are higher than expected, in particular for low current densities, i.e., small driving force.

The transition time following a concentration step at a vertical plate can be estimated from an approximate solution given by Siegel[145] and supplemented by Goldstein. The end of the one-dimensional conductive period (τ_1) and the end of the asymptotic approach to steady state (τ_2) are obtained by employing the method of characteristics and assuming similarity of the transient profiles.

The results are

	flux step	concentration step
period 1	$\tau_1^* = 1.71\ (1+2Sc^{-1})^{2/5}$	$\tau_1 = 2.37(1+Sc^{-1})^{1/2}$
period 2	$\tau_2^* = 4.33(1+1.68Sc^{-1})^{2/5}$	$\tau_2 = 5.72(1+0.59Sc^{-1})^{1/2}$

Here $\tau = \frac{Dt}{L^2}(GrSc)^{1/2}$ and $\tau^* = \frac{Dt}{L^2}(Gr^*Sc)^{2/5}$ (E.2)

The results for a flux step are given for comparison with Gebhart's solution. The exact transition time (to 1% from steady-state) is underestimated by τ_1 and overestimated by τ_2. In the calculations of Table

4.1 the transition time for a concentration step was taken to be $\tau = 3$.

It is interesting to compare this with experimental observations from the electrochemical literature, in cases where a constant potential was applied.

Böhm, Ibl and Frei[48] report a transition time of 3 minutes to reach steady-state in an 0.1 M $CuSO_4$ acidified solution. The vertical cathode was 2 cm high; the diaphragm used in their experiments was close to the electrode but remote enough (> 0.3 mm) to obtain limiting current values in agreement with the classical relation for free convection at a vertical plate. Using the physical properties: μ = 1.27 cp; ρ = 1.10 g/ml; $D = 5.3 \times 10^{-6}$ cm^2/sec, one obtains $\tau = 10.5$ ($Ra = 0.192 \times 10^{10}$). This is considerably longer than expected.

For ferricyanide reduction in equimolar solution the transition time was longer; up to 50 minutes if the distance cathode-diaphragm was made smaller than the critical distance referred to above (cf. equation 20 of Table 1.3). This indicates that the development of secondary convection, which dominates mass transfer in such narrow spaces open to the bulk (cf. p.37), may take a much longer time than one would calculate from the solutions for free convection at a vertical plate.

This is also suggested by the observation of Marchiano and Arvía[66] that development of a steady limiting current at a 1 cm high cathode in 0.005 M $CuSO_4$ (with 1.5 M H_2SO_4), following a potential step to -500 mv, required 20 minutes. This corresponds to:

$$\tau = 21 \qquad (Gr\ Sc = 9.75 \times 10^6) \quad ,$$

again much longer than expected. One should note that the cell employed had a volume of 64 cm^3 while the cathode occupied only a 1 x 1 cm area. Moreover, the driving force for the secondary convection was very small.

2. Lévêque-type mass transfer

A complete analytic solution for a concentration step at the surface has been given by Soliman and Chambré.[159] Here the characteristic time variable is (4.4):

$$\tau = t(S^2D/x^2)^{1/3} \quad , \qquad (E.3)$$

where $S = \tau_o/\mu$, i.e., the local velocity gradient at the wall. The one-dimensional diffusion transient is followed to approximately $\tau = 0.80$. The approach to the steady-state is exponential and complete to within 10% at $\tau = 0.92$, and to within 1% at $\tau = 1.25$. (Used in Table 4.1)

The procedure for solving the unsteady-state following a flux step at the surface has also been described by Soliman and Chambré, but numerical values are not given.

3. Rotating disk at high Sc number (see also Appendix B*)

The unsteady state at a rotating disk has dimensional similarity to that in Lévêque mass transfer, if it is taken into account that at the rotating disk $S(r) = -\alpha\omega^{3/2}\nu^{-1/2}r$. The variables in the two problems are:

---

*Note that τ is here identical with (4a) of Appendix B, and differs from $\tau = \omega t\, Sc^{-1/3}$ used in Chapters 3 and 4 by a factor $(\alpha/3)^{2/3} = 0.307$.

	Lévêque Problem	Rotating Disk
τ	$\frac{Dt}{(9Dx/S)^{2/3}}$	$\frac{Dt}{(3Dr/S)^{2/3}} = \omega t\left(\frac{\alpha^2 D}{9\nu}\right)^{1/3}$
η	$\frac{y}{(9Dx/S)^{1/3}}$	$\frac{y}{(3Dr/S)^{1/3}} = \frac{y\omega^{1/2}}{\nu^{1/2}}\left(\frac{\alpha\nu}{3D}\right)^{1/3}$

The equations differ by one term only:

$$\text{Lévêque:}\quad \frac{\partial c}{\partial \tau}(1-6\eta\tau) - 3\eta^2\frac{\partial c}{\partial \eta} = \frac{\partial^2 c}{\partial \eta^2} \quad ; \qquad \text{(E.4)}$$

$$\text{Rot. Disk:}\quad \frac{\partial c}{\partial \tau} - 3\eta^2\frac{\partial c}{\partial \eta} = \frac{\partial^2 c}{\partial \eta^2} \quad . \qquad \text{(B.5)}$$

The extra term in the Lévêque equation derives from the non-uniform thickness of the diffusion boundary-layer. The steady state is reached more slowly than in a uniform diffusion layer having the same velocity gradient: $\tau = Dt/(9Dx/S)^{2/3} = 1.25$ for the Lévêque transient, while the analogous time $Dt/(9Dr/S)^{2/3}$ is 0.31 for the rotating disk transient. Apparently the parallel convective inflow provides a more effective replenishment of the falling concentration in the diffusion layer than the convection perpendicular to the surface.

Hale[154] has numerically computed the transient concentration at the disk surface following a step in the flux. The transition is 90% complete at $\tau = 1.40$, 99 % complete at $\tau = 3.02$ (used in Table 3.4). This is significantly slower than the transition following a concentration step.

Appendix F. Transient diffusion following linear potential decrease at a redox electrode.

1. The equations describing pure diffusion of the oxidized species (ox) and the reduced species (red) are:

$$\frac{\partial c_{ox}}{\partial t} = D_{ox} \frac{\partial^2 c_{ox}}{\partial y^2} \quad , \tag{F.1}$$

$$\frac{\partial c_{red}}{\partial t} = D_{red} \frac{\partial^2 c_{red}}{\partial y^2} \quad , \tag{F.2}$$

with the initial conditions:

$$t = 0,\ y \geq 0,\ c_{ox} = c_{ox,b},\ c_{red} = c_{red,b} \quad ; \tag{F.3}$$

and the boundary conditions:

$$t > 0,\ y = 0,\ -D_{ox} \frac{\partial c_{ox}}{\partial y} = D_{red} \frac{\partial c_{red}}{\partial y} \tag{F.4a}$$

$$y = \quad ,\ c_{ox} = c_{ox,b},\ c_{red} = c_{red,b} \tag{F.4b}$$

The concentration ratio at the electrode is prescribed by:

$$t > 0,\ E = E^\circ + \frac{R_o T}{nF} \ln \frac{c_{ox}}{c_{red}} = E_{in} + a't \tag{F.4c}$$

where E° is the standard redox potential and E_{in} the initial potential. This is equivalent to

$$\Phi = E - E_{in} = \frac{R_o T}{nF} \ln \left[\frac{c_{ox}}{c_{red}} \Big/ \frac{c_{ox,b}}{c_{red,b}} \right] = a't \tag{F.4d}$$

In the following a' is supposed to be negative

2. In dimensionless variables $\theta_{ox} = c_{ox}/c_{ox,b}$;

$\theta_{red} = c_{red}/c_{red,b}$; $\phi = \Phi nF/RT$, the boundary conditions (3,4) can be restated:

$$t = 0,\ y \geq 0,\ \theta_{ox} = 1,\ \theta_{red} = 1 \quad ; \tag{F.5}$$

$$t > 0,\ y = 0,\ \frac{\partial \theta_{red}}{\partial y} = - \frac{\partial \theta_{ox}}{\partial y}\left(\frac{c_{ox,b} D_{ox}}{c_{red,b} D_{red}}\right) \tag{F.6a}$$

$$y = 0,\ \phi = \ell n\ \frac{\theta_{ox}}{\theta_{red}} = at \quad ; \tag{F.6b}$$

$$y = \infty,\ \theta_{ox} = 1,\ \theta_{red} = 1 \quad . \tag{F.6c}$$

Note that $\left(\frac{\partial \theta_{ox}}{\partial t}\right)_o$, i.e., at the electrode, is unknown but coupled to $\left(\frac{\partial \theta_{red}}{\partial t}\right)_o$ by

$$\left(\frac{\partial \theta_{ox}}{\partial t}\right)_o = \left(\frac{\partial \theta_{red}}{\partial t}\right)_o e^{at} + a\, \theta_{red,o}\, e^{at} \tag{F.7}$$

3. The solution of (1) for a prescribed variation of c_{ox} at the electrode is, according to the Duhamel (superposition) theorem:

$$c_{ox}(y,t) = \int_o^t \operatorname{erfc} \frac{y}{2\sqrt{D_{ox}(t-t')}} \left(\frac{dc_{ox}}{dt'}\right)_o dt' \quad . \tag{F.8}$$

In dimensionless variables the concentration gradient is then:

$$\left(\frac{\partial \theta_{ox}}{\partial y}\right)_o = \int_o^t \frac{1}{\sqrt{\pi D_{ox}(t-t')}} \left(\frac{d\theta_{ox}}{dt'}\right)_o dt' \tag{F.9}$$

For the reduced species an analogous equation can be written. The flux equality (6a) takes the form:

$$-R\int_0^t \frac{\left(\frac{d\theta_{ox}}{dt'}\right)_o}{(t-t')^{1/2}}\,dt' = \int_0^t \frac{\left(\frac{d\theta_{red}}{dt'}\right)_o}{(t-t')^{1/2}}\,dt' \quad , \tag{F.10}$$

$$\text{where } R = \frac{c_{ox,b}\sqrt{D}_{ox}}{c_{red,b}\sqrt{D}_{red}} \quad . \tag{F.11}$$

4. The integrals in (10) are conveniently evaluated by the method of Acrivos and Chambré. In this method the t axis is divided into n equal intervals of length $\Delta t'$ and the derivative $\left(\frac{d\theta}{dt'}\right)_o$ is written in difference form for each interval:

$$-\int_0^t \frac{\left(\frac{d\theta}{dt'}\right)_o}{(t-t')^{1/2}}\,dt' = -\sum_{k=1}^{n}\int_{(k-1)\Delta t}^{k\Delta t} \frac{\theta_o(k\Delta t)-\theta_o((k-1)\Delta t)}{\Delta t(k\Delta t-t')^{1/2}}\,dt' \quad . \tag{F.12}$$

Upon integration and rearrangement one obtains

$$-\sum_{k=1}^{n} \frac{\theta_o(k\Delta t)-\theta_o((k-1)\Delta t)}{\Delta t} \int_{(k-1)\Delta t}^{k\Delta t} \frac{dt'}{(k\Delta t-t')^{1/2}} =$$

$$\frac{2}{(\Delta t)^{1/2}}\left[\theta_o(1)\left\{(n-1)^{1/2} - (n-2)\right\}^{1/2} - \theta_o(n) + \sum_{k=1}^{n-1}\theta_o(k)A_{n-k}\right] \quad , \tag{F.13}$$

where $A_k = 2k^{1/2} - (k+1)^{1/2} - (k-1)^{1/2}$.

5. Applying this method to (10) one can write:

$$- R\left[\theta_{ox}(n) - \theta_{ox}(1)B_{n-1} - \sum_{k=1}^{n-1} \theta_{ox}(k)A_{n-1}\right] =$$

$$\theta_{red}(n) - \theta_{red}(1)B_{n-1} - \sum_{k=1}^{n-1} \theta_{red}(k)A_{n-k} =$$

$$\theta_{ox}(n)\exp\{-(n-1)a\Delta t\} - \theta_{ox}(1)B_{n-1}$$

$$- \sum_{k=1}^{n-1}\theta_{ox}(k) \exp\{-(k-1)a\Delta t\} A_{n-k} \quad , \qquad \text{(F.14)}$$

where (6b) has been used, and

$$B_k = k^{1/2} - (k-1)^{1/2} \quad .$$

The final expression for $\theta_{ox}(n)$ is:

$$\theta_{ox}(n) = \frac{B_{n-1}(R+1) + (R)(s_1) + s_2}{R + \exp\{-(n-1)a\Delta t\}} \quad . \qquad \text{(F.15)}$$

where $$s_1 = \sum_{k=1}^{n-1} \theta_{ox}(k)\ A_{n-k} \qquad \text{(F.16a)}$$

and $$s_2 = \sum_{k=1}^{n-1} \theta_{ox}(k)\ A_{n-k} \exp\{-(k-1)a\Delta t\} \qquad \text{(F.16b)}$$

The final expression for the current is:

$$I = \frac{-i}{c_{ox,b}nF}\left(\frac{\pi}{aD_{ox}}\right)^{1/2} =$$

$$\frac{2}{(a\Delta t)^{1/2}}\left[\frac{B_{n-1}\{\exp(-(n-1)a\Delta t) - 1\} + s_1\exp(-(n-1)a\Delta t) - s_2}{R + \exp(-(n-1)a\Delta t)}\right] \qquad (F.17)$$

6. The program THETRO reproduced at the end of this appendix calculates the current and $\theta_{ox,o}$ for a given value of the parameter R and a given value of the increment $a\Delta t$, i.e., the dimensionless potential. 401 meshpoints are used in the calculation. The initial increment of $a\Delta t = \Delta\phi$ is 2.5×10^{-5}. In the next time cycle the increment is multiplied by 10 and the first 40 meshpoints are selected from the last cycle. Seven decades were usually computed in this way.

7. The results for various values of R are shown in Table F.1: the maximum current I(17) and corresponding potential, as well as θ_{ox} at the electrode when the current peak occurs,

At small values of R the current maximum agrees to 5 significant figures with that of (4.28), i.e., for a deposition reaction.

At high values of R the current maximum agrees to three significant figures with that computed by Nicholson and Shain,[166] who used a similar integration technique.

As shown in Figure 4.17, the current maximum is displaced to more negative potentials as R is increased. The reason is that the depletion of the diffusion layer takes more time. The reactant concentration is high compared to the product concentration and the initial current by itself would produce a larger shift from equilibrium than in the case of

equimolar bulk concentration; because the potential is controlled, the effect will be indirect and the initial current will be depressed. This is clearly shown in Figure 4.17; also, as noted in Chapter 4, the maximum current will be less.

Reinmuth[171] has proved that the shift of the maximum to more negative potentials is proportional to the increase in ℓn R. In physical terms: at high values of R, i.e., at large anodic initial potentials, the potential of the maximum will be a fixed amount more negative than

$$E^o + \frac{RT}{nF} \ell n\ R \quad ; \tag{F.18}$$

if $c_{ox,b} = c_{red,b}$, (18) is recognized as the half-wave potential ($E_{1/2}$) of polarography. According to Nicholson and Shain[166] the peak potential is

$$E = E_{1/2} - 1.109 \frac{RT}{nF} \quad . \tag{F.19}$$

Table 1 shows that the agreement with the results of Nicholson and Shain is quite good at $R = 10^3$. At higher values of R the present method of numerical integration gives inaccurate results, because the more important contributions to the sums s_1 and s_2 (16) are made at potentials where the (at) increment is not small anymore (0.025 in the calculations of Table 1; Nicholson and Shain used a uniform increment $\Delta(at) = 0.01$.

Table F.1. Current maxima in linear potential decrease at a redox electrode.

R	I(eq.F.17)	$-\phi$	$\theta_{ox,0}$
10^3	0.7916	8.025	0.247
10^2	0.7952	5.725	0.249
10^1	0.8223	3.450	0.265
1.1	0.9346	1.600	0.347
1	0.9410	1.575	0.343
10^{-1}	1.0566	0.9400	0.413
10^{-2}	1.0793	0.8650	0.423
10^{-3}	1.0818	0.8550	0.426
10^{-4}	1.0821	0.8540	0.426
0 (theory)	1.08209	0.85403	0.4257
∞ (Ref. 166)	0.7911 $\pm$ 0.001	7.998	

```
      PROGRAM THETRO(INPUT,OUTPUT)
      DIMENSION TH(401),A(401),B(401),CUR(401),ETAA(401)
  102 FORMAT(X,I9,X,E10.3,X,E13.7,X,E13.6)
  103 FORMAT(1H0,    9H     NZ    ,                    10H     PHI    ,X,13H
     1THETA    ,X,15H      CURRENT    )
  104 FORMAT(10X,4HNZT=,I4,4H,DZ=,F12.8,6H,SIGN=,F5.0,6H,RATE=,F12.5,15H
     1,DECADES TIME= ,I6)
  106 FORMAT(23X,F7.3,10X,E11.5,X,E13.6)
  107 FORMAT(115X,4HDZ= ,E12.5)
  115 FORMAT (I3)
  125 FORMAT(115X,6HRATE= ,E8.1)
  126 FORMAT(115X,8HDECADE= ,I3)
  199 FORMAT(1H0,23X,      7H  PHI   ,9X           ,12H    THETA     ,14H
     1CURRENT     )
  343 FORMAT(10X,14HREDOX REACTION,X,5H R=   ,F12.5)
 1111 FORMAT(1H1)
 1112 FORMAT(1H0)
      MM=0
C       MMAX= NUMBER OF CASES WITH DIFFERENT R
      READ 115,MMAX
   70 TH(1)=1.
  111 FORMAT(I4,E12.3,F3.0,E12.5,I2,E12.5)
C     NZT=NUMBER TIME-STEPS IN ONE CYCLE , DZ= TIME INCREMENT
C     SIGN=SIGN SCAN , RATE = RATE, NDEC= NUMBER OF CYCLES , R=R
      READ 111,NZT,DZ,SIGN,RATE,NDEC,R
      DZ=0.5*DZ
      EX=0.5
      RR=R*10.**6
      ETAA(1)=0.
      CUR(1)=0.
      IDEC=0
      MM=MM+1
      IF(MM.GT.MMAX) GO TO1113
      JBEGIN=2
      KKMAX=(NZT-1)/10 + 1
      KKBEG=2+ (KKMAX-1)/10
C     FORM COEFFICIENTS OF ACRIVOS-CHAMBRE INTEGRATION PROCEDURE
      DO 61 NZ=1,NZT   $ ANZ=NZ
      A(NZ)=2.0*ANZ**EX  -(ANZ+1.)**EX  - (ANZ-1.)**EX
   61 B(NZ)=ANZ**EX    - (ANZ-1.)**EX
      PRINT 1111
      PRINT 343, R
      PRINT 104,NZT,DZ,SIGN,RATE,NDEC
      PRINT 103
      NK=NDEC -1
      DO 3 M=1,NK
      IDEC=IDEC+1
      DO 80  NZ=JBEGIN,NZT
      TW=2.
      Z=(NZ-1)*DZ
      ETA=RATE*SIGN*Z
      RON=EXP(-ETA)
C     FORM S1 =SUM AND S2=SUM2
      SUM=0.
      SUM2=0.
      SUM3=0.
      IF (NZ.LE.2)  GO TO 42
      TW=2.
      DO 40 J=3,NZ
```

```
      K=NZ -J +1
      SUM=SUM +  TH(J-1)*A(K)
      PO = -((J-2)*RATE*SIGN*DZ)
      SUM3 = SUM3 + TH(J-1)*A(K)*EXP(K*RATE*SIGN*DZ)
   40 SUM2= SUM2 +TH(J-1)*A(K)*EXP(PO)
   42 NJ= NZ -1
      IF(RR.LT.PON) GO TO 77
      TH(NZ)=(B(NJ)*(1.+R) + R*SUM  + SUM2)/ (R + EXP(-ETA))
      GO TO 78
   77 TH(NZ)=SUM3
   78 CUR(NZ)=TW*(TH(1)*B(NJ) - TH(NZ) +SUM)/DZ**EX
      PRINT 102,NZ  ,ETA,TH(NZ),CUR(NZ)
      IF(TH(NZ).LE.1.0E-290) GO TO 117
   80 CONTINUE
  117 DO 11 K=1,KKMAX
      J=K*10-9
      TH(K)=TH(J)
      CUR(K)=CUR(J)
      ETAA(K)=ETAA(J)
   11 CONTINUE
      DZ=10.*DZ
      PRINT 1111
      PRINT 125,RATE
      PRINT 126,IDEC
      PRINT 107,DZ
      PRINT 199
      PRINT 106,(ETAA(NZ),TH(NZ),CUR(NZ),NZ=1,KKMAX)
      PRINT 1112
      PRINT 103
      JBEGIN=KKMAX+1
    3 CONTINUE
      PRINT 1111
      PRINT 1112
      GO TO 70
 1113 CONTINUE
      STOP
      END
-
+10
+401+005.000E-05-1.+1.00000E-0007+1.00000E+05
+401+005.000E-05-1.+1.00000E-0007+1.00000E+04
+401+005.000E-05-1.+1.00000E-0007+1.00000E+03
+401+005.000E-05-1.+1.00000E-0007+1.00000E+02
+401+005.000E-05-1.+1.00000E-0007+1.00000E+01
+401+005.000E-05-1.+1.00000E-0007+1.00000E+00
+401+005.000E-05-1.+1.00000E-0007+1.00000E-01
+401+005.000E-05-1.+1.00000E-0007+1.00000E-02
+401+005.000E-05-1.+1.00000E-0007+1.00000E-03
+401+005.000E-05-1.+1.00000E-0007+1.00000E-04
```

Appendix G. Transient diffusion following linear potential decrease in a deposition reaction characterized by slow electrode kinetics.

1. The equation describing pure diffusion in a semi-infinite medium is

$$\frac{\partial c}{\partial t} = D \frac{\partial^2 c}{\partial y^2} \tag{G.1}$$

with the initial condition

$$t = 0, \quad y \geq 0, \quad c = c_b; \tag{G.2a}$$

and the boundary condition:

$$t > 0, \; y = \infty, \; c = c_b. \tag{G.2b}$$

The concentration at the electrode is related to the total overpotential, η, by the expression (2.29)

$$i = -nFD\left(\frac{\partial c}{\partial y}\right)_o = j_o \left\{ \exp \frac{\alpha(\eta-\eta_c)ZF}{R_o T} - \exp \frac{\alpha(\eta-\eta_c)ZF}{R_o T} \right\} \tag{G.3}$$

where the ohmic contribution is assumed equal to zero. The concentration-dependent exchange current density j_o can be replaced by $i_o(c_o/c_b)^{\gamma}$ where i_o is taken at $c = c_b$.

The total overpotential is prescribed:

$$\eta = a't, \quad \text{or} \tag{G.4a}$$

$$\phi = \eta ZF/R_o T \quad \text{at.} \tag{G.4b}$$

In the following a is assumed to be negative.

2. In terms of dimensionless concentration, θ, and potential (4b), the boundary conditions are:

$$t = 0,\ y \geq 0,\ \theta = 1 \tag{G.5a}$$

$$t > 0,\ y = \infty,\ \theta = 1 \tag{G.5b}$$

$$t > 0,\ y = 0,$$

$$-D\frac{\partial\theta}{\partial y} = \frac{i_o}{c_b nF}\left\{\theta^{\gamma-\alpha_e}e^{\alpha at} - \theta^{\gamma+\beta_e}e^{-\beta at}\right\} \tag{G.5c}$$

where the Nernst relation (2.22) has been used.

3. The solution of (1) for a prescribed variation of c at the electrode, $(dc/dt)_o$, is according to the superposition theorem:

$$c(y,t) = \int_o^t \operatorname{erfc}\frac{y}{2\sqrt{D(t-t')}}\left(\frac{dc}{dt'}\right)_o dt' \quad . \tag{G.6}$$

In dimensionless variables the concentration gradient at the electrode is then:

$$\left(\frac{\partial\theta}{\partial y}\right)_o = \int_o^t \frac{1}{\sqrt{\pi\, D(t-t')}}\left(\frac{d\theta}{dt'}\right)_o dt' \quad . \tag{G.7}$$

The current condition (3) can now be written:

$$\theta_o^{\gamma-\alpha_e}e^{\alpha at} - \theta_o^{\gamma+\beta_e}e^{-\beta at} = \frac{-i_o}{c_b nF}\sqrt{\frac{D}{\pi}}\int_o^t \frac{(d\theta/dt')_o}{\sqrt{t-t'}}\,dt' \tag{G.8}$$

Next, introducing a dimensionless time:*

*Note that τ here signifies a different dimensionless time from that used elsewhere.

$$\tau = \frac{\pi t}{D}\left(\frac{i_o}{c_b nF}\right)^2 \qquad (G.9)$$

and a dimensionless potential scan rate:

$$r = \frac{aD}{\pi}\left(\frac{c_b nF}{i_o}\right)^2 \quad , \qquad (G.10)$$

so that $\phi = at = r\tau$, one obtains an integral equation for θ which contains r, and α,β and γ, as parameters:

$$\theta_o^{\gamma-\alpha_e \alpha r\tau} - \theta_o^{\gamma+\beta_e-\beta r\tau} \int_0^{\tau} \frac{(d\theta/d\tau')_o}{\sqrt{\tau-\tau'}}\, d\tau' \qquad (G.11)$$

4. To solve (11) numerically, we use the method of Acrivos and Chambré[169] (see Appendix F). The righthand side of (11) is thereby reduced to a summation and (11) to an algebraic equation:

$$(\theta_o[n\Delta\tau]^{\gamma-\alpha_e \alpha r(n\Delta\tau)} - (\theta_o[n\Delta\tau])^{\gamma+\beta_e-\beta r(n\Delta\tau)} =$$

$$\frac{2}{\sqrt{\Delta\tau}}[\theta_o[1](\sqrt{n-1} - \sqrt{n-2} - \theta_o[n] + \sum_{k=1}^{n-1} \theta_o[k]A_{n-k} \qquad (G.12)$$

where $A_{n-k} = 2\sqrt{k} - \sqrt{k+1} - \sqrt{k-1}$.

Equation (12) is now solved for θ_o at every time-step, starting with $\theta_o[1] = 1$. The value of θ_o at the previous step is used as the first trial in a Newton-Raphson root-finding iteration. The current follows directly from (3):

$$i = i_o(\theta_o^{\gamma-\alpha_e \alpha r\tau} - \theta_o^{\gamma+\beta_e-\beta r\tau}) \quad , \qquad (G.13)$$

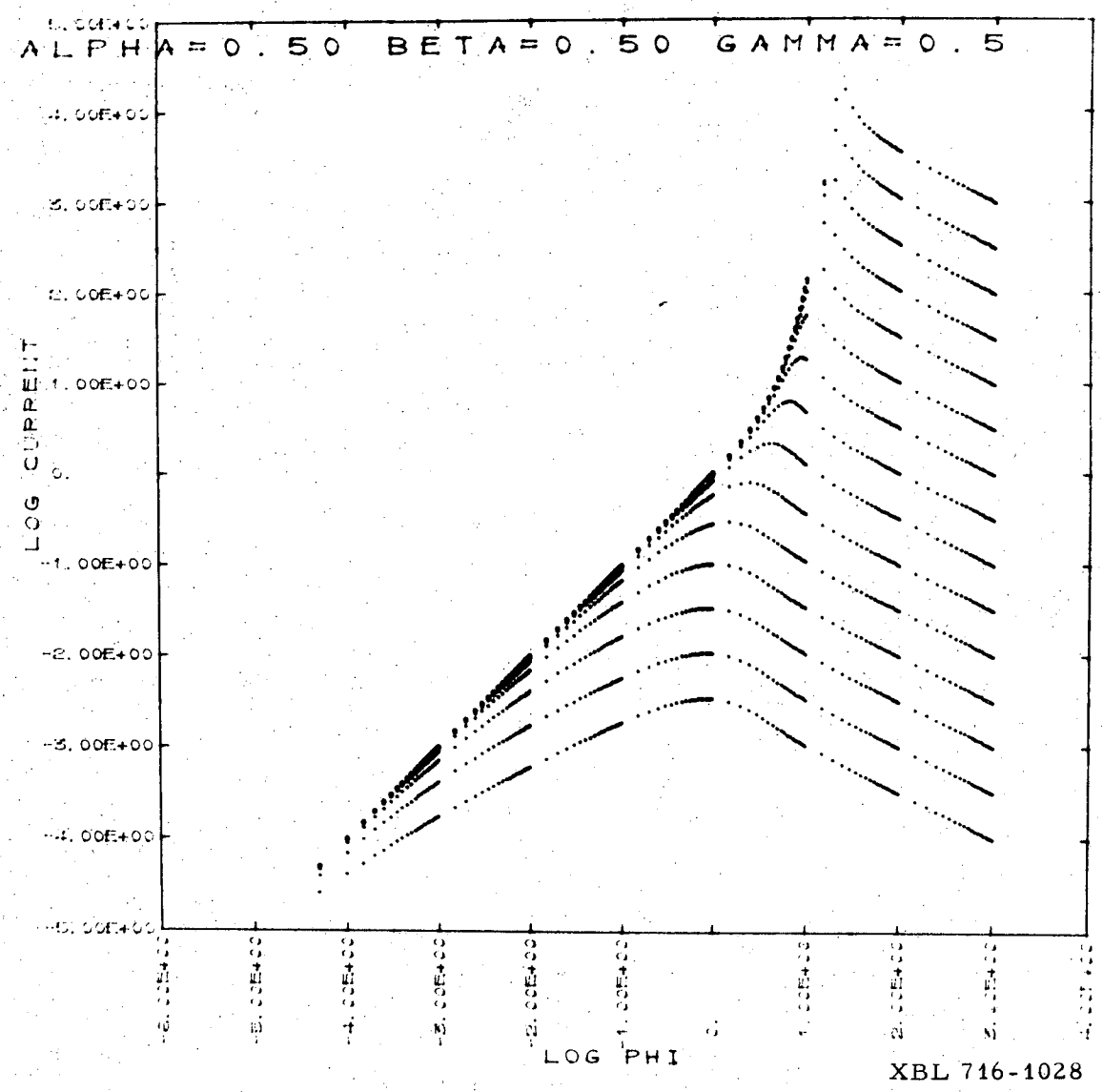

Fig. G.1. Current response to negative potential scan of a deposition reaction characterized by $\alpha = \beta = \gamma \geq 0.50$. PHI = ϕ; CURRENT = i/i_o. The scan rate

$$r = \frac{aD}{\pi} \left(\frac{c_b nF}{i_o}\right)^2$$

varies from 10^{-5} (lowest curve) to 10^{9} (top) by decades.

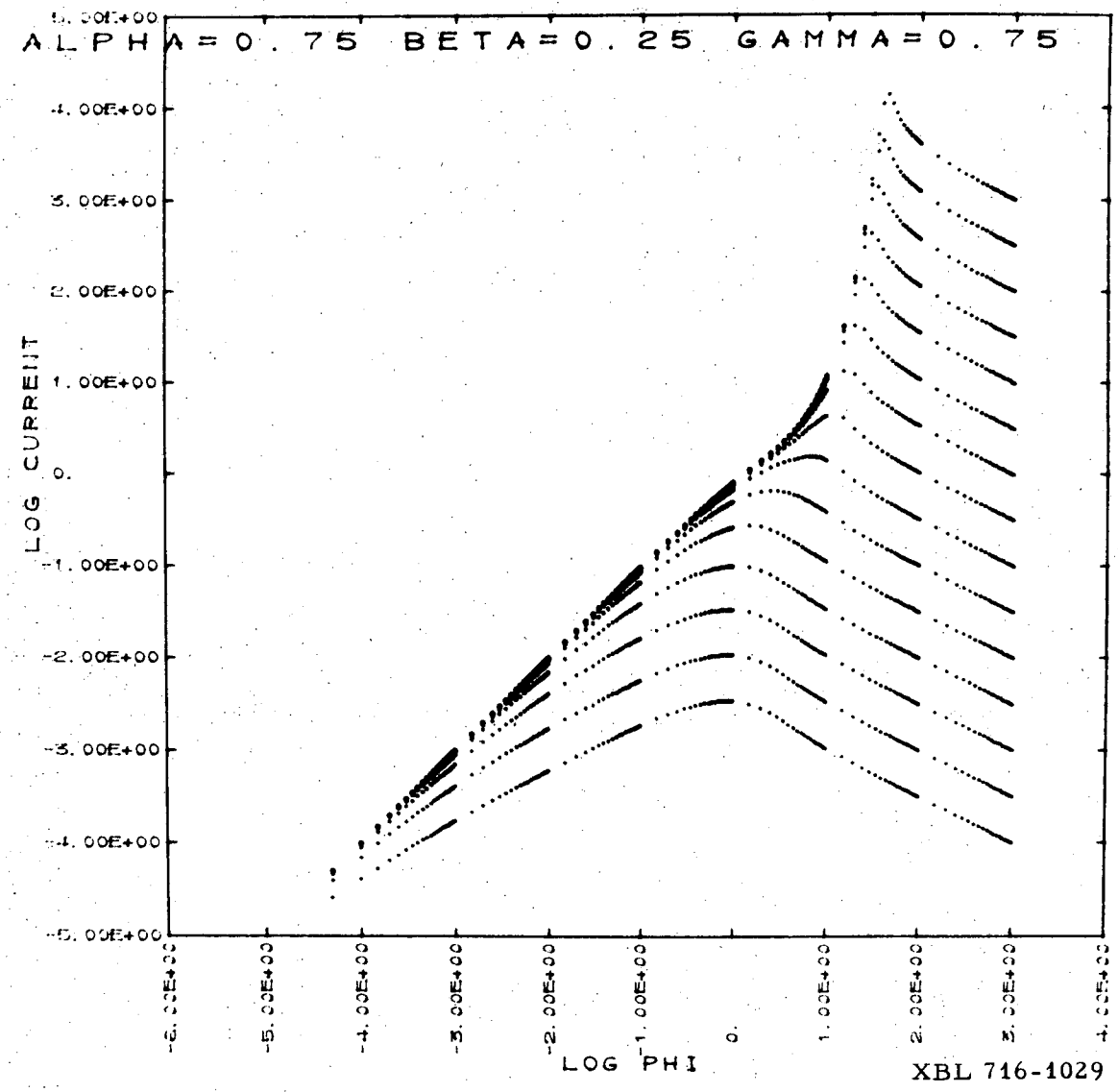

Fig. G.2. Current response to potential scanning of a deposition reaction characterized by $\alpha = \gamma = 0.75$, $\beta = 0.25$. PHI = ϕ; CURRENT = i/i_o. Scan rate increases by decades from $r = 10^{-5}$ (lowest curve) to $r = 10^{9}$ (top).

i.e., the left-hand or righthand side of (12) will give the current relative to i_o.

5. The program THETA reproduced at the end of this appendix calculates the concentration θ_o and the current i/i_o, given input parameters RATE(r), ALPHA(α), BETA(β), GAMMA(γ) and given an initial value of the potential increment $r\Delta\tau$. 201 meshpoints are used in the calculation. The initial increment of $\Delta\phi = r\Delta\tau$ is 5×10^{-5}. In the next time cycle the increment is multiplied by 10 and the first 20 meshpoints are selected from the last cycle. Seven decades were usually computed in this manner.

6. The results of principal interest are the value of the current maximum and the potential at which it occurs. Since a systematic variation of the four input parameters is not very meaningful, a few combinations of α,β and γ have been selected and r has been varied systematically.

Table G.1 presents values of $I = i/i_o$ and ϕ at the maximum for ($\alpha = 0.50$, $\beta = 0.50$, $\gamma = 0.50$), and for ($\alpha = 0.75$, $\beta = 0.25$) with four different values of γ; one of these values is 0.40 (cf. copper deposition electrode kinetics discussed in section 2.3).

7. Figures G.1 and G.2 illustrate the current response to a scan rate varying over 15 decades. The scale is logarithmic in both coordinates. This makes it possible to distinguish the characteristic features of the diffusion limitation modified by electrode kinetics:

a. All rates have a common short-time asymptote:

$$I = i/i_o = (\alpha+\beta)\phi \quad ; \tag{G.14}$$

this is the linear form of (2.29). The slope of the asymptote is +1.

b. They also have a common long-time asymptote, namely:

$$\frac{\partial\theta}{\partial y}_o = \frac{1}{\sqrt{\pi Dt}} \quad ; \tag{G.15}$$

this is the response to a unit step in concentration at the surface. Expressed in units $\log(i/i_o)$ and $r\tau$ (9), the long-term asymptote shifts a vertical distance $\log \sqrt{10}$ for every tenfold increase in r. The slope of the asymptote is -1/2.

c. The potential at which the maximum occurs is 0.860 at the lowest rates. This indicates that diffusion control is dominant, since it tends to the value found when kinetics are left out of account ($-0.8540 R_o T/nF$ mv, cf. section 4.7). The current peaks at low r follow the relation (4.28) which, expressed in I, r and τ, reads:

$$I_{max} = 1.0821\sqrt{r} \quad . \tag{G.16}$$

d. At high rates the maximum is shifted to more negative potentials by the electrode-kinetic constraint on the current. The envelope of the curves for high rates is the most simplified form of the Butler-volmer equation (2.29):

$$I = e^{\alpha\phi} - e^{-\beta\phi} \tag{G.17}$$

Note that the initial part of the envelope is linear, and also the part at very high ϕ (Tafel relation). The envelope for $\beta = 0.25$ differs from that for $\beta = 0.50$ by having an inflection, and by proportionately higher potentials for the same current.

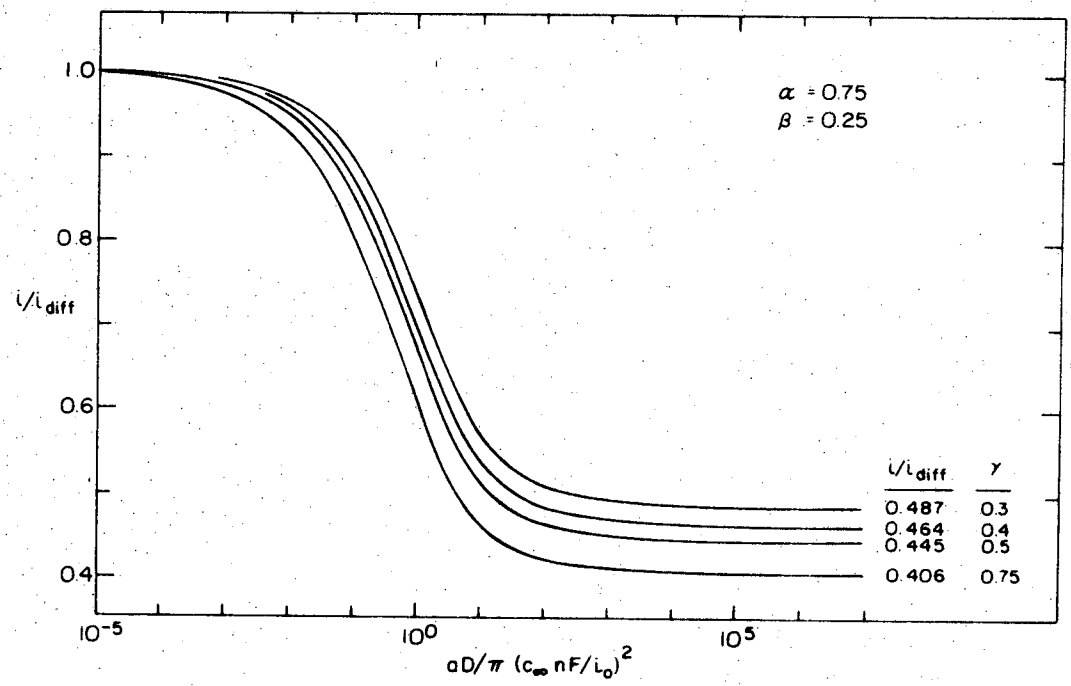

Fig. G.3. Dependence of the maximum current on the scan rate r, for a deposition reaction characterized by $\alpha = 0.75$, $\beta = 0.25$ γ variable. The current is relative to the diffusive current maximum $i_{diff} = 0.6105\ c_b nF(aD)^{1/2}$.

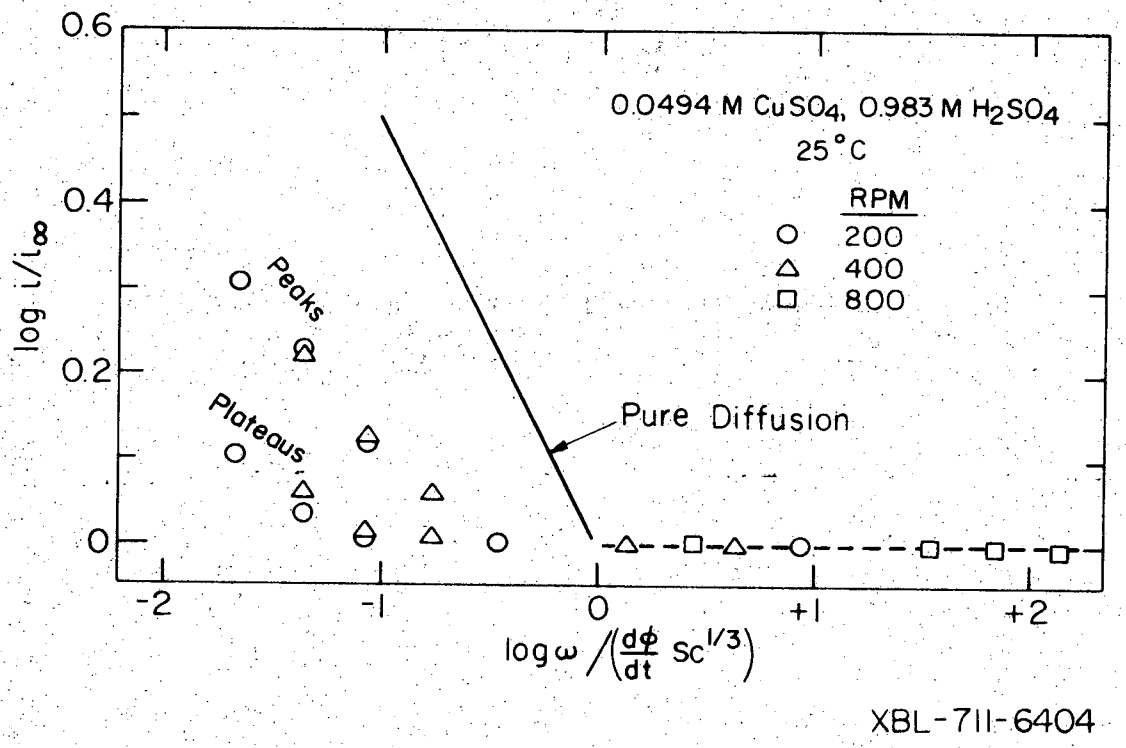

Fig. G.4. Current maxima and plateaux in potential scanning of copper deposition at a rotating disk. The solid line represents $i_{diff} = 0.6105\ c_b nF(aD)^{1/2}$.

e. As can be expected from the behavior of the envelope, the current peaks do not follow (16) anymore at rates above 10^{-3}, but at high rates ($> 10^{3}$) they again tend to follow a $\sqrt{r}$ dependence: the pure-diffusion limitation (15) is then reached almost instantaneously. There remains, however, an "overshoot" of the current so that the maximum is not simply given by the intersection of the lines

$$I = \sqrt{r}/\sqrt{\phi} \qquad \text{(G.15a)}$$

and

$$I = \exp(-\beta\phi) \qquad \text{(G.17a)}$$

f. The potential of the current maximum at high rates is strongly dependent on the value of β(see Table G.1). Delahay[172] first pointed out the importance of the shift in potential as an indicator of n for a particular reaction. The potential shift appears to be barely dependent on γ, for the case $\beta = 0.25$ (Table G.1). However, the current level at the peak is dependent on β and γ, as shown in Figure G.3, where it is plotted relative to the pure-diffusion current (16), for $\beta = 0.25$. If the value of β is known, a study of current peaks in potential scanning should yield information about γ.

Figure G.4 shows current peaks and plateaux obtained by potential scanning of copper deposition at a rotating disk electrode. The plot is similar to that of Figure 4.13. The solid line represents (4.28), or equation 16, in terms of rotating disk variables. One might now assume that the highest peak current of Figure G.4 lies already in that region of Figure G.3 where constant dependence on $\sqrt{r}$ is reached (r is by

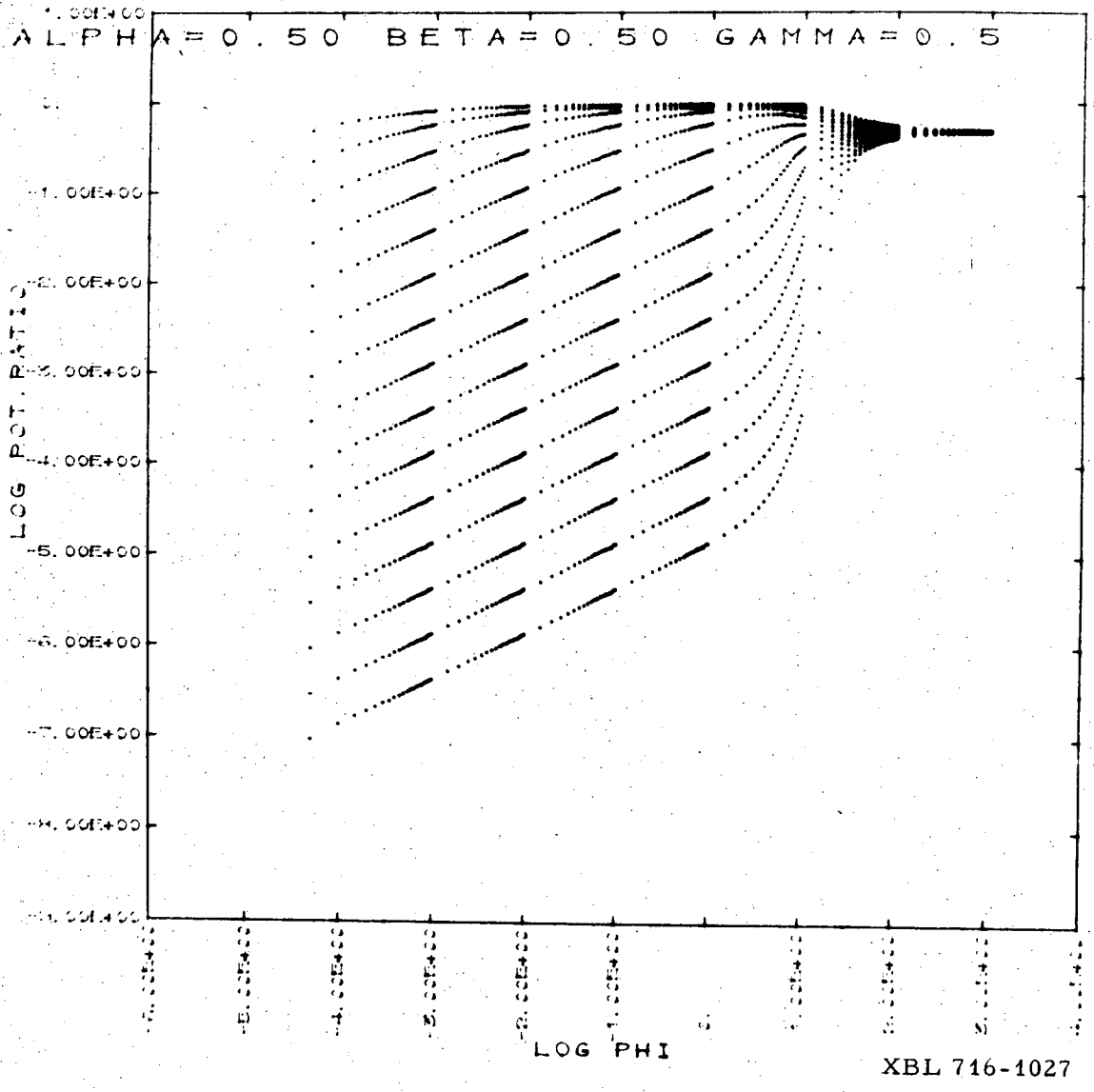

Fig. G.5. The ratio of concentration overpotential to surface overpotential in potential scanning at rates from $r = 10^{-5}$ (highest curve) to $2 = 10^{9}$ (lowest), for a deposition reaction with $\alpha = \beta = \gamma = 0.50$.

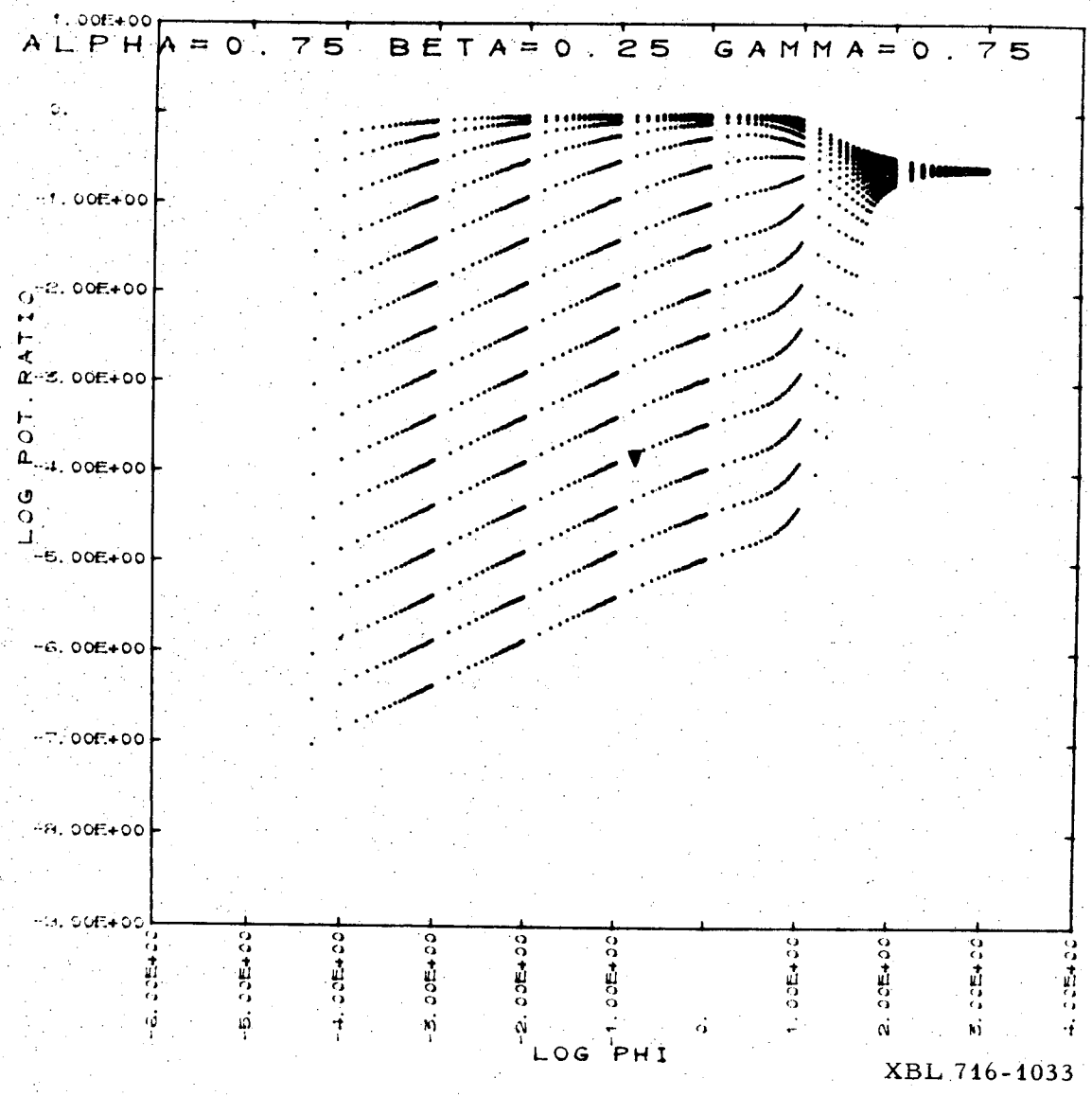

Fig. G.6. The ratio of concentration overpotential to surface overpotential in potential scanning at rates from $r = 10^{-5}$ (highest curve) to $r = 10^{9}$ (lowest), for a deposition reaction with $\alpha = \gamma = 0.75$, $\beta = 0.25$.

approximation 2.5×10^3). The value of the current is, compared with the pure-diffusion current,

$$i/i_{diff} = 0.32$$

This indicates a very high value of γ, in accordance with the findings of Chapter 4.

g. Figures G.5 and G.6 show the behavior of the ratio concentration to surface overpotential. The ratio is large for small rates and goes through a fairly flat maximum. For the higher rates a dependence on $\sqrt{r}$ exists at small times. This follows from:

$$i = 2c_b nFa \sqrt{Dt/\pi} \qquad (G.18)$$

which is the short-term approximation of (4.26), and (14).

At long times the ratios for all scan rates converge. The approximate convergence ratios are:

$\alpha = 0.50$	$\beta = 0.50$	$\gamma = 0.50$	$\eta_c/\eta_s = 0.50$
0.75	0.25	0.75	0.25
0.75	0.25	0.50	0.33
0.75	0.25	0.40	0.38
0.75	0.25	0.30	0.45

These values are accurate to $\pm$ 1%. For the same reason as indicated in Appendix F the accuracy of the numerical procedure is limited with respect to the behavior at large time. This explains why the values of θ_o in Table G.1 do not remain stable as r is increased but vary slightly.

Table G.1. Current maximum and corresponding potential for various scan rates.

	α=0.50 β=0.50 γ= 0.50			α=0.75 β=0.25 γ=0.75		
log r	I	ϕ	θ_o	I	ϕ	θ_o
-5	3.417E-3	0.860	0.425	3.413E-3	0.860	0.426
-4	1.077E-2	0.875	0.424	1.073E-2	0.875	0.425
-3	3.368E-2	0.925	0.418	3.335E-2	0.925	0.423
-2	1.032E-1	1.05	0.411	1.002E-1	1.05	0.427
-1	3.000E-1	1.45	0.380	2.757E-1	1.50	0.413
0	8.138E-1	2.40	0.336	6.618E-1	2.65	0.412
1	2.205E0	4.25	0.278	1.579E0	6.70	0.297
2	6.453E0	6.60	0.239	4.559E0	12.0	0.227
3	1.988E1	8.90	0.232	1.406E1	16.5	0.227
4	6.245E1	11.5	0.199	4.411E1	21.0	0.231
5	1.973E2	13.5	0.231	1.391E2	25.5	0.237
6	6.227E2	16.0	0.209	4.397E2	30.5	0.215
7	1.966E3	18.0	0.243	1.391E3	35.0	0.220
8	6.226E3	20.5	0.220	4.397E3	39.5	0.226
9	1.965E4	23.0	0.199	1.390E4	44.0	0.232

Table G1. (continued)

	α=0.75 β=0.25 γ=0.50			α=0.75 β=0.25 γ=0.40		
log r	I	ϕ	ϕ_o	I	ϕ	θ_o
-5	3.416E-3	0.860	0.425	3.417E-3	0.860	0.425
-4	1.077E-2	0.875	0.424	1.078E-2	0.875	0.423
-3	3.366E-2	0.925	0.418	3.377E-2	0.920	0.418
-2	1.029E-1	1.10	0.395	1.038E-1	1.10	0.390
-1	2.930E-1	1.50	0.381	2.998E-1	1.50	0.369
0	7.298E-1	2.70	0.354	7.617E-1	2.70	0.330
1	1.753EO	6.30	0.261	1.838EO	6.10	0.248
2	5.012EO	11.0	0.219	5.234EO	11.0	0.186
3	1.540E1	15.5	0.218	1.609E1	15.5	0.185
4	4.832E1	20.5	0.190	5.042E1	20.0	0.190
5	1.525E2	25.0	0.196	1.590E2	24.5	0.197
6	4.818E2	29.5	0.203	5.021E2	29.5	0.169
7	1.523E3	34.0	0.210	1.589E3	34.0	0.176

Table G.1. (continued)

α=0.75 β=0.25 γ=0.30

log r	I	ϕ	θ_o
-5	3.419E-3	0.860	0.425
-4	1.079E-2	0.875	0.423
-3	3.386E-2	0.920	0.417
-2	1.047E-1	1.05	0.403
-1	3.067E-1	1.50	0.356
0	7.967E-1	2.70	0.305
1	1.937E0	5.95	0.227
2	5.493E0	10.5	0.187
3	1.685E1	15.0	0.186
4	5.277E2	20.0	0.153
5	1.666E2	24.5	0.160
6	5.266E2	29.0	0.167
7	1.665E3	33.5	0.175

```
      PROGRAM THETA (INPUT,OUTPUT)
      DIMENSION  TH(201),A(201),B(201),CUR(201),ETAA(201),RAT(201)
  102 FORMAT(    10X,I4,11X,F9.3 ,X,F8.5,X,E11.5,X,E13.6)
  103 FORMAT(1HO,15X,4H NZ ,7X       ,7H  PHI  ,9H   RATIO ,12H   THET
     1  ,14H   CURRENT     )
  104 FORMAT(10X,4HNZT=,I4,4H,DZ=,F12.5,6H,SIGN=,F5.0,6H,RATE=,F12.5,1
     1,DECADES TIME= ,I6)
  105 FORMAT(19X,              7H ALPHA=,F7.3,7H, BETA=,F7.3,7H,GAMMA=,F
     13)
  106 FORMAT(23X,F7.3, X,F8.5,X,E11.5,X,E13.6)
  107 FORMAT(115X,4HDZ= ,F12.5)
  108 FORMAT(/10X,4H X1=,E13.5,4H,X2=,E13.5,4H,X3=,E13.5,5H,DX1=,E13.5
     15H,DX2=,E13.5,5H,SUM=,F8.5,3H,S=,F8.5,3H,N=,I4/)
  111 FORMAT  (I4,E12.3,F3.0,E12.5, I4)
  112 FORMAT(4E5.2)
  115 FORMAT(I2)
  125 FORMAT(115X,6HRATE= ,E8.1)
  126 FORMAT(115X,8HDECADE= ,I3)
  127 FORMAT(115X, 7HDEVM =    ,E9.2)
  199 FORMAT(1HO,23X,                  7H  PHI  ,9H   RATIO ,12H   THET
     1  ,14H   CURRENT     )
  999 FORMAT(1HO,4HPHI=,E13.6,8H,TH(NJ)=,E13.6,7H,B(NJ)=,E13.6,5H,SUM=
     113.6,3H,Z=,E13.6,3H,N=,I4/)
 1010 FORMAT (1HO,*NO CONVERGENCE AT*,F6.3)
 1111 FORMAT(1H1)
 1112 FORMAT (1HO)
      MP=2
      MM=0
      DEVI=0.000001
C     MMAX= NUMBER OF CASES WITH DIFFERENT RATES
      READ 115,MMAX
      READ 111,NZT,DZ,SIGN,RATE,NDEC
      READ 112,ALPHA,BETA,GAMMA
   70 TH(1)=1.
      S=TH(1)        $EX=0.5
      DEVM=DEVI $ ETAA(1)=0.  $ CUR(1)=0. $ RAT(1)=0.
      MM=MM+1
      IF(MM.GT.MMAX) GO TO 119
      RATE=RATE*10.  $ DZ=DZ/10.**NDEC
      JBEGIN=2
      KKMAX=(NZT-1)/10 + 1
      DO 61 NZ=1,NZT    $ ANZ=NZ
      A(NZ)=2.0*ANZ**EX  -(ANZ+1.)**EX  -(ANZ-1.)**EX
   61 B(NZ)=ANZ**EX  -(ANZ-1.)**EX
      PRINT 1111
      PRINT 104,NZT,DZ,SIGN,RATE,NDEC
      PRINT 105     ,ALPHA,BETA,GAMMA
      PRINT 103
      NK=NDEC-1
      DO 3 M=1,NK
      DO 80  NZ = JBEGIN,NZT
      TW = 2.356194448975
      Z = (NZ - 1)*DZ          $ETA=RATE*Z*SIGN
      SUM = 0.0
      IF (NZ .LE. 2) GO TO 42
      TW=2.
C     CALC. SUM(TH(J)*A(K))
      DO 40 J = 3,NZ
      K = NZ - J + 1
   40 SUM = SUM + TH(J - 1)*A(K)
```

```
   42 NJ=  NZ - 1
      DO 56 N = 1,20
      IF(S.GT.0.) GO TO 129
  128 FORMAT(105X,11HS NEG., IT.,I4)
      IF (JFLAG.EQ.0) PRINT 128,N
      JFLAG=1
      S=(CUR(NZ-1)*EXP(BETA*ETA))**(1.0/(GAMMA+BETA))
  129 X1   =        S**(GAMMA-ALPHA)*  EXP(ALPHA*ETA)
      DX1=  X1*(GAMMA-ALPHA)/S
      X2=  S**(GAMMA+  BETA)*  EXP(-BETA*ETA)
      DX2=X2*(GAMMA+BETA)/S
      X3=  TW *(TH(1)*B(NJ)  -  S  +  SUM)/ DZ**EX
      CUR(NZ)=X3
      DTH= S  - (((X1-X2)+X3)/(DX1-DX2 -TW/DZ**EX))
      IF(CUR(NZ).LE.0.0001)  PRINT 108,X1,X2,X3,DX1,DX2,SUM,S,N
      IF(N.LT.3) GO TO 56
      DEV = (S - DTH)/DTH
   53 IF (ABS(DEV) .LE. DEVM) GO TO 60
   56 S = DTH
      PRINT 1010,ETA
   60 TH(NZ) = DTH
      CUR(NZ)=TW*(TH(1)*B(NJ) - S  + SUM)/DZ**EX
   62 ETAC=ABS(ALOG(TH(NZ)))
      RAT(NZ)=ETAC/ETAA(NZ)
      PRINT 102,NZ,  ETA      ,RAT(NZ),TH(NZ),CUR(NZ)
   80 CONTINUE
  117 DO 11 K=1,KKMAX
      J=K*10-9
      TH(K)=TH(J)
      RAT(K)=RAT(J)
      CUR(K)=CUR(J)
      ETAA(K)=ETAA( J )
   11 CONTINUE
      DZ=10.*DZ
      PRINT 1111
      PRINT 125,RATE
      MMM=M+1
      PRINT 126,MMM
      PRINT 107,DZ
       PRINT 127, DEVM
      PRINT 199
      PRINT 106,(ETAA(NZ),RAT(NZ),TH(NZ),CUR(NZ),NZ=1,KKMAX)
      PRINT 1112
      PRINT 103
      JBEGIN=KKMAX+1
    3 CONTINUE
      PRINT 1111
      PRINT 1112
      GO TO 70
  119 CONTINUE
  113 CONTINUE
      STOP
      END
-
20
+201+005.000E+07-1.+1.000000E-06  07
 0.75 0.25 0.75
(
```

NOMENCLATURE

a	thermal diffusivity	[cm^2/sec]
a	dimensional coefficient (1.35)	[cm^{-2}]
a	radius of model sphere (Ch. 3)	[cm]
a	dimensionless potential scan rate (Ch. 4)	
a'	potential scan rate	[mv/sec]
a_i	activity of species i	[mole/cm^3]
a_r	critical electrode-diaphragm separation (1.25)	[cm]
A	area	[cm^2]
b	dimensional coefficient (1.35)	[cm^{-1}]
c	concentration	[mole/cm^3]
C	constant in mass-transfer correlations (Ch. 1)	
D	diffusivity	[cm^2/sec]
e^-	electron	
E	electrode potential	[v]
E°	standard electrode potential	[v]
ΔE	applied cell voltage	[v]
f	frequency (Ch. 1)	[sec^{-1}]
f	fraction of limiting current (2.31, App. A)	
f_i	activity coefficient of species i	
F	Faraday's constant	[96,494 C]
g	acceleration of gravity	[cm/sec^2]
G	mass flux	[g/cm^2sec]
h	distance between electrodes (Ch. 2)	[cm]
h	mesh size (App. B)	

i	current density	[ma/cm^2]
i_D	limiting diffusion current	[ma/cm^2]
i_L	limiting current	[ma/cm^2]
i_o	exchange current density	[ma/cm^2]
i_{lim}	limiting current	[ma/cm^2]
I	apparent ionic strength	[mole/ℓ]
I_r	true ionic strength	[mole/ℓ]
I_e	effective current on rough surface (3.14)	[ma]
I_o	current on smooth surface (3.14)	[ma]
I	dimensionless current density (App. F, G)	
k	mass-transfer coefficient	[cm/sec]
k	rate-constant electrochemical reaction (2.40)	[cm/sec]
K	dissociation constant (thermodynamic)	[mole/ℓ]
K'	dissociation constant (stoichiometric)	[mole/ℓ]
L	length or height	[cm]
M_i	species participating in charge-transfer reaction (2.1)	
n	number of electrons transferred in charge-transfer reaction (2.1)	
$\tilde{n}$	dimensionless frequency (Ch. 1)	
N	flux	[mole/cm^{2}sec]
ΔP	pressure drop	[dyne/cm^2]
Q	volume flow rate	[cm^3/sec]
r	radius (r_i: inner; r_o: outer radius)	[cm]
r	ratio of supporting to total electrolyte (2.3)	
r	dimensionless potential scan rate (G.10)	

R	ohmic resistance of electrochemical cell (Ch. 2)	[Ω]
R	diffusion parameter for redox reaction (4.33; App. F)	
R_o	gas-constant [8.3143 VC/mole °K]	
s	area per unit volume in packed bed (Ch. 1)	[cm^{-1}]
s	flux increase rate (4.16)	[cm/sec^2]
s_i	number of ions or molecules of species i participating in charge-transfer reaction (2.1)	
S	velocity gradient at mass-transfer interface	[sec^{-1}]
t	time	[sec]
t_i	transference number of species i	
T	temperature	[°K]
T	dimensionless time in Appendix B (B.23a)	
u_i	mobility of ionic species i	[cm^2mole/Jsec]
v	velocity	[cm/sec]
x	longitudinal distance from leading edge of electrode or interface	[cm]
y	distance perpendicular to electrode or interface	[cm]
z	valence of ionic species	
Z	charge transfer number defined by (2.29a,b)	

GREEK SYMBOLS

α	exponential coefficient (charge-transfer coefficient) in (2.29)	
α	degree of dissociation of HSO_4^- ion (App. C)	
α_i	densification coefficient due to concentration gradient of species i	$[cm^3/mole]$
β	exponential coefficient (charge-transfer coefficient) in (2.29)	
γ	curvature parameter in free convection (Fig. 1.2)	
γ	exponential coefficient in (2.30)	
$\Gamma(4/3)$	= 0.893	
δ	thickness of boundary-layer or film	[cm]
ε	porosity	
E	field strength	[v/cm]
ζ	densification coefficient due to temperature gradient	$[°K^{-1}]$
η	dimensionless distance variable (App. B,E)	
η	overpotential	[v]
η_c	concentration overpotential	[v]
η_s	surface overpotential	[v]
θ	dimensionless concentration (c/c_b)	
θ	degree of dissociation of $CuSO_4$, in App. C	
κ	ratio of inner and outer radii in annular channel or ring-disk (Ch. 1)	
κ	conductivity (Ch. 2, Ch. 4)	$[\Omega^{-1}cm^{-1}]$
λ	friction factor (Ch. 1)	
λ_i	mobility of ionic species i	$[cm^2/\Omega equiv]$

Subscripts

avg	averaged
b	in the bulk
B	pertaining to bisulfate dissociation
C	pertaining to copper sulfate association
d	with respect to equivalent diameter (Ch. 1)
h	pertaining to heat transfer
i	pertaining to species i
m	modified
o	at the electrode or interface
ox	pertaining to oxidized species
p	with respect to particle dimensions
red	pertaining to reduced species
R	pertaining to reacting species
s	pertaining to the molecule (salt) as a whole
ss	corresponding to steady state
+	with respect to wall-parameters (Ch. 1)
+,-	pertaining to positive or negative ion
∞	corresponding to steady state
∞	in the bulk (Figures 2.3, 2.8, 2.11)

Superscripts

o	at the electrode (Fig. 2.3)
-	averaged
*	corresponding to uniform flux condition
∞	in the bulk (Fig. 2.3)

μ	dynamic viscosity	[cp]
ν	kinematic viscosity	[cst]
ρ	density	[g/ml]
τ	dimensionless time $\omega t\ Sc^{-1/3}$ (Ch. 3,4)	
τ	dimensionless time $0.307\ \omega t\ Sc^{-1/3}$ (App. B,E)	
τ_o	shear-stress at the wall	[dyne/cm^2]
ψ	auxiliary function in App. B	
ϕ	parameter in laminar transfer equation for annular ducts (1.6, fig. 1.1)	
ϕ	dimensionless potential (Ch. 4, App. A, F, G)	
Φ	potential	[v]
ω	rotation rate	[radians/sec]

Dimensionless Numbers

Gr_x	Grashof number (uniform concentration)	$\frac{g\alpha\Delta c x^3}{\nu^2}$
Gr_x^*	Grashof number (uniform flux)	$\frac{g\alpha N x^4}{\nu D}$
j_D	Chilton-Colburn parameter	$\frac{k}{v}Sc^{2/3}$
J	current distribution parameter	$\frac{i_o LZF}{\kappa_b R_o T}$
N	current distribution parameter	(2.57)
N'	current distribution parameter	(2.38,252)
Nu_x	Nusselt number	kx/D
Pr	Prandtl number	ν/a
Ra_x	Rayleigh number (uniform concentration	$Gr_x Sc$
Ra_x^*	Rayleigh number (uniform flux)	$Gr_x^* Sc$
Sc	Schmidt number	ν/D

REFERENCES

1. C. Wagner; Trans. Am. Electrochem. Soc. 95, 161-173 (1949).
2. C. S. Lin, E. B. Denton, H. S. Gaskill, G. L. Putnam; Ind. Eng. Chem. 43, 2136-2143 (1951).
3. C. R. Wilke, M. Eisenberg, C. W. Tobias; J. Electrochemical Soc. 100, 513-523 (1953).
4. C. S. Lin, R. W. Moulton, G. L. Putnam; Ind. Eng. Chem. 45, 636-645 (1953).
5. C. R. Wilke, C. W. Tobias, M. Eisenberg; Chem. Eng. Progr. 49, 663-674 (1953).
6. M. Eisenberg, C. W. Tobias, C. R. Wilke; J. Electrochemical Soc. 101, 306-320 (1954).
7. N. Ibl, R. Müller; Z. Elektrochemie 59, 671-676 (1955).
8. N. Ibl; "Studies of Mass Transfer during Electrolysis with Natural Convection," Proc. 8th Reunion C.I.T.C.E., Madrid (Spain), 1956; pp.174-189.
9. N. Ibl, R. H. Müller; J. Electrochemical Soc. 105, 346-353 and 536-538 (1959).
10. S. Okada, S. Yoshizawa, F. Hine, K. Asada; J. Electrochemical Soc. Japan (Overseas Ed.) 27, E69-72 (1959).
11. E. J. Fenech, C. W. Tobias; Electrochimica Acta 2, 311-325 (1960).

11a. E. J. Fenech; Ph.D. Thesis, U. California (1960), UCRL-9079.

12. M. G. Fouad, N. Ibl; Electrochimica Acta 3, 233-243 (1960).
13. P. Grassmann, N. Ibl, Trueb; Chemie-Ing. Technik 33, 529-533 (1961).
14. J. Venczel; Diss., E. T. H. Zurich, Nr. 3019 (1961).
15. P. de Voogd; Ir. (M.Sc.) Report, T. H. Delft (1961).

16. G. Wranglen,O. Nilsson; Electrochimica Acta 7, 121-137 (1962).

17. A. J. Arvia, J. S. W. Carrozza; Electrochimica Acta 7, 65-78 (1962).

18. R. Jottrand, F. Grunchard; Proc. Symp. Interaction Fluids Particles, London, 211 (1962).

19. L. P. Reiss, T. J. Hanratty; A. I. Ch.E. Journal 8, 245-247 (1962).

20. L. P. Reiss, T. J. Hanratty; A. I. Ch. E. Journal 9, 154-160 (1963).

21. J. T. Holmes, C. R. Wilke, D. R. Olander; J. Phys. Chem. 67, 1469-1472 (1963).

22. P. Van Shaw, L. P. Reiss, T. J. Hanratty; A. I. Ch. E. Journal 9, 362-364 (1963).

23. R. N. O'Brien, C. Rosenfield; J. Phys. Chem. 67, 643-647 (1963).

24. G. Schütz; Int. J. Heat Mass Transfer 6, 873-879 (1963).

25. P. H. Vogtländer, C. A. P. Bakker; Chem. Eng. Sci. 18, 583-589 (1963).

26. C. H. M. Vinke; Ir. (M.Sc.) Report, T. H. Delft (1963).

27. P. Van Shaw, T. J. Hanratty; A. I. Ch. E. Journal 10, 475-482 (1964).

28. T. P. Hoar, G. P. Rothwell; Electrochimica Acta 9, 135-150 (1964).

29. George S. Springer; Rev. Sci. Instr. 35, 1277-1280 (1964).

30. R. N. O'Brien, L. M. Mukherjee; J. Electrochemical Soc. 111, 1358-1362 (1964) and 112, 1253-1254 (1965).

31. M. G. Fouad, T. Gouda; Electrochimica Acta 9, 1071-1076 (1964).

32. Ch. W. Tobias, R. G. Hickman; Z. Physikal. Chemie (L) 229, 145-166 (1965).

33. K. Somasundara Rao, G. J. V. Jagannaha Raju, C. Venkata Rao; Ind. J. Technol. 3, 38-42 (1965).

34. J. C. Bazán, A. J. Arvía; Electrochimica Acta 9, 17-30 (1964).

35. J. C. Bazan, A. J. Arvia; Electrochimica Acta 9, 667-684 (1964).

36. T. K. Ross, A. A. Wragg; Electrochimica Acta 10, 1093-1106 (1965).

37. J. C. Bazan, A. J. Arvía; Electrochimica Acta 10, 1025-1032 (1965).

38. G. Schütz; Int. J. Heat Mass Transfer 7, 1077-1082 (1964).

39. G. J. V. Jagannadharaju, C. V. Rao; Ind. J. Technol. 3, 201-205 (1965).

40. M. S. Krishna, G. J. V. Jagannadharaju; Ind. J. Technol. 3, 263-267 (1965).

41. J. Sinkovic; Diss. Univ. Ljubljana (1965).

42. D. W. Hubbard, E. N. Lightfoot; Ind. Eng. Chem. Fundamentals 5, 370-379 (1966).

43. B. Howland, G. S. Springer, M. G. Hill; J. Fluid Mech. 24, 697-794 (1966).

44. R. G. Colello, G. S. Springer; Int. J. Heat Mass Transfer 9,1391-1399 (1966).

45. M. S. Krishna, G. J. V. Jagannadha Raju, C. Venkata Rao; Ind. J. Technol. 4, 8-11 (1966).

46. A. J. L. P. M. Boeffard; M. S. Thesis, Univ. California, Berkeley, UCRL-16624 (1966), and Ext. Abstr. 17th Meeting C.I.T.C.E., Tokyo (Japan), 1966, pp. 23-24.

47. S. L. Gordon, J. S. Newman, C. W. Tobias; Ber. Bunsenges. Phys. Chem. 70, 414-420 (1966).

48. U. Böhm, N. Ibl, A. M. Frei; Electrochimica Acta 11, 421-434 (1966).

49. J. E. Mitchell, T. J. Hanratty; J. Fluid Mech. 26, 199-221 (1966).

50. T. J. Hanratty; Phys. Fluids Supplement "Boundary Layers and Turbulence," S126 (1967).

51. A. J. Arvía, S. L. Marchiano, J. J. Podestá; Electrochimica Acta 12, 259-266 (1967).

52. R. E. Davis, G. L. Horvath, C. W. Tobias; Electrochimica Acta 12, 287-297 (1967).

53. P. Noordsij, J. W. Rotte; Chem. Eng. Sci. 22, 1475-1481 (1967).

54. E. Weder, Diss. E. T. H. Zürich, Nr. 4075 (1967).

55. D. H. King, J. W. Smith; Can. J. Chem. Eng. 45, 329-333 (1967).

56. A. Iribarne, A. D. Gosman, D. B. Spalding; Int. J. Heat Mass Transfer 10, 1661-1676 (1967).

57. C. V. Rama Raju, G. J. V. Jagannadha Raju, C. Venkata Rao; Ind. J. Technol. 5, 305-309 (1967).

58. M. S. Krishna, G. J. V. Jagannadha Raju; Ind. J. Technol. 5, 171-173 (1967).

59. M. Daguenet; Int. J. Heat Mass Transfer 11, 1581-1596 (1968).

60. A. A. Wragg; Electrochimica Acta 13, 2159-2165 (1968).

61. A. A. Wragg; Int. J. Heat Mass Transfer 11, 979-984 (1968).

62. R. E. Hicks, W. G. B. Mandersloot; Chem. Eng. Sci. 23, 1201-1210 (1968).

63. A. A. Wragg, T. K. Ross;Electrochimica Acta 13, 2192-2194 (1968).

64. A. J. Karabelas, T. J. Hanratty; J. Fluid Mech. 34, 159-162 (1968).

65. J. A. de Leeuw den Bouter, B. de Munnik, P. M. Heertjes; Chem. Eng. Sci. 23, 1185-1190 (1968).

66. S. L. Marchiano, A. J. Arvía; Electrochimica Acta 14, 741-747 (1969).

67. J. S. Son, T. J. Hanratty; J. Fluid Mech. 35, 353-368 (1969).

68. A. Tvarusko, L. S. Watkins; Electrochimica Acta 14, 1109-1118 (1969).

69. K. K. Sirkar, T. J. Hanratty; Ind. Eng. Chem. Fundamentals 8, 189-192 (1969).

70. P. Le Goff, F. Vergnes, F. Coeuret, J. Bordet; Ind. Eng. Chem. 61, 8-17 (1969).

71. C. V. Rama Raju, A. Ramalinga Sastry, G. J. V. Jagannadha Raju; Ind. J. Technol. 7, 35-37 (1969).

72. K. R. Jolls, T. J. Hanratty; A. I. Ch. E. Journal 15, 199-205 (1969).

73. J. W. Rotte; Diss. T. H. Delft (1967).

74. J. W. Rotte, G. L. J. Tummers, J. L. Dekker; Chem. Eng. Sci. 24, 1009-10015 (1969).

75. M. G. Fouad, A. M. Ahmed; Electrochimica Acta 14, 651-666 (1969).

76. M. G. Fouad, A. A. Zatout; Electrochimica Acta 14, 909-919 (1969).

77. E. Ravoo, J. W. Rotte, F. W. Sevenstern; Chem. Eng. Sci. 25, 1637-1652 (1970).

78. A. Palade de Iribarne, S. L. Marchiano, A. J. Arvía; Electrochimica Acta 15, 1827-1836 (1970).

79. E. Ravoo; Chemie-Ing. Technik (to be published).

80. E. Ravoo; Ingenieur (to be published).

81. B. T. Ellison, I. Cornet; J. Electrochemical Soc. 118, 68-72 (1971).

82. A. Tvarusko, L. S. Watkins; J. Electrochemical Soc. 118, 248-251 (1971).

83. A. A. Wragg; Ext. Abstr. 20th Meeting C.I.T.C.E., Strasbourg (France) 1969, pp. 17-21.

84. E. Heitz, A. Hauptmann; Ext. Abstr. 20th Meeting C.I.T.C.E., Strasbourg (France) 1969, pp. 143-144.

85. L. Hsueh, J. Newman, "Currents Limited by Gas Solubility", UCRL-19098 (October 1969).

86. A. Regner, I. Rousar; Coll. Trav. Chim. Tchecoslov. 25, 1132-1142 (1960).

87. Yu. G. Siver, B. I. Kabanov; J. Phys. Chem. USSR 22, 53-57 (1948).

88. J. D. Newson, A. C. Riddiford; J. Electrochemical Soc. 108, 695-698 (1961).

89. H. G. Dimopoulos, T. J. Hanratty; J. Fluid Mechanics 33, 303-319 (1968).

90. H. G. Schmidt; Diss. ETH Zürich No. 3095 (1961).

91. J. S. Son, T. J. Hanratty; A. I. Ch. E. Journal 13, 689-696 (1967).

92. F. O. Mixon, W. Y. Chon, K. O. Beatty; Chem. Eng. Progr. Symp. 56, (1960), Nr. 30, 75-81.

93. A. A. Wragg, T. K. Ross; Electrochimica Acta 12, 1421-1428 (1967).

94. M. S. Krishna; D. Sc. thesis, Andhra University, Waltair (1962).

95. F. Coeuret; D. Sc. thesis, Nancy (1967).

96. L. Hsueh; Ph.D. thesis, U. of California, Berkeley (1968), UCRL-18597.

97. M. Eisenberg, C. W. Tobias, C. R. Wilke; J. Electrochemical Soc., 103, 413-416 (1956).

98. L. Hsueh, J. Newman; Electrochimica Acta 12, 429-438 (1967).

99. A. Eucken; Z. Elektrochemie 38, 341-345 (1932).

100. C. W. Tobias, M. Eisenberg, C. R. Wilke; J. Electrochemical Soc. 99, 359C-365C (1952).

101. N. Ibl, "Methods for the Study of the Diffusion Layer"; 7th Reunion C.I.T.C.E. Lindau (Switzerland) 1955, pp. 112-133.

102. N. Ibl; Chemie-Ing. Technik 35, 353-361 (1963).

103. J. Newman; Ind. Eng. Chem. 60, 12-27 (1968).

104. R. H. Müller; "Optical Techniques for the Study of Phase Boundaries," UCRL-11997 (1965).

105. B. Levich; Acta Physicochimica U.R.S.S. 17, 257-307 (1942) and 19, 117-138 (1944).

106. B. Levich; Disc. Faraday Soc. 1, 37-43 (1947).

107. J. N. Agar; Disc. Faraday Soc. 1, 26-37 (1947).

108. V. G. Levich; "Physicochemical Hydrodynamics," Prentice-Hall Inc., Englewood Cliffs, N. J., 1962.

109. J. Newman; Adv. Electrochem. Electrochemical Eng. 5, 87-135 (1967).

110. A. C. Riddiford; Adv. Electrochem. Electrochemical Eng. 4, 47-116 (1966).

111. S. Bruckenstein; "Rotating Disk, Ring and Ring-Disk Electrodes," Electrochemical Society Short Course.

112. J. Newman; "The Graetz Problem," UCRL-18646 (1969).

113. J. R. Selman, J. Newman; "Free-Convection Mass Transfer with a Supporting Electrolyte, UCRL-20306 (1970), to be published in J. Electrochemical Soc.

114. J. R. Selman, J. Newman; "Migration in Supported Electrolyte Solutions with Free Convection," UCRL-20322 (1971).

115. Kirk W. Beach; "Optical Methods for the Study of Convective Mass Transfer Boundary Layers on Extended Electrodes," UCRL-20324, (Ph.D. Thesis), June, 1971.

116. W. Nernst; Z. Physik. Chemie 47, 52-55 (1904).

117. E. Brunner; Z. Physik. Chemie 47, 56-102 (1904).

118. C. V. King, M. Schack; J. Am. Chem. Soc. 57, 1212-1217 (1935).

119. C. V. King, W. H. Cathcart; J. Am. Chem. Soc. 59, 63-67 (1937).

120. K. E. Gubbins, R. D. Walker, Jr.; J. Electrochemical Soc. 112, 469-471 (1965).

121. A. C. Makrides, N. Hackerman; J. Electrochemical Soc. 105, 156-161 (1958).

122. J. N. Agar, F. P. Bowden; Proc. R. Soc. (L) A169, 206-234 (1938).

123. J. Newman; Ind. Eng. Chem. Fund. 5, 525-529 (1966).

124. J. Newman; Int. J. Heat Mass Transfer 10, 983-997 (1967).

125. L. Hsueh, J. Newman; "The Role of Bisulfate Ions in Ionic Migration Effects," UCRL-19102, July 1970.

126. A. Brenner; Proc. Am. Electroplaters Soc. 95-98 (1940).

127. W. H. Smyrl, J. Newman; Trans. Far. Soc. 63, 207-216 (1967).

128. W. L. Friend, A. B. Metzner; A. I. Ch. E. J. 4, 393-402 (1958).

129. B. C. Sakiadis; A. I. Ch. E. J. 7, 26-28, 221-225, 467-472 (1961).

130. J. Newman; "The Graetz Problem," UCRL-18646, January 1969.

131. D. B. Spalding; Int. J. Heat Mass Transfer 7, 743-761 (1964).

132. W. R. Vieth, J. H. Porter, T. K. Sherwood; Ind. Eng. Chem. Fund. 2, 1-3 (1963).

133. R. G. Deissler; N. A. C. A. Report 1210, pp. 69-82 (1955).

134. E. Mattson, J. O'M. Bockris; Trans. Faraday Soc. 55, 1586-1601 (1959).

135. J. Newman; J. Electrochemical Soc. 113, 1235-1241 (1966).

136. W. R. Parrish, J. Newman; J. Electrochemical Soc. 116, 169-172 (1969).

137. W. R. Parrish, J. Newman; J. Electrochemical Soc. 117, 43-48 (1970).

138. O. R. Brown, H. R. Thirsk; Electrochimica Acta 10, 383-393 (1965).

139. L. Hsueh; "Mass Transfer and Poalrization at a Rotating Disk Electrode" (M.S. Thesis, U. California, Berkeley), UCRL-16607 (January 1966).

140. L. Hsueh, J. Newman, J. R. Selman, C. W. Tobias; "Physical Properties of Ternary Electrolytic Solutions Employed in Ionic Mass Transfer Studies," UCRL-20710 (June 1971).

141. A. F. W. Cole, A. R. Gordon; J. Phys. Chem. 40, 733-737 (1936).

142. A. J. Arvía, J. C. Bazán, J. S. W. Carrozza; Electrochimica Acta 11, 881-889 (1966).

143. H. Gerischer, W. Vielstich; Z. Physik. Chemie (F) 3, 16-33 (1955).

144. D. R. Olander; Int. J. Heat Mass Transfer 5, 825-836 (1962).

145. R. Siegel; Trans. Am. Soc. Mech. Eng. 80, 347-359 (1958).

146. V. Yu. Filinovskii, V. A. Kir'yanov; Doklady A. N. SSSR 156, 1412-1415 (1964), Engl. transl. 650-553 (1964).

147. F. G. Cottrell; Z. Physik. Chemie 42, 385-431 (1903).

148. B. Fedoroff; Ann. Chim. 11 16, 154-214 (1941).

149. H. S. Harned and R. M. Hudson; J. Am. Chem. Soc. 73, 3781-3783, 5880-5882 (1951).

150. N. Ibl, K. Schadegg; J. Electrochemical Soc. 114, 54-58 (1951).

151. T. F. Young, L. F. Maranville, H. M. Smith: "Raman Spectral Investigations of Ionic Equilibria in Solutions of Strong Electrolytes," in W. J. Hamer (Ed.), "The Structure of Electrolytic Solutions" pp. 35-63. New York: John Wiley & Sons, Inc., 1959.

152. G. A. Emelyanenko, E. Ya. Baibarova; Ukrain. Khim. Zh. 25, 727-734 (1959).

153. K. J. Vetter; "Elektrochemische Kinetick"; Berlin: Springer-Verlag, 1961.

154. J. M. Hale; J. Electroanal. Chem. 6, 87-97 (1963).

155. S. K. Arapkoske, J. R. Selman; "Transport Properties of $CuSO_4$-H_2SO_4-H_2O at 25 C", UCRL-20510 (March 1971).

156. R. G. Hickman; "The Effect of Buoyancy Forces on Forced Convection Ionic Mass Transfer at Horizontal Planar Electrodes" (Ph.D. Thesis, U. of California), December, 1963.

157. B. Gebhart; J. Heat Transfer 83, 61-70 (1961).

158. B. Gebhart, R. P. Dring, C. E. Polymeropoulos; J. Heat Transfer 89, 53-59 (1967).

159. M. Soliman, P. L. Chambré; Int. J. Heat Mass Transfer 10, 169-179 (1967).

160. N. Riley; J. Fluid Mechanics 17, 97-104 (1964).

161. B. T. Chao, L. S. Cheema; Int. J. Heat Mass Transfer 11, 1311-1324 (1968).

162. G. P. Girina, V. Yu. Filinovskii, L. G. Feoktistov; Elektrokhimiya 3, 941-945 (1967), Engl. transl. 831-835 (1967).

163. I. Fried, P. J. Elving; Anal. Chem. 37, 464-467 and 803-806 (1965).

164. H. S. Carslaw, J. C. Jaeger; "Conduction of Heat in Solids," 2nd ed., Oxford, 1959, p. 77.

165. M. Abramowitz, I. A. Stegun; "Handbook of Mathematical Functions," Nat. Bureau of Standards, Washington (1964), p. 319.

166. R. S. Nicholson, I. Shain; Anal. Chem. 36, 706-723 (1964).

167. N. Tanaka, R. Tamamushi, Electrochimica Acta 9, 963-989 (1964).

168. H. J. Read, A. K. Graham; Trans. Electrochemical Soc. 80, 329-340 (1941).

169. A. Acrivos, P. L. Chambré; Ind. Eng. Chem. 49, 1025-1029 (1957).

170. L. Karasyk, H. B. Linford; J. Electrochemical Soc. 110, 895-903 (1963).

171. W. H. Reinmuth; J. Am. Chem. Soc. 79, 6358-6360 (1957).

172. P. Delahay; J. Am. Chem. Soc. 75, 1190-1196 (1953).

173. P. H. Sih;"Mass Transfer to the Rear of Objects in Low Reynolds Number Flow" (Ph.D. Thesis), UCRL-20509, April 1971.

174. W. H. Smyrl, J. Newman; "Ring-Disk and Sectioned Disk Electrodes," UCRL-20379, December 1970.

LEGAL NOTICE

This report was prepared as an account of work sponsored by the United States Government. Neither the United States nor the United States Atomic Energy Commission, nor any of their employees, nor any of their contractors, subcontractors, or their employees, makes any warranty, express or implied, or assumes any legal liability or responsibility for the accuracy, completeness or usefulness of any information, apparatus, product or process disclosed, or represents that its use would not infringe privately owned rights.

TECHNICAL INFORMATION DIVISION
LAWRENCE BERKELEY LABORATORY
UNIVERSITY OF CALIFORNIA
BERKELEY, CALIFORNIA 94720